Application of Path-Independent Integrals to Soil-Structure Interaction

Thesis by
Antonio Joaquín García Suárez

In Partial Fulfillment of the Requirements for the
Degree of
Doctor of Philosophy

CALIFORNIA INSTITUTE OF TECHNOLOGY
Pasadena, California

2020
Defended September 27, 2019

Antonio Joaquín García Suárez
ORCID: 0000-0001-8830-4348

ACKNOWLEDGEMENTS

I would like to express my gratitude to the Spanish and European taxpayers that funded the Talentia Scholarship that brought me to Caltech to pursue my Master in Space Engineering, and thanks to the Andalusian Regional Government (Junta de Andalucía) that deemed me worthy of it. I would also like thank the Tyson family, who funded part of my graduate work through the Tyson Fellowship.

I am indebted to Prof. Pilar Ariza, Prof. Antonio Martínez and Prof. Fernando Medina (University of Sevilla) and Fernando Medina Reguera (NextForce Engineering), my guarantors back in Sevilla, who wrote their names beside mine when it came to apply to Caltech. I have heartfully tried to live up to the trust they put in me.

I would like to acknowledge the California Institute of Technology, as an institution, for providing an unmatchable stage to delve in scientific pursuits. Staff over at Chandler's and Red Door Cafe, the International Student Office, the Registrar's Office and the Health Center kept me healthy and compliant with both Institute and American requirements. I have had the privilege to learn from Caltech faculty by taking a fair number of classes over these years, my gratitude goes to them too. In particular, Prof. Ravichandran and Prof. Meiron, who also served as committee members of this thesis, provided me with some of the mathematical and mechanics tools I needed to carry this work to completion, so I remain sincerely grateful to them.

Prof. Ortiz's and Prof. Asimaki's group members granted me the opportunity to expand my knowledge and feed my curiosity during group meeting presentations and many discussions. Special mention to Carolina and Lydia, the "invisible hands" keeping the groups running. In Asimaki's group, I have to single out Elnaz and Danilo, as a considerable part of my contributions owes much to their engagement during our countless discussions over research issues in the basement of Gates-Thomas at unearthly hours.

My gratitude to Prof. Miguel Ortíz cannot be overstated. Not only he enabled my arrival in California, he also channeled my efforts to become a prudent solid mechanician, and acts as an inspiration to strive to ever-greater excellence.

Thanks are also in order to Prof. Domniki Asimaki, who has been the best adviser I could have wished for. Both her knowledge and her kindness became overwhelming at times during this PhD period. I must thank her for taking me as her PhD student,

and for her constant guidance while allowing me to risk following my curiosity at the same time.

To the friends I have made in California, words cannot do justice to how lucky I feel for having encountered you along my way. Thanks for sharing (either in Lees-Kubota, in Sierra Bonita or in El Rancho, in Chiapas, in Connecticut, in Mammoth Lakes, or wherever necessary!) these remarkable years and so much life and adventures.

To my family back home I would like to dedicate this work. I have been blessed with a tight-knit family: my cousins (in Arcos, in Álora, in Sebastián Trujillo and in Los Remedios), my uncles and aunts (some of my first references in academia), my parents and brothers. To my younger brothers, Víctor, Gonzalo, Pedro and Santiago, as everything I have done was intended to make them feel proud of their elder brother. To my mother, Reyes, for she is my admired lifelong role model, and to my father, Víctor, for he taught me, among many other things, to love Science.

Gracias.

Nuestras horas son minutos
cuando esperamos saber,
y siglos cuando sabemos
lo que se puede aprender.
– Proverbios y cantares (IV)
Antonio Machado

ABSTRACT

Assessing seismic pressure increment on buried structures is a critical step in the design of infrastructure in earthquake-prone areas. Due to intrinsic complexities derived from the need to match the solution in the far-field to the localized solution around the structure, the near-field, researchers have aimed at finding simplified models focused on engineering variables as the seismic earth thrust. One such model is the so-called Younan-Veletsos model, which pivots on a stringent assumption on the stress tensor.

At the same time, the might of the path-independent integrals of solid mechanics to deal with problems in Geotechnical Engineering at large, and Soil-Structure Interaction in particular, has remained unexplored, despite of a rich landscape of potential applications. The unbridled success of these path-independent integrals in Fracture Mechanics, a discipline which cannot be understood without them currently, may be mirrored in problems in Geotechnical Engineering, since the two fields, despite appearing very detached from each other at first glance, share deep traits: in both cases, the system under consideration can be conceptualized as a domain with simple, easy-to-assess regions (the areas where remote loading is applied and the far-field, respectively) and also with other complex, hard-to-understand regions (the crack tip, the near-field).

We present the first derivation of the exact solution of the Younan-Veletsos problem, which is later analyzed to reveal phenomena not captured by previous approximate solutions. Then, we introduce a novel model which relies on the path-independent Rice's J-integral, a customary tool in Fracture Mechanics, which is applied here in the Soil-structure Interaction context for the first time. This novel model captures those features of the exact solution that were missed by prior approximations. The capabilities of the J-integral to, first, find an upper bound of the force induced by earthquakes over the walls of underground structures, under some conditions, and, second, to understand the soil-structure kinematic interaction phenomenon are also assessed.

Additionally, the intermediate step of analyzing of the far-field yielded some results concerning Site Response Analysis which are also included in the text.

PUBLISHED CONTENT AND CONTRIBUTIONS

[GA19] Joaquin Garcia-Suarez and Domniki Asimaki. “On the fundamental resonant mode of inhomogeneous soil deposits”. In: *engrxiv.org* (2019). DOI: 10.31224/osf.io/a8fmx..
This work was a collaborative effort for which each author made substantial contributions to all aspects.

[GSA19] Joaquin Garcia-Suarez, Elnaz Seylabi, and Domniki Asimaki. “Seismic harmonic response of inhomogeneous soil: scaling analysis”. In: *Géotechnique* (accepted, 2019).
This work was a collaborative effort for which each author made substantial contributions to all aspects.

TABLE OF CONTENTS

LIST OF ILLUSTRATIONS

LIST OF TABLES

Chapter 1

INTRODUCTION

This first chapter aims to provide the reader with:

- Brief introductions to both soil-structure interaction and path-independent integrals, and motivation for the need of applying the second to the first.
- Objectives and scope of this text.
- Organization of the text.
- A list of supplementary materials.

1.1 Soil-structure interaction: a primer

By and large, civil structures are either partially or completely embedded in the soil. The soil, in and of itself, is an intricate system, made up of a large collection of microconstituents which interact with each other through (in general) contact forces, with either air or water filling the void spaces between them. These microconstituents are usually referred to as grains, although clayey soils display a more complex microstructure.

Due to the inherent uncertainty when dealing with it, civil engineers tend to avoid direct consideration of soil-structure interaction effects when designing or analyzing a structure, indirectly accounting for it by increasing safety margins. However, this procedure is unfeasible whenever the structure bears special standing (critical infrastructure, e.g., a nuclear power plant) or its value is deemed somewhat too high for the risk to remain unaccounted. A paramount source of peril is, of course, seismic activity.

Soil-structure interaction (SSI, from this point onward) effects are twofold. It is advantageous, on one hand, as the surrounding soil *radiates* a portion of energy away from the structure, which, if the soil was absent would have to be converted into either kinetic or deformation energy in the structure, or dissipated by internal processes within the structure which are, in general, way less efficient than this so-called *radiation damping* mechanism. This critical mechanism strongly depends on the soil's mechanical properties and layering [Wol85]. This is generally due

to the wave scattering produced by the presence of the structure, which is "seen" as an obstacle by the impinging wavefront. Such an event is labeled as *kinematic interaction* in SSI lexicon.
On the other hand, the coupling between structure and soil response (in particular for relatively soft soils) can trigger a pernicious cycle of increasing inertial forces in the structure, which induce larger deformations in the soil surrounding the structure or its foundation, and in turn may provoke further deflection and accelerations in the structure. This effect is labeled, in SSI, as *inertial interaction*.

The approaches to study the SSI phenomenon have ranged from analytical investigations, forerunners tracing back to the nineteenth century [Cer82; Bou85], to numerical simulations and experimental work.

The original push towards anchoring SSI as a discipline within Solid Mechanics saw initial successes [Ter16; Lov29], many of them supplied by the Austro-German tradition headed by Terzaghi [Kau10]. These first attempts were concerned with statics and aimed at obtaining the response of a linear-elastic half-space subjected to different types of loads applied at its free-surface. Equivalent problems in dynamic SSI have exhibit more difficulties than their quasi-static counterpart, as was expected. A collection of available solutions can be found in Kausel's compendium [Kau06]. The basic conceptual framework to understand this phenomenon is attributed to Prof. George Housner, who penned two milestone articles (the first one in collaboration with Prof. R.G. Merrit), [MH54; Hou57b], by the mid 1950s, wherein he explained the effect of man-made structures on the displacement field at the ground surface elicited by earthquakes. Once the conceptual pieces of the phenomenon were ascertained, simple-yet-insightful reduced models describing the main traits of the interplay between soil and structure were proposed by [SRW72], leading up to current practice recommendations codified, in the US, by the National Institute of Standards and Technology (NIST) [NIS12].

Despite remarkable progress, the ever-increasing complexity of these problems (e.g. considerations of soil layering, effect of embedment depth, etc) made a generation of researchers pivot towards numerical methods in order to gain insight on the influence of these features. In particular, the Boundary Element Method (BEM) proved itself a tool-of-choice to deal with the unbounded domain that represents the soil bulk. For instance, Prof. Domínguez Abascal [DR78a; DR78b] was the first to obtain the dynamic impedance of an embedded rectangular foundation by the aid of BEM. Nowadays, numerical codes can deal with more complex constitutive models, which

allow for the incorporation of more realistic material behavior than linear elasticity; as a token, see [Ana+08]. Results such as those provided by Prof. Gazetas [Gaz91] are already common tools in the trade. Regrettably, numerical parametric studies display limited capacity in assessment of the underlying physics and caution must be exercised when interpreting and extrapolating results from parametric analyses.

For more detail on both analytical and numerical work, the reader is referred to the comprehensive survey curated by Prof. Eduardo Kausel [Kau10].

Experiments remain the touchstone of scientific endeavors and the ultimate arbiter of suitability of engineering mdoels. Regarding SSI, efforts in the experimental front have been vexed by another factor: in reality, the soil is tantamount to a granular medium and not so much to a linear-elastic material. For the most part, analytical results in dynamic SSI are restricted to linear-elastic medium, and so are the aforementioned milestones in numerical work. This has hindered the reconciliation between these and experimental results [GS91], albeit it seems possible to find mechanical parameters so that the analytical and numerical methods can agree with the experiments [Sey+18]. On the bright side, profuse instrumentation of both buildings and sites [GAG19; Oka+04] is common in seismic areas nowadays, granting researchers with access to a large database amenable to gauge the accuracy of their models.

In any event, the push continues in all fronts, propelled by the necessity of assessing complex scenarios and systems that demand novel tools or deeper understanding.

The spark that initiated the work in this text was the construction of the Headworks Reservoir, in Los Angeles, California [Hud+14]. These 110-million-gallon (combined total) reinforced concrete structures posed, due to their singularity, a phenomenal design challenge on the Los Angeles Department of Water and Power (LADWP) and onerous economic effort to the State of California and its citizens. This remarkable project motivated a re-examination of the SSI physics concerning water underground water reservoirs subjected to seismic action [Hus+16a] as well as the available guidelines and numerical design tools [Har+14]. The inception and a sizeable part of this thesis may also be ascribed to this endeavor.

1.2 Path-independent integrals in Continuum Mechanics and its potential for solving problems in soil-structure interaction

Herein it follows a concise survey of the works concerning path-independent integrals (PIIs) in Solid Mechanics, with an admitted slant towards Fracture Mechanics,

Figure 1.1: Aerial view of Headworks Reservoir (under construction, 2018). Image credit: Los Angeles Dept. of Water and Power (downloaded from ladwpnews.com/epk-headworks-reservoir-construction)

divided by ambit (quasi-static or dynamic regime) and ordered chronologically. At the end of this section we will motivate the aptitude of these PII as useful tools to untangle problems in Soil-Structure Interaction.

1.2.1 The origins: quasi-static Fracture Mechanics

Eshelby is recognized as the first researcher that found a surface-integral representation for "force on an elastic singularity or inhomogeneity" [Esh56], in 1951 during the course of his studies on lattice defects, although an immediate antecedent can be found in the Peach-Kohler equation [Lub18], obtained one year earlier. Eshelby did note that in the absence of defects his result represented a conservation law for regular small-deformation elastostatic fields in homogeneous yet not-necessarily-isotropic bodies. Besides, he acknowledged that this result could be extended to finite kinematics.

A few years later, Prof. James Rice [Ric68] proposed a path-independent line integral for plane elastostatic problems with consequential implications for the study of Fracture Mechanics: the J-integral. It was in this work that a critical new insight was also presented: whatever happens at the crack tip (complex and unknown) can be directly related to the remote conditions (simple and well-known) through this path-independent integral. In other words, the identities derived from the J-integral allow one to establish a direct, exact relation between the well-understood part of

the domain and the to-be-understood regions, without needing to solve the field equations of the problem. The J-integral is nothing but a particular instance of a more general theory, of which the aforementioned work by Eshelby was but another example.

The equivalence of these results as well as a general theory of generalized conservation laws expressed in terms of path-independent integrals over elastic bodies was presented by Knowles and Sternberg [KS72], for both infinitesimal and finite kinematics, wherein it was also highlighted how these conservation laws relate to the classic Noether's theorem of mathematical physics [Bye98]. A similar text, which did not foresee connections to fracture, had been published by Günther previously [Gün62] in German, what hindered the dissemination of the findings to the extent that they had to be re-discovered independently a decade later.

Chen and Shield [CS77] explored a number of conservation laws in elastostatics connected to different types of strain-energy functionals. Moreover, they provided equivalent identities relating two different states, an approach that was later systematized by Zhang and Achenbach [ZA89], who also presented the so-called Boundary Integral Method (BIM).

Rice [Ric85] also noted the extent to which these relations resemble the classic Maxwell relations from Thermodynamics, both in appearance and content: the conserved integrals represent "energetic force" related to invariant transformations. One can find a "translational integral" (the J-integral itself, related to loss of translational symmetries), a "rotational integral" (the L-integral, related to loss of rotational symmetries), and a "scaling integral" (the M-integral, related to infinitesimal changes of scale). It was also acknowledged that the work done by these forces represents *dissipation* in accordance to the Second Law of Thermodynamics, and that then, logically, these become useful to establish *evolution criteria* (e.g. crack growth).

Rice's J-integral has enjoyed wide popularity in the Fracture Mechanics community, as it provided a simple parameter able of characterizing the stress concentration and energy dissipation occurring at the crack tip. In linear-elastic Fracture Mechanics, the relation between the J-integral and the ubiquitous stress intensity factors is common knowledge. In elastic-plastic fracture mechanics, under the use of deformation theory of plasticity, the value of J represents the strength of the HRR-singulairty field [Zha90]. It has also found applications in more complex scenarios in Fracture Mechanics, e.g., fracture of piezo-electric materials [YB95].

1.2.1.1 The extension to the dynamic setting

These path-independent integrals were originally intended to help deal with static or quasi-static problems, and their extension to more general dynamic settings was challenging: these path-independent integrals are intimately related to the elliptic nature of the static problem, such ellipticity being lost as one moves into the dynamic realm and appearance of inertial terms turn the equations hyperbolic and wave propagation phenomena take precedence.

Nevertheless, this issue was shown to be avoidable, as new dynamic approaches were developed to deal with problems in Dynamic Fracture Mechanics [Fre98], a logical extension of the pioneering work carried out by Rice and others.

Nilsson [Nil73] noted that translating the problem to the frequency domain, by means of application of Laplace's transform that would turn the original hyperbolic field equations into elliptic field equations (the inertial forces become regular body forces proportional to the displacement), which enables the definition of path-independent integrals relevant to the dynamic setting yet with a caveat: one is bound to interpret the results, firstly, not in the time domain but rather in the frequency domain. Once the results in frequency domain have been obtained, the Laplace's transform must be inverted in order to finally obtain results in time domain. That inversion can be expressed as the convolution of the product, and so was noted by Gurtin [Gur76] .

Nilsson's approach also hints at yet another way of dealing with the dynamic problem: assuming harmonic forcing and either neglecting free-vibration or assuming steady-state conditions, then, by virtue of linearity, the system of hyperbolic equations yield a system of elliptic equations wherein the unknowns are the (complex) amplitudes of the harmonic response. This framing is customary in the study of cracked bodies subjected to harmonic loading.

The literature in the field has increased dramatically, and it is beyond the scope of this text to delve too much into it. The reader in search of further details is referred to Prof. Maugin historical survey [Mau13], see Chapter 14 particularly, or to the monograph on configurational forces by the same author [Mau16], as well as Dynamic Fracture Mechanics monograph by Prof. Freund [Fre98], which remains an invaluable reference.

We have chosen to tilt our attention towards Fracture Mechanics because it provides a clean analogy that we move to exploit now. Equally fruitful is the analogy to dislocations, which will also be pursued. Be that as it may, keep in mind that

there exist many other applications of these path-independent integrals as work on this field has been steady during the last years insofar different flavours of continuum mechanics are concerned: strain discontinuities in solids [AK90] and phase transitions [AK93], just to name a few. Reasons for this positive turnout will also be given in the next section.

1.2.2 On an analogy between Fracture Mechanics and Soil-Structure Interaction: configurational forces

Despite the progress made in many branches of Continuum Mechanics by mediation of these path-independent integrals, geomechanics has remained untouched by them.

The might of the path-independent integrals resides, first and foremost, in its intrinsic capacity to reveal meaningful interrelations between different regions in the same domain, intertwining the response of those regions that are more complex to the one of those that are simpler to understand and assess. Therein their usefulness for fracture is found, as they allow to coonect the complex local response at the crack, which is hard to assess, to the pre-established, already-understood, loading conditions.

This remarkable capacity stems from the concept of *thermodynamic* forces, as opposed to, or rather, complementing, *mechanical* forces. For illustration purposes, consider another example: a dislocation, a certain type of defect in crystalline solids [RS50]. This defect is an alteration in the regular configuration of the material, its presence breaking the material internal homogeneity, that is, its internal symmetry. The dislocation does not possess, say, either mass or electric charge, but one it can experimentally be seen evolving within the solid. So this dislocation "moves", yet it does not do it according to a force given by Newton's second law, neither given by Coulomb's law, but, following the analogy with the two foregoing, there must be a different type of "force" making the configuration of the material evolve. Such force that drives the evolution of the defect is dubbed a *configurational force*, or *material force*, or *thermodynamic driving force*. The cause whose effect is the dislocation movement is known as the Peach-Koehler force. Incidentally, the cause that drives the movement (growth) of the crack tip is Rice's J-integral, and both of these forces, as well as other equivalent ones, find their natural articulation by means of the path-independent integrals we have been presenting: these integrals represent nothing but the *balance laws* of these forces, in the same way that Newton's Second Law explains the balance of forces that act directly "over matter" (e.g., mediated by mass

or electric charge, neither of them present in either the crack or the dislocation). In the absence of sources or sinks, these balance laws may as well be dubbed *conservation laws*.

The prior relation between the crack and the plate, or between the regular atomic lattice and the dislocation, can forthrightly be mapped to a structure surrounded by soil: the presence of the structure (either a foundation, a pipe, an excavation...) alters the symmetry of the soil domain (in other words, introduces an heterogeneity).
Hence, the path-independent integrals establish a relation between the response at the *far-field*, the region far from the structure/inclusion (which is simpler to analyze and plays the role of the known loading condition in the analogy to fracture) and the *near-field*, viz. the region of the soil domain surrounding the inclusion (which plays the role of the crack tip in the analogy). Let us also link the prior discussion on dislocations to the presence of a man-made structure on ground, a foundation for instance. Even before considering the mass or the stiffness of the structure, one can recognize that it does represent a change in the geometrical configuration in an otherwise homogeneous system, and thus it is as if there was a kind of *defect* within the material. Now consider some sort of excitation on the whole system, say, an earthquake. The whole system moves, but the zone around the foundation (*near-field*) moves differently compared to the rest of the soil, and thus we may say some extra force, that does not appear anywhere else, is being applied to it and changing the configuration locally. These configurational forces can be devised through the path-independent integrals (the new conservation laws), as we have already mentioned and we shall illustrate. Of course, this phenomenon has to represent a new rendition of the *kinematic interaction* phenomenon that was introduced in the previous section.
Besides, adding mechanical properties and mass to the foundation would bring other forces (internal elastic, inertial) into the picture, but the configurational force will remain.

We present yet one more item upon which the analogy could be extended: see how, as in the case of the crack tip, the work of the thermodynamic forces is a dissipation term, then, what about the underground structure? The dissipation mechanism in this case must be the *radiation* associated with the scattered wavefield.

The nature of these forces is the subject of debate [BR16], and herein we do not intend to settle such debate. In any event, it appears they are an efficient way, a bypass one may say, of conceptualizing some physical phenomena, which eases the

comprehension of problems like those that concern us.

Finally, we should notice that these conservation laws can be of much utility even when there is no structure but just changes within the soil domain. We surmise that changes in stratigraphy, slopes, and other common geomechanical affairs may be also studied from the viewpoint of PII.

1.3 Objectives and scope

This thesis chief objective is motivating and illustrating the potential of path-independent integrals, developed originally in the ambit of Fracture Mechanics, for analyzing SSI problems, which appears to have gone unexplored.

To make this precise, we shall focus first on the problem considered by Dr. Younan and Prof. Veletsos in two landmark papers [VY94b; VY94a], which we shall refer as the Younan-Veletsos problem from this point onward. We shall show how considerations derived from PIIs help elucidating relevant features in the problem. In the course of study of the Younan-Veletsos problem, we will provide the exact solution of the problem with smooth-rigid walls, complementing the classic solution obtained by Wood for a system with two of these walls [Woo73]. We must clarify that this solution is given in wavenumber space, since the inversion of Fourier transform that allows moving from wavenumber back to spatial coordinates has not been achieved yet. Nevertheless, this shall not prevent us from evaluating some relevant parameters, as the earth thrust, numerically.

Another basic application of PII to a more complex problem, namely a reservoir within a thick soil layer resting on soil, shall also be demonstrated. In spite of requiring the introduction of a number of simplifying assumptions, the result is deemed interesting, as it shows how the PII can be used to obtain bounds of certain parameters in geometric configurations that do not lend themselves to finding a simple closed-form solution. This result can be considered a first attempt towards an answer of a rather general and consequential question: how much information on *mechanical* forces acting on a certain certain can be retrieved from the analysis of *configurational* forces?

Finally, in the last chapter, the aforementioned soil-structure kinematic interaction is re-framed in terms of a balance of configuratinal forces. It is shown that such an approach presents some critical advantages, which shall enable us to obtain a simple model for foundation input motion[EMR77] that compares satisfactorily, provided some assumptions, to classic results in the field obtained through simulations.

Additionally, there are a number of ancillary topics addressed in this text.

One of them consists of providing a general framework wherein the problem of seismic response of underground water reservoirs can be assessed. The chosen instrument to fulfill this effort is none other than Dimensional Analysis, as outlined by Buckingham's Pi Theorem [Lan51]. We shall put forward a descriptive model of this scenario, including a bevy of parameters describing the response of soil, water, and structure, as well as features of the seismic load. Once this is done, we shall interpret the physical significance of the dimensionless groups that derive from this set of parameters. Once the meaning of each has become apparent, we shall map specific configurations of the physical configuration to distinct points in the parameter space. We hesitate referring to this contribution as novel, since it so appears that the use of Dimensional Analysis is gaining standing among theoreticians in our field of Geotechnical Earthquake Engineering; here one must mention a notable paper by Prof. Conti and collaborators [CMV17]. We must also mention that the comparable section in this text was written prior to the author being aware of their work. In a private communication, Prof. Conti rightly pointed out that this wherewithal has already been used extensively by experimentalists in the field [Woo14].

Another relevant theme in this thesis has been One-dimensional Site Response (1D-SR). Devoting a full chapter to the topic in a thesis primarily concerned to SSI may seem an unnecessary digression at first, but this is far from being the case, as there are good reasons to do so. First and foremost, due to its relation to SSI (far-field analysis). Moreover, in and of itself, it is a relevant problem that concerns geotechnical engineering experts as much as SSI, and it has some unexpected ramifications [Gaz87]. We shall focus on two questions: how to characterize, in first place, the high-frequency response of sites, and secondly, idem for the fundamental resonance mode. This front has been limited 1D-SR, and the extension of the conclusions to SSI is a pending task, although we already provide some results bearing direct consequences to SSI recommendations [NIS12].

The scope limitation of the results will be thoroughly discussed in the text, especially with aid of the dimensionless groups that we devise to characterize the problem of seismic response of underground reservoirs.
In any event, let us make clear that the classic assumptions of isotropy, homogeneity and linearity will pose the main restrictions to most results contain in this text. We expect future work will relieve this burden.

1.4 Organization of the text

Chapter 2 considers the basic theory Elasticity and Elastodynamics, including Path-independent integrals, necessary for upcoming discussion. In addition, fundamentals of soil behavior and 1D Site Response are revisited.

Chapter 3 is concerned with new results in 1D-SR. These range from explicitly presenting and displaying interrelations between the two possible manners of conceptualizing the problem when there exists rigid bedrock (i.e. in terms of either relative or total displacements), to a characterization of the high-frequency regime and the first resonant mode in these systems. The consequences of these results for SSI are not included in the text as they are still in the early stages, but relevant comments on the matter are included by the end of the chapter.

Chapter 4 presents an overarching study, assisted by Dimensional Analysis, of seismic response of underground water reservoirs. Thorough discussion of the different parameters and regimes in the problem is pursued. Then, the main object of study, the Younan-Veletsos problem, is presented, solved, and its main qualitative features discussed. Finally, a relaxation of the Younan-Veletsos problem, wherein there is soil between structure and bedrock, is considered in the long-wavelength regime, and, providing certain conditions, a bound for the earth thrust is derived in terms of the far-field response.

Chapter 5 delves into how to use the insight from PIIs and the qualitative features of the problem to propose a new simplified model that captures most distinct features of the exact solution. Such a model is proposed and compared to the new exact solution and to other simplified models.

Chapter 6 is occupied with developing a new framework to understand soil-structure kinematic interaction within the theory of configurational forces. A simple model for foundation input motions is drawn out from the general expressions and compared to the classic results by Elsabee and Morray [EMR77].

Chapter 7 provides conclusions and outline future research avenues.

A number of appendices provide supporting material like step-by-step derivations, as well as address other topics of interest that have been studied but that surpass the scope of the thesis.

1.5 Supporting material

In an effort to ease the dissemination of the findings contained in the text, a number of *Mathematica* [Wol00] notebooks are provided as supporting material. These contain details on derivations and also implement the main results of this study. A list, including brief description, of these notebooks follows:

- “Chapter3 1D Site Response.nb" was used to generate the transfer functions displayed in plots for Chapter 3.
- “Chapter4 Exact Solution YV Problem.nb” contains some details of the derivation of the main result in the chapter, as well as implementation of the exact solution of the problem being considered. This notebook can be used to generate the data displayed in figures in Chapter 4.
- “Chapter5 Evaluation Dynamic J Integral.nb”,likewise, implements and evaluates the results in Chapter 5.
- “Chapter6 Kinematic Interaction.nb” was used to generate the main results in Chapter 6 (namely those contained in Figure 6.2).

Files can be found in the author’s GitHub repository (`github.com/jgarciasuarez`).

Chapter 2

BACKGROUND

Here we aim to present the fundamentals upon which the upcoming study hinges:

- Modeling of soil as linear-elastic material.
- Elastostatics and Elastodynamics, including Williams solution for notches.
- Variational formulation in Continuum Mechanics (due to its relevance to path-independent integrals).
- Path-independent integrals.
- One-dimensional site response.

2.1 The soil as a linear-elastic medium and its dynamic properties

The constitutive law used to describe the soil response poses a bottleneck to any effort of predicting response of soil-structure systems. As the customary saying goes, the accuracy of predictions by a model can be as good as, but not better than, the material description one adopts. Accordingly, finding a simple-yet-accurate constitutive relation to describe the soil behavior is paramount.

In general, most clays, silts, and sands present a linear stress-strain relation up to strains $\sim 10^{-4}$ [PD74], although for some peculiar clay types the range can be extended up to $\sim 10^{-3}$ [DV87]. Let us keep these orders in magnitude in mind, as we shall resurface them when the discussion of range of validity of our analysis ensues in section 4.2.

The question of how to assign values to the mechanical properties of such linear-elastic medium still demands an answer. Contrasted experimental data is widely available for both static and dynamic response [IZ93]. Hertzian theory [Joh82], which does not involve irregular grains but perfect spheres, at least provides insight on how the mechanical macromechanical properties of the ensemble depend on the overburden pressure, and, by extension, on how mechanical properties of the soil vary with depth [HD72]. Another effect arising from overburden pressure has to see with the intrisic soil anisotropy mainly due to this compression acting primarily

only in one direction [Gib74], although oftentimes it tends to be ignored. In our work, we shall consider, whenever necessary, either that the depth is not excessive so that the degree of anisotropy remains small, or that the wave propagation elicits response in just one direction. Should there be cases such that neither suppoition is possible, our results must be interpreted as limited to specific materials whose properties are such that it can be considered isotropic.

Another concern is how to model internal dissipation in the granular material from a *macro* perspective. An unvarnished way to accomplish this would be considering soil as a viscous medium where dissipation is proportional the deformation rate; experiments contradict this last assertion, though. Dissipation in most soils subjected to cyclic load follow from an hysteresis loop that appears to be proportional to deformation amplitude instead of rate, and dissipation is present at even very low strain levels [Kra96]. Besides, confinement pressure has been proved to affect dissipation too [IZ93].
The customary, simple approach of adding this dissipation is through a *loss factor*, turns the elastic constants from real parameters to complex parameters, as it adds a factor $(1 + \mathrm{i}\delta_d)$, δ_d (real number, also referred to as *hysteretic* damping factor, sometimes appearing with an extra factor 2) will be adopted ("i" is the imaginary unit). Note that this approach is limited to frequency-domain analyses.

2.2 Elastostatics

Before starting, a word on notation: bold symbols represent vectors and tensors, Einstein's index convention is in effect, unless otherwise stated, we shall use the letters x, y and z to refer to indices, and thus, for instance, the displacement vector can be equivalently expressed as $\boldsymbol{u} = u_i = [u_x, u_y, u_z]^\top = [u, v, w]^\top$, the second triad (u, v, w) shall be used whenever referring to specific components directly.

We begin by considering an homogeneous body occupying a domain $\Omega \subset \mathbb{R}^3$ which undergoes deformations elicited by external loads and prescribed displacements. The boundary of the domain is referred to as $\partial\Omega = \partial\Omega_1 \cup \partial\Omega_2$ (such that $\partial\Omega_1 \cap \partial\Omega_2 = \varnothing$). As a cardinal assumption, this problem will be framed using infinitesimal kinematics. Moreover, in this section we shall consider deformation rates such that the inertial forces appearing anywhere within the body happen to be negligible. Let $\boldsymbol{x}$ denote the position o a point in Ω. Hence, we seek displacements $\boldsymbol{u} = u_i(\boldsymbol{x})$, strains $\boldsymbol{\epsilon} = \epsilon_{ij}(\boldsymbol{x})$ and stresses $\boldsymbol{\sigma} = \sigma_{ij}(\boldsymbol{x})$ satisfying the field equations and boundary

conditions governing the evolution of the system:

$$\epsilon_{ij} = \frac{1}{2}\left(\frac{\partial u_i}{\partial x_j} + \frac{\partial u_j}{\partial x_i}\right) \qquad \text{in } \Omega\,, \tag{2.1}$$

$$\sigma_{ij,j} + \rho b_i = 0 \qquad \text{in } \Omega\,, \tag{2.2}$$

$$\sigma_{ij} = \frac{\partial W}{\partial u_{i,j}} \qquad \text{in } \Omega\,, \tag{2.3}$$

$$\boldsymbol{u} = \bar{\boldsymbol{u}} \qquad \text{on } \partial\Omega_1\,, \tag{2.4}$$

$$\sigma_{ij} n_j = \bar{t}_i \qquad \text{on } \partial\Omega_2\,, \tag{2.5}$$

where $W(\boldsymbol{x})$ represents the corresponding strain energy density, n_j is the outwards-facing normal. Thermal considerations are intentionally left out of the picture, as these are irrelevant for the problems we shall focus on.

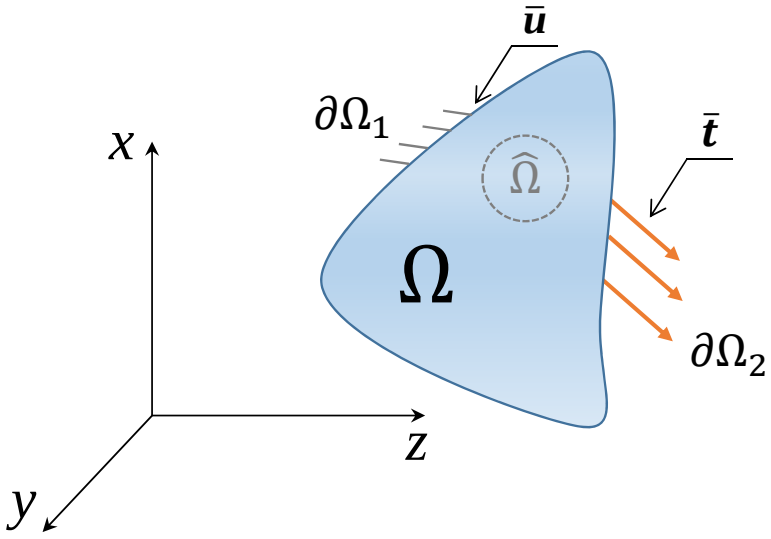

Figure 2.1: Scheme of the boundary-value problem

If we were to add the hypothesis of linear material response, then

$$W = \frac{1}{2}\sigma_{ij}\varepsilon_{ij}\,. \tag{2.6a}$$

If we allow for elastic (anisotropic) behavior

$$W = \frac{1}{2}c_{ijkl}\varepsilon_{ij}\varepsilon_{kl}\,, \tag{2.6b}$$

c_{ijkl} being the tensor of elastic constants (which must satisfy the symmetry conditions $c_{ijkl} = c_{jikl} = c_{ijlk} = c_{klij}$). If eq. (2.6b) holds, it implies the so-called anisotropic Hooke's (constitutive) law:

$$\sigma_{ij}(\boldsymbol{x}) = c_{ijkl}\varepsilon_{kl}(\boldsymbol{x})\,, \tag{2.7}$$

which in turn can be generalized to heterogeneous media by rendering the elastic constants function of the position,

$$\sigma_{ij}(\boldsymbol{x}) = c_{ijkl}(\boldsymbol{x})\varepsilon_{kl}(\boldsymbol{x})\,. \tag{2.8}$$

Combining eq. (2.7) and eq. (2.1) into eq. (2.2), the Navier equations (formulation in terms of displacements) are obtained, moreover, they can be also used into Equation (2.5) to express the traction boundary conditions in terms of displacement gradients as well, hence the problem defined by eqs. (2.1) to (2.5) becomes

$$(c_{ijkl}u_{k,l})_{,j} + \rho b_i = 0 \qquad \text{in } \Omega\,, \tag{2.9}$$

$$u = \bar{u} \qquad \text{on } \partial\Omega_1\,, \tag{2.10}$$

$$(c_{ijkl}u_{k,l})n_j = \bar{t_i} \qquad \text{on } \partial\Omega_2\,. \tag{2.11}$$

This problem belongs in the category of linear-elliptic boundary-value (mixed boundary conditions) problems, made up by systems of partial differential equations. Solution existence and uniqueness are not guaranteed. We shall, nevertheless, from this point forward, assume that any condition that existence and uniqueness necessitate are granted.

Finally, if the material is homogeneous and isotropic, then the tensor of elastic constants must be of the form

$$c_{ijkl} = \lambda\,\delta_{ij}\delta_{kl} + \mu\,(\delta_{ik}\delta_{jl} + \delta_{il}\delta_{jk})\,, \tag{2.12}$$

where δ_{ij} represents the Kronecker delta tensor and λ, μ (shear modulus) are the "Lamé constants" of the isotropic material. It suffices to set $\lambda(\boldsymbol{x})$ and $\mu(\boldsymbol{x})$ in order to consider a material that is isotropic yet heterogeneous.
Using eq. (2.12) in eq. (2.6b) becomes

$$W = \mu\,\varepsilon_{ij}\varepsilon_{ij} + \frac{1}{2}\lambda\,(\varepsilon_{kk})^2\,, \tag{2.13}$$

whereas eq. (2.6b)

$$\sigma_{ij} = 2\mu\varepsilon_{ij} + \lambda\varepsilon_{kk}\delta_{ij} = \mu\,(u_{i,j} + u_{j,i}) + \lambda u_{k,k}\,, \tag{2.14}$$

and eqs. (2.9) to (2.11)

$$\mu\,u_{i,jj} + (\mu + \lambda)\,u_{j,ij} + \rho b_i = 0 \qquad \text{in } \Omega\,, \tag{2.15}$$

$$u = \bar{u} \qquad \text{on } \partial\Omega_1\,, \tag{2.16}$$

$$\left[\mu\,(u_{i,j} + u_{j,i}) + \lambda u_{k,k}\delta_{ij}\right] n_j = \bar{t_i} \qquad \text{on } \partial\Omega_2\,. \tag{2.17}$$

2.2.1 Stress concentration at corners: Williams Solution

It is well-known that the linear elastostatic stress field, and the linear elastodynamic one too [Fre98], around a crack tip is singular, and the singularity scales as the inverse of the square-root of the distance from the crack-tip.

The foregoing does not preclude other configurations from presenting different singular stress fields; actually, any configuration with sharp-edge intersections (a corner or a notch) will present a stress singularity at the intersection, albeit its scaling will not be "as singular as" the one of the crack tip.

The linear-elastic stress concentration at notch tips was settled by Williams [Wil52] (himself a Galcit graduate).

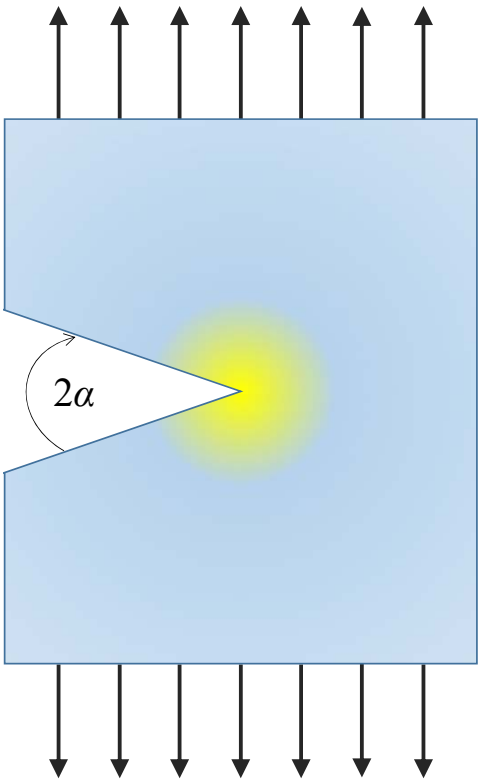

Figure 2.2: Notch scheme

The preeminent outcome of his study was ascertaining the existence of singular values of stresses, compatible with finite strain energy, at notch tips. The acuter the notch, the more singular the stress field; in the limit corresponding to the notch folding over itself, an idealized crack, the most-singular field is attained and it scales inversely to the square-root of the distance from the crack tip.

We will consider a configuration with rectangular corners in both section 4.4 and Chapter 6, that is, configurations corresponding to $\alpha = \pi/4$ (see fig. 2.2), hence $\sigma_{ij} \sim r^{-0.495}$, where r represents distance from the tip of the corner. When it comes to consider contour integrals around these domains, the customary approach is to add a circumferential contour enclosing the singularity (so that no elastic singularities are enclosed in the domain). In such scenario, it is easy to realize that the contribution of this piece of contour to both the stress integral (the thrust) and to the integral of the energy-momentum tensor (proportional to the square of the stresses, to be formally presented in section 2.5.1.1) vanishes as the radius of the circumference tends to zero. The latter is due to the perimeter contour tending to zero as $\sim r$ when $r \to 0$ whereas the integrand scales, in this case, no faster than $\sim (r^{-0.495})^2$ as $r \to 0$; thus, in the limit, the whole integral goes as $r^{1-2\cdot 0.495} \to 0$ (although very slowly) since the exponent is still positive (note that the same happens for any notch except when $\alpha = 0$, that is, the crack is recovered and the contribution of the integral of the energy momentum tensor over the infinitesimal contour is finite [Ric68]).

Acoording to Luco [LW72], a similar result abscribed to the problem of settlements of rigid foundations was derived by Muskhelishvili [Mus13] and by Abramov [Abr37] independently.

2.3 Elastodynamics

Let us lift the restriction on negligible inertial forces. Time, t, enters the formulation explicitly as an independent variable. Hence, now we seek displacements $\boldsymbol{u} = u_i(\boldsymbol{x}, t)$, strains $\boldsymbol{\varepsilon} = \varepsilon_{ij}(\boldsymbol{x}, t)$ and stresses $\boldsymbol{\sigma} = \sigma_{ij}(\boldsymbol{x}, t)$ satisfying the field equations and boundary conditions governing the evolution of the system:

$$\varepsilon_{ij} = \frac{1}{2}\left(\frac{\partial u_i}{\partial x_j} + \frac{\partial u_j}{\partial x_i}\right) = u_{(i,j)} \qquad \text{in } \Omega\,, \tag{2.18}$$

$$\sigma_{ij,j} + \rho b_i = \rho \ddot{u}_i \qquad \text{in } \Omega\,, \tag{2.19}$$

$$\sigma_{ij} = \frac{\partial W}{\partial u_{i,j}} \qquad \text{in } \Omega\,, \tag{2.20}$$

$$u = \bar{u} \qquad \text{on } \partial\Omega_1\,, \tag{2.21}$$

$$\sigma_{ij} n_j = \bar{t}_i \qquad \text{on } \partial\Omega_2\,. \tag{2.22}$$

Initial conditions are necessary in order to complement the dynamic picture. For the purpose of this text, assume evolution starting from quiescent conditions at $t = 0$, hence $\boldsymbol{u}(\boldsymbol{x}, t = 0) = \boldsymbol{0}$, and $\dot{\boldsymbol{u}}(\boldsymbol{x}, t = 0) = \boldsymbol{0}$.

Following the same the chain of assumptions that lead us to the (quasi-)static definition of the elastic problem in terms of displacements, eqs. (2.9) to (2.11), we can reach their dynamic analogue:

$$\mu\, u_{i,jj} + (\mu + \lambda)\, u_{j,ij} + \rho b_i = \rho \ddot{u}_i \qquad \text{in } \Omega\,, \tag{2.23}$$

$$u = \bar{u} \qquad \text{on } \partial\omega_s\,, \tag{2.24}$$

$$\left[\mu\,(u_{i,j} + u_{j,i}) + \lambda u_{k,k}\delta_{ij}\right] n_j = \bar{t}_i \qquad \text{on } \partial\Omega_2\,. \tag{2.25}$$

Basically, the only difference is that inertial forces have to be added to eq. (2.15) so that the equilibrium in the bulk of the body is achieved among internal forces, external body forces, and the supplementary action of inertial forces, eq. (2.23).

At this point, let us introduce the Cartesian frame of reference that has been implicit so far. This, the position vector comes defined as $\boldsymbol{x} = [\, x,\, y,\, z\,]^\top$, and eq. (2.23) can be expanded into

$$\mu\left(\frac{\partial^2 u}{\partial x^2} + \frac{\partial^2 u}{\partial y^2} + \frac{\partial^2 u}{\partial z^2}\right) + (\lambda+\mu)\frac{\partial}{\partial x}\left(\frac{\partial u}{\partial x} + \frac{\partial v}{\partial y} + \frac{\partial w}{\partial z}\right) + \rho b_x = \rho\frac{\partial^2 u}{\partial t^2}\,, \tag{2.26a}$$

$$\mu\left(\frac{\partial^2 v}{\partial x^2} + \frac{\partial^2 v}{\partial y^2} + \frac{\partial^2 v}{\partial z^2}\right) + (\lambda+\mu)\frac{\partial}{\partial y}\left(\frac{\partial u}{\partial x} + \frac{\partial v}{\partial y} + \frac{\partial w}{\partial z}\right) + \rho b_y = \rho\frac{\partial^2 v}{\partial t^2}\,, \tag{2.26b}$$

$$\mu\left(\frac{\partial^2 w}{\partial x^2} + \frac{\partial^2 w}{\partial y^2} + \frac{\partial^2 w}{\partial z^2}\right) + (\lambda+\mu)\frac{\partial}{\partial z}\left(\frac{\partial u}{\partial x} + \frac{\partial v}{\partial y} + \frac{\partial w}{\partial z}\right) + \rho b_z = \rho\frac{\partial^2 w}{\partial t^2}\,. \tag{2.26c}$$

Note that we do not have an elliptic problem anymore, so now the problem belongs to the linear-hyperbolic class.

2.3.1 Plane-strain elastodynamics

The plane-strain idealization consists of conceptualizing the body as infinite along a certain spatial direction, and accepting that no disturbances of any kind (e.g., body forces, material changes) take place as that spatial coordinate is traversed (at least not during sufficiently long stretches). Another way of conceptualizing this scenario is by stating that at any point on the axis running along such coordinate one can define a plane of mechanical symmetry (geometrical, material, and load symmetry). Then focusing on a representative plane perpendicular to such axis would be enough as to define the response of the system. This idealization can be used to describe the response of an intermediate cross-section of a very slender body, despite the aforesaid symmetry conditions not being fulfilled due to the presence of three-dimensional effects at the edges of the body.

Let us assume that $z = 0$ represents such symmetry plane, and that there are no forces whatsoever nor gradients of any kind along its normal direction. Under these suppositions, it follows that $u_{,z} = v_{,z} = w_{,z} = 0$ and $w = 0$ itself at this representative section (recall that $\sigma_{33} = \lambda\,(u_{,x}+v_{,y}) \neq 0$ necessarily), eq. (2.26c) is trivially satisfied and eq. (2.26a) simplify into

$$(\lambda + 2\mu)\frac{\partial^2 u}{\partial x^2} + (\lambda + \mu)\frac{\partial^2 v}{\partial x \partial y} + \mu\frac{\partial^2 u}{\partial y^2} + \rho b_x = \rho\frac{\partial^2 u}{\partial t^2}\,, \tag{2.27a}$$

$$(\lambda + 2\mu)\frac{\partial^2 v}{\partial y^2} + (\lambda + \mu)\frac{\partial^2 u}{\partial x \partial y} + \mu\frac{\partial^2 v}{\partial x^2} + \rho b_y = \rho\frac{\partial^2 v}{\partial t^2}\,. \tag{2.27b}$$

2.4 Variational formulation of Continuum Mechanics

In some systems, it is acknowledged that the observed states coincide with those that extremize a certain functional defined over the variables describing the system. For such systems, it is said that its evolution is governed by an *extremum principle*. Moreover, in even more general terms, for some systems the observed state are identified as stationary points of a certain functional, this it is said that the system abides by a *stationarity principle*. See that extrema are stationary points, and stationary points that are not extrema are referred to as *saddle points*.

Consider a functional $\Phi : X \to \mathbb{R}$ of the form

$$\Phi[\boldsymbol{u}] = \int_\Omega \mathcal{W}(\boldsymbol{x}, \boldsymbol{u}, \nabla\boldsymbol{u})\, dV + \int_{\partial\Omega_2} \mathcal{F}(\boldsymbol{x}, \boldsymbol{u})\, dS\,, \tag{2.28}$$

where X is an affine space referred to as the space of *admissible solutions*. Consider V to be the translational space of X, which is itself a linear space, and is referred to as the space of *admissible variations*. For our purposes, both X and V are finite-dimensional spaces. The *first variation* of Φ at a point $\boldsymbol{u} \in X$ in the direction of $\mathfrak{u} \in V$ is

$$\langle D\,\Phi[\boldsymbol{u}], \mathfrak{u}\rangle = \left[\frac{d}{d\epsilon}\Phi(u + \epsilon\mathfrak{u})\right]_{\epsilon=0^+}\,, \tag{2.29a}$$

since the working spaces are finite dimensional

$$= \frac{\partial\Phi}{\partial x_i}(\boldsymbol{x})\mathfrak{u}_i \tag{2.29b}$$

hence using eq. (2.28) and integration by parts

$$= \int_\Omega \left(\frac{\partial\mathcal{W}}{\partial u_i} - \frac{\partial}{\partial x_j}\frac{\partial\mathcal{W}}{\partial u_{i,j}}\right)\mathfrak{u}_i\, dV + \int_{\partial\Omega_2}\left(\frac{\partial\mathcal{F}}{\partial u_i} + \frac{\partial\mathcal{W}}{\partial u_{i,j}}n_j\right)\mathfrak{u}_i\, dS\,. \tag{2.29c}$$

A point $\boldsymbol{u} \in X$ is said to be a *stationary point* of Φ in X when

$$\langle D\,\Phi[\boldsymbol{u}], \mathfrak{u}\rangle = 0\,, \qquad \forall\, \mathfrak{u} \in V\,. \tag{2.30}$$

Thus, for eq. (2.30) to be verified in eq. (2.29c) both integrands must vanish for any value of the admissible variation. This condition yields the so-called *Euler equations* of Φ:

$$\frac{\partial \mathcal{W}}{\partial u_i} - \frac{\partial}{\partial x_j}\frac{\partial \mathcal{W}}{\partial u_{i,j}} = 0 \qquad \text{in } \Omega, \tag{2.31a}$$

$$\frac{\partial \mathcal{F}}{\partial u_i} + \frac{\partial \mathcal{W}}{\partial u_{i,j}} n_j = 0 \qquad \text{on } \partial\Omega_2. \tag{2.31b}$$

Satisfying these equations is a necessary condition for stationarity. Note that the definition of the equations themselves is contingent upon the capacity of defining some derivatives properly.

By this as it may, the next step is realizing that the problem defined by eqs. (2.1) to (2.5) is but the Euler equations corresponding to the stationaity condition of the celebrated *Hu-Washizu functional*:

$$\begin{aligned}\Phi[\boldsymbol{u}, \boldsymbol{\varepsilon}, \boldsymbol{\sigma}] = &\int_\Omega \left[W(\boldsymbol{\varepsilon}) + \sigma_{ij}(u_{(i,j)} - \varepsilon_{ij}) - \rho b_i u_i\right]\, dV \\ &- \int_{\partial\omega_s} \sigma_{ij} n_j (u_i - \bar{u}_i)\, dS - \int_{\partial\Omega_2} \bar{t}_i u_i\, dS\,,\end{aligned} \tag{2.32}$$

in this case $\mathcal{W} = W(\boldsymbol{\varepsilon}) + \sigma_{ij}(u_{(i,j)} - \varepsilon_{ij}) - \rho b_i u_i$ and $\mathcal{F} = -(\sigma_{ij} n_j (u_i - \bar{u}_i) + \bar{t}_i u_i)$.

Therefore, solving the problem posed by eqs. (2.1) to (2.5) amounts to finding stationay points of the function in eq. (2.32). Assuming the functional satisfies convexity requirements, stationarity requires the functional to be minimized with respect to the strain field, maximimized with respect to the stress field and finally minimized with respect to the displacement field:

$$\text{Stationarity} \iff \min_{\boldsymbol{u}} \min_{\boldsymbol{\sigma}} \min_{\boldsymbol{\varepsilon}} \Phi[\boldsymbol{u}, \boldsymbol{\varepsilon}, \boldsymbol{\sigma}]\,. \tag{2.33}$$

One can obtain a reduced variational principle, the so-called *Hellinger-Reissner Principle*, by minimizing eq. (2.32) with respect to the strain field, that is, enforcing eq. (2.3) a priori.

A further-reduced principle is the *Principle of Minimum Potential Energy*, obtained from maximizing Hellinger-Reissner's with respecto to the stress field, what amounts

to satisfying eq. (2.1) and eq. (2.4) a priori. The corresponding functional is

$$\Phi[\boldsymbol{u}] = \int_\Omega \left[W\left(u_{(i,j)}\right) - \rho b_i u_i \right] \, dV - \int_{\partial\Omega_2} \bar{t}_i u_i \, dS \,,$$

and the Euler equations are simply eqs. (2.2) and (2.5). A displacement field satisfying these equations solves the problem, but, more generally, one can also express the solution of the problem, call it $\boldsymbol{u}^*$, directly from the variational priciple, eq. (2.34), as

$$\boldsymbol{u}^* = \arg\min \left\{ \Phi[\boldsymbol{u}] \, : \, \boldsymbol{u} = \bar{\boldsymbol{u}} \text{ on } \partial\Omega_2 \right\} \,. \tag{2.34}$$

The bevy of assumptions that were leveled in section 2.2 (isotropy, heterogeneity, linearity...) have a direct translation into the specific actual architecture of Φ. In any case, see that the formulation holds.

The variational approach can also be extended to the dynamic setting, by means of the action functional

$$\mathscr{A}[\boldsymbol{u}] = \int_{t_1}^{t_2} \left(T[\boldsymbol{u}] - \Phi[\boldsymbol{u}] \right) \, dt, \tag{2.35}$$

where T is the potential energy functional:

$$T[\boldsymbol{u}] = \int_\Omega \frac{\rho}{2} |\dot{\boldsymbol{u}}|^2 dV \,. \tag{2.36}$$

The *Action Principle* states that the solution $\boldsymbol{u}^*(\boldsymbol{x}, t)$ renders the action functional stationary.

Dynamic problem, as those mentioned in section 2.3, require of the Action Principle to be analyzed. However, we will not appeal to it, as there are strategies that, under some circumstances, will allow to fit the dynamic problem within the Principle of Minimum Potential Energy, eq. (2.34). These will prove more convenient for our purposes, since allow for definition of dynamic path-independent integrals without resorting to time convolutions, as we shall describe in section 2.5. Two possible manners of removing time from the equations is by either invoking Laplace's transform, or by assuming the steady-state being in effect and working with amplitudes. For the latter, simply decompose $u_i(\boldsymbol{x}, t) = \hat{u}_i(\boldsymbol{x}) e^{\mathrm{i}\varpi t}$ For example, eq. (2.23) would yield

$$\frac{\partial \hat{\sigma}_{ij}}{\partial x_j} + \rho(\hat{b}_i + \varpi^2 \hat{u}_i) = 0 \,, \tag{2.37}$$

where In conclusion, the dynamic problem can be recast as a static problem in which there exists a body force vector proportional to the amplitude of the displacements.

Conversely, the same problem can be also expressed in the so-called variational form. To do so, the potential energy of the body is redefined as

$$\Phi[\hat{\boldsymbol{u}}, \nabla \boldsymbol{u}] = \int_B \left[\hat{W}(\nabla \boldsymbol{u}) - \rho \left(\hat{b}_i + \frac{\varpi^2}{2} \hat{u}_i \right) \hat{u}_i \right] dV - \int_{\partial B_2} \hat{t}_i \hat{u}_i dS \,, \tag{2.38}$$

where $\partial W / \partial \hat{u}_{i,j} = \hat{\sigma}_{ij}$. The stationary condition for this functional corresponds to eq. (2.37); in other words, that equation is the Euler-Lagrange equation of the system.

2.5 Path-independent integrals and configurational forces

The existence of path-independent integrals, alternatively referred to as conservation laws, was spelled out by Knowles and Sternberg [KS72] for elastostatics, crystallizing previous work of other scholars [Ric68; Che67; San59], and by Fletcher [Fle76], a student of Knowles, for elastodynamics. We will review the classic formulation, quasi-static in the absence of body forces [Ric85], first, and then will move to the dynamic realm.

2.5.1 Quasi-static, no body forces

As explained by Knowles and Sternberg [KS72], there are *up to* three path-independent integrals in infinitesimal elastostatics: the vector J and L integral, and the scalar M integral. These represent a total of seven conservation laws in the three-dimensional framework, four in the two-dimensional.

2.5.1.1 The energy-momentum tensor

The introduction of the *Eshelby's energy momentum tensor*, $\boldsymbol{E} = E_{ij}$, allows for a common treatment of all of these integrals. In the absence of inertia and body forces, the tensor is defined as [1]

$$E_{ij} = W \delta_{ij} - u_{k,i} \sigma_{kj} \,. \tag{2.39}$$

If, moreover, we presuppose a linear constitutive law, as in eq. (2.6a), the entries of the tensor can be expressed as

$$E_{xx} = \frac{1}{2} \Big[- \sigma_{xx} \frac{\partial u}{\partial x} + \sigma_{yy} \frac{\partial v}{\partial y} + \sigma_{zz} \frac{\partial w}{\partial z} + \tau_{xy} \left(\frac{\partial u}{\partial y} - \frac{\partial v}{\partial x} \right) + \tau_{xz} \left(\frac{\partial u}{\partial z} - \frac{\partial w}{\partial x} \right)$$

[1] Beware that other scholars [Mau16] define this tensors differently, as in the end they compensate the change by tweaking the surface normal accordingly. This innocent difference has caused more than one scare to this student.

$$+ \tau_{yz}\left(\frac{\partial v}{\partial z} + \frac{\partial w}{\partial y}\right)\Big], \tag{2.40a}$$

$$E_{xy} = -\left(\tau_{xy}\frac{\partial u}{\partial x} + \sigma_{yy}\frac{\partial v}{\partial x} + \tau_{zy}\frac{\partial w}{\partial x}\right), \tag{2.40b}$$

$$E_{xz} = -\left(\tau_{xz}\frac{\partial u}{\partial x} + \tau_{yz}\frac{\partial v}{\partial x} + \sigma_{zz}\frac{\partial w}{\partial x}\right), \tag{2.40c}$$

$$E_{yy} = \frac{1}{2}\Big[\sigma_{xx}\frac{\partial u}{\partial x} - \sigma_{yy}\frac{\partial v}{\partial y} + \sigma_{zz}\frac{\partial w}{\partial z} + \tau_{xy}\left(\frac{\partial v}{\partial x} - \frac{\partial u}{\partial y}\right) + \tau_{xz}\left(\frac{\partial u}{\partial z} + \frac{\partial w}{\partial x}\right) + \tau_{yz}\left(\frac{\partial w}{\partial z} - \frac{\partial w}{\partial y}\right)\Big], \tag{2.40d}$$

$$E_{yx} = -\left(\sigma_{xx}\frac{\partial u}{\partial y} + \tau_{yx}\frac{\partial v}{\partial y} + \tau_{zx}\frac{\partial w}{\partial y}\right), \tag{2.40e}$$

$$E_{yz} = -\left(\tau_{xz}\frac{\partial u}{\partial y} + \tau_{yz}\frac{\partial v}{\partial y} + \sigma_{zz}\frac{\partial w}{\partial y}\right), \tag{2.40f}$$

$$E_{zz} = \frac{1}{2}\Big[\sigma_{xx}\frac{\partial u}{\partial x} + \sigma_{yy}\frac{\partial v}{\partial y} - \sigma_{zz}\frac{\partial w}{\partial z} + \tau_{xy}\left(\frac{\partial u}{\partial y} + \frac{\partial v}{\partial x}\right) + \tau_{xz}\left(\frac{\partial w}{\partial x} - \frac{\partial u}{\partial z}\right) + \tau_{yz}\left(\frac{\partial w}{\partial y} - \frac{\partial v}{\partial z}\right)\Big], \tag{2.40g}$$

$$E_{zx} = -\left(\sigma_{xx}\frac{\partial u}{\partial z} + \tau_{yx}\frac{\partial v}{\partial z} + \tau_{zx}\frac{\partial w}{\partial z}\right), \tag{2.40h}$$

$$E_{zy} = -\left(\tau_{xy}\frac{\partial u}{\partial z} + \tau_{zy}\frac{\partial w}{\partial z} + \sigma_{yy}\frac{\partial v}{\partial z}\right). \tag{2.40i}$$

This tensor is not symmetric .

2.5.2 Invariance with respect to coordinate translation: the J-integral

The presence of some sort of "inclusion" within the otherwise homogeneous solid elicits *configurational forces*, that is, energetic forces conjugated to the dissipation induced by the presence of the inclusion either on the contour or within the bulk of the domain.

The energy-momentum tensor is instrumental when it comes to consider configurational forces, as it allows to relate total configurational force within a subbody to their flux through the boundary of the subbody. The total configurational force acting on a subbody $\widehat{\Omega} \subset \Omega$ along the i-th direction is referred to as $\mathrm{J}_i(\widehat{\Omega})$ and it is equal to

$$\mathbf{J}(\widehat{\Omega}) = \int_{\widehat{\Omega}} \nabla \cdot \boldsymbol{E}\, dV = \int_{\partial\widehat{\Omega}} \boldsymbol{E}\boldsymbol{n}\, dS\,. \tag{2.41}$$

Note that, in the absence of heterogeneities or singularities inside $\widehat{\Omega}$,

$$\mathrm{J}_i(\widehat{\Omega}) = 0\,. \tag{2.42}$$

A couple of observations:

1) The definition of this path-independent integral only requires the existence of a stress potential (the strain energy density) as in eq. (2.3). Nevertheless, it is necessary condition for eq. (2.42) that the potential depends on $\boldsymbol{\varepsilon}$ through its invariants [KS72], what amounts to guarantee stresses being invariant under rigid body movement (translation plus rotation).

2) It does not behoove the material to be linear, as in eq. (2.6a), nor isotropic eq. (2.6b) for eq. (2.42) to hold.

Alternatively, eq. (2.42) can be also expressed, with no appeal to the energy-momentum tensor, in a more suggestive manner which allows to judge the influence of applied tractions more easily

$$\mathrm{J}_i = \int_{\partial\widehat{\Omega}} (W\, n_i - t_k u_{k,i})\, dS = 0\,. \tag{2.43}$$

2.5.3 Invariance with respect to coordinate rotations: the L-integral

Likewise, one may consider configurational torques. The total configurational torque acting on the subbody is

$$\mathbf{L}(\widehat{\Omega}) = \int_{\widehat{\Omega}} \boldsymbol{x} \times (\nabla \cdot \boldsymbol{E})\, dV\,, \tag{2.44a}$$

and assuming, in addition, isotropic material

$$\mathbf{L}(\widehat{\Omega}) = \int_{\partial\widehat{\Omega}} \boldsymbol{x} \times (\boldsymbol{E}\boldsymbol{n})\, dS = 0\,, \tag{2.44b}$$

if there are no singularities within the body. The latter can also be expressed as

$$\mathrm{L}_i = \int_{\partial\widehat{\Omega}} \epsilon_{kji} \left(W x_k n_j - t_p u_{p,j} x_k + t_j u_k\right)\, dS = 0\,. \tag{2.44c}$$

In conclusion, to attain these conservation laws, one has to accept the restrictions that yielded eq. (2.42) *plus* isotropic material response additionally.

2.5.4 Invariance with respect to scale changes: the M-integral

Consider a particular case of a self-similar expansion about the origin. Considering the configurational pressures associated with this scenario:

$$\mathrm{M}(\widehat{\Omega}) = \int_{\widehat{\Omega}} \boldsymbol{x} \cdot (\nabla \cdot \boldsymbol{E})\, dV\,, \tag{2.45a}$$

and assuming, in addition, linear material, as in eq. (2.6b),

$$\mathrm{M}(\widehat{\Omega}) = \int_{\partial\widehat{\Omega}} \boldsymbol{x} \cdot (\boldsymbol{E}\boldsymbol{n})\, dS = 0\,, \tag{2.45b}$$

if there are no singularities within the body. The latter can also be expressed as

$$\mathrm{M} = \int_{\partial\widehat{\Omega}} \left(W x_i n_i - t_j u_{j,i} x_i - \frac{t_i u_i}{2} \right) dS = 0\,. \tag{2.45c}$$

In conclusion, to attain this new conservation law, one has to accept (in linearized kinematics) the restrictions that yielded eq. (2.42) plus linear (not necessarily isotropic) material response additionally.

2.5.5 Dynamic, no body forces

As mentioned in the introduction, a number of ways of using these path-independent integrals have been proposed for the last 40 years. We shall favor the customary approach utilized in analysis of crack tips of specimens subjected to harmonic loading, in which case one can work with the amplitudes of the harmonics rather than with functions that depend on time.

Note that the M-integral is absent from the analysis. As explained by Fletcher [Fle76], this integral requires a cumbersome treatment in time domain, as it includes terms that scale linearly with time. For this reason, and following common practice, this integral is disregarded in the steady-state dynamic setting.

Derivations of some results that follow, those that the author could not find in the literature, can be found in Appendix A.

2.5.5.1 Steady-state harmonic, total displacement

Let us begin by re-stating the decomposition $\sigma_{ij} = \hat{\sigma}_{ij} e^{\mathrm{i}\varpi t}$ and $u_i = \hat{u}_i e^{\mathrm{i}\varpi t}$, and recall that the amplitudes are complex number whose phase represent the phase lag of the variable with respect to $e^{\mathrm{i}\varpi t}$. In the absence of body forces, eq. (2.37) turns into

$$\hat{\sigma}_{ij,j} + \rho\varpi^2 \hat{u}_i = 0\,, \tag{2.46}$$

if now we define properly an *equivalent* strain-energy density as the potential meeting the relation

$$\hat{\sigma}_{ij} = \frac{\partial \hat{W}}{\partial \hat{u}_{i,j}}\,, \tag{2.47}$$

and the *equivalent* kinetic energy as,

$$\hat{T} = \frac{1}{2}\varpi^2 \hat{u}_i \hat{u}_i \,, \tag{2.48}$$

notice that in order to render this quantity coherent with the classic definition, one should include a minus sign. See next how eq. (2.46) represents the Euler-Lagrange equations corresponding to the functional eq. (2.38), that can be written in this case as

$$\Phi[\hat{\boldsymbol{u}}, \nabla\hat{\boldsymbol{u}}] = \int_\Omega \left[\hat{W}\left(\nabla\hat{\boldsymbol{u}}\right) - \hat{T}\left(\hat{\boldsymbol{u}}\right)\right] \, dV - \int_{\partial\Omega_2} \bar{\hat{t}}_i \hat{u}_i \, dS \,,$$

Using the same formalism as used for quasi-statics, we ca define a dynamic J-integral $\hat{\mathrm{J}}_i$ and dynamic L-integral $\hat{\mathrm{L}}_i$ as

$$\hat{\mathrm{J}}_i = \int_{\partial\Omega} \left[(\hat{W} - \hat{T})n_i - \hat{t}_j \hat{u}_{j,i}\right] \, dS = 0 \,, \tag{2.49}$$

$$\hat{\mathrm{L}}_i = \int_{\partial\widehat{\Omega}} \epsilon_{kji} \left[(\hat{W} - \hat{T})x_k n_j - \hat{t}_p \hat{u}_{p,j} x_k + \hat{t}_j \hat{u}_k\right] \, dS = 0 \,. \tag{2.50}$$

For eq. (2.50) to hold, it is required the material being isotropic.

2.5.5.2 Steady-state harmonic, relative displacement

For our purposes, oftentimes it will be useful to introduce a change of variables to consider time-varying imposed boundary conditions. Such change of variable consists of expressing the displacement field as relative displacements with respect to an uniform displacement field that also oscillates harmonically in time.
In other words, we shall consider the substitution $\hat{u}_i \longrightarrow \hat{u}_i + X_i$ in the previous conservation laws. Note that, by our very own choice, these X_i do not depend on the spatial variables. We grant this may not be the most general case that one can consider, but it is the very one we need for subsequent work. See that, since X_i does not change in space, new terms do not appear along gradients of displacements, but wherever straight amplitudes are relevant, that is, in the kinetic energy. In the same fashion as X_i was introduced, we may also use $\ddot{X}_i = -\varpi^2 X_i$, where, recall, ϖ is the frequency of the harmonic under consideration.

Then, these steady-state dynamic J and L integrals are expressed in terms of relative displacements as

$$\hat{\mathrm{J}}_i = \int_{\partial\Omega} \left[\left(\hat{W} - \hat{T} + \rho\ddot{X}_l \hat{u}_l\right) n_i - \hat{t}_j \hat{u}_{i,j}\right] \, dS = 0 \,, \tag{2.51}$$

$$\hat{\mathrm{L}}_i = \int_{\partial\widehat{\Omega}} \epsilon_{kji} \left[\left(\hat{W} - \hat{T} + \rho\ddot{X}_l \hat{u}_l\right) x_k n_j - \hat{t}_p \hat{u}_{p,j} x_k + \hat{t}_j (\hat{u}_k + X_k)\right] dS = 0 \,, \tag{2.52}$$

now $\hat{u}$ has to be understood as the amplitude of the relative displacement.

2.5.5.3 Quasi-static approximation enabled by relative displacement

Finally, the quasi-static peers can also be formally obtained from eqs. (2.49) and (2.50), by assuming an expansion of the variables in terms of a small parameter [BO13] that can represent either the quotient between the frequency of the harmonic load over a characteristic frequency or the ratio between a characteristic geometric length in the problem over the wavelength of the wave in the domain. The leading order term of such expansion is understood as the imposed displacement at the border that was introduced in the previous section. First, eq. (2.49) yields

$$\hat{\mathrm{J}}_i = \int_{\partial\Omega} \left[\left(\hat{W} + \rho \ddot{\hat{X}}_l \hat{u}_l \right) n_i - \hat{t}_j \hat{u}_{i,j} \right] \, dS = 0 \,, \tag{2.53}$$

while in eq. (2.50),

$$\hat{\mathrm{L}}_i = \int_{\partial\widehat{\Omega}} \epsilon_{kji} \left[\left(\hat{W} + \rho \ddot{\hat{X}}_l \hat{u}_l \right) x_k n_j - \hat{t}_p \hat{u}_{p,j} x_k + \hat{t}_j (\hat{u}_k + X_k) \right] dS = 0 \,. \tag{2.54}$$

When deciding if using or not these low-frequency approximations, one must bear in mind that they entail errors that scale quadratically with frequency. See Appendix A for further details.

2.5.6 Equivalent contour integrals for Plane Strain

If the system conforms to the requirements of plane strain, one can rephrase the previous surface integrals as contour integrals, just by parametrizing the contour as a tube whose cross-section is delimited by a section curve Γ. The contribution of the surfaces tapping the tube vanish in plain strain, so that only the flank surfaces remain, but the contour integral along Γ must be zero itself for the contribution of the flanks to vanish and yield the identity equal to zero. Thus, in 2D plane-strain problems, there are four non-trivial path-independent integrals [BR73]:

$$\mathrm{J}_x(\Gamma) = \int_\Gamma (W n_x - t_i u_{i,x}) \, dl = 0 \,, \tag{2.55}$$

$$\mathrm{J}_y(\Gamma) = \int_\Gamma (W n_y - t_i u_{i,y}) \, dl = 0 \,, \tag{2.56}$$

$$\mathrm{L}_z(\Gamma) = \int_\Gamma \epsilon_{3ij} \left(W x_j n_i + t_i u_j - t_k u_{k,i} x_j \right) \, dl = 0 \,, \tag{2.57}$$

$$\mathrm{M}(\Gamma) = \int_\Gamma \left(W x_i n_i - t_j u_{j,i} x_i - \frac{t_i u_i}{2} \right) \, dl = 0 \,, \tag{2.58}$$

where $i, j = x, y$ in this case, and dl represents a differential element of curve arc-length. The conditions for the identities to be in effect are the same as in the 3D case.

Similarly, eqs. (2.49), (2.51) and (2.53) (different flavors of dynamic J-integral) as well as eqs. (2.50), (2.52) and (2.54) (L-integral), can be also re-defined as contour integrals over a contour.

2.6 Far-field Analysis

In this section we review two important results concerning 1D wave propagation. This section serves as skeleton for the new results to be presented in next chapter.

2.6.1 Introduction

The importance of one-dimension wave propagation to the study of Soil-Structure Interaction cannot be overstated. A crucial idea permeating much of SSI theory is relating whatever happens at the interface between soil and structure to the behavior of the soil in the absence of structure. For this very reason, understanding the behavior of the far-field is a prerequisite. The customary first step of the study tends to be analyzing the response of the soil with no structure, what, under assumptions of plane-strain and vertically-propagating waves, becomes a one-dimension wave-propagation problem.
Moreover, in and of itself, 1D Site Response is a problem possessing special interest for the geotechnical earthquake engineering community, with interesting applications in unexpected areas, as for instance, seismic design of gravity dams [Gaz87].

The part of the domain that is referred to as the *far field*, or *free field* corresponds to a region where the presence of the structure does not affect the rest of the domain. Same behavior as in this region would be encountered all over the domain if the symmetry had not been broken by the addition of a discontinuity (the structure).

In static problems, this zone can be defined in an unequivocal fashion, as the solutions are strongly spatially localized. Conversely, defining the same concept when in the dynamic setting becomes more cumbersome, due to the wave-propagation nature of the solutions: as time progresses, the local effects induced by the existence of the structure breaking the system symmetry spread through the soil domain, reaching any point, no matter how far away, if enough time is provided and damping is small enough. Thus, the definition of the far-field is contingent upon the definition of a characteristic time: if considerations on the response were restricted to time

spans of the order of the characteristic time of the loading, the far-field can be conceptualized as the region away from the structure a distance much greater than the wave propagation velocity in the soil times the characteristic time of the load, that is, the distance traveled by a signal emanating at the structure in time spans of the order of the characteristic time of the load. Additionally, should the soil have any internal damping, the amplitude of the waves would diminish after traveling a certain distance, whereas scattering fields already decay by their very own nature.

As mentioned earlier, the far-field problem is always easier to understand, as the absence of the structure reduces the "dimensionality" of the problem by allowing us to disregard spatial change in the direction that conduces to the structure.

Let us put forward the following assumptions:

1) Plane-strain conditions.

2) Linear-elastic isotropic behavior (not necessarily homogeneous).

3) Restrict attention to vertically propagating (no incidence angle) SH-wave along direction $y \equiv z$ (for a matter of convenience this coordinate is redefined to adapt to the classic notation [Kra96]), eliciting horizontal displacements u.

4) The soil domain is limited by a horizontal top free surface.

5) No body forces.

Hence of motion, eq. (2.19), reduces to

$$\frac{\partial}{\partial z}\left(\mu\frac{\partial u}{\partial z}\right) = \rho\frac{\partial^2 u}{\partial t^2}\,. \tag{2.59}$$

If, moreover, the soil is uniform

$$\mu\frac{\partial^2 u}{\partial z^2} = \rho\frac{\partial^2 u}{\partial t^2}\,. \tag{2.60}$$

2.6.2 Uniform soil on elastic bedrock

For further comments regarding this topic, see Prof. Kramer's book [Kra96].

In this first case, a harmonic monochromatic wave propagating inside the rock stratum towards a free-surface at the top of an overlying soil stratum has frequency ϖ, wavenumber k_r, and amplitude A_r, and is partially reflected and a portion is transmitted into the soil, where it keeps the same frequency ϖ, wavenumber

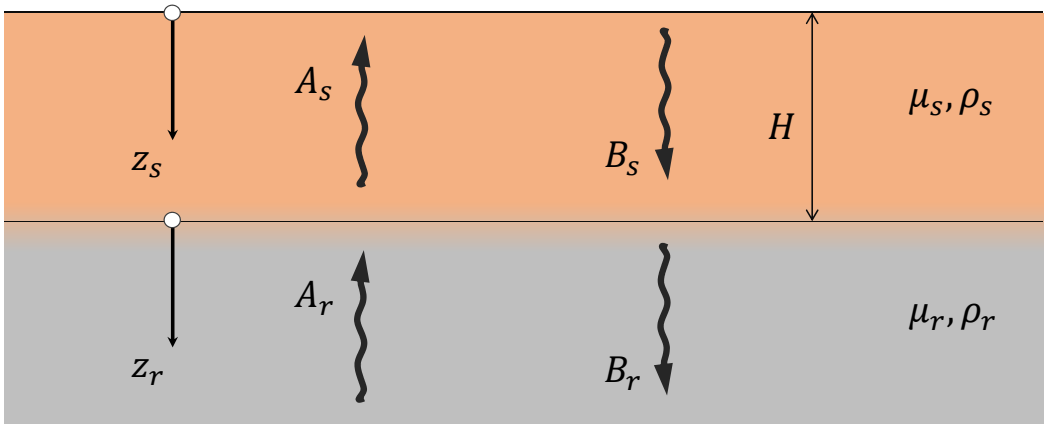

Figure 2.3: Scheme of transient wave propagation in soft soil resting on elastic bedrock

becomes k_s, and amplitude A_s. The propagation phenomenon is described by eq. (2.60) in both layers.

Once this transmitted wave interacts with the free-surface, it will alter its amplitude to B_s, since the superposition of impinging and reflected wave satisfies the boundary condition, wavelength, and frequency remain the same. The wave switches direction after it is reflected at the free-surface, and eventually encounters the bedrock it emanated from. At the interface between the two a portion of energy is transmitted and another portion is reflected, the transmitted part moves into the rock downwards with amplitude B_r, same frequency, and corresponding wavelength λ_r.

The auxiliary coordinates z_s and z_r (see fig. 2.3) help in describing the upward and downward propagation in the strata. With help of these auxiliary coordinates an ansatz conforming to eq. (2.59):

$$u_s = A_s e^{i(\omega t - k_s z_s)} + B_s e^{i(\omega t + k_s z_s)}, \tag{2.61a}$$

$$u_r = A_r e^{i(\omega t - k_r z_r)} + B_r e^{i(\omega t + k_r z_r)}. \tag{2.61b}$$

$A_r = A_{input}$ is the amplitude of the impinging wave and it is assumed to be known. The three other unknowns, B_r, A_s and B_s, are found by enforcement of the following conditions: stress free boundary condition at the free surface

$$\tau_{xz}|_{z_s=0} = 0 \rightarrow \left.\frac{\partial u_s}{\partial z_s}\right|_{z_s=0} = 0 \tag{2.62}$$

plus displacement compatibility and stress compatibility at the interface between

soil and rock

$$\tau_{xz}|_{z_s=H} = \tau_{xy}|_{z_r=0} \rightarrow \mu_s \frac{\partial u_s}{\partial z_s}\Big|_{z_s=H} = \mu_r \frac{\partial u_r}{\partial z_r}\Big|_{z_r=0}, \tag{2.63a}$$

$$u_s(z_s = H) = u_r(z_r = 0)\,. \tag{2.63b}$$

After imposing these boundary conditions one finds

$$A_s = B_s = \frac{A_{input}}{\cosh(k_s H) + i\alpha \sinh(k_s H)}, \tag{2.64a}$$

$$B_r = A_{input}\left(\frac{\cosh(k_s H) - i\alpha \sinh(k_s H)}{\cosh(k_s H) + i\alpha \sinh(k_s H)}\right), \tag{2.64b}$$

$\alpha = \sqrt{\rho_s \mu_s}/\sqrt{\rho_r \mu_r}$ is referred to as the interface impedance ratio; it provides a measure of the amount of energy that is filtered through the interface from one medium (rock) to the other (soil) and back after the wave is reflected at the free-surface. Note the following limit scenarios:

a) $\alpha = 0$ corresponds to the limit case of rock infinitely more either rigid or dense than the soil, in such a case the rock moves independently from the upper soil, the phenomena in the soil not perturbing its response.

b) $\alpha = 1$ corresponds to no impedance contrast at the interface, and thus wave moves in its entirety past the interface as if there was no interface whatsoever.

c) $\alpha \gg 1$ denotes an scenario wherein the soil is much more rigid than the (alleged) rock. The interface works as a rigid interface, no portion of the wave enters the upper stratum and the reflected wave does not amend its amplitude.

A magnitude of great practical interest for earthquake engineers is the amplitude amplification between the impinging wave at some depth with respect to the one at the surface (which is a crucial design parameter for man-made structures located in seismic-prone areas). Once all the amplitudes are quantified any of these relations can be evaluated. In particular, the amplification at the surface level with respect to the amplitude of the *incoming* wave traveling in the rock (A_{input}) is

$$A(\varpi) = \frac{|u_s|}{A_{input}} = \frac{2}{\sqrt{\cos^2(r) + \alpha^2 \sin^2(r)}}, \tag{2.65}$$

where $r = \varpi H/c_s$ represents a dimensionless frequency (very handy when it comes to represent results in a compact form, see that this is also referred to as a_0 oftentimes in the SSI literature). See how this result agrees to the prior discussion: for $\alpha = 0$

a fraction of the energy inputted by the wave is trapped within the soft soil layer, and meaningful dynamic amplification are possible. The latter scenario can be interpreted as the absence of a damping mechanism within the soft soil layer, namely *radiation damping*. The fact that a portion of energy is evacuated from the soil through the interface and towards the rock bulk, and it does not ever return, is effectively felt by the soil as a kind of dissipation (energy loss). This phenomenon is not present if the rock-to-soil impedance is zero.

2.6.3 Layered soil on elastic bedrock

Consider a variation of the fig. 2.3, a succession of layers instead of one homogeneous layer, resting on top of elastic bedrock. Each layer is itself homogeneous, and thus the propagation within it can be described by means of eq. (2.60).

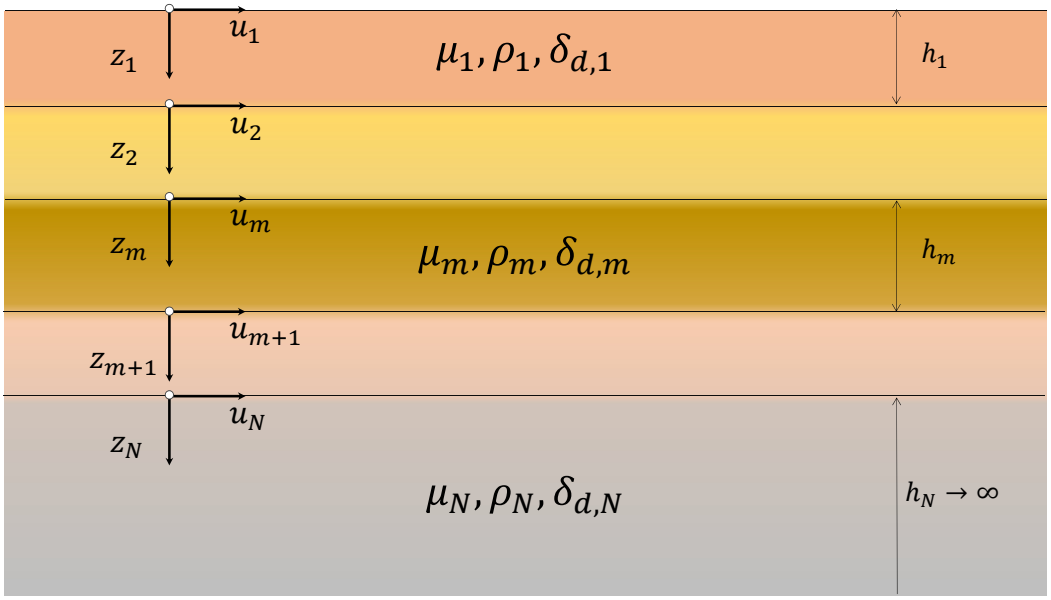

Figure 2.4: Scheme of transient wave propagation in multilayered soft soil ($N-1$ layers) resting on elastic bedrock (N^{th} layer)

Stress and displacements compatibility constraints, as those in eq. (2.63a) and eq. (2.63b), can be leveled at each interface between consecutive layers. Likewise, ansatze as in eqs. (2.61a) and (2.61b) can be used to yield the following inter-layer relations:

$$A_{m+1} = \frac{A_m}{2}(1+\alpha)e^{ik_m h_m} + \frac{B_m}{2}(1-\alpha_m)e^{-ik_m h_m}, \tag{2.66a}$$

$$B_{m+1} = \frac{A_m}{2}(1-\alpha_m)e^{ik_m h_m} + \frac{B_m}{2}(1+\alpha)e^{-ik_m h_m}, \tag{2.66b}$$

$k_m = (\varpi/\sqrt{\mu_m/\rho_m})^{-1}$ for $m = 1 \dots N-1$. See how a certain recurrence can be written in matrix form:

$$\boldsymbol{A}_{m+1} = \begin{bmatrix} A_{m+1} \\ B_{m+1} \end{bmatrix} = \frac{1}{2} \begin{bmatrix} (1+\alpha_m)e^{ik_m h_m} & (1-\alpha_m)e^{-ik_m h_m} \\ (1-\alpha_m)e^{ik_m h_m} & (1+\alpha_m)e^{-ik_m h_m} \end{bmatrix} \begin{bmatrix} A_m \\ B_m \end{bmatrix} = \boldsymbol{L}_m \boldsymbol{A}_m \,, \quad (2.67)$$

and thus it follows that

$$\boldsymbol{A}_{m+1} = \boldsymbol{L}_m \boldsymbol{A}_m = \boldsymbol{L}_m(\boldsymbol{L}_{m-1}\boldsymbol{A}_{m-1}) = \dots = \prod_{j=1}^{m} \boldsymbol{L}_j \boldsymbol{A}_1 = \prod_{j=1}^{m} \boldsymbol{L}_j \begin{bmatrix} 1 \\ 1 \end{bmatrix} A_1 \,. \quad (2.68)$$

If we wanted to calculate the wave propagation within the last layer, set $m+1 = N$:

$$\boldsymbol{A}_N = \boldsymbol{L}_{N-1}\boldsymbol{A}_{N-1} = \underbrace{\prod_{j=1}^{N-1} \boldsymbol{L}_j}_{\boldsymbol{L}} \begin{bmatrix} 1 \\ 1 \end{bmatrix} A_1 = \boldsymbol{L} \begin{bmatrix} 1 \\ 1 \end{bmatrix} A_1 = \begin{bmatrix} L_{11} + L_{12} \\ L_{21} + L_{11} \end{bmatrix} A_1 = \begin{bmatrix} A_N \\ B_N \end{bmatrix} . \quad (2.69)$$

This procedure can be seen as an instantiation of the classic method of *propagation matrices* used in Seismology [AR02].

The amplitude at the N^{th} layer must coincide with the amplitude in bedrock, and therefore

$$A_N = A_{input} = (L_{11} + L_{12})A_1 \rightarrow A_1 = \frac{A_{input}}{L_{11} + L_{12}} \,, \quad (2.70)$$

thus, similarly as in eq. (2.65), the amplitude of the displacement at the top of the layer with respect to the amplitude of the *incoming wave* will be given by

$$A = \frac{|u_s(z_s = 0)|}{A_{input}} = \frac{2A_1}{A_{input}} = \frac{2}{L_{11}(\varpi) + L_{12}(\varpi)} \,. \quad (2.71)$$

2.6.3.1 Soft-layers on bedrock

If the last layer was effectively rigid rock, simply take the last impedance equal to zero. Then, calculate $\boldsymbol{A}_N$ as previously, in this case, A_N, B_N must represent the propagation within bedrock, and thus

$$u_N = A_N e^{i(\varpi t + k_r z_r)} + B_N e^{i(\varpi t - k_r z_r)} \quad (2.72)$$

the displacement at the base level corresponds to $z_r = 0$

$$\begin{aligned} u_{base} &= u_N(z_r = 0) = A_N e^{i\varpi t} + B_N e^{i\varpi t} = \\ &= (A_N + B_N)e^{i\varpi t} = (L_{11} + L_{12} + L_{21} + L_{22})A_1 e^{i\varpi t} = A_{input} e^{i\varpi t} \,, \end{aligned} \quad (2.73)$$

and thus we can define the ratio between the *displacement at the top* (at the free surface) and the *displacement at the base of the deposit* (the displacement at the contact between soil and rigid bedrock) as

$$A = \frac{|u_1(z_s = 0)|}{|u_N(z_r = 0)|} = \frac{2A_1}{A_N + B_N} = \frac{2}{L_{11}(\varpi) + L_{12}(\varpi) + L_{21}(\varpi) + L_{22}(\varpi)} \,. \quad (2.74)$$

Note that this parameter is slightly different from eq. (2.65).

Chapter 3

NOVEL RESULTS CONCERNING ONE-DIMENSIONAL SITE RESPONSE ANALYSIS

The following items are pursued in this chapter:

- The connection between the general framework and the one corresponding to rigid bedrock is posited.
- The definition of equivalent homogeneous properties for heterogeneous sites is discussed. The connection to Fermat's Principle, and to other results in Physics, in the high-frequency regime is highlighted.
- An estimate for the amplitude of the first resonant peak in heterogeneous deposits overlying rigid bedrock is proposed in order to complement previous work.

3.1 Introduction

In recent years, it has been well-established that site conditions and soil layering strongly influence ground motions during seismic events [Ben90]. The stiffness gradients in the soil (either discrete or continuous) entail a concentration of seismic energy in the softer layers [Tow96], which usually are those closer to the surface, and in turn translates into higher risk for man-made ground and underground structures.

Consequently, a number of researchers have been occupied with studying the modification of ground seismic response due to the presence of inhomogeneous stratification in the soil by means of simplified one dimensional (1D) wave propagation models under the assumption of linear viscoelastic medium [DWV71; Gaz82; Vre13; Vre90; Zha97; AP02; TG04; SP09]. Most of them have focused on finding steady-state solution in frequency domain, which happens to be the dominant component of the response, except under some specific circumstances (low-frequency fundamental mode, high-frequency excitation) as described by Sarma [Sar94].

Finding the natural frequencies of the inhomogeneous system requires solving transcendental equations (which usullay involves Bessel's functions of different orders) numerically, and therefore no closed-form expression for the natural frequencies of

the inhomogeneous can be attained. Zhao [Zha97] studied the seismic response of both layered soils and soils with continuous variation of stiffness using a slightly different approach based on modal analysis. Relevant observations for this same problem, concerning the definition of an equivalent soil, were posited and verified, yet were not formally anchored in the mathematics of the problem. In spite of representing the exact solutions, these solutions do not lend themselves to easy interpretation, and it attests to this point that prior work by Rovithis et al. [RPM11] investigated a number of potential equivalent homogeneous soils without reaching conclusive results on which one should be used. As a way to partially circumvent this problem, the same authors [MRP13] put forward a new method for estimation of the natural frequencies based on Rayleigh quotient [Wei12], which yield simple closed-form estimates for the first natural frequency, which were proved to perform well although the corresponding modal shape had to be presupposed. In spite of providing a simple expression for the fundamental frequency, information on the higher modes could not be retrieved as easily by means of application of the method since surmising the mode shapes for higher modes is certainly not a prosaic task. Moreover, an estimate of the amplitude at resonance, what amounts to having an appraisal of the effect of inhomogeneity on the amplitude at the fundamental resonance, is still pending.

Excessive complexity that hinders definition of simplified models is a ubiquitous shortcoming present in the body of prior scholarly work. In the own words of Gazetas [Gaz82]:

> *Despite all the progress made, simple analytical solutions have always been in demand since they allow parametric studies to be easily performed and since they can be incorporated in building codes.*

The general procedure presented in section 2.6 contains the particular case of having as large a contrast as to be able of considering the upper layers to be resting upon what may be deemed utterly rigid bedrock: we just have to take the last impedance to zero. However, this particular case, sometimes referred to as soft-soil deposit on rigid bedrock, permits a different treatment of its own, which will come in handy in the next sections where we will add a structure to the picture, but always assuming there is a rigid bedrock at some depths below (in the case that will occupy most of our time, the bedrock will lie directly underneath the structure).

In this chapter a number of new results are presented: from minor discussion addressing some misconceptions (section 3.2), to a wholly-new treatment of 1D site analysis in high-frequency regime, solidly anchored in classic physics results (e.g. Fermat's Principle [KO90]) in section 3.3.2, including a new assessment of the fundamental resonance mode of soft soil deposits section 3.3.3.

Also, observe that in this chapter we will revamp the third coordinate z, which would not appear as the problems herein are restricted to plane strain, but it will be re-defined as the complement of the vertical coordinate, meaning $y + z = H$.

3.2 Homogeneous soil on rigid bedrock

In prior sections, it was implicitly taken for granted that either $\alpha \neq 0$ or $\alpha_m \neq 0$. The case in which the impedance between bedrock and adjacent layer is zero corresponds to the limit case of soft soil on rigid bedrock. The prior developments include this as a particular case, relevant results can be obtained by simply setting $\alpha = 0$ or $\alpha_m = 0$ in the corresponding equations.

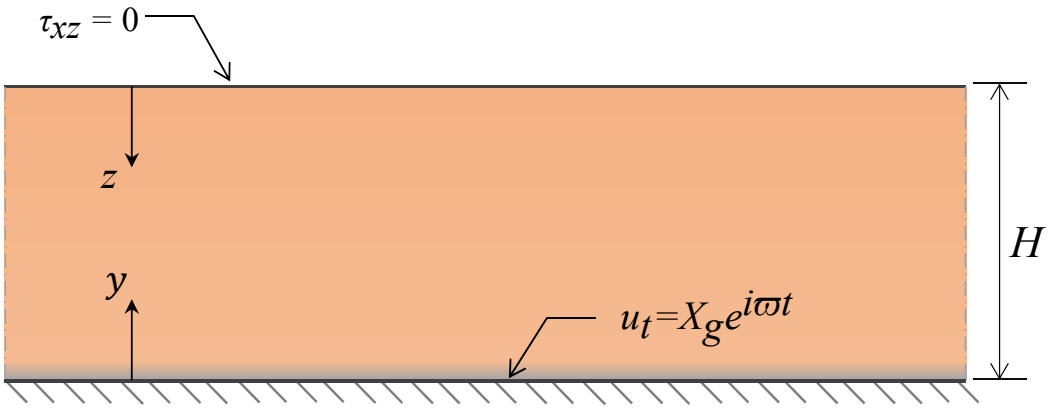

Figure 3.1: Scheme of wave propagation in homogeneous soil resting on rigid bedrock (total displacement)

Nevertheless, there are a couple of important qualitative differences between rigid and elastic bedrock:

1) When the reflected wave encounters the bedrock, it is reflected back in its entirety. Thus, there is no energy portion leaked out of the soft soil, and there are no changes in the displacement field within bedrock, hence we say that the displacement at the base of the soft soil (top of the rock stratum) *comes imposed*, as it is indifferent to whatever happens in the upper layer.

This prompts a logical definition of *total* displacement (u_t, referred to some motionless frame of reference) and *relative* displacement ($u = u_t - X_g e^{i\varpi t}$, displacement *with respect to the base*).

2) Once a portion of energy enters the upper soil layer, it remains trapped within it. Hence, there is no radiation damping as this in the system as no energy is lost to the underlying subspace. This scenario can give rise to *spurious resonances* (as we shall see), as the dissipation can rely only on other mechanisms less efficient than radiation.

Let us re-state eq. (2.60)

$$\mu \frac{\partial^2 u_t}{\partial y^2} - \rho \frac{\partial^2 u_t}{\partial t^2} = 0\,, \tag{3.1}$$

and introducing relative displacements

$$\mu \frac{\partial^2 u}{\partial y^2} - \rho \frac{\partial^2 u}{\partial t^2} = \rho \ddot{X}_g e^{i\varpi t}\,, \tag{3.2}$$

with boundary conditions

$$u(y=0,t) = 0 \quad \text{and} \quad \tau_{xz}(y=0,t) = \tau_{xy}(y=0,t) = 0 \rightarrow \left.\frac{\partial u}{\partial y}\right|_{y=H} = 0\,. \tag{3.3}$$

The implicit assumption $\ddot{X}_g = -\varpi^2 X_g$ being constant along the layer in horizontal direction is necessary to maintain the problem unidimensional.

As we shall focus on frequency domain analysis, let us skip the definition of initial conditions.

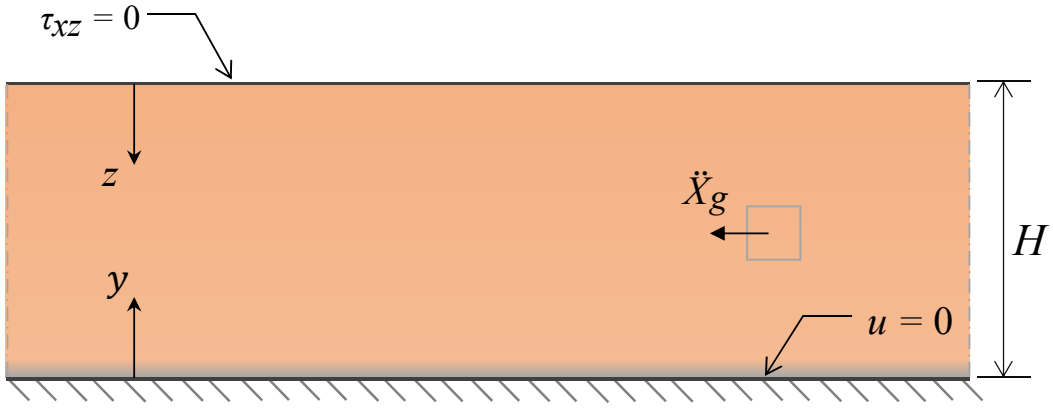

Figure 3.2: Scheme of wave propagation in homogeneous soil resting on rigid bedrock (N^{th} layer)

The steady-state solution of eq. (3.1) is

$$u_t(y,t) = X_g e^{i\varpi t} \frac{\cos(r(1-\eta))}{\cos(r)}, \tag{3.4}$$

where $r = \varpi H/c_s = \pi\varpi/2\omega_s$, ω_s being the fundamental frequency of the stratum, $c_s = \sqrt{\mu/\rho}$ is the shear-wave velocity of the material, and $\eta = y/H$.

In particular, it follows from 3.4 that the corresponding base-to-top amplification in this uniform stratum overlying rigid bedrock is

$$A(\varpi) = \frac{u_t(y=H,t)}{X_g e^{i\varpi t}} = \frac{1}{\cos(r)} = \frac{1}{\cos\left(\frac{\varpi}{c_s/H}\right)}, \tag{3.5}$$

an intuitive result that shall be summoned later as we consider heterogeneous soft layer. Moreover, the amplitude at resonance can be approximated for low values of damping δ_d [Roe77] as

$$A(\varpi = \omega_n) \approx \frac{4}{\pi} \frac{1}{(2n-1)\delta_d}, \tag{3.6}$$

where $\omega_n = (2n-1)\pi c_s/2H = (2n-1)\omega_s$ is the n-th natural frequency of the stratum.

The propagation equation in terms of total displacements, eq. (3.1), admits a treatment in terms of separation of variables, so that the vertical profile can be decomposed as a superposition of normal modes.
Similarly, the steady-state response in terms of relative displacements, eq. (3.2) has also been studied in the same way, by means an eigenfunction expansion composed of $\sin(k_n y/H)$, where $k_n = (2n-1)\pi/2$ for $n = 1, 2, \ldots$, although not much attention has been dedicated to the formal complications that arises from using such expansion as the basis upon which the forcing term is projected. In any event, the issue vanishes as the equation is integrated (for detailed discussion, see Appendix B). The steady-state solution of eq. (3.2) is

$$u(y,t) = Ue^{i\varpi t} \sum_{n=1}^{\infty} \tilde{u}_n \sin(k_n\eta) = -Ue^{i\varpi t} \sum_{n=1}^{\infty} \frac{2}{k_n^3\left(1-r_n^2\right)} \sin(k_n\eta), \tag{3.7}$$

where $r_n = r/k_n$ and $U = \rho\ddot{X}_g H^2/\mu$ represents a characteristic value of relative displacement in the far-field. See how the denominator in eq. (3.4) yields the same resonances as the one of eq. (3.7), yet through different mathematical expressions.

For a demonstration of the equivalence of eq. (3.7) and eq. (3.4), also see Appendix B.

3.2.1 Quasi-static setting

See how eq. (3.2) allows for the definition of a quasi-static regime as there is now an elastic force and an inertial force balancing an external load.

The next point is to prove that the quasi-static solution, which can be readily derived using the model with body force having the inertial term removed, is asymptotically equivalent to the dynamic solution for "low" frequencies, low being meant in comparison to the fundamental frequency of the stratum, hence $\varpi \ll \omega_s$; evidently, if the frequency is small in comparison to any natural frequency, then the aforesaid non-dimensional parameter $r = \varpi H/c_s$ must be small as well. Complementarily, bear in mind that low frequencies are synonym to long wavelengths, where "long" is meant with respect to any geometric characteristic length of the problem.

First, let us derive the quasi-static solution by direct double integration of eq. (3.2), prior removal of inertial forces, and imposing the boundary conditions (3.3):

$$u^{qs}(y,t) = u^{qs}(\eta,t) = U\Big(\frac{\eta^2}{2} - \eta\Big)e^{i\varpi t}\,, \tag{3.8}$$

where the superscript qs stands for "quasi-static".

To find the equivalence, assume r is a small parameter, then take eq. (3.4), rewrite it in a more convenient form and use the Taylor expansion around $r = 0$:

$$\begin{aligned} u(y,t) &= u_t(y,t) - X_g e^{i\varpi t} = X_g e^{i\varpi t}\Big[\frac{\cos(r(1-\eta))}{\cos r} - 1\Big] \\ &= X_g e^{i\varpi t}[\cos(r\eta) + \tan r \sin(r\eta) - 1] = \\ &= X_g e^{i\varpi t}[1 - \frac{1}{2}(r\eta)^2 + r\cdot r\eta - 1 + O(r^4)] = \\ &= \underbrace{-X_g r^2}_{\rho\ddot{X}_g H^2/\mu}\Big(\frac{\eta^2}{2} - \eta\Big)e^{i\varpi t} + O(r^4) = \\ &= U\Big(\frac{\eta^2}{2} - \eta\Big)e^{i\varpi t} + O(r^4) = \\ &= u^{qs}(y,t) + O(r^4)\,; \end{aligned} \tag{3.9}$$

thereby, the quasi-static solution using the body-force approach is equivalent to the dynamic solution for imposed displacement at the base if terms $O(r^4)$ are neglected. This relation is useful since it provides an estimate of the error one incurs when using the quasi-static approximation in the infinite stratum.

Before closing this apostrophe, a final clarification: see that r appears in the definition of the characteristic displacement U; therefore, the complete expansion around

$r = 0$ should be expressed in terms of total displacements as

$$\begin{aligned} u_t(y,t) &= X_g e^{i\varpi t} + u^{qs}(y,t) + O(r^4) = \\ &= X_g e^{i\varpi t} - \left[X_g \left(\frac{\eta^2}{2} - \eta \right) e^{i\varpi t} \right] r^2 + O(r^4) = \\ &= X_g e^{i\varpi t} \left[1 - \left(\frac{(y/H)^2}{2} - (y/H) \right) \left(\frac{\varpi}{c_s/H} \right)^2 \right] + O(\varpi^4) \,. \end{aligned} \tag{3.10}$$

In light of eq. (3.10), one can acknowledge that, as common sense dictates, the soft soil moves exactly as the bedrock in the limit $\varpi \to 0$, and there are no relative displacements whatsoever and the system moves as a rigid body. However, a first-order correction introduces relative displacements u^{qs}.

The same conclusions would have been attained had classic perturbation methods [BO13] been leveled at eq. (3.1). The approach displayed above was deemed more convenient, as it enables us to motivate the introduction of the surrogate body force and a quasi-static approximation.

These observations are aimed, partially, to correct the misconception of the quasi-static approximation lacking interest on its own right. For the upcoming discussion on retaining walls, see for example the paper by Kloukinas et al. [KLM12]:

> *The pseudostatic condition, although idealized (recall that imposing constant base acceleration at zero frequency requires an infinite amount of displacement), is of fundamental importance for problems of this type, for it allows comparisons against results from limit analysis methods.*

We intended to show here that the quasi-static approximation corresponds to a simple approximate solution for the low-frequency (long-wavelength) regime. This observation is valid for both the 1D as well as 2D problem (layer with retaining wall at one flank).

3.3 Heterogeneous soil on rigid bedrock

Next, we shall consider the case wherein the mechanical properties of the soil vary within the stratum in continuous fashion. This heterogeneity will be conceptualized by an evolving shear-wave velocity, that is, defining $c_s(y) = c_{s,base} f(y)$, where it is assumed:

1) The function is continuous within its domain of definition; in mathematical terms, $f(y) \in C^1([0,H])$,

2) The function is strictly positive within the interval, $f(\eta) > 0 \quad \forall y \in [0,H]$.

Both assumptions are relevant for the reasonings we will pursue. No more assumptions are necessary for now.

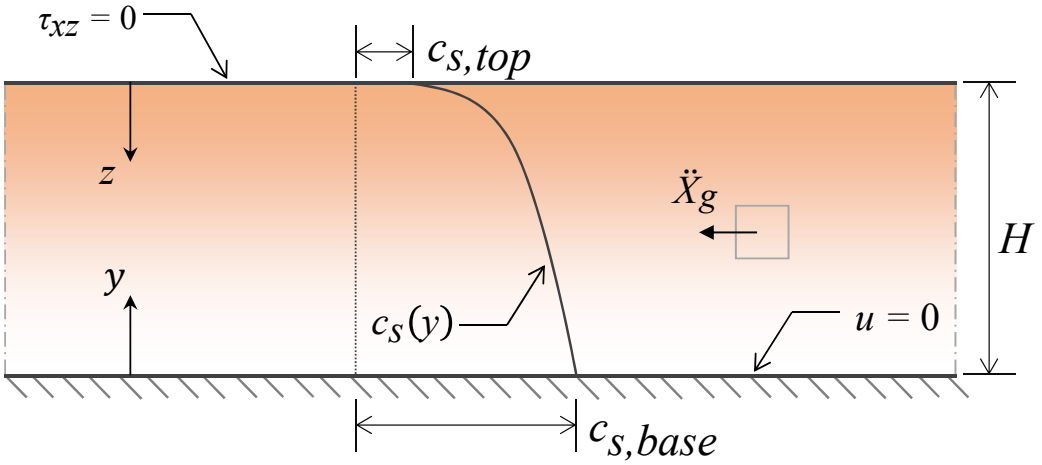

Figure 3.3: Scheme of wave propagation in inhomogeneous soil resting on rigid bedrock (N^{th} layer)

In this situation, eq. (2.59) is in effect. Let us concentrate on analyzing the frequency domain (what amounts to consider steady-state response), and thus introduce $u_t(y,t) = \hat{u}_t(y)e^{i\varpi t}$ in the prior equation, moreover, divide by ρ and $e^{i\varpi t}$ to obtain

$$\frac{d}{dy}\left(c_s^2(y)\frac{d\hat{u}_t}{dy}\right) + \varpi^2\hat{u}_t = 0\,, \tag{3.11}$$

which can be expressed in relative displacements as eq. (3.2)

$$\frac{d}{dy}\left(c_s^2(y)\frac{d\hat{u}}{dy}\right) + \varpi^2\hat{u} = \ddot{X}_g\,. \tag{3.12}$$

The last equation can be conveniently expressed in dimensionless form by means of the following non-dimensional parameters and variables:

$$\eta = \frac{y}{H} \quad , \quad \tilde{u} = \frac{\hat{u}}{\ddot{X}_g H^2/c_{s,base}^2} \quad , \quad r = \frac{\varpi}{c_{s,base}/H}\,. \tag{3.13}$$

These are, by and large, a re-definition based on the mechanical properties at the base of those presented in the previous section. Using these in eq. (3.12) we obtain

$$\frac{d}{d\eta}\left(f^2(\eta)\frac{d\tilde{u}}{d\eta}\right) + r^2\tilde{u} = 1\,, \tag{3.14}$$

while the boundary conditions, as in eq. (3.3), are

$$\tilde{u}(\eta = 0) = 0 \quad \text{and} \quad \left.\frac{d\tilde{u}}{d\eta}\right|_{\eta=1} = 0\,. \tag{3.15}$$

Logically, the solution of the equation depends dramatically on the specific $f(\eta)$ choice.

3.3.1 Results for generalized-parabola distribution

Holl [Hol41] pioneered the use of continuous distributions of mechanical properties as a way to consider the effect of overburden pressure on the response of soils. Kassir [KC74] proposed a power law with non-zero stiffness at the free surface of the layer, a choice that has been echoed since then. Rovithis et al. [RPM11] proposed modeling the shear-wave distribution as

$$\frac{c_s(z)}{c_{s,base}} = \left(b + (1-b)\,\frac{z}{H}\right)^n \Rightarrow f(\eta) = (1 + (b-1)\,\eta)^n\,, \tag{3.16}$$

where $b = (c_{s,top}/c_{s,base})^{1/n}$ and n is referred to as "inhomogeneity parameter" (also referred to as "inhomogeneity parameter", see [DG85]). The parameter b controls the maximum variation of c_s, which in this case always corresponds to top-to-bottom or vice versa, since the function only allows for monotonic evolution across the layer.

This profile, usually referred to as "generalized parabola", has received wide attention given that it works well as a continuous approximation to profiles corresponding to real sites.

These authors found that, assuming eq. (3.16), the exact solution of eq. (3.12) yields a base-to-surface displacement ratio (A) is

$$A(b,n,r) = \frac{u_t(z=0)}{X_g} = \frac{2}{\pi}\frac{b^{\psi-\ell/2}}{\lambda}\left[J_{\nu+1}(\lambda b^{\ell/2})Y_\nu(\lambda) - J_\nu(\lambda)Y_{\nu+1}(\lambda b^{\ell/2})\right]^{-1}\,, \tag{3.17}$$

where J_i and Y_i are the Bessel functions of i-th kind, $\ell = 2(1-n)$, $\psi = (1-2n)/2$, $\nu = (2n-1)/2(1-n)$, $\lambda = 2r/\ell(1-b)$ and r as in eq. (3.13). See that the frequency dependence takes place through the function $\lambda = \lambda(r) = \lambda(\varpi)$, which should be mistaken by either the Lamé constant or a wavelength.

3.3.1.1 Equivalent-homogeneous properties for high-frequency

A fair critic to be aimed at eq. (3.17) is its genuine complexity, even more apparent when it is contrasted to eq. (3.5), its homogeneous analogue. Due to this and

similar issues when considering heterogeneous soils, there has been a persistent research effort towards finding an adequate definition of "equivalent homogeneous" soil profiles, that is, an uniform layer whose shear-wave velocity is such that its dynamic response mimics the one embedded into eq. (3.17). In other words, one might pose the problem of finding an "equivalent homogeneous" profile as to find $c_{s,eq}$ in

$$A_{eq}(\varpi) = \frac{1}{\cos\left(\frac{\varpi}{c_{s,eq}/H}\right)} \tag{3.18}$$

such that the discrepancies between eq. (3.17) and eq. (3.18) are minimized according to some criterion (e.g. reducing error when predicting either resonant frequencies or amplitudes or amplitudes at resonance).

We assessed, among other matters, in what ways the asymptotic behavior of eq. (3.17) can guide the definition of equivalent-homogeneous properties [GSA19]. It was found (see appendix for details) that eq. (3.17) can be expressed as

$$A(\beta, n, r) = \frac{\beta^{-1/2}}{\cos\left(\frac{r}{1-n}\left(\frac{1-\beta^{(1-n)/n}}{1-\beta^{1/n}}\right)\right)} + O\left(\frac{(1-n)}{r}\frac{(1-\beta^{1/n})}{\beta^{(1-n)/n}}\right), \tag{3.19}$$

where $\beta = c_{s,top}/c_{s,base} = b^n$. This result prompts us to define

$$c_{s,eq} = c_{s,base}\frac{(1-n)(1-\beta^{1/n})}{\beta^{(1-n)/n}}, \tag{3.20}$$

whence

$$\omega_{s,eq} = \frac{\pi}{2}\frac{c_{s,eq}}{H} = \frac{\pi}{2}\frac{c_s}{H}\frac{(1-n)(1-\beta^{1/n})}{\beta^{(1-n)/n}}, \tag{3.21}$$

and also

$$A(\beta, n, r) = \frac{\sqrt{c_{s,base}/c_{s,top}}}{\cos\left(\frac{\varpi}{c_{s,eq}/H}\right)} + O\left(\frac{c_{s,eq}/H}{\varpi}\right) = \frac{\sqrt{c_{s,base}/c_{s,top}}}{\cos\left(\frac{\pi}{2}\frac{\varpi}{\omega_{s,eq}}\right)} + O\left(\frac{\omega_{s,eq}}{\varpi}\right). \tag{3.22}$$

This last expression does very much resemble eq. (3.18). Some salient features of eq. (3.22) demand comments:

1) The first addend corresponds to the asymptotic limit of the exact solution as the argument in the cosine goes to infinity, which happens to be the same factor as the second addend is inversely proportional to. Large values in this argument are attained by either

a) increasing the frequency ($\varpi \to \infty$),

b) decreasing the top-to-bottom contrast ($\beta \to 1$). The latter is mathematically confirmed by realizing that the limit as $\beta \to 1$ of eq. (3.22) is eq. (3.5).

2) The eq. (3.22) not only suggests the value of $c_{s,eq}$ but also clearly states that the amplitude of the amplification depends on the heterogeneity too, yet not so much on the distribution but on the limit values of shear-wave velocity. This equation makes physical sense as one would expect more energy to be trapped at the softer layers, hence if the softer layers are at the top ($c_{s,base}/c_{s,top} > 1$) then the with-respect-to-base amplification will be greater than the homogeneous soil (defined over the properties at the base), whereas, conversely, this amplification will be smaller if the soft layers are at the bottom, as less energy will reach the top. Actually, eq. (3.22) claims even further, as it states that the relation *scales as the square-root* of the top-to-bottom velocity contrast.

3) Besides, the preceding scaling can also be interpreted as a damping factor update to account for the soil heterogeneity: see that, ignoring the second added, the amplitude at resonance, eq. (3.6), for eq. (3.22) is

$$A\left(\beta, n, \varpi = \omega_{k,eq}\right) \approx \frac{4}{\pi} \frac{\sqrt{c_{s,base}/c_{s,top}}}{(2k-1)\delta_d} = \frac{4}{\pi} \frac{1}{(2k-1)\delta_{d,eq}}, \tag{3.23}$$

thus defining $\delta_{d,eq} = \sqrt{c_{s,top}/c_{s,base}}\delta_d$ as an equivalent-homogeneous damping factor the amplitude of resonant spikes would be properly captured by equivalent-homogeneous model as well. Keep in mind these conclusions are contingent upon the second addend having relatively small magnitude.

Among a number of different alternatives, Rovithis et al. [RPM11] realized that defining an equivalent soil profile by taking

$$c_{s,eq} = H\left(\int_0^H \frac{dy}{c_s(y)}\right)^{-1}, \tag{3.24}$$

that is, the *harmonic mean* of the distribution given by eq. (3.16) (referred to as "V_{hom4}" in their paper). This was not the first time this fact was pointed out: Zhao [Zha97], by means of numerical experiments and assuming a distribution similar to eq. (3.16), realized that using this harmonic mean it is possible to obtain good

predictions of the actual natural frequencies of the heterogeneous layer, and that the higher the frequency, the better the prediction. In his nomenclature, the *travel time for vertical incidence* and the *nominal frequency of a site* and an estimate for the higher mode frequencies are given, respectively, by

$$T_0 = \int_0^H \frac{dy}{c_s(y)} \quad , \quad f_0 = \frac{1}{4T_0} \quad , \quad \omega_k = 2\pi(2k-1)f_0\,, \tag{3.25}$$

assuming $k \geq 2$. In his very own words (see the section titled "Main Conclusions"):

> *It has been shown that the nominal frequency of a site, i.e. the inverse of four times the total travel time of the soil layers, is an important parameter for estimating high mode frequencies. A simple equation for estimating high mode frequencies is presented and its accuracy is well within the requirement for engineering applications. The nominal frequency is, however, not a very good estimate for the first mode frequency of the site.*

It seems that the possibility of defining an average shear-wave velocity had been considered even earlier by, at least, Steedman and Zheng [SZ90], albeit no critical assessment of the range of suitability of this choice was pursued. After all, defining equivalent shear-wave velocity in this fashion is currently being recommended with no restrictions [NIS12].

By realizing that actually eq. (3.20) is just eq. (3.24) wherein the generalized-parabola distribution eq. (3.16) is used, all these observations can now be rooted in the mathematics of the model, in light of eq. (3.19): we acknowledge that what Zhao described [Zha97] and what Rovithis et al. confirmed [RPM11], simply corresponds to the asymptotic behavior of the exact solution, eq. (3.17) as the frequency increases.

Some pressing questions at this point are: how general is this result? Would we obtain the same conclusion if a different distribution was used? What conditions should the distribution fulfill for the harmonic-mean equivalent homogeneous to remain valid? Is the square-root law for the amplitude dependent on the shape distribution?

In the end, all the answers to these questions will be traced back to an elemental physics theory: *ray theory*, also referred to as *geometrical optics* [KO90]. We shall delve into this matter in section 3.3.2.

3.3.1.2 Verification

A suite of figures displaying a comparison between the exact solution eq. (3.17) and the asymptotic approximation in eq. (3.22) can be found next. They are followed by tables showcasing errors both in amplitude and resonance location estimation. These are intended to demonstrate quantitatively the conclusions derived in the previous section.

Comparisons include base-to-top S-wave velocity ratio 10% ($\beta = 0.1$), 50% ($\beta = 0.5$), and 90% ($\beta = 0.9$). Damping $\delta_d = 0.05$ is assumed in all comparisons. Results for different values of the inhomogeneity factor n (namely: 0.9, 0.5, 0.1) are displayed in fig. 3.4, fig. 3.5, and fig. 3.6 and condensed in Table table 3.1 and Table table 3.2.

In all these figures $\omega_{s,base} = \pi c_{s,base}/2H$ represents the first natural frequency of the soil column (homogeneous stratum) based on the stiffness at the base ($c_s = c_{s,base}$). Then, fig. 3.4, fig. 3.5, and fig. 3.6 and table 3.2 show that good agreement is obtained for low-to-medium ratios when it comes to predict the amplitude of the resonant spikes as long as n is not too low. Note that eq. (3.19) delivers similar results as it scales amplitudes in the same fashion. Agreement worsens dramatically when either β or n decrease below 0.5, leading to severe errors notwithstanding the amplitude is never underestimated.

The main observation to be learned from the comparisons is the capacity of eq. (3.21) to predict natural frequencies of the stratum above the fundamental one (table 3.1), even under cases of poignant both ratios and inhomogeneity gradient, yielding reasonable errors (below 10%) even for the most extreme cases herein considered. Note how the error term in the aforementioned equation scales as $\sim r^{-1}$, that is, decreases with increasing frequency, this explaining why the estimation of the second and third natural frequencies is sensibly more accurate than the one corresponding to the fundamental mode. Besides, this explains why the approximation based on asymptotics perform rather poorly in the low-frequency range: as the error terms in eq. (3.19) are inversely proportional to the frequency, the magnitude of these becomes as large as the other addend, and thus ignoring them in the low-frequency regime entails large errors, to the extent that at $\varpi = 0$ the asymptotic approximation yields dynamic amplification ($A(\varpi = 0) > 1$) when there must be none ($A(\varpi = 0) = 1$).

Finally, the lack of influence of damping is confirmed in table 3.3, table 3.4, and

fig. 3.7. These results indicate that the parameter δ_d does not play a relevant role in the precision of the approximations, as long as high frequencies are considered.

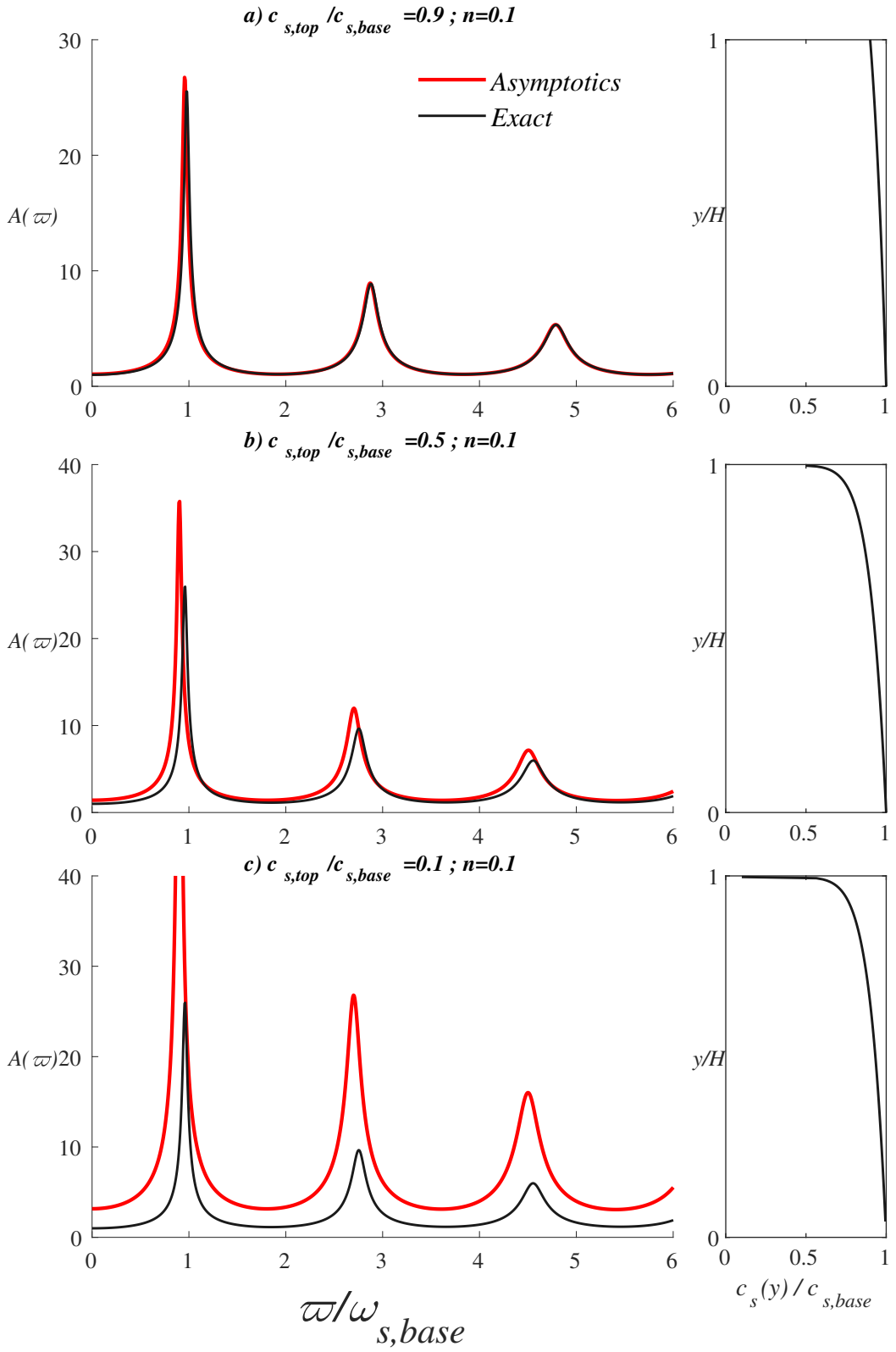

Figure 3.4: Base-to-top dynamic amplification $A(\varpi)$ (with corresponding vertical S-wave profile $c_s(y)$), comparison between eq. (3.17) (*Exact*) and eq. (3.22) (*Asymptotics*) for inhomogeneity factor $n = 0.1$

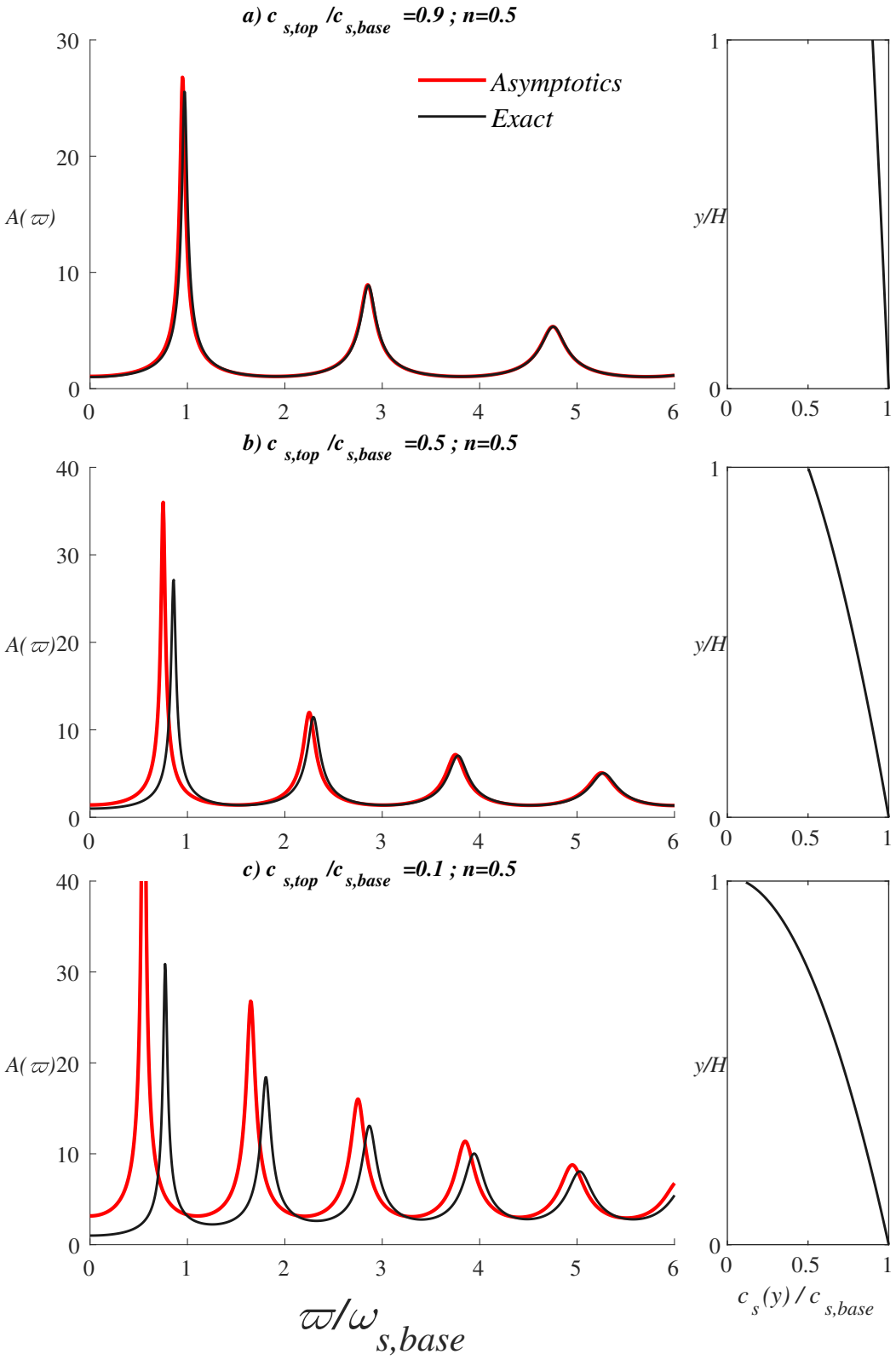

Figure 3.5: Base-to-top dynamic amplification $A(\varpi)$ (with corresponding vertical S-wave profile $c_s(y)$), comparison between eq. (3.17) (*Exact*) and eq. (3.22) (*Asymptotics*) for inhomogeneity factor $n = 0.5$

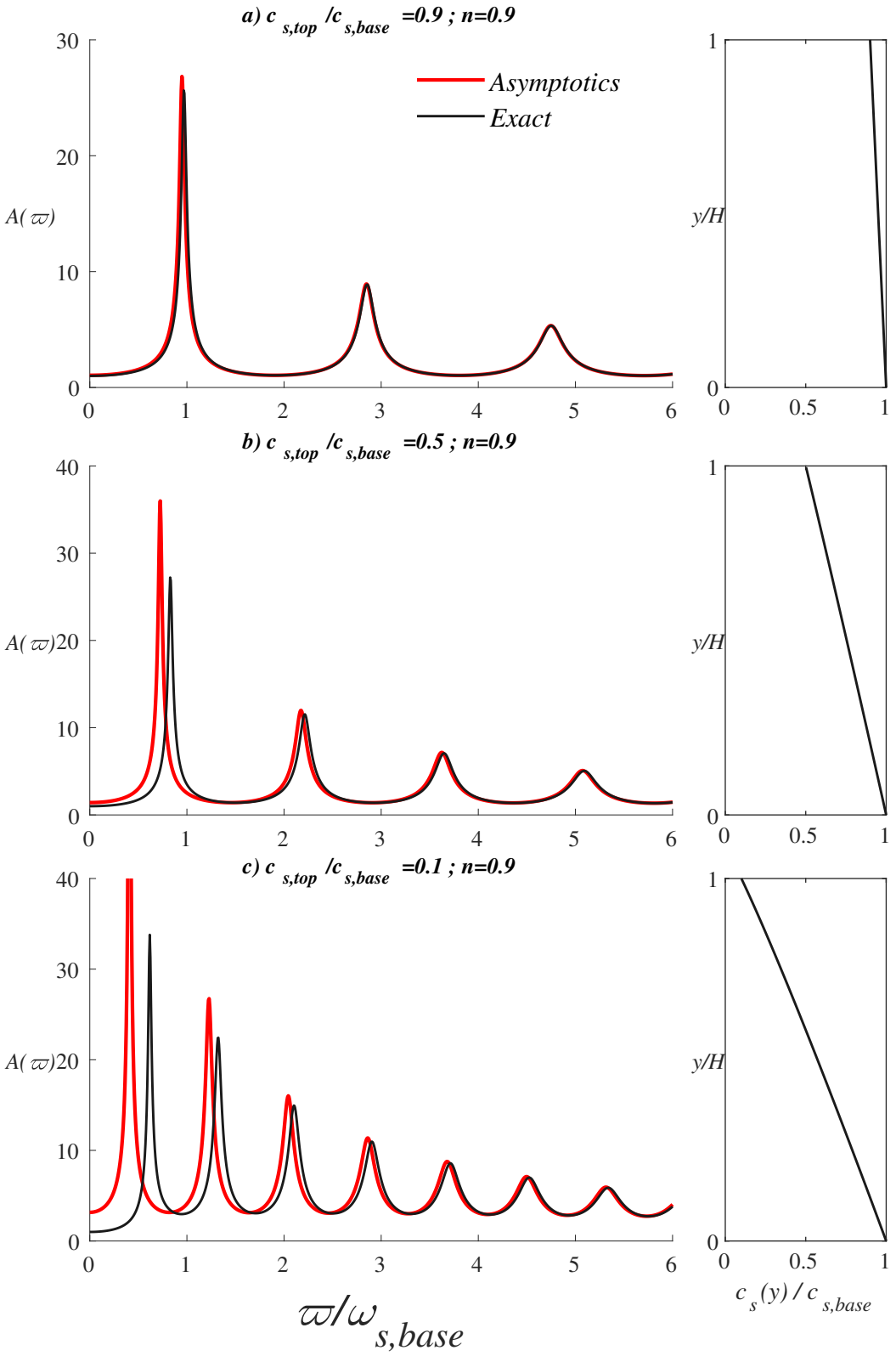

Figure 3.6: Base-to-top dynamic amplification $A(\varpi)$ (with corresponding vertical S-wave profile $c_s(y)$), comparison between eq. (3.17) (*Exact*) and eq. (3.22) (*Asymptotics*) for inhomogeneity factor $n = 0.9$

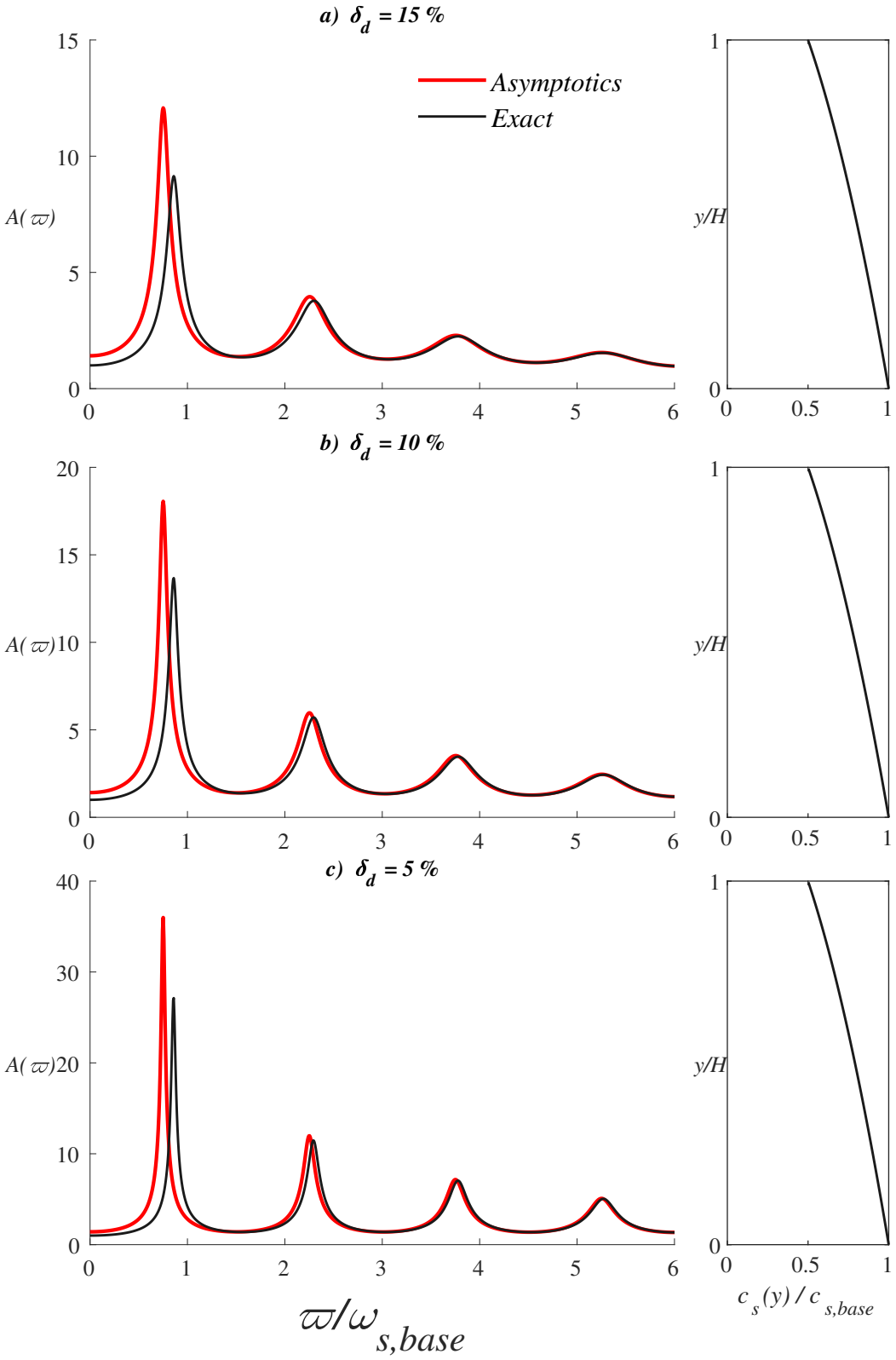

Figure 3.7: Base-to-top dynamic amplification $A(\varpi)$ (with corresponding vertical S-wave profile $c_s(y)$), comparison between eq. (3.17) (*Exact*) and eq. (3.22) (*Asymptotics*) for $n = 0.5$ and $\beta = 0.5$, analysis of damping sensitivity

		Inhomogeneity factor (n)		
	$c_{s,top}/c_{s,base}$	0.9	0.5	0.1
First resonance peak	0.9	2.0	2.0	2.0
	0.5	12.2	12.5	5.9
	0.1	33.7	28.7	6.6
Second resonance peak	0.9	0.44	0.22	0.22
	0.5	1.7	1.7	1.8
	0.1	7.2	8.8	2.1
Third resonance peak	0.9	<0.1	0.1	0.1
	0.5	0.7	0.7	1.0
	0.1	2.7	4.0	1.1

Table 3.1: Error (%) in estimation by eq. (3.22) of the natural frequency corresponding to the three first resonance peaks

		Inhomogeneity factor (n)		
	$c_{s,top}/c_{s,base}$	0.9	0.5	0.1
First resonance peak	0.9	-4.7	-4.9	-4.8
	0.5	-32.2	-32.7	-37.7
	0.1	-136.4	-156.4	-208.3
Second resonance peak	0.9	-0.5	-0.5	-0.7
	0.5	-3.8	-4.4	-24.2
	0.1	-19.2	-45.4	-177.7
Third resonance peak	0.9	-0.2	-0.2	-0.3
	0.5	-1.4	-1.7	-19.9
	0.1	-7.2	-22.5	-167.7

Table 3.2: Error (%) in estimation by eq. (3.22) of the amplitude corresponding to the three first resonance peaks

	Damping factor (δ_d)		
Resonance Peak	0.9	0.5	0.1
First	-32.7	-32.1	-32.1
Second	-4.4.	-4.6	-4.7
Third	-1.7	-1.7	-1.8

Table 3.3: Error (%) in estimation by eq. (3.22) of the amplitude corresponding to the three first resonance peaks for different values of damping

	Damping factor (δ_d)		
Resonance Peak	0.9	0.5	0.1
First	12.5	12.5	12.5
Second	1.7	1.9	1.9
Third	0.7	0.7	0.7

Table 3.4: Error (%) in estimation by eq. (3.22) of the natural frequency corresponding to the three first resonance peaks for different values of damping

3.3.2 General 1D high-frequency response of continuously-heterogeneous soil layers on rigid bedrock

Recall the assumptions that were made at the beginning of section 3.3 (i.e., $f(y) \in C^1([0,H])$ and $f(y) > 0 \quad \forall y \in [0,H]$). We shall show that an expression equivalent to eq. (3.22) holds for any distribution $f(y)$ verifying just these two conditions. To do so, it turns out to be more convenient re-adopting the formulation in terms of total displacements.

Thus, let us use eq. (3.2) in dimensionless form, where in this case the non-dimensional *total* displacement is $\tilde{u}_t = \hat{u}_t / X_g$, and thus

$$\frac{d}{d\eta}\left(f^2(\eta)\frac{d\tilde{u}_t}{d\eta}\right) + r^2\tilde{u}_t = 0\,, \tag{3.26a}$$

or

$$f^2(\eta)\frac{d^2\tilde{u}_t}{d\eta^2} + 2f(\eta)f'(\eta)\frac{d\tilde{u}_t}{d\eta} + r^2\tilde{u}_t = 0\,. \tag{3.26b}$$

The boundary conditions in dimensionless form are

$$\tilde{u}_t(\eta = 0) = 1 \quad \text{and} \quad \left.\frac{d\tilde{u}_t}{d\eta}\right|_{\eta=1} = 0\,. \tag{3.27}$$

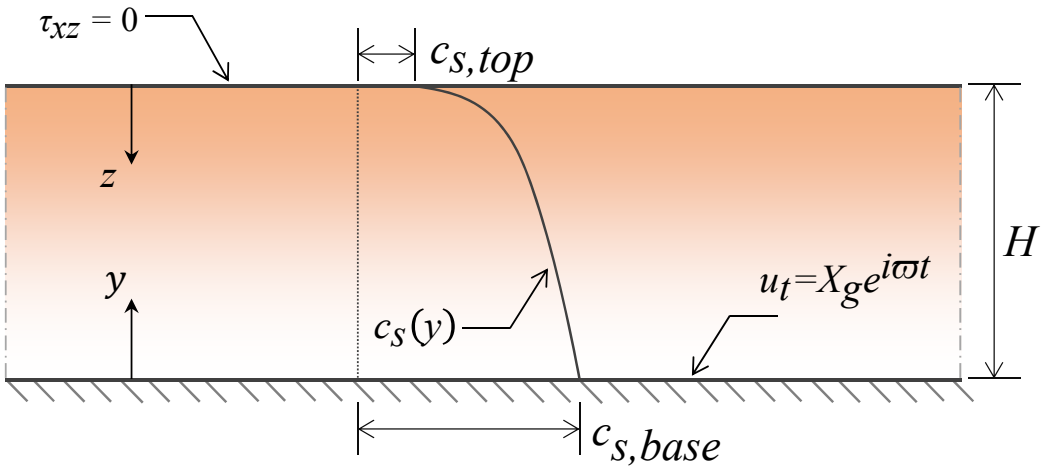

Figure 3.8: Scheme of wave propagation in heterogeneous soil resting on rigid bedrock (total displacement)

We are interested in understanding the high-frequency regime. In terms of the only dimensionless group in the problem, such regime corresponds to $r \gg 1$, therefore $\epsilon = 1/r$ may be considered as a small parameter. Thus, rewrite eq. (3.26b) multiplying by ϵ^2, and also dividing by $f^2(\eta) = 0$:

$$\epsilon^2 \frac{d^2\tilde{u}_t}{d\eta^2} + 2\epsilon^2 \frac{f'(\eta)}{f(\eta)} \frac{d\tilde{u}_t}{d\eta} + \frac{1}{f^2(\eta)} \tilde{u}_t = 0\,, \tag{3.28a}$$

and, for the sake of brevity, call $q(\eta) = 1/f^2(\eta)$ (see that this function is always positive and bounded based on the restrictions of positive and non-zero wave velocity) and $m(\eta) = f'(\eta)/f(\eta)$ (finite and positive too)

$$\epsilon^2 \frac{d^2\tilde{u}_t}{d\eta^2} + 2\epsilon^2 m(\eta) \frac{d\tilde{u}_t}{d\eta} + q(\eta)\tilde{u}_t = 0\,. \tag{3.28b}$$

This is a singular perturbation problem with spatially-changing coefficients. The classic WKB method [BO13] is the tool-of-choice to find an approximate solution. See that the condition $f(\eta) \neq 0\ \forall y \in [0, H]$ is critical as it precludes the existence of turning points.

In a nutshell, the WKB advocates the use of the ansatz

$$\tilde{u}_t(\eta) \sim \exp\left(\frac{1}{\delta} \sum_{n=0}^{\infty} \delta^n S_n(\eta)\right) \tag{3.29}$$

in eq. (3.28b). A painstaking derivation can be found in Appendix B. We proceed to state the main results that utilizing the method yields:

$$S_0(\eta) = \pm i \int_1^{\eta} \sqrt{q(\eta')} d\eta' = \pm i \int_1^{\eta} \frac{d\eta'}{f(\eta')}\,, \tag{3.30}$$

recall that $q(\eta) = 1/f^2(\eta) = (c_{s,base}/c_s(y))^2$, and moreover

$$S_1(\eta) = C + \ln(f(\eta)^{-1/2}), \tag{3.31}$$

where C represents a constant. Combining this two contributions of the phase (the only ones that do not vanish in the high-frequency limit) we obtain the so-called *physical optics* approximation, which for top-to-bottom displacement amplification yields

$$A(\varpi) = \frac{f(\eta = 1)^{-1/2}}{\cos\left(\frac{\varpi H}{c_{s,eq}}\right)} = \frac{\sqrt{c_{s,base}/c_{s,top}}}{\cos\left(\frac{\varpi H}{c_{s,eq}}\right)}, \tag{3.32}$$

where $c_{s,eq}$ is the harmonic mean defined in eq. (3.24). It is interesting to note that utilizing just S_0 yields the denominator and the harmonic mean homogeneous-equivalent velocity whereas including S_1 adds the amplitude correction.

The formal validity of the approximation is discussed in Appendix B. If we wanted to display the damping factor, δ_d, explicitly in eq. (3.32), just substitute $c_{s,eq}$ by $c_{s,eq}\sqrt{1 + \mathrm{i}\delta_d}$.

One must also mention that a similar result would have been obtained had we allowed the density to be a function depending on the position in the stratum. Had we done so, considering $\mu = \mu(y) = \mu_{base}g(\eta)$, $\rho = \rho(y) = \rho_{base}h(\eta)$ (hence $f(\eta)^2 = g(\eta)/h(\eta)$) , the auxiliary coefficients $m(\eta)$ and $q(\eta)$ would have become

$$m(\eta) = \frac{1}{2}\frac{g'(\eta)}{g(\eta)}, \tag{3.33a}$$

$$q(\eta) = \frac{h(\eta)}{g(\eta)}. \tag{3.33b}$$

These expressions yield a generalization of eq. (3.32):

$$A(\varpi) = \frac{(h(\eta = 1)g(\eta = 1))^{-1/4}}{\cos\left(r\int_0^1 \frac{d\eta}{f(\eta)}\right)}, \tag{3.34}$$

reversing the non-dimensionalization,

$$A(\varpi) = \left(\frac{\mu_{base}\rho_{base}}{\mu_{top}\rho_{top}}\right)^{1/4} \sec\left(\frac{\omega H}{c_{s,eq}}\right), \tag{3.35}$$

where $c_{s,eq}$ is still being given by the harmonic mean of $f(\eta) = \sqrt{g(\eta)/h(\eta)}$, eq. (3.24), and now the change of amplitude depends on the base-to-top relative evolution both of stiffness and the density and density (observe that eq. (3.32) simply corresponds to $\rho_{base} = \rho_{top}$).

3.3.2.1 Physical significance

Interpretation

The physical interpretation of these results is straightforward once it is framed in terms of wavelength: high frequencies entail short wavelengths, with respect to H, propagating inside the material bulk. Short wavelengths tend to "filter out" those spatial features of the medium larger than themselves, and thus, one may say, the wave does not "see" the shift in stiffness and it behaves as if there was only uniform soil all around, while long wavelengths "see" each relatively-small stiffness alteration, and hence it tends to move around "chunks" of heterogeneous soil. The reason for obtaining the harmonic mean instead of the arithmetic mean derive from the fact that in this problem the travel distance is kept constant, not the travel time. Let us illustrate this point carefully: the stratum in fig. 3.8 can be conceptualized as a series of infinitely many slices each with the same infinitesimal thickness, $h = H/N$ where the number of slices N tends to infinity, hence we calculate the average velocity of the propagating wave as the ratio between the total travel distance over the total time that the trip takes

$$c_{s,mean} = \frac{\sum_{i=1}^{N} h_i}{\sum_{i=1}^{N} T_i} = \frac{H}{\sum_{i=1}^{N} (H/N c_{s,i})} \rightarrow \frac{1}{\int_0^H \frac{d(y/H)}{c_s(y)}} = c_{s,eq} \tag{3.36}$$

as N tends to infinity. The subscript i denotes properties concerning the i-th layer. This means that the proper average to consider in this kind of problem is the harmonic mean.

Fit in Ray Theory

The previous results can be considered as the outcome of application of so-called *ray approximation methods* to the problem occupying us. In a nutshell, these employ the short-wavelength (high-frequency) limit to analyze wave propagation phenomena (electromagnetic, acoustic or elastic). Ray methods are a powerful tool that has already been used in Elastodynamics; see for example the monograph by Prof. Achenbach and coworkers [AGM82], wherein these methods are applied to the study of the effect of cracks over waves propagating within *homogeneous* elastic bodies. The physical intuition behind these results has been common currency in the physics community, including seismology, see Aki and Richards' treaty on Quantitative Seismology [AR02], in particular, Chapter 4, section 4, concerning ray methods as a means to consider seismic wave propagation in the heterogeneous earth. However, these appraisals had not been passed on to the geotechnical engineering

community at large nor, it appears, explicitly spelled out in the mathematical terms of the WKB approximation applied to considerations of unidimensional propagation in a finite domain, although similar expansions are usually discussed in the geometrical optics literature [AGM82; KO90], including the renowned *Debye expansion*, which does not rely on the definition of small parameters directly.

In order to perform a one-to-one mapping between the classic theory and prior results, let us state that the first component to the phase, S_0 is equivalent to the *eikonal function* (is actually equal to it times an extra factor $\pm$i), the refraction index corresponds to the inverse of the velocity distribution, and, just like the general theory foresees, the eikonal function is proportional to the integral of the refraction index over the arc-length of the trajectory followed by the ray [KO90]. The second component of the phase, S_1, yields the leading-order approximation of the amplitude, which is provided by solving of a transport equation.

Moreover, the amplification factor in both eq. (3.35) and eq. (3.32) can be retraced to the *ray divergence* parameter, which is but a consequence of the energy flux conservation in the system. See [KO90] for details.

This physical intuition also allows us to reply to the question posed earlier, namely, what does it happen when $f(y) \notin C^1([0,H])$ but $f(y) \in C^0([0,H])$ (continuous function, non-continuous first derivative) or even $f(y) \in C^{-1}([0,H])$ (non-continuous function)? The reasoning that was followed before is prevented as $f'(\eta)$ cannot be defined. The answer is found in Fermat's Principle. Basically, Fermat's Principle states that the problem we are solving possesses a variational structure, and hence the equations we are solving are nothing but its corresponding Euler equations. If the functions describing the parameter evolution do not have enough continuity, this may prevent us from defining the Euler equations properly, but the underlying stationarity condition [KO90] remains in effect. The phenomenon at the intersection of different mediums can be described by an analogue of Snell's law in optics. This intuition suggests to further generalization of the conclusions previously derived.

Finally, let us mention, on one hand, that the case corresponding to $\delta_d = \delta_d(y) \ll 1$ can be assimilated into a classic scenario referred to as *medium with weak absorption*, and, secondly, that the case of vanishing stiffness at the top of the layer can be understood as the presence of a *caustic* surface at the top of the stratum. [KO90]. The only "exotic" feature that our problem introduces concerns *where* the inhomogeneity is localized. Normally, the wave propagates in a medium with varying refraction index, hence the elliptic operator that appears in Euler equations is simply

a Laplacian, which in the 1D-case boils down to a neat second derivative in space, $\partial^2(\cdot)/\partial y^2$, where the dot represents the dependent variable; in our case, at least part of the homogeneity is confined within the operator due to the change in stiffness of the medium, hence the operator we deal with is $\partial(\mu(y)\partial(\cdot)/\partial y)/\partial y$, then we can recognize an instantiation of the Sturm-Liouville problem [Wei12] in our problem. Aki and Richards [AR02] studied this case.

3.3.2.2 Comparison to numerical results

Let us illustrate how and when the approximate formula eq. (3.32) agrees well with an exact solution that could still be obtained numerically for cases of complicated profiles.

Increasing contrast

First, let us consider a "toy" profile that may allow us confirm the influence of sudden property gradients on fitness of the approximation. For such purpose, consider

$$f(\eta) = 1 - \frac{3}{8}\left[1 + \tanh\left(p\left(\eta - \frac{1}{3}\right)\right)\right]. \tag{3.37}$$

This profile gives a contrast between base and top of $1/4$, where all the variation is concentrated at $\eta = 1/3$. The parameter p controls the gradient in that zone, the higher p the quicker the evolution and the more sudden the change. In the limit $p \to \infty$ the function becomes an step function and the gradient is infinite. Three different cases have been solved in *Mathematica*.

We observe in fig. 3.9 how the approximate formula eq. (3.32) successfully captures the behavior in most of the frequency range, but the agreement worsens as the smooth change becomes a localized snap at $p = 100$. This result illustrates how it behooves the gradient to remain bounded everywhere for the approximation to match the exact solution.

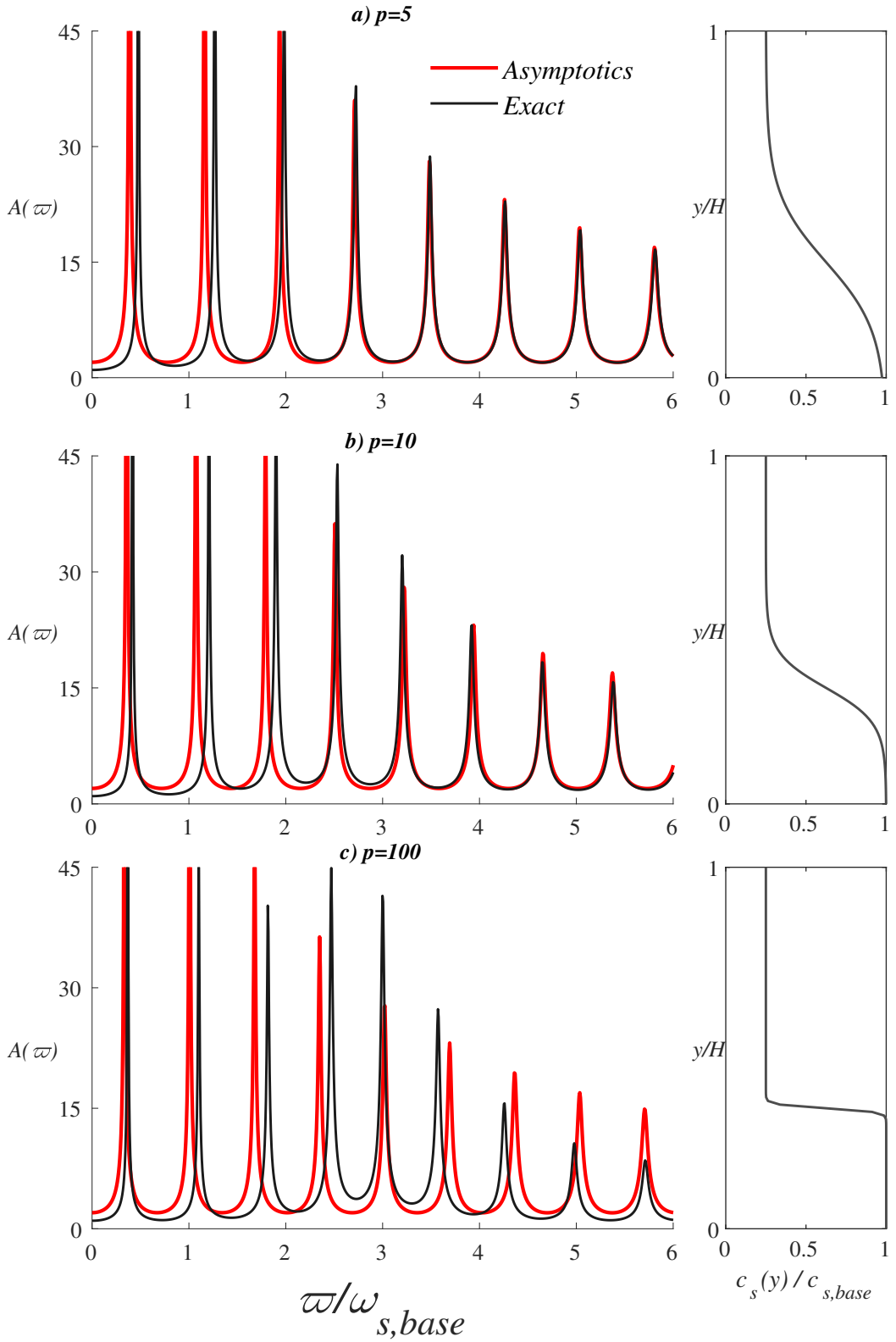

Figure 3.9: Base-to-top dynamic amplification $A(\varpi)$ (with corresponding vertical S-wave profile $c_s(y)$), comparison between numerical solution of eqs. (3.2) and (3.3) (*Exact*) and eq. (3.32) (*Asymptotics*)

Profile reversal

This time, let us consider a profile with reversals, meaning softer regions in between stiffer ones. For this job, we propose using

$$f(\eta) = 1 + \Delta \sin\left(K\frac{\pi}{2}\eta\right), \tag{3.38}$$

where Δ controls the amplitude of the reversals whereas K does the same for the number of reversals that happen within the layer.

We acknowledge in fig. 3.10 that the number of oscillations, K, and their amplitude Δ, in and of itself, do not influence the convergence of the approximation to the exact value, but the gradient, which in this case is linearly proportional to both K and Δ, is the parameter to control, and obviously the more turns within the finite layer and the acuter these are have a direct translation on the gradient magnitude. This explains the deterioration from the fist case to the last one. This display embodies the lack of necessity of imposing monotonicity requirements on the profile evolution for eq. (3.32) to work.

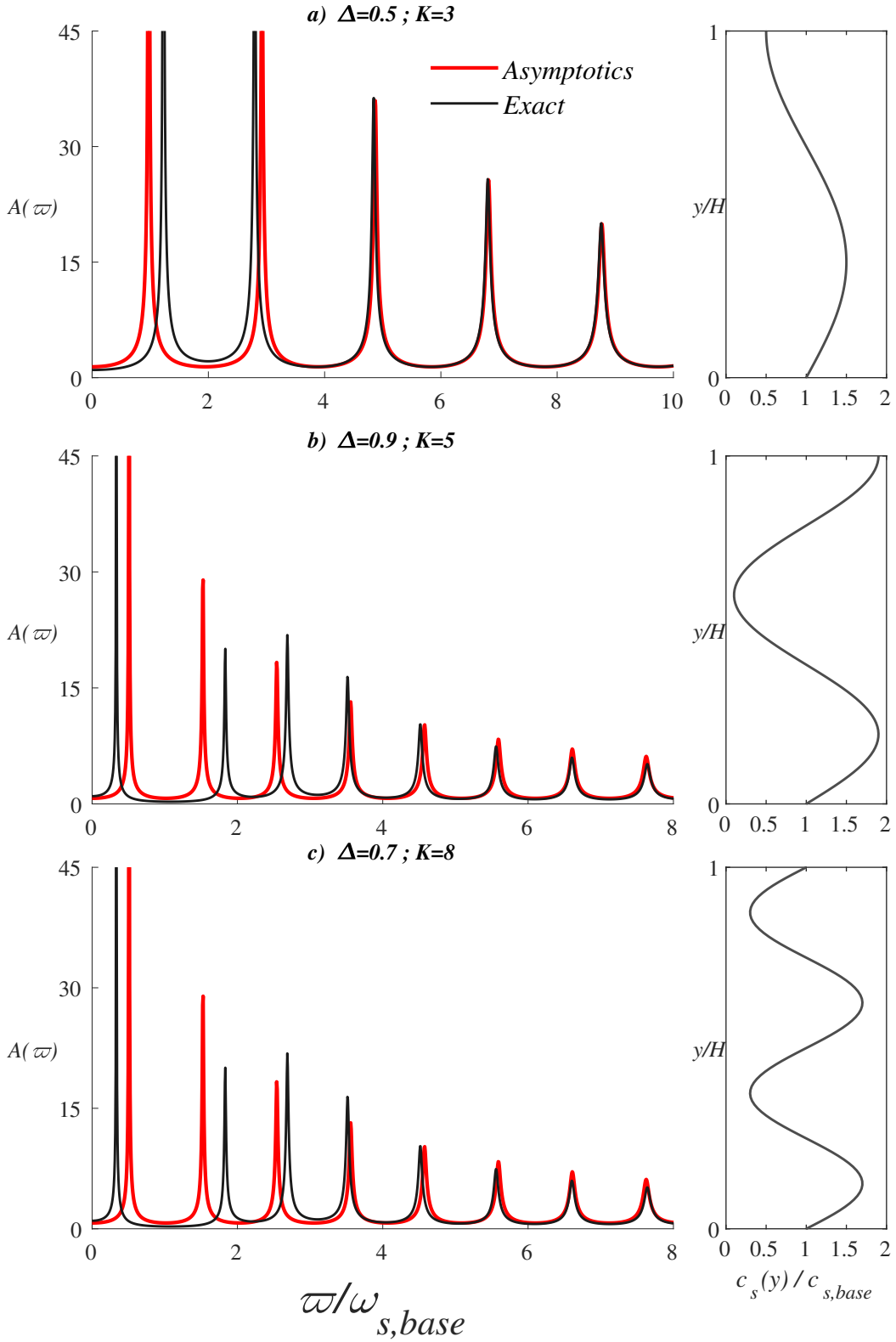

Figure 3.10: Base-to-top dynamic amplification $A(\varpi)$ (with corresponding vertical S-wave profile $c_s(y)$), comparison between numerical solution of eqs. (3.2) and (3.3) (*Exact*) and eq. (3.32) (*Asymptotics*)

3.3.3 Characterization of the first resonant spike

It has been argued that the high-frequency amplification conforming to eq. (3.11) can be described by 3.32 where the equivalent shear-wave velocity is but the harmonic mean of the shear-wave velocity distribution across the stratum. Nevertheless, the fundamental mode remains out of the scope of this result, at least for the cases wherein there is any meaningful heterogeneity, in loose terms, when there is some point for which $f(y)$ is not (even close to) 1.

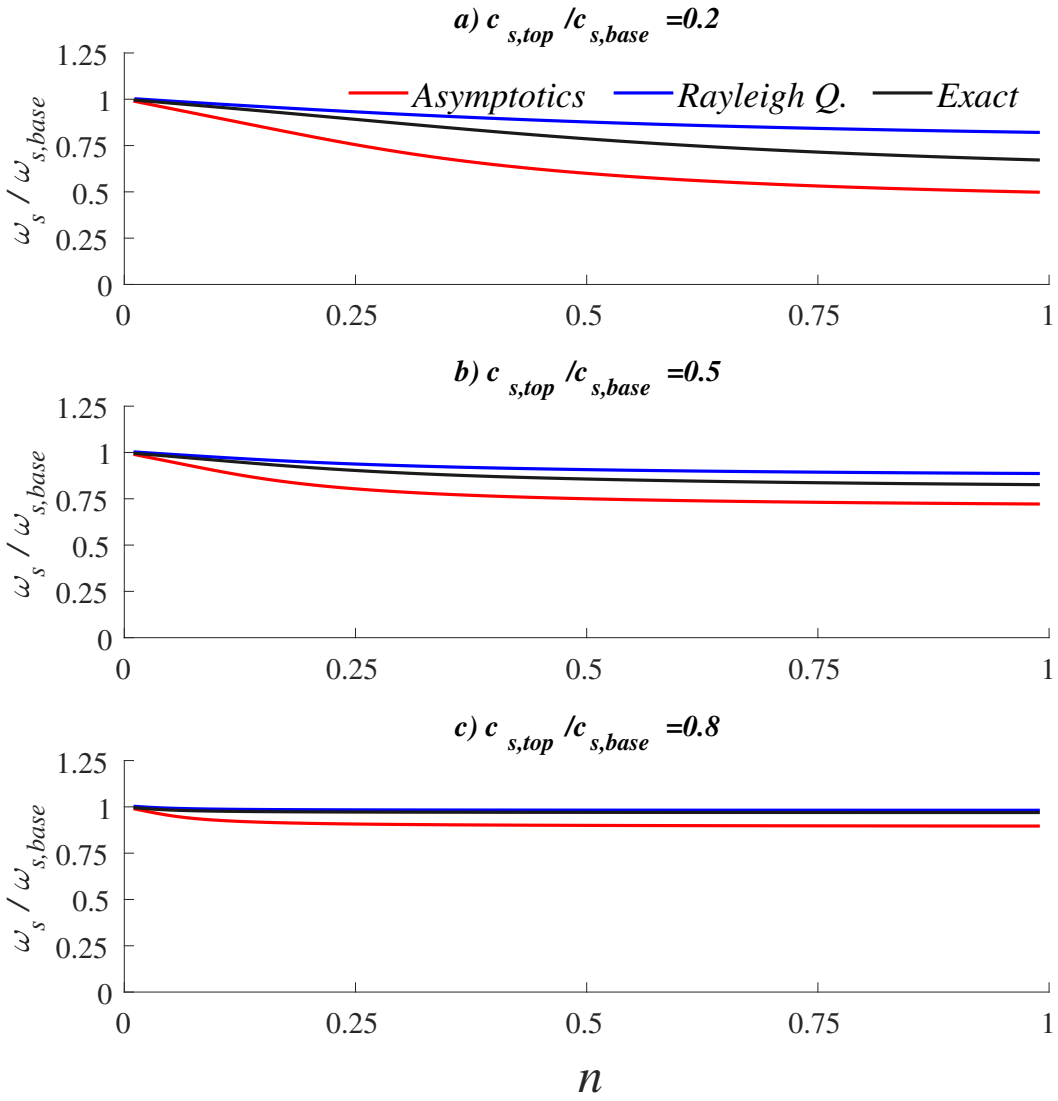

Figure 3.11: Comparison of fundamental frequency: roots of denominator of eq. (3.22) (*Asymptotics*), eq. (3.39) (*Rayleigh Q.*), roots of denominator of eq. (3.17) (*Exact*)

The work by Mylonakis et al.[MRP13] becomes relevant for this reason. The

authors proposed applying the Rayleigh quotient of the governing ODE eq. (3.12), to estimate the natural frequencies (i.e., the eigenvalues of the operator):

$$\mathcal{R}^2 = \frac{\int_0^1 f^2(\eta)\left(\frac{d\psi_1(\eta)}{d\eta}\right)^2 d\eta}{\int_0^1 \psi_1^2(\eta) d\eta} \approx \left(\frac{\omega_s}{c_{s,base}/H}\right)^2 , \tag{3.39}$$

where ψ_1 must be point-wise close to the fundamental shape in order for the estimation to work. The method relies on "guessing" a good approximation of the first mode shape, but it appears that using simple profiles, as parabolic or sinusoidal, fulfils to obtain good results, at least in those models conforming to eq. (3.16) with $\beta < 1$ (softer upper layers). In spite of providing good estimates for the *location* of the first resonance (see fig. 3.11) the method does not provide an amplitude for the resonance peak that accounts for the inhomogeneity.

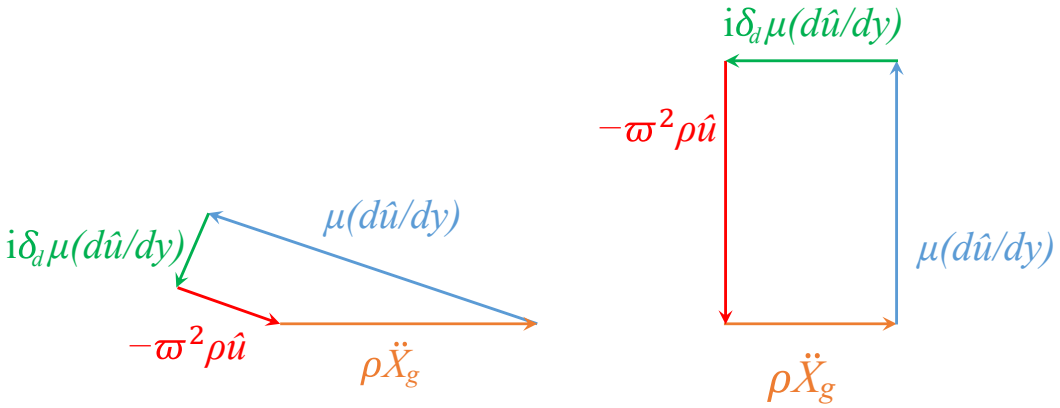

Figure 3.12: Schematic representation of two possible equilibria (red = inertial forces, green = damping forces, blue = elastic forces , orange = external load).

Thus the next approach is proposed: recall eq. (3.12) and that this is but a classic equation of a one-degree-of-freedom system, wherein elastic, damping, and inertial forces team up to balance an external load [HH59].

It may not be so easy to appraise this as the damping is not of viscous type but hysteretic. Let us show this clearly by explicitly substituting $\mu(y)$ by $\mu(y)(1 + i\delta_d)$ in

$$\frac{d}{dy}\left(\mu(y)\frac{d\hat{u}}{dy}\right) + i\delta_d\frac{d}{dy}\left(\mu(y)\frac{d\hat{u}}{dy}\right) + \rho(y)\varpi^2\hat{u} = \rho(y)\ddot{X}_g . \tag{3.40}$$

Now it is easy to recognize each term in the left-hand side: from left to right, the first addend corresponds to elastic forces, the second one to hysteretic damping forces and the third to inertial forces. The right-hand side is the external load.

The diagram fig. 3.12 represents two possible admissible configurations in eq. (3.40):

- To the left, a configuration wherein elastic forces are dominant and hence, for the most part, these take care of balancing the external load. See that elastic force magnitude rely on straining (gradient of displacements), and thus large displacements are not necessarily required to balance the excitation. Damping and inertial forces remain relatively small. See that the phase difference between inertial and elastic forces is π rad, that is, half a period.

- To the right, a configuration we may refer as *resonance*: the elastic forces and the inertial forces reach equal magnitude, and, since they are out of phase, cancel each other, leaving the damping force solely in charge of compensating the external load. Given that δ_d tends to be small ($\delta_d < 1$), it follows that the gradient magnitude must surge to compensate the adverse influence of δ_d, but in this situation the magnitudes of both displacement and displacement gradient are directly linked through the condition of inertia balancing elastic forces, and thus the displacement amplitude surges as well.

In conclusion, let us, from this point onward, consider resonance as the dynamic setting wherein elastic and inertial forces cancel each other (as they attain the same magnitude but their phases are shifted π radians), and thus leaving the damping forces on their own to balance the external loading. In such a scenario we may particularize eq. (3.40) as

$$\mathrm{i}\delta_d \frac{d}{dy}\left(\mu(y)\frac{d\hat{u}}{dy}\right) = \rho(y)\ddot{X}_g \,. \tag{3.41}$$

This equation can be directly integrated if we assume (as it is customary notwithstanding) that the density is constant and $\mu(y)/\rho = c_s^2(y) = (c_{s,base} f(\eta))^2$, and after imposing boundary conditions (3.15) one attains the displacement at resonance

$$\frac{\hat{u}}{X_g} = -\frac{\mathrm{i}}{\delta_d}\left(\frac{\omega_s}{c_{s,base}/H}\right)^2 \int_0^\eta \frac{(1-\eta')}{f^2(\eta')} d\eta' \,. \tag{3.42}$$

There is a consequential presupposition that we must point out before going any further: eq. (3.40) represents equilibrium *point-wise*, that is, the forces therein are forces per unit of volume, not the total force acting on the system. The fact that *at one point* inertial and elastic forces balance does not entail necessarily that the same happens at all points in the cross-section simultaneously. In other words, it is not guaranteed that we are allowed integrate eq. (3.41) to obtain eq. (3.42), and

therefore such result must be considered a simplification. There exists a neat way of realizing this limitation: since elastic and inertial forces are equal, eq. (3.41) can be also written as

$$\mathrm{i}\delta_d \left(-\rho(y)\omega_s^2 \hat{u}\right) = \rho(y)\ddot{X}_g = -\omega_s^2 \rho(y) X_g \,, \tag{3.43}$$

hence an expression for the displacement, alternative to eq. (3.42), can be found from it:

$$\frac{\hat{u}}{X_g} = -\frac{\mathrm{i}}{\delta_d} \,, \tag{3.44}$$

which, evidently, holds at the point level but it cannot be extended to the whole layer as it would not satisfy the boundary conditions at the base. The meaning of eq. (3.44) is interesting: it indicates that a point that is undergoing resonance experiences a relative displacement equal to the displacement at the base divided by the damping factor, and a change of phase of half a period.

Once this discussion has been cleared and the simplification accepted, let us proceed to study the top to obtain the amplification during resonance:

$$A(\omega_s) = 1 + \frac{1}{\delta_d}\left(\frac{\omega_s}{c_{s,base}/H}\right)^2 \int_0^1 \frac{(1-\eta)}{f^2(\eta)} d\eta \,. \tag{3.45}$$

Note how the integral provides an amplification radically different to the one of the high-frequency regime: the amplitude of eq. (3.32) at resonance scales as the square-root of the base-to-top contrast, whereas in this case, the whole heterogeneity distribution affects as revealed by the integral in eq. (3.45). Let us take a moment to carefully assess this integral: the amplitude at resonance depends not on the shear-wave velocity distribution, $f(\eta)$, but on the distribution of the compliance, the inverse of the shear modulus $1/f^2(\eta)$, and it is also averaged linearly over the stratum, favoring the compliance of the lower layers ($\eta \approx 0$) over layers close to the surface ($\eta \approx 1$).

In addition, see how in these developments we have not required of continuity or smoothness conditions to be laid over the distribution of shear-velocity $f(\eta)$. We request but for the function to be positive (so we can invert it) and that its inverse can be integrated. Nothing stop us from using this expression to deal with layered stratum where there are stark contrasts between layers. Let us therefore assume that we also had a (potentially discontinuous) distribution of density and damping, $\rho(y)$ and $\delta_d(y)$, in addition to $\mu(y)$, and thus starting from eq. (3.41) we reach the

corresponding analogue of eq. (3.45):

$$A(\omega_s) = 1 + \omega_s^2 \int_0^H \frac{F(y)}{\mu(y)} d\eta \,, \tag{3.46}$$

where $F(y)$ represents

$$F(y) = \int_H^y \rho(y')/\delta_d(y') dy' \,, \tag{3.47}$$

where y' represents a dummy integration variable.

It still remains to identify the value of the fundamental frequency. The estimate provided by the Rayleigh quotient, eq. (3.39), could be used. Hence, assuming once again the stiffness varies whereas the density and the damping stay constant across the stratum, we propose the following estimate for the fundamental frequency

$$A(\omega_s) = 1 + \frac{\mathcal{R}^2}{\delta_d} \int_0^1 \frac{(1-\eta)}{f^2(\eta)} d\eta \,. \tag{3.48}$$

This estimate is completely general, but it requires a good guess of the mode shape (what may be difficult to ascertain in complex profiles presenting "reversal", i.e., soft intermediate layers).

In order to check this estimate, consider homogeneous stratum, $f(\eta) = 1$, and the exact mode shape $\sin(\pi\eta/2)$:

$$A_{hom}(\omega_s) = 1 + \frac{1}{\delta_d} \frac{\pi^2}{8} \approx \frac{1.23}{\delta_d} \,, \tag{3.49}$$

where 1 has been neglected as it will be much smaller than the second, since $\delta_d \ll 1$. Comparing to the value suggested by Roesset [Roe77], that is, $4/\pi\delta_d \approx 1.27/\delta_d$, it seems that, as it also happens in viscously-damped 1-dof systems [CP92], the maximum amplitude is slightly shifted towards a higher frequency due to the presence of damping. Nevertheless, the estimate, at least in this case, yields a value just about a 3% smaller.

3.3.3.1 Results concerning profiles with gradients of mechanical properties localized in upper layers

Focusing our attention now to profiles given by eq. (3.16), particularly those with $n << 1$.

In many practical cases, there is evidence of substantial stiffness changes being confined in a narrow region close to the surface; once this first zone of rapid growth

of stiffness is left behind, the stiffness continues increasing with depth yet at slower pace. This behavior adjusts to values of the inhomogeneity factor $n \leq 0.1$.

Let us re-assess eq. (3.48) bringing this fact to bear.

a) In first place, as $\mathcal{R}$ depends on the integral of the mode shapes, if most inhomogeneity is intensely localized in a narrow upper layer, wheres in the rest of the domain is similar to the one at the base, it seems logical to assume that the shape will resemble the one of the homogeneous profile except at a narrow region at the top. However, as the quotient entails a *global* comparison to the exact shape (through the integral), as opposed to point-wise local comparison, then we argue the value of the integrals will not differ too much from the one of the homogeneous stratum with properties as at the base, and hence $\mathcal{R} \approx \pi/2$.

b) A similar, even-more-convincing argument can be leveled at the integral factor in eq. (3.45): see how the integral was argued to represent an averaged compliance wherein the weights start from zero at the surface and increase the deeper the point under consideration; this means the integral weights automatically diminish the contribution of the upper narrow region where the stiffness differ the most from the one at the base. Hence, under these circumstances, this integral value must be controlled by the value at the base (which has the most favorable weighting and it is, by the assumption $n \leq 0.1$, the largest), then the integral value must be close to the value corresponding to $f(\eta) = 1$ (the whole stratum having base stiffness).

Let us deploy this arguments within eq. (3.48):

$$A(\omega_s) \approx 1 + \frac{\pi^2}{4\delta_d} \int_0^1 \frac{(1-\eta)}{1} d\eta = 1 + \frac{\pi^2}{8\delta_d} \,. \tag{3.50}$$

This is the same result that we obtained in eq. (3.49), that is, when we used the formula to calculate the amplification corresponding to the homogeneous layer.

In conclusion, for the case when n is relatively small, the behavior of the inhomogeneous stratum shall resemble the one of the homogeneous one having by properties those of the bottom (base) layer. Under these premises, the response of the fundamental mode can be considered, in the first instance, as independent of both the contrast, i.e., β, and the particular shape of the distribution of shear-wave velocity, i.e., n.

For instance, compare the value that the estimate would deliver for the fundamental mode in the previous plots ($\delta_d = 0.05$), in next table

	Top-to-base contrast (β)		
Inhomogeneity factor (n)	0.1	0.5	0.9
0.9	33.8	27.2	25.6
0.5	30.8	27.1	25.5
0.1	26.0	26.0	25.5

Table 3.5: Amplitudes at the fundamental mode in figs. 3.4 to 3.6

to the estimate from eq. (3.50):

$$A(\omega_s) \approx 1 + \frac{\pi^2}{8 \cdot 0.05} \approx 1 + \frac{1.23}{0.05} = 25.6\,. \tag{3.51}$$

The maximum error, is 24.3% (amplitude is underestimated), but it corresponds to $n = 0.9$ and $\beta = 0.1$, a 90% decrease in stiffness happening almost linearly, then the premises upon which the reasoning was developed (gradient localized at the top) does not hold in any way. Is interesting to note that for $n = 0.5$ still get less than 6% error (underestimation), we ascribe this to the helpful effect on the weight in the integral factor.

Clearly, the trends that were predicted are the ones observed.

All the prior results concern $\delta_d = 0.05$. Since we have data on the influence of damping available in table 3.4 and fig. 3.7, corresponding to a convenient value of $n = 0.5$, let us use the information concerning the fundamental modes to test eq. (3.50) even further. We shall use $A_{exact}(n = 0.5, \beta, \delta_d)$ to represent the evaluation of eq. (3.17) then to be compared to the result that eq. (3.50) yields.

$$A_{exact}(n = 0.5, \beta = 0.1, \delta_d = 0.15) = 9.1\,, \text{compare to } A(\omega_s) \approx 1 + \frac{1.23}{0.15} = 9.2\,, \tag{3.52a}$$

$$A_{exact}(n = 0.5, \beta = 0.5, \delta_d = 0.10) = 13.7\,, \text{compare to } A(\omega_s) \approx 1 + \frac{1.23}{0.15} = 13.3\,, \tag{3.52b}$$

$$A_{exact}(n = 0.5, \beta = 0.9, \delta_d = 0.05) = 27.2\,, \text{compare to } A(\omega_s) \approx 1 + \frac{1.23}{0.15} = 25.6\,. \tag{3.52c}$$

The last result is redundant (it is already in table 3.5) but it is shown anyways for completeness sake. The error ranges from -1.1% to a 5.8%.

Extension to discontinuous velocity profile

Hitherto, everything has been referred to profiles under the umbrella of the "generalized parabola", eq. (3.16), but, as it has already been discussed, one could work directly with the down-hole data since there are no requirements of any kind over continuity in mechanical properties profile. The estimate (3.50) should work well if the same conditions discussed above are met: heterogeneity concentrated in upper layer.

In order to illustrate this point, let us pick three real profile from the Kiban-Kyoshin Network (*KiK-net*) database [Oka+04]. One being used corresponds to Kasumigaura station (Ibaraki prefecture), code name IBRH17, another one from Taiki (Tokachi Subprefecture, Hokkaido) and the last one from Ishige (Yuki District, Ibaraki Prefecture). The available borehole data is displayed in the next tables:

No.	Thickness (m)	Depth (m)	c_p (m/s)	c_s (m/s)
1	1.00	1.00	160	90
2	9.00	10.00	500	250
3	80.00	90.00	1700	380
4	145.00	235.00	1700	470
5	65.00	300.00	1900	540
6	80.00	380.00	1900	660
7	80.00	460.00	2100	820
8	–	–	5300	2300

Table 3.6: Information concerning KiK-net site IBRH17

No.	Thickness (m)	Depth (m)	c_p (m/s)	c_s (m/s)
1	4.00	4.00	300	130
2	32.00	36.00	1850	480
3	42.00	78.00	1850	590
4	22.00	100.00	5000	2800

Table 3.7: Information concerning KiK-net site TKCH08

No.	Thickness (m)	Depth (m)	c_p (m/s)	c_s (m/s)
1	20.00	20.00	540	110
2	170.00	190.00	1560	380
3	220.00	410.00	1800	530
4	108.00	518.00	2150	850
5	182.00	700.00	4360	2350
6	–	–	0	0

Table 3.8: Information concerning KiK-net site IBRH10

Let us consider the last layer in each case as rigid bedrock, then calculate the transfer function numerically as detailed in section 2.6.3.1. The calculation result is contained in fig. 3.13, the damping values used have been $\delta_d = 0.147$ for IBRH17, 0.068 for TKCH08 and 0.035 for IBRH10.

The numerical amplitude of the fundamental mode is, from the first to the third case, 9.34, 20.54, and 37.87, whereas the estimate eq. (3.50) yields 9.38, 19.09, and 36.25, and thus the error ranges from less than 1% to less than 8% at most. It is instructive to note that the estimation is accurate in spite of the natural frequency being far from the one of the homogeneous stratum with $c_{s,base}$, as it can be readily seen from fig. 3.13.

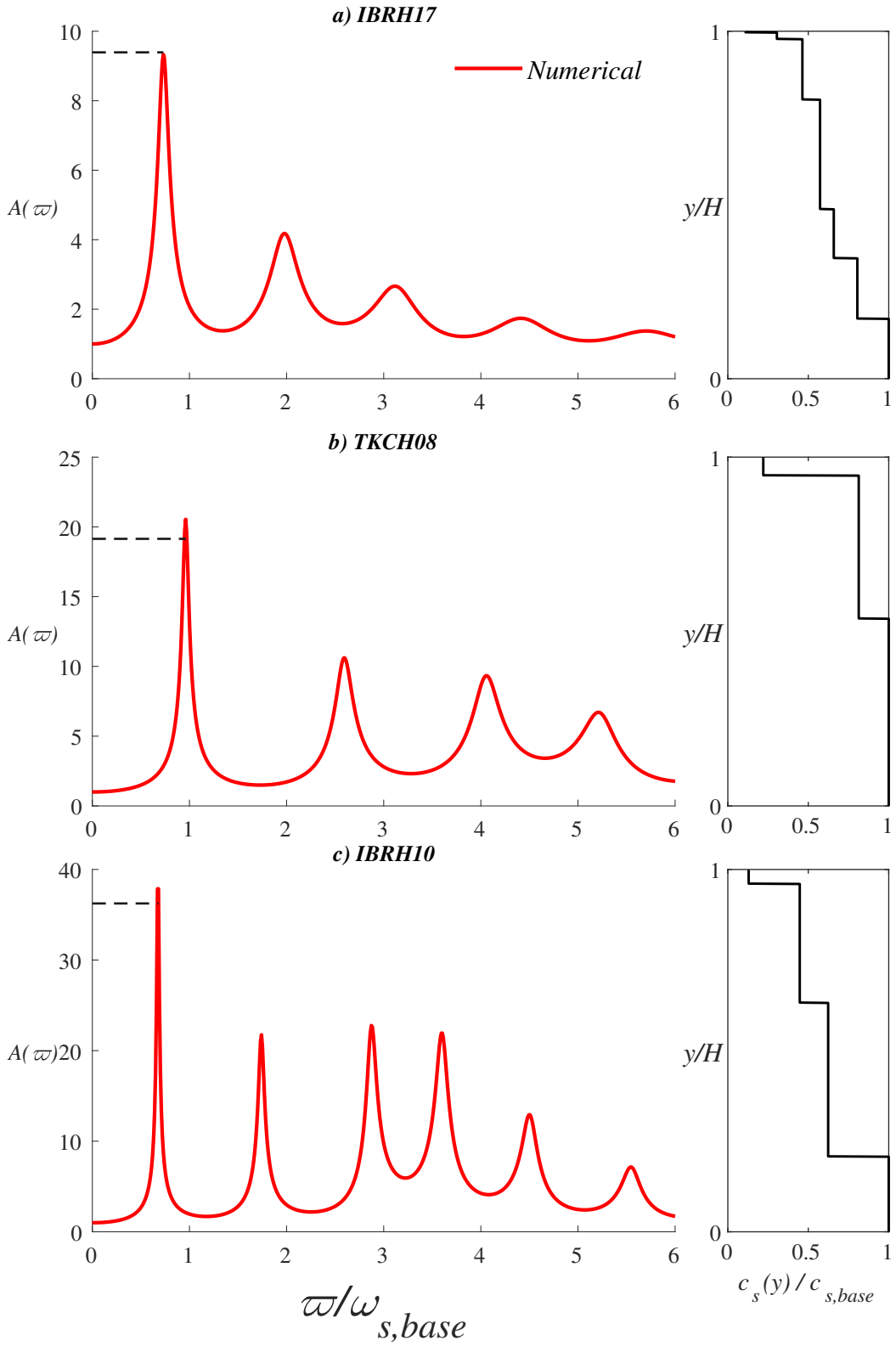

Figure 3.13: Transfer function and profile corresponding to KiK-net sites (discontinuous line marks the estimate eq. (3.50)).

3.4 Disclaimer: on the scope of these results

These novel results have been derived upon three strong pressumptions:

1) Rigid bedrock, therefore the contribution of radiation damping is being effectively neglected.

2) Steady-state frequency domain analysis, which allow us to work with standing waves instead of trasiently propagating waves.

3) Linear-viscoelastic soil response.

These assumptions clearly delimit the range of validity of the results derived in this chapter.

Should the first assumption be the one not met, the results can still be used and considered as an upper bound in terms of maximum amplification that could take place (the presence of radiation damping would take energy away from the stratum and would decrease the top-to-base amplification). The tightness of the bound will depend on the impedance contrast between the last layer and the rock base, the tighter the lower the contrast.

The second assumption requires for the stratum thickness to be short enough as to allow waves to "fill it" rapidly, so much so that transient effects can be overlooked [Sar94], establishing an effective steady-state (any transient effect vanishes) depicted as the standing-wave we have assumed. Were we using Fourier series to decompose a complex excitation, this point should be kept in mind when handling the results.

The last assumption limits the range of validity of earthquake intensities that may fit in the description. Strong shake would elicit a non-linear response of the soil, what would require further painstaking description and analysis [Kak+15]. Nevertheless, these viscoelastic solutions may still be used as an upper bound, should the other two conditions be met. We will provide a criterion to gauge the linearity assumption adequacy in section 4.2. This criterion takes only the PGA and the soil stiffness.

3.5 Coda: on the connection to Soil-Structure Interaction

These results pertain to the discipline of 1D Site Response proper, but, as it has been argued, they find applications and some natural extensions in the field of SSI.

On some direct applications, let us point out that the current recommendations [NIS12] by the National Institute of Standards and Technology (NIST) regarding

SSI instruct the use of the harmonic mean of shear-wave velocity distribution when considering rocking, swaying and other phenomena regarding the response of foundations resting over heterogeneous soil. This recommendation may be re-evaluated in light of the new results (e.g. eqs. (3.32), (3.45) and (3.50)) contained in this chapter: it appears to be unfitting to use the harmonic mean of the velocity distribution as the equivalent one for the whole range of excitation frequencies, this choice should be limited to specific combinations of frequency, soil mechanical properties c_s and depth to bedrock H. When it comes to consider the amplitude of the fundamental mode, properties of the soil layer in contact with the bedrock may be used in sites where most change is concentrated closer to the surface layers.

Talking about extensions, the discussion in section 3.2.1 concerning the interpretation of provides rationale to consider quasi-static earth pressures on retaining walls in their own right, and not as a mathematical trinket [KLM12].

The main two gains from this chapter are a new approach to the high-frequency regime based and an analytical assessment of the fundamental resonance mode. Both approaches can potentially be extended, for instance, to the determination of seismic pressures on underground structures.

Chapter 4

SEISMIC PRESSURES ON BURIED STRUCTURES: A COMPREHENSIVE APPROACH AND TWO PARTICULAR CASES

In this chapter we shall address the following items:

- The problem of determining the forces acting over buried structures when a seismic event occurs is considered. A general geometrical configuration and parameters will be presented and scrutinized in light of Buckingham's Π Theorem.
- The Younan-Veletsos [VY94b] problem is related to the general scenario. The problem's exact solution is presented. The qualitative behavior of the system is discussed.
- An extension of the Younan-Veletsos problem wherein the structure does not rest directly on rigid bedrock is considered under certain simplifying assumptions.

4.1 Overarching assessment of seismic pressures on underground structures

The objective of this section is to assess the problem of seismically-induced pressures on structures either totally or partially embedded within the soil, in a rather general way. We shall begin with a brief review of the state of the art. Once that the modelization of each subsystem has been agreed, Dimensional Analysis will be invoked as to elucidate the role of each parameter. Along the chapter, many simplifications based on specific values of dimensionless groups stemming from Dimensionl Analsysis will be discussed.

4.1.1 Previous work

The study of underground water reservoirs by means of analytical methods has remained somewhat limited, as the complexity of the system plays a dissuading role.

Before moving into the releveant literature, we must mention the line of work pioneered by Prof. Housner [Hou57a] that considered the effects of fluid-structure

interaction on elevated fluid tanks. Thanks to efforts on this regard, the role of fluid pressure on the vessel is already well understood. Moreover, further research concerning fluid-structure-soil interaction in dams [MD89; DM89] provides acumen on the effect of adding the soil domain to the picture.

Although there has been a fruitful push towards characterizing the response of underground tunnels [Has+01] and pipes [Dav03b], the typology that concerns us here does not fit under the same umbrella. Thereby, Davis [Dav03a] proposed a method for evaluating the lateral forces induced by vertically-propagating seismic shear waves on rigid buried structures within a inhomogeneous half-space. The current state-of-the-art model was developed by Brandenberg and collaborators [BMS15], and combine results derived for retaining walls [KLM12] and foundations [Gaz91], properly tuned to render the model coherent to the actual geometrical configuration.

Recent experiments carried out at the centrifuge facility at University of Colorado Boulder [Hus+16b] explored the influence of different features and compared experimental response to the available analytical assessment methods. The capacity of linear-elastic methods to capture main traits of the transient response obtained from these experiments was demonstrated by means of numerical simulations performed by Prof. Esmaielzadeh Seylabi and collaborators [Sey+18].

By and large, aforementioned analytical results rely on studying portions of the structure (walls and base) independently in order to later assemble them. There are no available results derived from direct considerations of the full model of an underground water reservoir. This chapter may be considered as an initial move to amend this circumstance.
First, we shall provide, by aid of Dimensional Analysis, a comprehensive framework in which the problem may be systematically considered. Then we shall focus on the specific case corresponding to the Younan-Veletsos problem, the very same simplification that other researchers have used to consider the walls independently from the rest of the structure. Finally, a first, admittedly-oversimplified, result will be derived for a more complex configuration resembling closely a realistic scenario.

4.1.2 Presentation of Dimensional Analysis

Dimensional Analysis has been a critical element in the physicist's and engineer's toolbox since the 19^{th} century. It has been successfully applied by many including some of the most relevant names in Physics, see for instance [Cle90], [Str15]. Even

though the name is Buckhingham is traditionally associated to it, it is also ascribed with Vaschy, Robachinski, and others [Gib74]. Its renown arises from the deep and consequential connections that reveals, which intertwine the reality as the scientist strives to understand it to the mathematical models devoted to the purpose.

Dimensional Analysis provides a formal procedure to assess the influence of the parameters of a system on the response, even if the form of the underlying equation connecting them remains unknown. Its deepest underpinning can be considered to be the realization that *the laws of Nature can not depend on either the particular frame of reference or the system of units that one chooses to express them*. As a consequence, the nondimensional response has to depend on the parameters through dimensionless combinations of them, as it has to be indifferent to the system of units we use in our prosaic computations.

This method is widely applied for experiment design and in several research fields (see, e.g., [Zlo12; Kur13; Hor13]), since it is capable of yielding insight on the behavior of systems that require many parameters to be described, as it reduces the relevant parameter space by positing how each physical quantity must relate to the others to configure the response of the system. The dimensionless response comes given as a function of dimensionless groups of parameters. Such groups are obtained through the celebrated Buckingham's theorem [Lan51], which also provides the formal framework to introduce new dimensionless parameters to replace others.

By this as it may, there exists, still nowadays, a lack of familiarity to such a versatile tool among the geotechnical earthquake engineering and soil dynamics communities. Quoting Kausel [Kau13]:

> *An additional important lesson to be learned in Soil Dynamics – a lesson which is well known in other areas of science and engineering – is that dimensional analysis can be of invaluable help in establishing the form of some physical phenomena, but it cannot guarantee that such formulas will be physically meaningful.*

The exception to the rule seem to be the geotechnical experimentalists [ITN05; Woo14], an elegant application put forward by Gibson during the course of his Rankine Lecture[1] [Gib74], and the recent work by Conti and collaborators [CMV17],

[1] It is indeed enlightening to revisit this particular line: "By Riebouchinski's theorem (Buckingham, 1921) or by employing *reasoning encountered in elementary fluid mechanics*, these dimen-

wherein Dimensional Analysis is effectively used to judiciously reduce the parameter space concerning foundation motion filtering.

4.2 Application of Dimensional Analysis to underground water reservoirs

Dimensional Analysis [RS05] will be applied to the most general scenario, so that the different cases to be considered later can be related to certain combinations of the non-dimensional parameters.

Systems as our object of study are made up of three main subsystems or subcomponents, namely, the reservoir structure itself, the water enclosed within the reservoir, and the soil that confines the structure. All these are jostled by a propagating wavefront, elicited by a seismic event.

The response of the system is defined by the properties of the subsystems, and on how they are coupled to each other. These features can be modeled in a number of ways, but any modelization is composed of certain physical parameters, and the global response will depend on the set of parameters in each subsystem and those parameters defined at the contact interfaces: soil and structure, and fluid and structure.

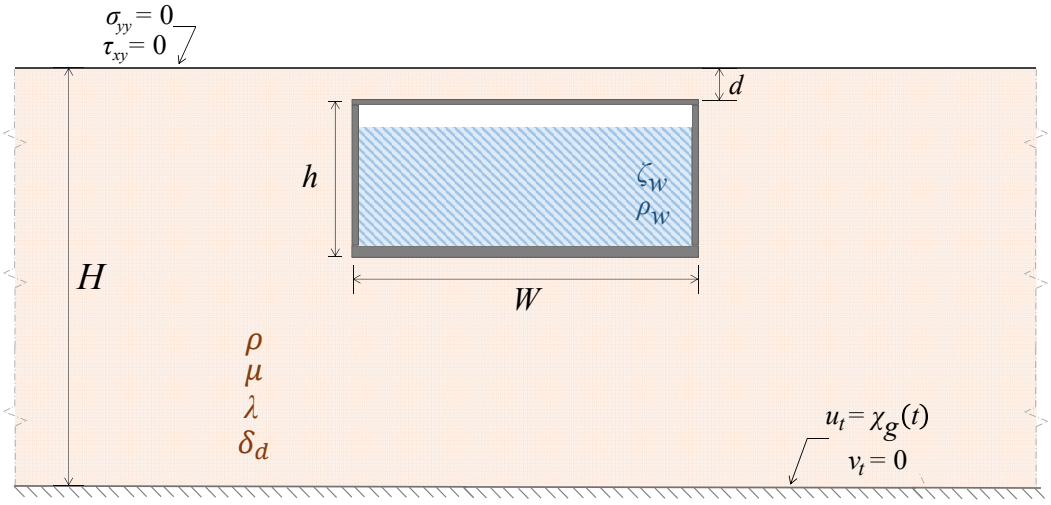

Figure 4.1: Schematic representation of a representative cross-section of the system being surveyed, including some relevant parameters

As our earliest simplification, let us say that the conditions at interface of two subsystems do not add extra parameters to the count; for example, we shall not

sionless groups must be connected functionally by a relation of the form [...]". The conception of Dimensional Analysis as a gizmo concerning fluid mechanics, first and foremost.

pursue considerations of friction between the wall ad the soil, nor roughness of the wall influencing the flow.

A second simplification, another parameter that has been purged away from the kick-off, is gravity itself. Gravity is critical in the study of these structures, as it enables the static forces that act simultaneously to dynamic ones during a seismic event and is also the agent in charge of consolidating the soil around or below structures. In any case, effects from gravity and seismic accelerations can be considered independently under the pretext of linearity. Therefore, we aim to develop a framework for the assessment of the dynamic increment of pressures over the structure, leaving the geostatics pressures to be appraised by other means.
Additionally, we shall not pursue considerations of vertical seismic accelerations, only horizontal ones.

Let us perform a survey of the rest of parameters before moving into the procedural application of Dimensional Analysis:

- Soil: for the purpose of this section, it will be assumed that the soil can be described as an homogeneous linear-elastic isotropic solid. As it is well-known, the response of such a material is characterized by two material constants, e.g., the so-called Lamé constants, μ (shear modulus) and λ, see eq. (2.14). The ratio between these two is a function of the soil Poisson's ratio, ν, and thus one of the Lamé constants can be replaced by it; this is precisely what will be done, considering μ and ν as the constants describing the soil response instead of μ and λ.
  Additionally, there is necessity of modeling internal dissipation within the soil. As mentioned before, when working in frequency domain or when assuming steady-state cyclic time response, the soil is assumed to behave as a viscoelastic material, whose internal dissipation can be modeled by means of a loss modulus, which relates to the shear modulus by means of the hysteretic factor δ_d. Considering more complex descriptions of the soil is always possible, at the expense of using a more involved consitutive law and increasing the number of parameters used in the characterization.

- Reservoir: underground structures as this have traditionally been built with reinforced concrete. An exhaustive quantitative description of the response of structural members made of this material, when subjected to complex, realistic loading, is certainly a challenge, owing to the highly-nonlinear re-

sponse of both the concrete (which includes the appearance and propagation of cracks even for low relatively amplitude loads) and the steel rebars (plastic yielding occurring at high load levels). Such detailed modelization would require oodles of parameters. In order to carry out a first approximation while keeping the parameter space in an amenable size, let us assume that the deformation of the structure will be limited so that the behavior can be described by means of the linear-elastic theory of thin plates, so-called Kirchoff-Love plate theory [Den87]. Under the tenets of this theory and the assumption of material isotropy (unrealistic yet still included for tractability sake), the relation between forces acting on the structure and the deflection of the middle plane of the walls and slab takes place through one parameter, which encompasses material and geometric properties, referred to as plate's flexural rigidity, D_p. This parameter depends on the mechanical properties of the material the members are made of and on the element's thickness. The material is being assumed to be homogeneous linear-elastic and isotropic, therefore its mechanical response can be described by (subscript "p" stands for plate) its shear modulus, μ_p and its Poisson's ratio ν_p, and its inertia by its density ρ_p (this is a regular density, not mass per unit of length). The thickness of the members is referred to as t_p. The relation between these parameters and the flexural rigidity is

$$D_p = \frac{\mu_p t_p^3}{6(1-\nu_p)}\,. \tag{4.1}$$

One must highlight the "quick" (cubic) scaling of this rigidity with the wall thickness, t_p. Thus, the relevant properties of the local structural mechanics can be condensed in four parameters: D_p, ρ_p, μ_p, and ν_p. Information about the reservoir geometry, h (wall height), W (in-plane width) and W_z (out-of-plane width), completes the description of this subsystem (note that only prismatic shapes fit in the current description). The positioning of the reservoir with respect to the layer is described by the parameter d, depth at which the upper surface of the reservoir lays, and H, stratum height, are introduced. $d = 0$ would correspond to an excavation, whereas $H = h$ corresponds to the structure base resting directly on the rigid bedrock.

- Water: it will be assumed that the medium contained in the reservoir is water at normal conditions of both pressure and temperature. Under these conditions, the fluid properties are density ρ_w (assumed to be constant in

space and time as the fluid is incompressible) and the kinematic viscosity ζ_w. The flow conditions will be discussed later, yet one may foresee that the flow will correspond to high Reynolds number. Sloshing and other more advanced considerations [Hou57a] are left out of the scope of this study and laid out as potential future work.

- Seismic load: this subcomponent of the problem requires thorough commentary as its characteristics arbitrate the response of the other subsystems. An all-encompassing characterization of the seismic excitation is a phenomenal task relying on seismologists and geophysicists, for the most part. For the aim of this study, information about the wavefront propagating within the soil bulk is desirable. However, oftentimes only information at the surface is available and bulk characteristic can be obtained at the expense of dealing inverse problems [JE18].

  Despite this first characterization challenge, let us assume that one had a complete description of the time evolution of the wavefront as a superposition of harmonics of certain amplitudes and frequencies. Some kind of linearity could be invoked at every instance, and the principle of superposition summoned to allow the decomposition of the response of the system as a superposition of the individual harmonic responses, by assuming the load amplitudes, and the displacements that it would elicit, were to be small enough. The drawback of such approach, which necessitates of linearity, is that it limits the intensity of the earthquakes that can be considered. Since in this first section we will retrain the scope to Dimensional Analysis considerations, one could compromise to simply considering a characteristic value of the amplitude $\ddot{X}_g$, representing e.g. the *peak ground acceleration* (PGA) that was recorded at a ground station, which may vary from imperceptible to up to ~ 3 g [Fur+11], and a characteristic value of frequency, ϖ, that could vary in the customary range for seismic excitation: from 0.1 Hz to 10 Hz. This will be enough for what the ensuing discussion concerns. The linearity assumptions shall be recovered later as a consequence of Dimensional Analysis and as a condition *sine qua non* it would be much harder to attain closed form expressions. We provide a criterion to gauge, in terms of PGA and soil stiffness, if assuming linearity is fitting or not, see eq. (4.10b).

  For the purpose of this work, it will be assumed that the seismic motion comes in terms of S-waves, propagating perpendicularly to the horizontal free-surface, therefore the incidence angle will not be considered as a param-

eter either.

A summary of the parameters in the problem is displayed in the following table:

Parameters		
Label	Dimension	Description of the physical variable
h	L	Reservoir wall height.
H	L	Distance from free surface to rock bedrock.
W	L	In-plane reservoir base length.
W_z	L	Out-of-plane reservoir base length.
d	L	Reservoir burial depth.
μ	$ML^{-1}T^{-2}$	Shear modulus of soil.
ν	$-$	Poisson's ratio of soil.
δ_d	$-$	Soil hysteretic damping factor.
ρ	ML^{-3}	Soil density.
ζ_w	L^2T^{-1}	Water kinematic viscosity.
ρ_w	ML^{-3}	Water density.
D_p	ML^2T^{-2}	Structure flexural rigidity.
μ_p	$ML^{-1}T^{-2}$	Shear modulus of reinforced concrete.
ν_p	$-$	Poisson's ratio of reinforced concrete.
ρ_p	ML^{-3}	Reinforced concrete density.
$\ddot{X}_g$	LT^{-2}	Wavefront characteristic amplitude (acceleration).
ϖ	T^{-1}	Wavefront characteristic frequency.

Table 4.1: The n-physical parameters of the soil-structure-interaction problem to be considered through dimensionless analysis.

Thus, the system response shall be characterized through these 17 parameters henceforth. Recall that to complete this set one should have added the incidence angle (taken to be equal to zero with respect to the vertical in this case), gravity, and whatever parameters were to be defined at the interface between subsystems.

For illustration purposes, the total thrust acting on a wall per unit of length of wall in z-direction, Q, will be the output considered in this section, yet a similar process could be carried out for any other dependent variable. Let us take advantage of its

mention to introduce its components

$$Q_x = \int_{H-h}^{H} \sigma_{xx}|_w dy\,, \tag{4.2a}$$

$$Q_y = \int_{H-h}^{H} \tau_{xy}|_w dy\,, \tag{4.2b}$$

and itself proper as the modulus of the vector having these two components

$$Q = |\boldsymbol{Q}| = \left| \int_{H-h}^{H} \boldsymbol{t}|_w dy \right| = \left(Q_x^2 + Q_y^2 \right)^{1/2} . \tag{4.3}$$

Therefore,

$$Q = Q(h, H, W, W_z, d, \mu, \nu, \delta_d, \rho, \zeta_w, \rho_w, D_p, \mu_p, \nu_p, \rho_p, \ddot{X}_g, \varpi)\,. \tag{4.4}$$

Let us choose a dimensional basis made up by h, $\ddot{X}_g$ and ρ, and thus a characteristic length is h, a characteristic time $\sqrt{h/\ddot{X}_g}$ and a characteristic mass ρh^3. Using this basis, eq. (4.4) in dimensionless form becomes

$$\begin{aligned} \frac{Q}{\rho \ddot{X}_g h^2} = \tilde{Q}\Big(& \frac{H}{h}, \frac{W}{h}, \frac{W_z}{h}, \frac{d}{h}, \frac{\mu}{\rho \ddot{X}_g h}, \nu, \delta_d, \\ & , \frac{\zeta_w}{h^{3/2} \ddot{X}_g^{1/2}}, \frac{\rho_w}{\rho}, \frac{D_p}{\rho \ddot{X}_g h^4}, \frac{\mu_p}{\rho \ddot{X}_g h}, \nu_p, \frac{\rho_p}{\rho}, \frac{\varpi}{\sqrt{\ddot{X}_g / h}} \Big) = \\ = \tilde{Q}\,(& \Pi_1, \Pi_2, \Pi_3, \Pi_4, \Pi_5, \Pi_6, \Pi_7, \Pi_8, \Pi_9, \Pi_{10}, \Pi_{11}, \Pi_{12}, \Pi_{13}, \Pi_{14})\ ; \end{aligned} \tag{4.5}$$

thus the non-dimensional response depends on fourteen dimensionless Π groups. Before proceeding, let us perform some algebra on the Π groups to come up with better-suited dimensional groups:

1) Define $\Pi'_8 = \Pi_8 \Pi_{14} / \Pi_2 = \zeta_w \varpi / W \ddot{X}_g$ to replace Π_8.

2) $\Pi'_{14} = \Pi_{14} \Pi_1 / \sqrt{\Pi_5} = \varpi / \sqrt{\mu / \rho H}$ substitutes Π_{14}.

3) $\Pi'_{13} = \Pi_{14} \sqrt{\Pi_{13} / \Pi_{10}} = \varpi / \sqrt{D_p / \rho_p h^5}$ replaces Π_{13}.

4) $\Pi'_9 = \Pi_9 \Pi_2 / \Pi_{14}^2 = \rho_w \ddot{X}_g / \rho \varpi^2 W$ enters so that Π_9 can be removed.

5) Finally, $\Pi'_{10} = \Pi_{10} / \Pi_5 = D_p / \mu h^3$ substitutes Π_{10}.

Thus,

$$\begin{aligned}\frac{Q}{\rho\ddot{X}_g h^2} = \tilde{Q}\Big(&\frac{H}{h}, \frac{W}{h}, \frac{W_z}{h}, \frac{d}{h}, \frac{\mu}{\rho\ddot{X}_g h}, \nu, \delta_d, \\ &, \frac{\zeta_w \varpi}{W\ddot{X}_g}, \frac{\rho_w \ddot{X}_g}{\rho\varpi^2 W}, \frac{D_p}{\mu h^3}, \frac{\mu_p}{\rho\ddot{X}_g h}, \nu_p, \frac{\varpi}{\sqrt{D_p/\rho_p h^5}}, \frac{\varpi H}{\sqrt{\mu/\rho}}\Big) = \\ = \tilde{Q}&\left(\Pi_1, \Pi_2, \Pi_3, \Pi_4, \Pi_5, \Pi_6, \Pi_7, \Pi'_8, \Pi_9, \Pi'_{10}, \Pi_{11}, \Pi_{12}, \Pi'_{13}, \Pi'_{14}\right) .\end{aligned} \tag{4.6}$$

These are the working Π groups the system response shall be referred to. Let us analyze the physical meaning of each of them, and point some assumptions concerning them.

- $\Pi_1 = \frac{H}{h}$: this geometric ratio discloses the relation between wall and stratum heights. It is obvious that $\Pi_1 \geq 1$ always, $\Pi_1 = 1$ corresponding to structure resting directly on bedrock. The diametric limit, $\Pi_1 \to \infty$ corresponds to a scenario where the structure is resting on a elastic sub-space.

- $\Pi_2 = \frac{W}{h}$: it represents a shape factor defining in-plane slenderness of the structure. For real-life applications, either $\Pi_2 \sim 1$ or $\Pi_2 \gg 1$, the latter corresponding to elongated reservoirs as this is a simpler manner of augmenting the deposit volume (enlarging the excavation instead of making it deeper).

- $\Pi_3 = \frac{W_z}{h}$: this ratio represents a shape factor defining in-plane slenderness of the structure. The plane-strain assumption is recommended for cases such that $\Pi_3 \gg 1$ and $\Pi_3 \gg \Pi_2$ simultaneously, as long as the cross-section to be studied is located far from the edges of the structure (close to the edges 3D effects will inevitably become relevant, unless very particular boundary conditions are also presented) and the loading is also two-dimensional (as it will be the case).

- $\Pi_4 = \frac{d}{h}$: it represents the relative burial depth. If $\Pi_4 \ll 1$ then the reservoir is basically an excavation; $\Pi_4 \sim 1$ corresponds to a buried reservoir that is relatively close to the surface, so the surface effects could be relevant in the determination of its seismic response; finally, $\Pi_4 \gg 1$ would entail the reservoir is deeply buried, so deep that it could be considered, at least in first approximation, that the structure is oblivious to the presence of the free-surface (note that if, in addition, $\Pi_4 \gg 1$ then the structure in virtually unaware of both the free-surface and the rigid bedrock, and thus behaving,

at least insofar this intermediate asymptotics are valid, as if it was engulfed within an infinite body).

- $\Pi_5 = \frac{\mu}{\rho \ddot{X}_g h}$: the interpretation of this ratio is more intricate, yet it pays off. The denominator ($\rho \ddot{X}_g h$) represents a characteristic stress induced by the presence of the structure, assuming elastic forces are dominant, hence dividing it by the shear modulus represents a characteristic strain of the soil in the structure surroundings. The ratio is just the inverse of this characteristic strain. This strain will be much smaller than one as long as the amplitude of the load remains within certain limits. Should that be the case, infinitesimal strain/small displacement theory would be in effect. Therefore, the assumption $\Pi_5 \gg 1$ is tantamount to granting linear-elastic soil behavior. If $\Pi_5 \sim 1$, non-linear effects would certainly be triggered: finite deformations in the soil, inelasticity (plasticity) would render opting for Linear Elasticity to describe the soil mechanics utterly inadequate.

- $\Pi_6 = \nu$: this is just the soil Poisson's ratio, which relates shear deformation and volume-change stiffness of the soil.

- $\Pi_7 = \delta_d$: it corresponds to the hysteretic damping factor, which controls the amount of energy dissipation.

- $\Pi'_8 = \frac{\zeta_w \varpi}{W \ddot{X}_g}$: it is the inverse of the Reynolds number of the flow of water induced by the horizontal shaking. Logically, this flow pertains to the category of inviscid flows, and thus our attention shall be restricted to the case $\Pi'_8 \gg 1$.

- $\Pi'_9 = \frac{\rho_w \ddot{X}_g}{\rho \varpi^2 W}$: it represents the ratio between a characteristic value of the pressure induced by the water impact on the wall to a characteristic value of the pressure induced by deformation of the soil. Let us prove this assertion: first, the characteristic stress at the soil-wall interface

$$|\sigma_{soil}| \sim \rho \ddot{X}_g h \,, \tag{4.7a}$$

whereas the dynamic pressure that the water exerts on the inner face of the wall

$$|\sigma_{water}| \sim \rho_w (\ddot{X}_g / \varpi)^2 \,, \tag{4.7b}$$

hence,

$$\frac{|\sigma_{water}|}{|\sigma_{soil}|} \sim \frac{\rho_w \ddot{X}_g}{\rho \varpi^2 h} \,. \tag{4.7c}$$

The ratio hints that the contribution of the soil deformation will outplay the dynamic pressures associated to the water flow when $\Pi'_9 \ll 1$. In the limit $\Pi_9 \to 0$, either the reservoir is empty or the effect of the water on the structure can be disregarded.

- $\Pi'_{10} = \frac{D_p}{\mu h^3}$: represents a ratio between the characteristic displacement in the soil elicited by the load and the characteristic displacement of the plate. Let us prove this assertion as well: first, the characteristic displacement in the soil will be equal to the characteristic strain, Π_5^{-1}, times a characteristic length, h,

$$|u_{soil}| \sim h\frac{\rho\ddot{X}_g h}{\mu} = \frac{\rho\ddot{X}_g h^2}{\mu}, \tag{4.8a}$$

whereas a characteristic value of the plate deflection (taking for granted that water pressures can be, at most, of the soil order of magnitude as soil pressures, $\Pi'_9 \sim 1$) is

$$|u_{plate}| \sim \frac{\rho\ddot{X}_g h^5}{D_p}, \tag{4.8b}$$

hence

$$\frac{|u_{soil}|}{|u_{plate}|} \sim \frac{D_p}{\mu h^3}. \tag{4.8c}$$

Thus, if the ratio happens to be much smaller than one, the deformation in the soil is much more substantial than the wall deflection; contrariwise, if Π'_{10} was large, the wall would be extremely compliant and incapable of acting as buffer between soil and water. Recalling eq. (4.1), see that this relation scales with the cube of the slenderness ratio of the wall, t_p/h, and thus small changes in this ratio result in larger variations of the dimensionless parameter.
Note that this parameter is the inverse of the one referred to as "d_w" by Veletsos and Younan [YV00].
So far, only the flank walls fit into the discussion. A rationale for the structure base to be considered rigid must be develop in the same fashion lest only the wall and not the whole structure can be considered rigid. Hence, for the structure, both walls and base, to be considered rigid also $\Pi'_{10} \ll \Pi_2$ must hold.

- $\Pi'_{11} = \frac{\mu_p}{\rho\ddot{X}_g h}$: it is to the structure material what Π_5 is to the soil's: a measurement of how good the small deformations assumption is. $\Pi'_{11} \ll 1$, then the material response can be assumed to be linear-elastic, otherwise relevant non-linear effects would be being left out of the picture.

- $\Pi_{12} = \nu_p$: it is just the Poisson's ratio of the structure material.

- $\Pi'_{13} = \frac{\varpi}{\sqrt{D_p/\rho_p h^5}}$: it represents, up to an irrelevant $O(1)$ constant dependent on boundary conditions, the ratio between the load characteristic frequency and the natural frequency of the plate. Therefore, this quotient also represents the ratio between inertial forces and elastic forces present in the structure. Hence, for $\Pi'_{13} \ll 1$ the response of the structure members shall be quasi-static, whereas if $\Pi'_{13} \sim 1$ or $\Pi'_{13} \gg 1$ inertial effects associated to structure deformation must be retained in the analysis.

- $\Pi'_{14} = \frac{\varpi H}{\sqrt{\mu/\rho}}$: likewise, it represents, up to $O(1)$ constant dependent on boundary conditions, the ratio between the load characteristic frequency and the natural frequency of the soil stratum at the far-field, and thus it represents a ratio between characteristic values of inertial forces over elastic forces in the soil. Note a possible alternative interpretation:

$$\Pi'_{14} = \frac{\varpi}{\sqrt{\mu/\rho}/H} = \frac{H}{c_s/\varpi} = 2\pi\frac{H}{\lambda_s}, \tag{4.9}$$

  therefore, it is also a ratio between the height of the stratum to the wavelength of the excitation. In cases wherein the wavelengths is very big in comparison to the stratum height slow changes in the forcing can be accommodated by the soil without eliciting large inertial forces, this is just another depiction of the quasi-static regime of the soil response, which, as shown in section 3.2.1, and enables an approach of its own. Note also that, in the limit $\Pi_{14} \to 0$ the wave propagates so quickly that it "fills" the stratum right away, the response is instantaneous and it does not elicit relative displacements between the base and the upper soil, there is no free vibration either, and the stratum, for base to top surface, moves as a rigid body, see eq. (3.10). It must be noted that this group corresponds to the dimensionless frequenct "a_0", encountered usually in SSI. Finally, let us mention that had the the original Π_{14} been used, the last group would have corresponded to the Strouhal number of the flow (based on h).

Next, we can narrow down the systems we are to consider based on the actual physical values each parameter can take. Next table displays the order of magnitude of characteristic values of all parameters involved, and the range of values of the dimensionless parameters that derive from them. Take into account that table 4.2 does not intend to display actual values but possible orders of magnitude; therefore

if, e.g., a characteristic value of the shear modulus of reinforced concrete is, say, $\mu_p = 25$ GPa, we shall say $\mu_p \sim 10$ GPa, meaning that this parameter is of the order of tens of gigapascals.

Parameter	Charac. values	Π-group	Charac. values
h	~ 1 m – 10 m	$\Pi_1 = \frac{H}{h}$	$\sim 0.01 - 1$
H	~ 10 m – 1000 m	$\Pi_2 = \frac{W}{h}$	$\sim 10 - 100$
W	~ 1 m – 100 m	$\Pi_3 = \frac{W_z}{h}$	$\sim 10 - 100$
W_z	~ 1 m – 100 m	$\Pi_4 = \frac{d}{h}$	$\sim 0 - 10$
d	~ 1 m – 10 m	$\Pi_5 = \frac{\mu}{\rho \ddot{X}_g h}$	$\sim 1 - 10^6$
μ	~ 10 kPa – 100 MPa	$\Pi_6 = \nu$	$\sim 0.1 - 0.49$
ν	$\sim 0.1 - 0.49$	$\Pi_7 = \delta_d$	$\sim 0.01 - 0.3$
δ_d	$\sim 0.01 - 0.3$	$\Pi_8 = \frac{\zeta_w \varpi}{W \ddot{X}_g}$	$\sim 10^{-3} - 10$
ρ	~ 1 ton/m^3	$\Pi_9 = \frac{\rho_w \ddot{X}_g}{\rho \varpi^2 W}$	$\sim 10^{-4} - 1$
ζ_w	~ 1 m^2/s	$\Pi_{10} = \frac{D_p}{\mu h^3}$	$\sim 10^{-4} - 10^6$
ρ_w	~ 1 ton/m^3	$\Pi_{11} = \frac{\mu_p}{\rho \ddot{X}_g h}$	$\sim 100 - 10^8$
D_p	~ 10 MNm – 10GNm	$\Pi_{12} = \nu_p$	$\sim 0.1 - 0.25$
μ_p	~ 10 GPa	$\Pi'_{13} = \frac{\varpi}{\sqrt{D_p/\rho_p h^5}}$	$\sim 10^{-3} - 100$
ν_p	$\sim 0.1 - 0.25$	$\Pi'_{14} = \frac{\varpi H}{\sqrt{\mu/\rho}}$	$\sim 10^{-4} - 100$
ρ_p	~ 1 ton/m^3	-	
$\ddot{X}_g$	~ 0.1 m/s^2 – 10 m/s^2	-	
ϖ	~ 1 Hz – 10 Hz	-	

Table 4.2: Characteristic values of physical parameters of the soil-structure-interaction problem and corresponding range of dimensionless groups.

In the ensuing, these assumptions will be taken for granted (unless otherwise stated):

a) $\Pi_3 \gg 1$, plane-strain behavior of the 2D cross-sections to be considered for analysis.

b) $\Pi_4 = 0$, there is no soil cover over the reservoir.

d) $\Pi_5 \gg 1$, small strains in the soil, then linear Elasticity can rightfully be used to describe the soil response.

e) $\Pi'_9 \ll 1$, and thus the main component of the thrust on the wall derives from the soil straining, not on the dynamic pressure associated with the interior water flow. The wall integrity is challenged only by the earth thrust.

f) $\Pi'_{10} \gg 1$, therefore the (quasi-static) wall deflection is small enough so that it can be neglected in favour of soil deformation, and thus the wall is considered rigid.

g) $\Pi_{11} \gg 1$, small strains in the structure, Linear Elasticity is rightly being used to describe the structure response.

h) $\Pi'_{13} \ll 1$ thus the walls of the structure are rigid enough so that there are no inner inertial forces developing within the members. This in conjunction to $\Pi'_{10} \gg 1$ reassures the suitability of considering the structure as rigid when compared to the surrounding soil.

Since the structure is being idealized as rigid, it effectively behaves as a buffer zone between soil and water, therefore decoupling their respective responses from each other. Moreover, as it is assumed that $\Pi_9 \ll 1$, the contribution of the flow to the pressures acting on the wall is meager, by assumption, therefore the detailed characterization of the flow lacks interest for the purpose of calculating the effective pressures on the wall. Thus, Π'_8 could be removed from the parameter space as well, as it shall not affect in any way the dependent variables of relevance.

A final note on the pivotal assumption $\Pi_5 \gg 1$: as discussed in section 2.1, linear-elastic soil response is an assumable assumption as long as the soil strain remains small, say, less than 10^{-4}. Since the ratio is the inverse of the characteristic strain in the soil, we enunciate this condition in more specific terms:

$$\Pi_5^{-1} = \frac{\ddot{X}_g H}{c_s^2} \sim \frac{\mathrm{PGA} \cdot H}{c_s^2} < 10^{-4} \Rightarrow \mathrm{PGA}|_{max} < 10^{-4} \frac{c_s^2}{H}, \tag{4.10a}$$

this relation can be refined by assuming characteristic values of the structure height and density (say $H \sim 1$ m and $\rho \sim 1000$ kg/m^3); thus, let us divide the PGA by g, the gravitational acceleration

$$\left(\frac{\mathrm{PGA}}{\mathrm{g}}\right)\left(\frac{100\mathrm{MPa}}{\mu}\right) < 1\,. \tag{4.10b}$$

This last inequality hints that, earthquakes of up to $\sim$ 1 g may be considered using this framework if the soil shear stiffness is greater than $\sim$ 100 MPa, what encompasses some stiff soil types [SM05]. The condition expressed by (4.10b) can

be used as to gauge the validity of the conclusions extracted from this and subsequent studies. This estimate is based on the supposition that elastic forces possess greater magnitude and hence the response is controlled by them; hence the estimate can be used for systems with enough damping, either hysteretic or raditional yet at least (say) 10%, or if the excitation can be deemed to be "low frequency", $\Pi'_{14} \ll 1$ independently of PGA. We recommend using the more specific values of height and density, if available, to tailor the estimate to specific application. The previous discussion is contingent on no deflections in the structure that would allow gravity to induce a soil flow to fill the space left.

Assuming all the aforementioned limits represent regular processes and the asymptotic limit can be taken in all and each one of them, the parameter-space reduction becomes, symbolically

$$\begin{aligned}\frac{Q}{\rho \ddot{X}_g h^2} = \tilde{Q}(\Pi_1, \Pi_2, \Pi_3 \gg 1, \Pi_4 = 0, \Pi_5 \gg 1, \Pi_6, \Pi_7, \Pi'_8, \Pi_9 \ll 1, \\ \Pi'_{10} \gg 1, \Pi_{11} \gg 1, \Pi_{12}, \Pi'_{13} \ll 1, \Pi'_{14}) \approx Q\left(\Pi_1, \Pi_2, , \Pi_6, \Pi_7, \Pi'_{14}\right) \\ = \tilde{Q}\left(\frac{H}{h}, \frac{W}{h}, \nu, \delta_d, \frac{\varpi H}{\sqrt{\mu/\rho}}\right) .\end{aligned} \tag{4.11}$$

Thus the dimensionless parameter space is reduced from fourteen parameters to (only) five parameters. These five furnish the dynamic response of rigid excavations assuming viscoelastic soil deforming in plane strain, a relevant fact to be utilized in Chapter 6. Many scenarios of interest can be understood as particular instantiations of this general scenario corresponding to specific values of these five dimensionless parameters.

4.3 The Younan-Veletsos problem

4.3.1 Introduction

Each realization of the general model requires assigning values to the whole set of dimensionless groups in eq. (4.11) to be fully defined.

The problem considered by Veletsos and Younan [VY94a] originally, and by many others later, corresponds to

$$\Pi_1 = 1 \quad , \quad \Pi_2 = 0 , \tag{4.12}$$

thus any dependent variable, including the thrust, depends only on $\{\nu, \delta_d, \omega H/c_s\}$. The system is conformed by a rigid wall which is connected to the rigid base

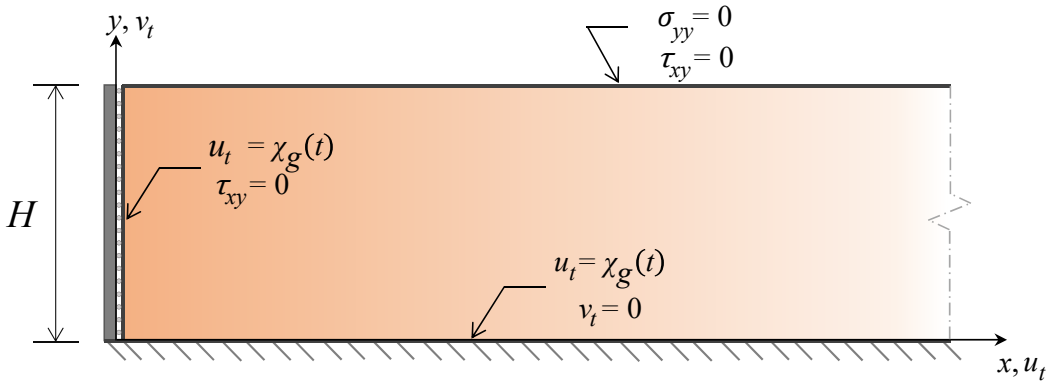

Figure 4.2: Scheme of the Younan-Veletsos problem (expressed in total displacement)

(bedrock) and restrains a layer of soil. No specific boundary conditions, other than rigidity, were used for the wall, as the assumptions introduced by the authors to propose a simplified solution precluded its consideration anyway. A concise survey on previous work concerned with this problem will be present in next chapter. For the moment, let us just say that every effort of tackling this very problem relied on introducing some simplification. Wood, another student of Housner at Caltech, derived the exact solution for a similar problem [Woo73], wherein instead of one wall there are two facing each other with soil in between them. In spite that this configuration may resemble a different system at first, intuition hints that if the distance between walls increases, the effects of a wall over the other one must fade, leaving the system virtually equivalent to the one-wall configuration insofar the displacement field around the wall is concerned. Hence, the problem may well be dubbed the *singular* Wood's problem.

One must also highlight that problems in Elastic Waveguide Theory [Mik12] resemble the problem at hand, the solution of wave propagation in plates in plane stress being very similar to ours in particular, and thus it does not come as a surprise that solution techniques in this area can be also used for our problem.

Following Wood [Woo73], we shall consider that the wall is *smooth*, i.e., frictionless, and thus no shear stress develops the interface.

4.3.2 Exact solution

First, we will provide the exact steady-state solution in wavenumber domain. In summary, the solution is accomplished by:

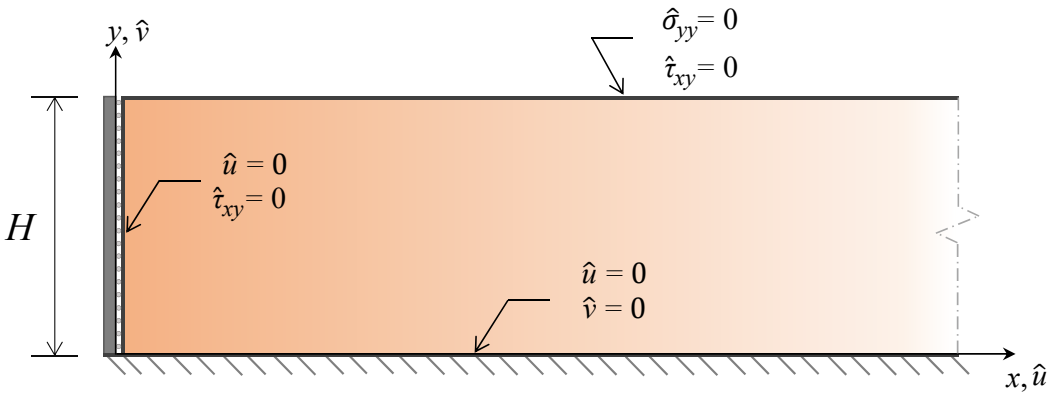

Figure 4.3: Scheme of the Younan-Veletsos problem (expressed in relative displacement)

1) Re-expressing the problem in terms of relative displacements.

2) Translate problem to amplitudes in frequency domain, see fig. 4.3, by assuming

$$\ddot{\chi}_g(t) = \ddot{X}_g e^{i\varpi t} \tag{4.13a}$$

$$u_t(x,y,t) - \chi(t) = u(x,y,t) = \hat{u}(x,y)e^{i\varpi t}\,, \tag{4.13b}$$

$$v_t(x,y,t) = v(x,y,t) = \hat{v}(x,y)e^{i\varpi t}\,. \tag{4.13c}$$

3) Realizing that the original semi-infinite layer in fig. 4.2 can be converted into an infinite layer to which classic Fourier Transform [Wei12] can be applied as to move into wavenumber (k) space.

4) Recast the problem as a first-order vector ODE of the sort $\boldsymbol{X}' = \boldsymbol{D}\,\boldsymbol{X}$, where the primed symbol entails derivative along the vertical coordinate. The solution is therefore a matrix exponential times a matrix of constants that can be obtained from the boundary conditions.

All the details of the derivation, plus comments on some technicalities, are contained in Appendix C.

The procedure yields the exact steady-state solution in the frequency-wavenumber domain. If the main goal was to characterize the displacement field everywhere in the domain we would have to invert Fourier Transforms. However, keep in mind that the main deliverable of this study is the earth thrust that acts on the wall and related quantities. Therefore, one can deal with the integrals to reduce the calculation of the

thrust to the evaluation of a certain integral, which can be, first, truncated so that it does not extend to infinity (we will discuss this truncation in coming sections), and then approximated numerically. The software *Mathematica*, [Wol00], was used.

The expression we obtain for the dimensionless thrust is

$$\frac{\hat{Q}}{\rho \ddot{X}_g H^2} = \frac{1}{\sqrt{2\pi}} \int_{-\infty}^{+\infty} \left\{ \frac{\sqrt{2/\pi}}{\beta^2} + c^2(A+B) - 2(Ae^{-\alpha} + Be^{\alpha}) + \right. \\ \left. + \left[c^2 \left(1 - \left(\frac{k}{\beta} \right)^2 \right) - 2 \right] \left(Ce^{-\beta} + De^{\beta} \right) + \left(\frac{ck}{\beta} \right)^2 (C+D) \right\} dk \,, \quad (4.14)$$

where $\alpha = \sqrt{k^2 - (\varpi H/c_s)^2}$ and $\beta = \sqrt{k^2 - (\varpi H/c_p)^2}$ are dimensionless wavenumbers for S and P waves respectively [Kau06], k is a dimensionless wavenumber, $k = \mathrm{k}H$, and the coefficients A, B, C and D are functions of the wavenumber whose expressions are given in the Appendix C as the solution of a (tortuous) system of algebraic equations.

4.3.2.1 Verification

Results derived from this exact solution are going to be compared to FEM analysis performed on *Abaqus* [Sim10]. This package, at the time the simulations were run, does not contain elements suitable to model *open boundaries* [Esm16]. For this reason, as the unboundedness in the horizontal direction can not be accounted formally, a very slender model ($H/L = 100$, L being the horizontal length of the part) was used. This approach mirrors the one advocated recently by Durante and collaborators [Dur+18], which delivered satisfactory results in the quasi-static regime, yet it had not been tested in frequency-domain dynamic analysis previously.

The parameter models are encapsulated in the following table. Keep in mind that *Abaqus* does not require to input units, and the user is solely responsible for ensuring the use of a consistent set of units.

Young's modulus E (GPa)	Density ρ (kg/m^3)	Height H (m)	Acceleration $\ddot{X}_g$ (m/s^2)
10	2000	2	0.73

Table 4.3: Base parameters used in finite-element simulations

As mentioned earlier, the three dimensionless groups controlling the response in this simplified scenario are $\Pi_6 = \nu$ (soil's Poisson's ratio), $\Pi_7 = \delta_d$ (soil's loss

factor), and $\Pi'_{14} = \varpi H/c_s = \pi\varpi/2\omega_s$, where $\omega_s = \pi c_s/2H$ is the fundamental frequency of the soil column. In order to analyze the system we shall consider different combinations of these three parameters.

Vertical displacement at the top of the wall

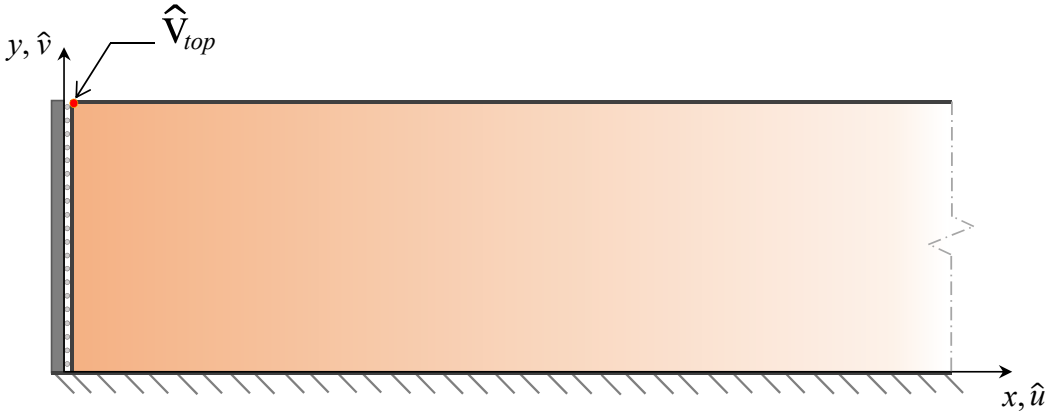

Figure 4.4: Scheme of probe location for "vertical displacement at the top of the wall"

The soil displacement at the corner delimited by the wall and the free surface is a parameter we can regard as useful for comparison purposes, moreover, it possesses a relatively simple expression in terms of the coefficients that conform the exact solution:

$$\hat{\mathrm{v}}_{top} = \frac{1}{\sqrt{2\pi}} \int_{-\infty}^{+\infty} \left(Ae^{-\alpha} + Be^{\alpha} + Ce^{-\beta} + De^{\beta} \right) dk \,. \tag{4.15}$$

The displacement is normalized with a characteristic displacement given by $U = H/\Pi_5 = \rho \ddot{X}_g H^2/\mu$. Recall that the integration is limited to $k = \pm 10$, as this interval encapsulates most of the spectrum (see how considering this interval is equivalent to limiting the wavelengths taken into consideration to those longer than $0.1H$). Next, we display the comparison of eq. (4.15) evaluated in *Mathematica* to the results obtained in *Abaqus*, once properly expressed in non-dimensional form. The first plot corresponds to $\Pi_7 = 0.05$ and the second one to $\Pi_7 = \delta_d = 0.16$, and in both bases $\Pi_6 = \nu = 0.1$ and $\Pi'_{14} = \pi\varpi/2\omega_s \in [0, 5\pi/4]$.

Complete agreement is acknowledged. We would like to highlight that, for $\nu = 0.1$ we observe a second resonance, that would not be present in the far-field response, at $\varpi \approx 1.5\omega_s = \omega_p$, since $c_p/c_s = 1.5$ when $\nu = 0.1$.

Earth thrust acting on the wall

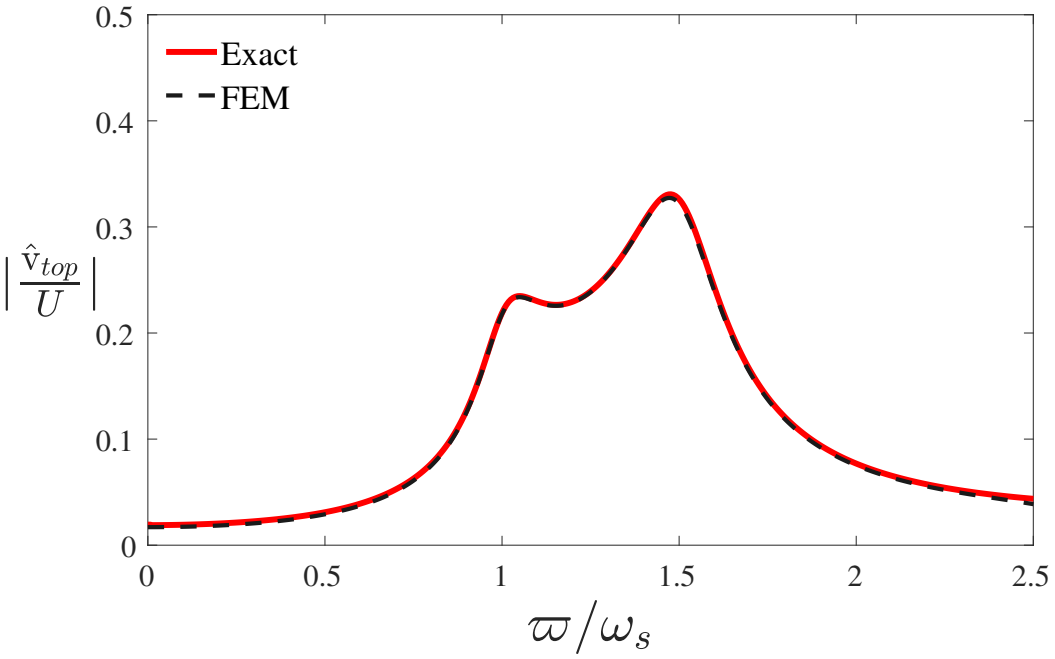

Figure 4.5: Transfer function for the vertical displacement at the top of the wall, $\nu = 0.1$, $\delta_d = 0.16$

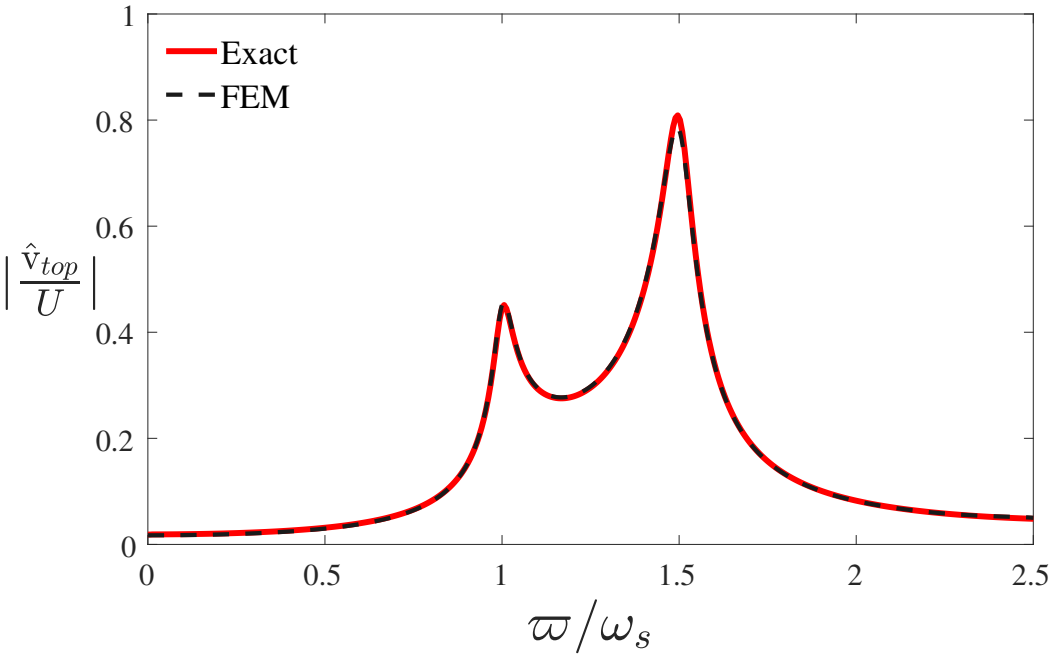

Figure 4.6: Transfer function for the vertical displacement at the top of the wall, $\nu = 0.1$, $\delta_d = 0.05$

Next, compare eq. (4.14) to its counterpart obtained from FEM.

First, set $\Pi_6 = \nu = 1/3$ and $\Pi_7 = \delta_d = 0.01$, $\Pi'_{14} = \pi\varpi/2\omega_s \in [0, 7\pi/4]$.

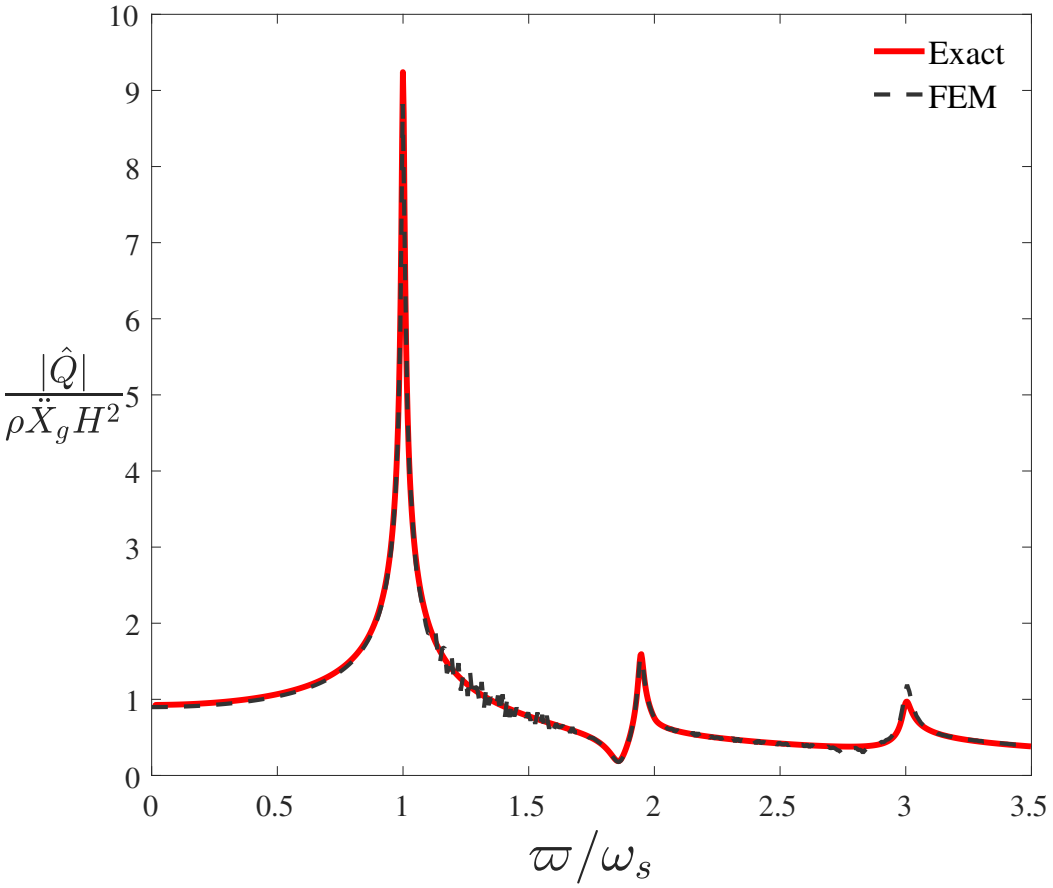

Figure 4.7: Transfer function for the earth thrust the wall, $\nu = 1/3$, $\delta_d = 0.01$

Let us spend a moment commenting this result before moving to the next comparison. First, the agreement is excellent. Again, there is a resonant spike happening at $\varpi \approx 2\omega_s = \omega_p$, since $c_p/c_s = 2$ as $\nu = 1/3$. This secondary resonance would have been overlooked had we assumed the thrust resonates at the same natural frequencies as the 1D soil column in the far-field. There seems to be some numerical artifact the author has not yet identified, which makes the numerical result oscillate mildly between the first two spikes. Other than that, the agreement is virtually complete. All the features predicted by the exact solution are present in the FEM analysis, including a substantive "dip" (deamplification) right before the second peak.

The effect of damping on the thrust is addressed in the following plot. The figures correspond to $\Pi_6 = \nu = 0.1$ (so one should expect, again, to find resonance at $\varpi/\omega_s = 1, 1.5, 3$ and so on), three new increasing values of damping are used $\Pi_7 = \delta_d = 0.05, 0.1, 0.2$,, and, again, $\Pi'_{14} = \pi\varpi/2\omega_s \in [0, 7\pi/4]$.

Once again, there is total compliance of numerical to analytical results, in the three

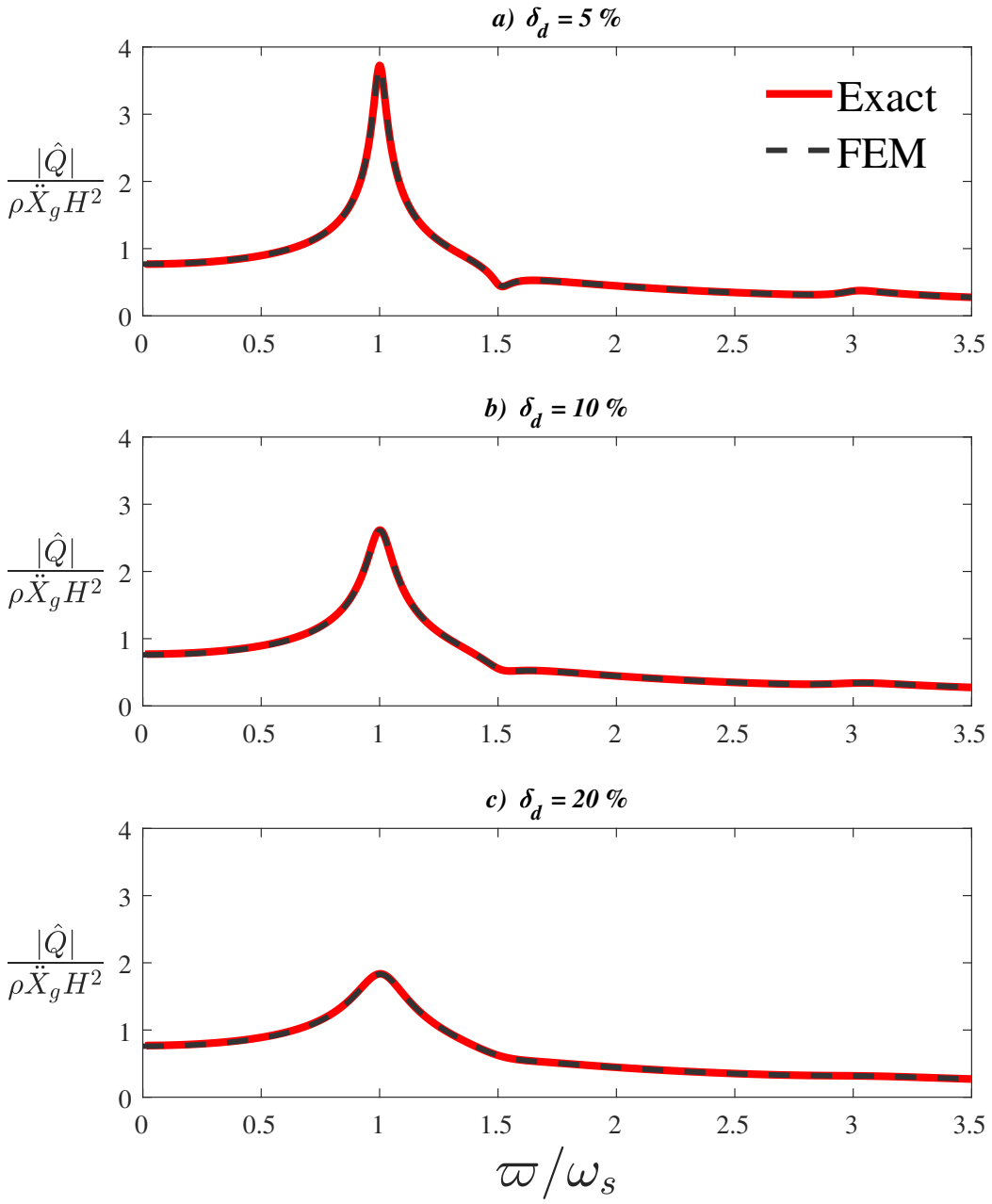

Figure 4.8: Transfer function for the earth thrust the wall, $\nu = 0.1$, $\delta_d = 0.05, 0.1, 0.2$

cases. It is instructive to note how increasing damping scratches out the two second resonant peaks and the aforesaid dip that happens before the resonance associated to ω_p. Hence, it is logical to assume that only the fundamental mode will introduce meaningful harm as long as the damping is not too small.

4.3.3 Qualitative analysis: from the wall to the far-field

The exact solution does not lend itself to easy interpretation. It does provide all the information one may need, yet not in a convenient manner: on one hand, the results come given in the wavenumber domain, what hinders the extraction of useful insights on the inner workings of the system. On the other hand, even if we were able of inverting all the transforms and move to "natural" space, the complexity of the solution would difficult the understanding of the evolution along the domain and the effects derived from the presence of the wall.

This motivates a quantitative study aimed at understanding the underpinnings of the system. We shall start by drawing attention to the different length scales involved in the problem in order to grasp how the qualitative features of the solution are reshaped along the soil layer. Later, we shall appeal to PII to gain more insight.

4.3.3.1 Characteristic Length Scales

The only geometric length-scale present in the problem is H, the wall height, which is taken to be the same as the height of the stratum.

The magnitude of the external load, $\ddot{X}_g$ (ground acceleration amplitude) defines another characteristic length:

$$\ell_s = \frac{c_s^2}{\ddot{X}_g}, \tag{4.16}$$

where $\ddot{X}_g$, in this case, refers to the amplitude of the harmonic under consideration. For the purpose of defining this characteristic length, some characteristic amplitude of the load must be specified, for example we may consider the maximum amplitude and say $\ddot{X}_g \sim$ PGA, viz. the peak ground acceleration.

A natural interpretation of this length scale is in terms of characteristic strain and stress: note that H is a geometric characteristic length, and $U = H(H/\ell_s)$ defines a characteristic displacement, recall eq. (3.8) and realize that this is the same U that defined the characteristic displacement in the far-field, therefore the ratio H/ℓ_s defines a characteristic strain, which we will refer as ϵ hereafter. Note that for realistic values of soil properties and ground accelerations, ℓ_s will be much larger than H, so $H/\ell_s \ll 1$ can be taken as a premise.

Before continuing, let us note that it follows that a characteristic stress, let it be called σ, would have magnitude $\sigma \sim \mu\epsilon = \rho\ddot{X}_g H$, and then, resorting to eq. (4.42a), a characteristic value of the earth thrust must be $Q_x \sim \sigma H = \rho\ddot{X}_g H^2$. In previous

work [VY94b], the result $|Q_x| \approx \rho \ddot{X}_g H^2$, derived under quasi-static conditions, was interpreted as an indication of the wall "supporting" approximately a $H \times H$ square of soil attached to it, in their own words:

> *Similarly, the corresponding [quasi-static] base shear [...] is approximately equal to the body force exerted over a square of side length equal to the wall height. These results suggest that the wall pressures and forces in this case are controlled by the action of the medium in the immediate vicinity of the wall rather than by its far-field action.*

Such observation has also been echoed by other researchers later [GM11; KLM12]. Even though we shall agree with the second part of their assessment (forces on the wall independent from, yet related to, far-field), our analysis suggests, rather, that this result simply suggests that the value of the thrust has to be of the order of its characteristic value, as long as the elastic forces in the soil take the lead in balancing the external load. In other circumstances, the characteristic value may be different (as an analogy, recall eq. (3.40) during the discussion of 1D site response in section 3.3.3).

The dynamic behavior of the load is described by the frequency ϖ, and thus a second characteristic length arises:

$$\lambda_s = \frac{c_s}{\varpi} = \frac{c_s T}{2\pi}, \tag{4.17}$$

λ_s represent the wavelength of the excitation, i.e., the distance an S-wave entering the system travels in the time it takes for the load to complete one period. This parameter indicates how fast the load changes with respect to the capacity of the soil to "adapt" to changes, or to "spread information" within its bulk. $T = 2\pi/\varpi$ defines the characteristic period of the load. The ratio r, which will be thoroughly used hereafter, is defined as:

$$r = \frac{\varpi}{c_s/H} = \frac{2}{\pi}\frac{\varpi}{\omega_s} = \frac{H}{\lambda_s} \tag{4.18}$$

This ratio is instrumental for the consideration of the three classical regimes in dynamic response of linear systems: low frequency (quasi-static behavior), high frequency (attenuated or no response), and resonance (amplification of natural vibration by externally imposed vibration).

Finally, acknowledge that $\Pi_5 = \ell_s/H$ and $\Pi'_{14} = r$ and therefore the prior discussion and its conclusions stem naturally from the Dimensional Analysis conducted earlier for the general case.

4.3.3.2 Scaling of Equilibrium Equations: from Far-Field to Wall Surroundings

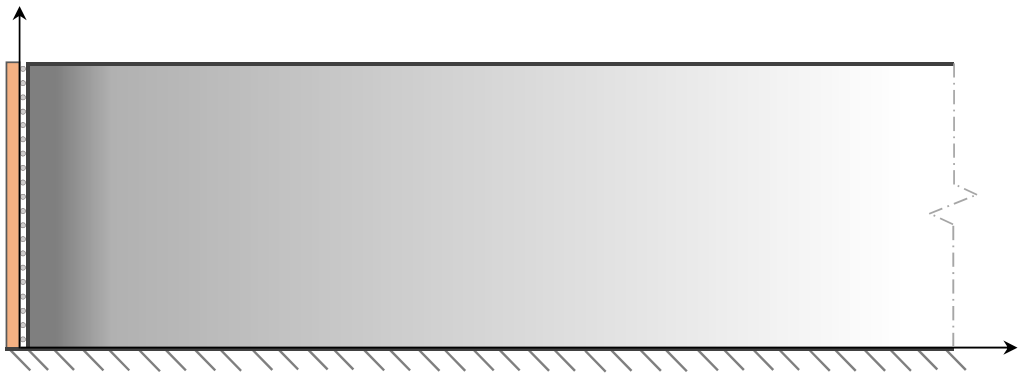

Figure 4.9: Three regions in the Younan-Veletsos problem: dark grey is the narrow layer around the wall controlled by the boundary conditions, light grey is the transition region and white the far-field

Let us conceptualize the soil domain as composed of three overlapping regions, each characterized by different qualitatively and quantitative features of the displacement field. These three regions are schematically depicted in fig. 4.9.

In order to describe and compare these different zones of the domain the following non-dimensional variables will be used:

$$\tau = \varpi t \quad , \quad \eta = \frac{y}{H} \quad , \quad \tilde{x} = \frac{x}{\ell_s} \quad , \quad \xi = \frac{x}{H} \quad , \quad \tilde{u} = \frac{u}{U} \quad , \quad \tilde{v} = \frac{v}{U} \, . \tag{4.19}$$

Let us motivate their usage:

1) Variation along the vertical direction is expected to occur in distances of order H (since this is the only length scale in vertical direction), then $\Delta y \sim H$, and thus we introduce a non-dimensional variable to measure vertical distance as portions of H, $\eta = y/H$.

2) With respect to the variation along the horizontal direction: if we focus on changes that happen along large spans, mathematically, we may interpret

this as considering $\Delta x \sim \ell_s$, and therefore $\tilde{x} = x/\ell_s$ should be used. We also have to consider displacement perturbations that happen across shorter spans, namely, adjustments associated to the presence of the wall, which are postulated to occur across spans of the order of the geometrical feature of the wall, its height H, then $\xi = x/H$.

3) To account for time variations, it is logical to expect that the solution will develop in time spans of the order of magnitude of the period of the external loading, then $t \sim 1/\varpi \Rightarrow \tau = \varpi t$. This is a wave-propagation problem: the wall sheds waves into the semi-infinite layer, which propagate rightwards. If we are to define the problem either in time or frequency domain precisely, we must provide a proper definition of the far-field. Such definition requires no wave shed by the wall reaching the far-field, which can be achieved by defining the far-field at a distance $\Delta x \gg c_s/\varpi$ or by relying on some internal mechanism to damp off the amplitude of the waves.

4) Displacements are supposed to be potentially of the same order of magnitude, and thus of the order of the characteristic displacement, U, that has already been introduced and discussed. Therefore, we define dimensionless displacements with respect to this characteristic value $\tilde{u} = u/U$ and $\tilde{v} = v/U$.

Let us also introduce the parameter

$$c = \frac{c_p}{c_s} = \sqrt{\frac{\lambda + 2\mu}{\mu}} = \sqrt{\frac{2(1-\nu)}{(1-2\nu)}} \tag{4.20}$$

that represents the ratio between the two wave propagation velocities in the linear elastic medium.

Far away from the wall

Let us consider first those changes that happen across large distances in the horizontal equation. Hence, choose $\tilde{x}$ over ξ to write the equation in dimensionless fashion, as it has been already discussed during the presentation of dimensionless variables and parameters. Thus, eqs. (2.27a) and (2.27b) are turned into the following non-

dimensional ones:

$$c^2\epsilon^2\frac{\partial^2\tilde{u}}{\partial\tilde{x}^2}+(c^2-1)\epsilon\frac{\partial^2\tilde{v}}{\partial\tilde{x}\partial\eta}+\frac{\partial^2\tilde{u}}{\partial\eta^2}=r^2\frac{\partial^2\tilde{u}}{\partial\tau^2}+e^{i\tau}\qquad\rightarrow\frac{\partial^2\tilde{u}}{\partial\eta^2}+O(\epsilon)=r^2\frac{\partial^2\tilde{u}}{\partial\tau^2}+e^{i\tau} \tag{4.21a}$$

$$c^2\frac{\partial^2\tilde{v}}{\partial\eta^2}+(c^2-1)\epsilon\frac{\partial^2\tilde{u}}{\partial\tilde{x}\partial\eta}+\epsilon^2\frac{\partial^2\tilde{v}}{\partial\tilde{x}^2}=r^2\frac{\partial^2\tilde{v}}{\partial\tau^2}\qquad\rightarrow c^2\frac{\partial^2\tilde{v}}{\partial\eta^2}+O(\epsilon)=r^2\frac{\partial^2\tilde{v}}{\partial\tau^2}\,, \tag{4.21b}$$

where the characteristic strain $\epsilon = H/\ell_s$ is understood as a small parameter henceforth. The boundary conditions, rewritten in non-dimensional form, read as follows:

At $\eta = 0$:

$$\tilde{u}(\tilde{x},0)=0\,, \tag{4.22a}$$

$$\tilde{v}(\tilde{x},0)=0\,. \tag{4.22b}$$

At $\eta = 1$:

$$\frac{\partial\tilde{u}}{\partial\eta}\Big|_{\eta=1}+\epsilon\frac{\partial\tilde{v}}{\partial\tilde{x}}\Big|_{\eta=1}=0\qquad\rightarrow\frac{\partial\tilde{u}}{\partial\eta}\Big|_{\eta=1}+O(\epsilon)=0\,, \tag{4.22c}$$

$$\frac{\partial\tilde{v}}{\partial\eta}\Big|_{\eta=1}+\epsilon\Big(\frac{c^2-2}{c^2}\Big)\frac{\partial\tilde{u}}{\partial\tilde{x}}\Big|_{\eta=1}=0\qquad\rightarrow\frac{\partial\tilde{u}}{\partial\eta}\Big|_{\eta=1}+O(\epsilon)=0\,. \tag{4.22d}$$

Once the boundary value problem is expressed in non-dimensional form and the small parameter has been identified, a standard analysis for the limit $\epsilon \rightarrow 0$ can be pursued.

By simple inspection of the equations, one can acknowledge that this problem admits a Boundary Layer solution [BO13] around the wall. Let us elaborate on this matter: First, assume an expansion in terms of the small parameter, $\tilde{u} = \sum_{j=0}^{\infty}\tilde{u}_j\epsilon^j$, and then fix $\epsilon = 0$ to find the zeroth-order approximation in ϵ of the solution. This simplifies the general equations into the equations of the infinite stratum (meaning the scenario where there is no wall and any vertical cross-section is identical to any other one); therefore, the outer solution (out of the boundary layer) in first approximation, will be the infinite stratum solution (soil column), which was extensively discussed in section 3.2 during the study of the far field. The equilibrium equations effectively decouple in this region, and the vertical equilibrium, given these boundary conditions, renders the vertical displacement equal to zero.
One more way of putting this, calling $\tilde{u}_{ff}$ to the infinite stratum/far-field solution, then we can say $\tilde{u} = \tilde{u}_{ff} + O(\epsilon)$ and $\tilde{v} = O(\epsilon)$ in this region.

A comment on the choice $\Delta x \sim \ell_s$ is compelled in light of this result. When setting $x = O(\ell_s)$, the response "fluctuations" that take place across distances much smaller than ℓ_s are "filtered out" of the response. Framing the problem in the terms of Fourier Analysis, one may see the displacement field as a superposition of many waveforms of different wavelengths, which in the end team up to yield the global displacement field, therefore, setting $\Delta x \sim \ell_s$ entails focusing on the part of the response associated to relatively long wavelengths, or, in other words, the part of the response that represents "slow" variations over horizontal spans.
An alternative reading of the result would be acknowledging that one incurs in errors $O(\epsilon)$ (very small) when approximating the displacement field at a distance $x \sim \ell_s$ by the infinite stratum solution. Everything that has been said is contingent upon the definition of the far-field being consistent, as discussed above when considering the dimensionless time τ.

The region surrounding the wall

The equation that governs the inner behavior, the one that is valid inside the boundary layer, is the one where $\tilde{x}$ is stretched as to traverse just the boundary layer width, this width being referenced as δ. Thus, let us introduce ξ, the inner horizontal coordinate for the boundary layer, then $\tilde{x} = \delta\xi$, and substitute into the eqs. (4.21a) and (4.21b):

$$c^2\left(\frac{\epsilon}{\delta}\right)^2\frac{\partial^2\tilde{u}}{\partial\xi^2} + (c^2-1)\left(\frac{\epsilon}{\delta}\right)\frac{\partial^2\tilde{v}}{\partial\xi\partial\eta} + \frac{\partial^2\tilde{u}}{\partial\eta^2} = e^{i\tau} + r^2\frac{\partial^2\tilde{u}}{\partial\tau^2}\,, \tag{4.23a}$$

$$c^2\frac{\partial^2\tilde{v}}{\partial\eta^2} + (c^2-1)\left(\frac{\epsilon}{\delta}\right)\frac{\partial^2\tilde{u}}{\partial\xi\partial\eta} + \left(\frac{\epsilon}{\delta}\right)^2\frac{\partial^2\tilde{v}}{\partial\xi^2} = r^2\frac{\partial^2\tilde{v}}{\partial\tau^2}\,. \tag{4.23b}$$

Dominant balance [BO13] requires $\delta \sim \epsilon$ and hence the equations governing the solution in the boundary layer are

$$c^2\frac{\partial^2\tilde{u}}{\partial\xi^2} + (c^2-1)\frac{\partial^2\tilde{v}}{\partial\xi\partial\eta} + \frac{\partial^2\tilde{u}}{\partial\eta^2} = e^{i\tau} + r^2\frac{\partial^2\tilde{u}}{\partial\tau^2}\,, \tag{4.24a}$$

$$c^2\frac{\partial^2\tilde{v}}{\partial\eta^2} + (c^2-1)\frac{\partial^2\tilde{u}}{\partial\xi\partial\eta} + \frac{\partial^2\tilde{v}}{\partial\xi^2} = r^2\frac{\partial^2\tilde{v}}{\partial\tau^2}\,, \tag{4.24b}$$

with boudary conditions:

At $\eta = 0$:

$$\tilde{u}(\xi, 0) = 0 \tag{4.25a}$$

$$\tilde{v}(\xi, 0) = 0\,. \tag{4.25b}$$

At $\eta = 1$:

$$\frac{\partial \tilde{u}}{\partial \eta}\Big|_{\eta=1} + \frac{\partial \tilde{v}}{\partial \xi}\Big|_{\eta=1} = 0 \tag{4.25c}$$

$$\frac{\partial \tilde{v}}{\partial \eta}\Big|_{\eta=1} + \Big(\frac{c^2-2}{c^2}\Big)\frac{\partial \tilde{u}}{\partial \xi}\Big|_{\eta=1} = 0\,. \tag{4.25d}$$

Note that $\delta \sim \epsilon$ implies $\tilde{x}/\xi \sim H/\ell_s$, therefore $\xi \sim \tilde{x}(\ell_s/H) = x/H$, whence we conclude that the physical width of the boundary layer around the wall is $\sim H$. The wall induces noticeable disturbances in a region around itself up to distances of the order of magnitude of its geometrical features (in this case, its height).

Additionally, observe that all the terms in eqs. (4.24a) and (4.24b) have the same order of magnitude. This fact precludes assumptions of negligible either displacements or stresses inside the boundary layer, that is, in the wall surroundings. Such an event demands considering the problem in all its complexity, including the coupling between vertical and horizontal displacement gradients through their relative contribution to the stress field.

On the wall

No small parameter appears within the "wall-surroundings" equations eqs. (4.24) to (4.25), but the distance from the wall to a point in the soil domain, i.e. ξ, the non-dimensional horizontal distance, can still be interpreted as a small parameter notwithstanding, at least when it comes to consider the displacement field very close to the wall.

First of all, let us express the displacement variables as an expansion in terms of the new small "parameter":

$$\tilde{u}(\xi,\eta,\tau) = \sum_{k=0}^{\infty} \frac{\tilde{u}_k(\eta,\tau)}{k!}\xi^k \quad , \quad \tilde{v}(\xi,\eta,\tau) = \sum_{k=0}^{\infty} \frac{\tilde{v}_k(\eta,\tau)}{k!}\xi^k\,, \tag{4.26}$$

these series represent simply the Taylor polynomial corresponding to $\tilde{u}$, $\tilde{v}$ around $\xi = 0$, that is, at the wall, and therefore $\tilde{u}_k(\eta,\tau) = \partial^k \tilde{u}/\partial \xi^k|_{\xi=0}$. Recall once again that calculating the earth thrust only requires knowing displacement gradients at $\xi = 0$.

If the series are introduced into eqs. (4.24a) and (4.24b), also (4.25), and terms corresponding to same powers of the small parameter are group together, the following

recurrence is obtained

$$c^2\tilde{u}_{k+2} + (c^2-1)\frac{\partial \tilde{v}_{k+1}}{\partial \eta} + \frac{\partial^2 \tilde{u}_k}{\partial \eta^2} = \mathbb{I}_k + r^2\frac{\partial^2 \tilde{u}_k}{\partial \tau^2}\,, \tag{4.27a}$$

$$\tilde{v}_{k+2} + (c^2-1)\frac{\partial \tilde{u}_{k+1}}{\partial \eta} + c^2\frac{\partial^2 \tilde{v}_k}{\partial \eta^2} = r^2\frac{\partial^2 \tilde{v}_k}{\partial \tau^2}\,, \tag{4.27b}$$

where $k = 0, 1, 2, \ldots$ and $\mathbb{I}_0 = e^{i\tau}$ and $\mathbb{I}_k = 0$ for $k > 0$.

Hitherto, no information concerning the boundary conditions on the wall (its smoothness or rigidity, for instance) as been utilized, in an aim to keep the framework as general as possible. Boundary conditions on the wall provide pieces of information that, in conjunction with the partial differential equations themselves, may lead to a local solution, or, at least, to an understanding of how the solution must behave.

To clarify this step, let us analyze the case of a rigid and frictionless wall that pertains to the Younan-Veletsos problem, as this is the object of study of section 4.3. Such a wall entails

$$\tilde{u}(0,\eta) = 0 \qquad \text{(rigid wall, no deflection)}, \tag{4.28a}$$

$$\left.\frac{\partial \tilde{v}}{\partial \xi}\right|_{\xi=0} = 0 \qquad \text{(smooth wall, no soil shearing at the interface)}. \tag{4.28b}$$

what amounts to $\tilde{u}_0 = 0$ and $\tilde{v}_1 = 0$ in terms of the previous notation. Let us move to gather terms with the same power and simplify the equations in accordance to the boundary conditions:

$O(1)$ terms.

$$c^2\tilde{u}_2 + (c^2-1)\underbrace{\frac{d\tilde{v}_1}{d\eta}}_{=0} + \underbrace{\frac{d^2\tilde{u}_0}{d\eta^2}}_{=0} = e^{i\tau} + r^2\underbrace{\frac{d^2\tilde{u}_0}{d\tau^2}}_{=0} \quad \rightarrow \quad \tilde{u}_2 = \frac{e^{i\tau}}{c^2}\,, \tag{4.29a}$$

$$\tilde{v}_2 + (c^2-1)\frac{d\tilde{u}_1}{d\eta} + c^2\frac{d^2\tilde{v}_0}{d\eta^2} = r^2\frac{d^2\tilde{v}_0}{d\tau^2}\,. \tag{4.29b}$$

$O(\xi)$ terms:

$$c^2\tilde{u}_3 + (c^2-1)\frac{d\tilde{v}_2}{d\eta} + \frac{d^2\tilde{u}_1}{d\eta^2} = r^2\frac{d^2\tilde{u}_1}{d\tau^2}\,, \tag{4.29c}$$

$$\tilde{v}_3 + (c^2-1)\frac{d\tilde{u}_2}{d\eta} + c^2\underbrace{\frac{d^2\tilde{v}_1}{d\eta^2}}_{=0} = r^2\underbrace{\frac{d^2\tilde{v}_1}{d\tau^2}}_{=0} \quad \rightarrow \quad \tilde{v}_3 = -(c^2-1)\frac{d\tilde{u}_2}{d\eta} = 0\,. \tag{4.29d}$$

$O(\xi^2)$ terms:

$$c^2\tilde{u}_4 + (c^2-1)\underbrace{\frac{d\tilde{v}_3}{d\eta}}_{=0} + \underbrace{\frac{d^2\tilde{u}_2}{d\eta^2}}_{=0} = r^2\underbrace{\frac{d^2\tilde{u}_2}{d\tau^2}}_{=-e^{i\tau}/c^2} \quad \rightarrow \quad \tilde{u}_4 = -r^2\frac{e^{i\tau}}{c^4}\,, \tag{4.29e}$$

$$\tilde{v}_4 + (c^2-1)\frac{d\tilde{u}_3}{d\eta} + c^2\frac{d^2\tilde{v}_2}{d\eta^2} = r^2\frac{d^2\tilde{v}_2}{d\tau^2}\,. \tag{4.29f}$$

$O(\xi^3)$ terms:

$$c^2\tilde{u}_5 + (c^2-1)\frac{d\tilde{v}_4}{d\eta} + \frac{d^2\tilde{u}_3}{d\eta^2} = r^2\frac{d^2\tilde{u}_3}{d\tau^2}\,, \tag{4.29g}$$

$$\tilde{v}_5 + (c^2-1)\frac{d\tilde{u}_4}{d\eta} + c^2\underbrace{\frac{d^2\tilde{v}_3}{d\eta^2}}_{=0} = r^2\underbrace{\frac{d^2\tilde{v}_3}{d\tau^2}}_{=0} \quad \rightarrow \quad \tilde{v}_5 = -(c^2-1)\frac{d\tilde{u}_4}{d\eta} = 0\,, \tag{4.29h}$$

and so on and so forth. This means that all the odd x-derivatives of the vertical displacement will be equal to zero

$$\left.\frac{\partial v}{\partial x}\right|_{x=0} = \left.\frac{\partial^3 v}{\partial x^3}\right|_{x=0} = \left.\frac{\partial^5 v}{\partial x^5}\right|_{x=0} = \ldots = 0\,. \tag{4.30}$$

We notice how the vanishing of certain derivatives suggests specific functional forms for the variables.

Likewise, a similar treatment can be carried out for the boundary conditions. For the sake of briefness, let us state just the zeroth-order boundary conditions (the higher orders can be obtained in similar orderly fashion).

At $\eta = 0$:

$$\tilde{u}_0(0,\tau) = 0 \tag{4.31a}$$

$$\tilde{v}_0(0,\tau) = 0 \tag{4.31b}$$

At $\eta = 1$:

$$\left.\frac{\partial \tilde{u}_0}{\partial \eta}\right|_{\eta=1} + \tilde{v}_1(1,\tau) = 0 \rightarrow \tilde{v}_1(1,\tau) = 0 \quad \text{(redundant, since } \tilde{v}_1 = 0 \text{ on wall)} \tag{4.31c}$$

$$\left.\frac{\partial \tilde{v}_0}{\partial \eta}\right|_{\eta=1} + \left(\frac{c^2-2}{c^2}\right)\tilde{u}_1(1,\tau) = 0 \tag{4.31d}$$

the $O(1)$-order equilibrium very close (that is, $\xi \to 0$ or $x/H \ll 1$) to the smooth, rigid wall is:

$$c^2 \frac{\partial^2 \tilde{u}}{\partial \xi^2}\bigg|_w = e^{i\varpi t}, \tag{4.32a}$$

$$c^2 \frac{\partial^2 \tilde{v}}{\partial \eta^2}\bigg|_w + (c^2 - 1)\frac{\partial^2 \tilde{u}}{\partial \xi \partial \eta}\bigg|_w + c^2 \frac{\partial^2 \tilde{v}}{\partial \xi^2}\bigg|_w = \frac{\partial^2 \tilde{v}}{\partial \tau^2}\bigg|_w, \tag{4.32b}$$

where $X|_w = X|_{x=0} = X|_{\xi=0}$, i.e., the variable "$X$" evaluated on the wall. Note this indicates decoupling of horizontal equilibrium from the vertical, in similar fashion as it happened in the far-field. In physical units,

$$(\lambda + 2\mu)\frac{\partial^2 u}{\partial x^2}\bigg|_w = \rho \ddot{X}_g e^{i\varpi t}, \tag{4.33a}$$

$$(\lambda + 2\mu)\frac{\partial^2 v}{\partial y^2}\bigg|_w + (\mu + \lambda)\frac{\partial^2 u}{\partial x \partial y}\bigg|_w + \mu \frac{\partial^2 v}{\partial x^2}\bigg|_w = \rho \frac{\partial^2 v}{\partial t^2}\bigg|_w. \tag{4.33b}$$

This information shall be taken into account at the moment of proposing a reduced-order model.

4.3.4 Insight from path-independent integrals

Let us complement the information derived in section 4.3.3 by analyzing the conservation laws applied to this domain.

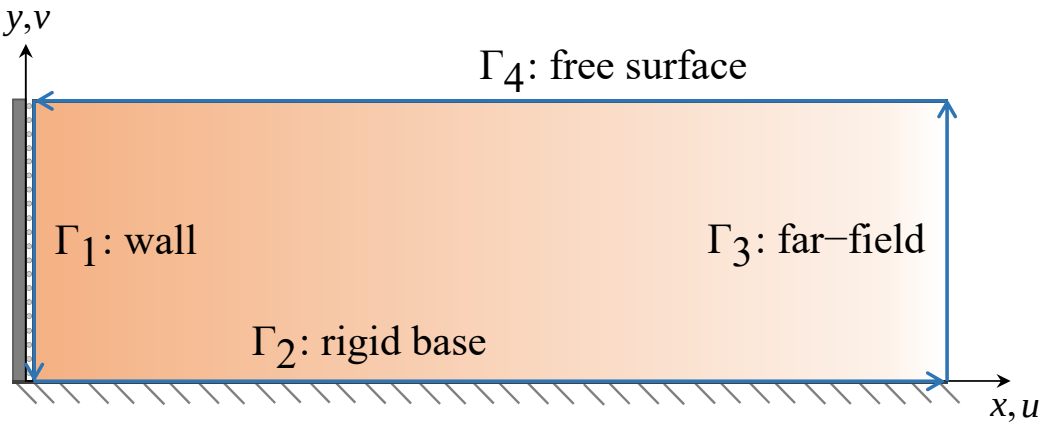

Figure 4.10: Contour to be used to evaluate the path-independet integrals

We shall use the expression of the dynamic integrals in terms of total displacements. Some of them will be particularized to the quasi-static regime later. Before displaying the result from each integral, let us inspect the value of the terms in the integrand

corresponding to each contour. Start by Γ_1 (wall), assuming smooth and rigid wall:

$$x = 0\,, \qquad n_x = -1\,, \qquad n_y = 0\,, \tag{4.34a}$$

$$\hat{t}_x = -\hat{\sigma}_{xx}\,, \qquad \hat{t}_y = -\hat{\tau}_{xy} = 0\,, \tag{4.34b}$$

$$\hat{T} = \frac{\rho\varpi^2}{2}(X_g^2 + \hat{v}^2)\,, \tag{4.34c}$$

$$\hat{W} = \frac{1}{2}\left(\hat{\sigma}_{xx}\frac{\partial\hat{u}}{\partial x} + \hat{\sigma}_{yy}\frac{\partial\hat{v}}{\partial y}\right) = \frac{(\lambda+2\mu)}{2}\left(\left(\frac{\partial\hat{u}}{\partial x}\right)^2 + \left(\frac{\partial\hat{v}}{\partial y}\right)^2\right)\,. \tag{4.34d}$$

Continue with Γ_2 (rigid wall):

$$y = 0\,, \qquad n_x = 0\,, \qquad n_y = -1\,, \tag{4.35a}$$

$$\hat{t}_x = -\hat{\tau}_{xy}\,, \qquad \hat{t}_y = -\hat{\sigma}_{yy}\,, \tag{4.35b}$$

$$\hat{T} = \frac{\rho\varpi^2}{2}X_g^2\,, \tag{4.35c}$$

$$\hat{W} = \frac{1}{2}\left(\hat{\sigma}_{yy}\frac{\partial\hat{v}}{\partial y} + \hat{\tau}_{xy}\frac{\partial\hat{u}}{\partial y}\right) = \frac{1}{2}\left(\left((\lambda+2\mu)\frac{\partial\hat{v}}{\partial y}\right)^2 + \mu\left(\frac{\partial\hat{u}}{\partial y}\right)^2\right)\,. \tag{4.35d}$$

Then Γ_3 (far-field):

$$x \to \infty\,, \qquad n_x = 1\,, \qquad n_y = 0\,, \tag{4.36a}$$

$$\hat{t}_x = \hat{\sigma}_{xx} = 0\,, \qquad \hat{t}_y = \hat{\tau}_{xy}\,, \tag{4.36b}$$

$$\hat{T} = \frac{\rho\varpi^2}{2}(X_g + \hat{u})^2\,, \tag{4.36c}$$

$$\hat{W} = \frac{1}{2}\left(\hat{\tau}_{xy}\frac{\partial\hat{u}}{\partial y}\right) = \frac{\mu}{2}\left(\frac{\partial\hat{u}}{\partial y}\right)^2\,. \tag{4.36d}$$

And finally Γ_4 (free surface):

$$y = H\,, \qquad n_x = 0\,, \qquad n_y = 1\,, \tag{4.37a}$$

$$\hat{t}_x = \hat{\tau}_{xy} = 0\,, \qquad \hat{t}_y = \hat{\sigma}_{yy} = 0\,, \tag{4.37b}$$

$$\hat{T} = \frac{\rho\varpi^2}{2}\left((X_g + \hat{u})^2 + \hat{v}^2\right)\,, \tag{4.37c}$$

$$\hat{W} = \frac{1}{2}\left(\hat{\sigma}_{xx}\frac{\partial\hat{u}}{\partial x}\right)\,. \tag{4.37d}$$

4.3.4.1 J-integral

For $J_x = 0$ first:

$$\int_0^H \left[\frac{\mu}{2} \left(\frac{\partial \hat{u}}{\partial y} \right)^2 - \frac{\rho \varpi^2}{2} (X_g + \hat{u})^2 \right]_{x \to \infty} dy = \int_0^H \left[\frac{(\lambda + 2\mu)}{2} \left(\left(\frac{\partial \hat{u}}{\partial x} \right)^2 - \left(\frac{\partial \hat{v}}{\partial y} \right)^2 \right) + \frac{\rho \varpi^2}{2} (X_g^2 + \hat{v}^2) \right]_{x=0} dy \,. \quad (4.38)$$

Next, $J_y = 0$ can be expressed, making use of the special form of the tensor vector at the base, as:

$$\int_0^\infty \left[\hat{W} + \hat{T} \right]_{y=0} dx = \int_0^\infty \left[\hat{W} - \hat{T} \right]_{y=H} dx \,, \quad (4.39)$$

this expression being only valid inasmuch hookean solids are concerned. More explicitly:

$$\int_0^\infty \left[\frac{1}{2} \left(\mu \left(\frac{\partial \hat{u}}{\partial y} \right)^2 + \lambda \left(\frac{\partial \hat{v}}{\partial y} \right)^2 \right) - \frac{\rho \varpi^2}{2} X_g^2 \right]_{y=0} dx = \int_0^\infty \left[\frac{1}{2} \left((\lambda + 2\mu) \left(\frac{\partial \hat{u}}{\partial x} \right)^2 + \mu \left(\frac{\partial \hat{v}}{\partial y} \right) \left(\frac{\partial \hat{u}}{\partial x} \right) \right) - \frac{\rho \varpi^2}{2} \left(\left(X_g + \hat{u} \right)^2 + \hat{v}^2 \right) \right]_{y=0} dx \,. \quad (4.40)$$

4.4 Reservoir on soft soil overlying rigid bedrock

Consider the system displayed in fig. 4.11. It represents a logical extension of the Younan-Veletsos model discussed the prior section.

4.4.1 Quasi-static regime, wide reservoir with rigid-rough walls

Let us consider the quasi-static regime, which is characterized by $\Pi'_{14} \ll 1$, hence eq. (4.11) is reduced even more. Moreover, the damping will not be significant in this short-wavelength regime, and thus Π_7 can also be removed from the parameter space. Additionally, let us add the assumption of "wide reservoir", entailing $W >> h$, and thus we can take the limit $\Pi_2 \to \infty$. After considering all these simplifications, eq. (4.11) boils down to

$$\frac{Q}{\rho \ddot{X}_g h^2} = \tilde{Q} \left(\frac{H}{h}, \nu \right) \,. \quad (4.41)$$

Apropos the boundary conditions at the soil-wall interface: the wall shall be considered, aside from rigid, *rough*, meaning that the soil is "welded" to the wall

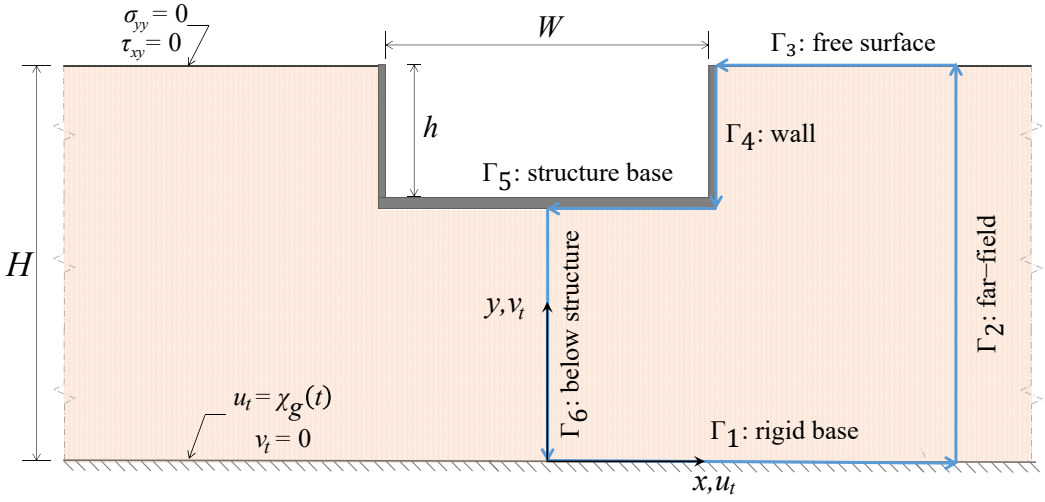

Figure 4.11: Schematic representation of excavation within soil resting over rigid bedrock

and therefore it moves with it and there are no relative displacements between the two, and thus $u|_w = 0$ and $v|_w = 0$, whence it follows that $\partial u/\partial y|_w = 0$ and $\partial v/\partial y|_w = 0$ and the stresses at the wall reduce to $\sigma_{xx}|_w = (\lambda + 2\mu)\partial u/\partial x|_w$ and $\tau_{xy}|_w = \mu(\partial v/\partial x|_w)$, hence

$$Q_x = \int_{H-h}^{H} \left[(\lambda + 2\mu) \frac{\partial u}{\partial x} \right]_w dy \,, \tag{4.42a}$$

$$Q_y = \int_{H-h}^{H} \left[\mu \left(\frac{\partial v}{\partial x} \right) \right]_w dy \,. \tag{4.42b}$$

4.4.1.1 A bound for the thrust

Let us examine eq. (4.3) under these conditions:

$$|\boldsymbol{Q}|^2 = |Q_x|^2 + |Q_y|^2 = \left| \int_{H-h}^{H} \sigma_{xx}|_w dy \right|^2 + \left| \int_{h-h}^{H} \tau_{xy}|_w dy \right|^2 \tag{4.43a}$$

these integrals can be understood as inner products, so Cauchy-Schwarz inequality can be applied,

$$\leq \left(\int_{H-h}^{H} |\sigma_{xx}|_w|^2 dy \right) \left(\int_{H-h}^{H} |1|^2 dy \right) + \left(\int_{H-h}^{H} |\tau_{xy}|_w|^2 dy \right) \left(\int_{H-h}^{H} |1|^2 dy \right) \tag{4.43b}$$

$$= h \left(\int_{H-h}^{H} |\sigma_{xx}|_w|^2 dy + \int_{H-h}^{H} |\tau_{xy}|_w|^2 dy \right) = h \left(\int_{H-h}^{H} \left(|\sigma_{xx}|_w|^2 + |\tau_{xy}|_w|^2 \right) dy \right) , \tag{4.43c}$$

using the boundary conditions corresponding to rigid wall with roughness,

$$= h\left(\int_{H-h}^{H}\left[(\lambda+2\mu)^2\left(\frac{\partial u}{\partial x}\right)^2+\mu^2\left(\frac{\partial v}{\partial x}\right)^2\right]_w dy\right) \tag{4.43d}$$

$$= h(\lambda+2\mu)\left(\int_{H-h}^{H}\left[(\lambda+2\mu)\left(\frac{\partial u}{\partial x}\right)^2+\left[\frac{\mu}{(\lambda+2\mu)}\right]\mu\left(\frac{\partial v}{\partial x}\right)^2\right]_w dy\right), \tag{4.43e}$$

note that necessarily $\mu/(\lambda+2\mu)<1$, hence,

$$< h(\lambda+2\mu)\left(\int_{H-h}^{H}\left[(\lambda+2\mu)\left(\frac{\partial u}{\partial x}\right)^2+\mu\left(\frac{\partial v}{\partial x}\right)^2\right]_w dy\right). \tag{4.43f}$$

In conclusion, the thrust can be bounded from above as follows:

$$\begin{aligned}|Q|^2 < h(\lambda+2\mu)\left(\int_{H}^{H-h}\left[(\lambda+2\mu)\left(\frac{\partial u}{\partial x}\right)^2+\mu\left(\frac{\partial v}{\partial x}\right)^2\right]_w dy\right)\\ = h(\lambda+2\mu)\left(\int_{H}^{H-h} W|_w dy\right),\end{aligned} \tag{4.44}$$

where $W|_w$ represents the strain energy density at the wall. This inequality will be summoned later on.

4.4.2 Application of $\mathrm{J}_x = 0$

Let us move to define a possible contour one may use to analyze the J-integral. The contour is made up of the following pieces (see fig. 4.11): rigid base (Γ_1), far-field soil to the left (Γ_2), right free surface (Γ_3), right wall (Γ_4), half structure base (Γ_5), from mid-point beneath the structure vertically to the rigid base (Γ_6). Thus the integral for J_x in this case is

$$\begin{aligned}\mathrm{J}_x = \int_{\Gamma_1}(-E_{12})dx+\int_{\Gamma_2}E_{11}dy+\int_{\Gamma_3}(-E_{12})dx+\\ \int_{\Gamma_4}E_{11}dy+\int_{\Gamma_5}(-E_{12})dx+\int_{\Gamma_6}E_{11}dy = 0\,.\end{aligned} \tag{4.45}$$

Here the piece of contour Γ_6 (corresponding to the far-field) is

$$\int_{\Gamma_2}E_{11}dy = \int_0^H\left[\rho\gamma u_{ff}+\frac{\mu}{2}\left(\frac{\partial u_{ff}}{\partial y}\right)^2\right]dy\,, \tag{4.46}$$

note that the integration could be carried out right away as the far-field displacement field is known. On the other hand, the integral along Γ_7 (below the structure) is

$$\int_{\Gamma_6}E_{11}dy = \int_{H-h}^{0}\left[\frac{1}{2}\left(\sigma_{yy}\frac{\partial v}{\partial y}-\sigma_{xx}\frac{\partial u}{\partial x}+\tau_{xy}\left(\frac{\partial u}{\partial y}-\frac{\partial v}{\partial x}\right)\right)+\rho\gamma u\right]_{x=0}dy\,. \tag{4.47}$$

The displacement field corresponding to this contour, unlike in the prior case, is unknown, yet a simplifying assumption can be argued: if the height of the wall was much smaller than the height of the stratum ($h/H \ll 1$), the disturbances introduced by the presence of the structure should not severely affect the displacement field out of a localized region around the structure; in the limit case of absence of structure the displacement field would be identical to the far-field's. Thus, it follows that, under this assumption, the displacement field below the structure will resemble the one of the far-field at similar height. With respect to the eq. (4.47), this would lead to

$$\int_{\Gamma_6} E_{11} dy \approx \int_{H-h}^{0} \left[\rho\gamma u_{ff} + \frac{\mu}{2} \left(\frac{\partial u_{ff}}{\partial y} \right)^2 \right]_{x=0} dy \,. \tag{4.48}$$

Including eq. (4.46) and eq. (4.48) into eq. (4.45) yields

$$\begin{aligned} -\int_{\Gamma_4} E_{11} dy &= \int_{\Gamma_2} E_{11} dy + \int_{\Gamma_6} E_{11} dy \\ &\approx \int_0^H \left[\rho\gamma u_{ff} + \frac{\mu}{2} \left(\frac{\partial u_{ff}}{\partial y} \right)^2 \right] dy - \int_0^{H-h} \left[\rho\gamma u_{ff} + \frac{\mu}{2} \left(\frac{\partial u_{ff}}{\partial y} \right)^2 \right] dy \\ &= \int_{H-h}^H \left[\rho\gamma u_{ff} + \frac{\mu}{2} \left(\frac{\partial u_{ff}}{\partial y} \right)^2 \right] dy \,. \end{aligned} \tag{4.49}$$

Finally, the piece of contour Γ_4 (corresponding to the wall), assuming the rough wall properties ($\partial u/\partial y|_w = 0$, $\partial v/\partial y|_w = 0$), becomes

$$\begin{aligned} -\int_{\Gamma_5} E_{11} dy &= -\int_H^{H-h} \left[\rho\gamma u - \frac{(\lambda + 2\mu)}{2} \left(\frac{\partial u}{\partial x} \right)^2 - \frac{\mu}{2} \left(\frac{\partial v}{\partial x} \right)^2 \right]_{x=L/2} dy \\ &= \int_{H-h}^H [\rho\gamma u]_{x=L/2} dy + \int_H^{H-h} \left[\frac{(\lambda + 2\mu)}{2} \left(\frac{\partial u}{\partial x} \right)^2 + \frac{\mu}{2} \left(\frac{\partial v}{\partial x} \right)^2 \right]_{x=L/2} dy \,, \end{aligned} \tag{4.50}$$

substitute this expression into eq. (4.49) and moving the first integral to the right-hand side:

$$\begin{aligned} &\int_H^{H-h} \left[\frac{(\lambda + 2\mu)}{2} \left(\frac{\partial u}{\partial x} \right)^2 + \frac{\mu}{2} \left(\frac{\partial v}{\partial x} \right)^2 \right]_{x=L/2} dy \\ &\quad \approx \int_{H-h}^H \left[\rho\gamma u_{ff} + \frac{\mu}{2} \left(\frac{\partial u_{ff}}{\partial y} \right)^2 \right] dy - \int_{H-h}^H [\rho\gamma u]_{x=L/2} dy \,, \end{aligned} \tag{4.51}$$

the second integral in the right-hand side represents a contribution from the movement of the wall. By prolonging the reasoning that yielded eq. (4.48), one more simplification is introduced: if the displacement field below the structure is alike the one at the far-field, then the displacement of the structure base must be similar to the one at the far-field corresponding to the same depth, and thus, as the structure is assumed to be rigid and rocking is being ignored, the structure itself must translate horizontally by the same amount as the far-field. In conclusion:

$$\int_{H}^{H-h} \left[\frac{(\lambda+2\mu)}{2} \left(\frac{\partial u}{\partial x} \right)^2 + \frac{\mu}{2} \left(\frac{\partial v}{\partial x} \right)^2 \right]_{x=L/2} dy \approx \tag{4.52a}$$

$$\int_{H-h}^{H} \left[\rho\gamma u_{ff} + \frac{\mu}{2} \left(\frac{\partial u_{ff}}{\partial y} \right)^2 \right] dy - \int_{H-h}^{H} [\rho\gamma u]_{x=L/2} dy \approx \tag{4.52b}$$

appealing to the argument discussed before

$$\int_{H-h}^{H} \left[\rho\gamma u_{ff} + \frac{\mu}{2} \left(\frac{\partial u_{ff}}{\partial y} \right)^2 \right] dy - \int_{H-h}^{H} [\rho\gamma u_{ff}]_{y=H-h} dy = \tag{4.52c}$$

$$\int_{H}^{H-h} \left[\rho\gamma \Delta u_{ff} + \frac{\mu}{2} \left(\frac{\partial u_{ff}}{\partial y} \right)^2 \right] dy \,. \tag{4.52d}$$

Evaluate this last integral by appealing to eq. (3.3) to conclude that eq. (4.52a) has to verify

$$\int_{H}^{H-h} \left[\frac{(\lambda+2\mu)}{2} \left(\frac{\partial u}{\partial x} \right)^2 + \frac{\mu}{2} \left(\frac{\partial v}{\partial x} \right)^2 \right]_{x=L/2} dy \approx \frac{(\rho\gamma)^2 h^3}{6\mu} \,, \tag{4.52e}$$

where $\Delta u_{ff} = u_{ff}(y) - u_{ff}(y = H - h)$, for $y \geq H - h$. This result has been derived from presuming the displacement profile under the structure to be similar to the one under the far-field, so the difference between the two is just the extra contribution of the far-field throughout the level the wall occupies. Note the following:

1) The same expression would have been obtained under the assumption of $h \approx H$, i.e., extending the wall from the free-surface down to (or almost to) the bedrock. In such case, the contribution from under the structure (the integral along Γ_6) will be small, so the main contribution will be just the contribution of the far-field (Γ_2).

2) Owing to the properties of the parabola, the value of the integral in eq. (4.52e) is the same as if a layer of height h had been considered in the classic

configuration 4.2. In other words, integral (4.52d) is equivalent to

$$\int_0^h \left[\rho\gamma u_{ff} + \frac{\mu}{2}\left(\frac{\partial u_{ff}}{\partial y}\right)^2 \right] dy \quad \text{where} \quad u_{ff}(y) = \frac{\rho\gamma h^2}{\mu}\left(\frac{1}{2}\left(\frac{y}{h}\right)^2 - \left(\frac{y}{h}\right)\right). \tag{4.53}$$

This result suggests that, under these assumptions, the current configuration, fig. 4.11, could be mapped to the classic configuration where both soil and structure rest directly on bedrock, 4.2, by taking the soil layer depth to be h.

Finally, recognize that the integral (4.52a) appears in the upper-bound of the thrust derived in the previous section, eq. (4.44), and thus the final result is reached by combining the two:

$$|Q| < \rho\gamma h^2 \sqrt{\frac{\lambda + 2\mu}{3\mu}} = \rho\gamma h^2 \sqrt{\frac{2(1-\nu)}{3(1-2\nu)}} = \rho\gamma h^2 \frac{c(\nu)}{\sqrt{3}}, \tag{4.54}$$

where $c(\nu) = \sqrt{2(1-\nu)/(1-2\nu)} = c_p/c_s$.

Provided all the aforementioned assumptions are substantiated, the bound has to be observed under any variation of the parameters. This entails a couple of relevant scaling results:

1) The bound scales as $\sim h^2$, therefore the actual thrust cannot scale faster than that.

2) The stratum height, H, does not appear in the expression of the bound. This means that the scaling of the thrust in independent of H under these approximations.

In conclusion, the bound also hints that the earth thrust caused by long-wavelength excitation (quasi-static thrust), under these geometric assumptions, is independent of the depth of the stratum, and it increases quadratically with the wall height, what agrees with previous results derived for retaining walls resting directly on rigid bedrock [VY94b].

4.4.3 Verification

Results for the bound, in the case $H = h$, are displayed fig. 4.12. The tightness the bond is remarkable at low Poisson's ratio, and it deteriorates as we approach undrained conditions, yet keep providing an upper bound.

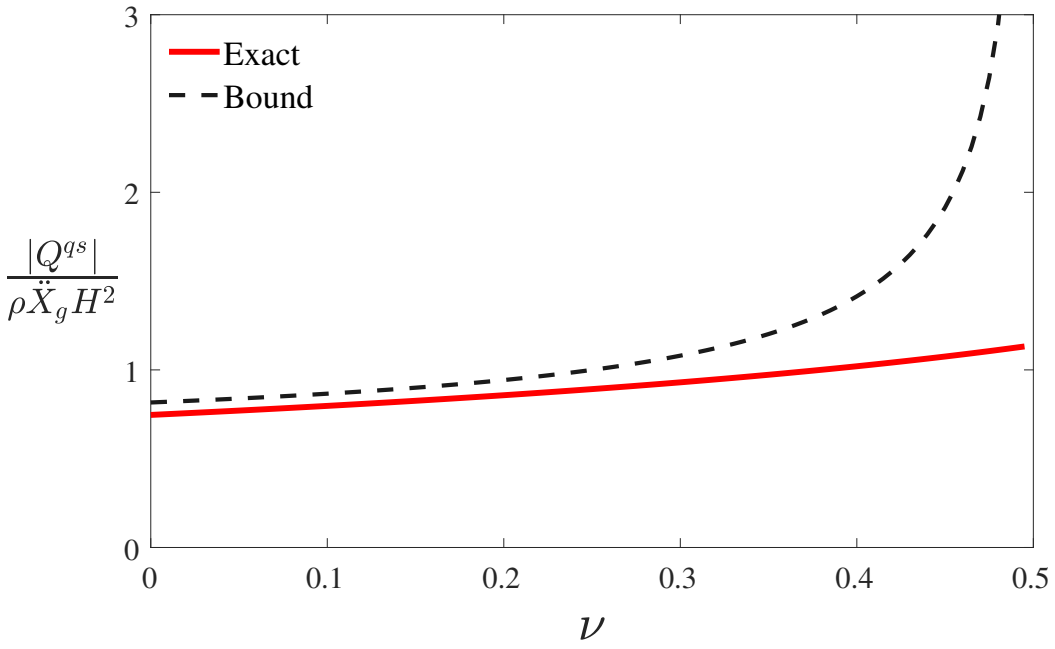

Figure 4.12: Exact solution of the quasi-static thrust derived from eq. (4.14) and comparison to the bound (4.54).

Further verification is still necessary, but we have preferred to develop the results in Chapter 6, as the study carried out in this section does connect naturally with those.

Chapter 5

REDUCED MODELS FOR THE YOUNAN-VELETSOS PROBLEM

In this chapter we tackle:

- A simplified model for the Younan-Veletsos problem is motivated.
- Comparison between the outcome of the reduced model, the exact solution and previous simplified models is pursued.

5.1 Historical survey of simplified models for the Younan-Veletsos problem

The study of the forces that soil exerts over retaining structures dates back centuries. A first clear distinction can be made, based on the methods used for the study:

- Methods based on plastic behavior of soils, foremost, limit-state theory [Lub08], for so-called *yielding* walls, that is, walls that move enough as to elicit plastic response in the soil.
- Those that use the theory of Linear Elasticity to describe both soil and structure [Lov13], which presupposes small deformation in both soil and wall, and thus the wall in this case is called *unyielding*.

The proper approach for the analysis does depend on the typology of the wall that is to be assessed or designed. Static load scenarios can be designed following the classic methods [Cou73]; on the contrary, when it comes to considerations in the dynamic earthquake setting, the right path remains unclear to this day.

On one hand, yielding walls require to consider the soil plastic behavior, what is rather complicated in time-domain, and thus researchers have proposed *pseudo-static* methods, that, in spite of intrinsic limitations, deliver satisfactory, even conservative, outcomes for free-standing gravity or cantilever walls (except if resting on stiff rock). On the other hand, approaches based on Linear Elasticity are suitable to ascertain seismic pressures on unyielding walls (as, e.g., restrained basement walls or rigid-enough underground structures), as long as the structure whose walls are being analyzed does not experiment other SSI effects (rocking). The National

Earthquake Hazard Reduction Program (NEHRP) recommendations [BSS09] sanction this classification. It also suggests that a wall whose top deflects around 0.002 times its height already triggers plastic behavior in its soil vicinity, ergo the threshold to consider a wall as yielding is in practice quite narrow.

The influence of soil-structure interaction (as the aforementioned rocking), the effect of water in the backfill, the role of soil cohesion on the seismic response, as well as other topics, are still a matter of ongoing study.

5.1.1 Approaches based on limit-state theory

Pertaining to the first group, the forerunner is the classic method devised by Coulomb [Cou73], under the tenets of what nowadays is called limit-state theory [Lub08]. This method was developed to describe the response of yielding walls (sliding or rotating) under the action of its own weight and the one of the soil in the backfill. Its adaptation, for cohesionless soils, to attempt to consider also accelerations due to earthquakes came after the great Kanto earthquake (1923), which devastated a number of retaining walls (in paticular, the quay walls of the harbor of Yokohama), and it is referred to as the Mononobe-Okabe (M-O) Method [Oka24].

A number of similar improved schemes were developed later [See70; SZ90], leading to the a state-of-the-art model by Mylonakis and collaborators [MKP07].

All these methods framed the problem in a pseudo-static setting, wherein the earthquake load boils down to another acceleration to consider concurrently with gravity. One can acknowledge the inherent limitations of such approaches:

- They assume that the wall has already deformed outward (away from the soil) so as to generate an active earth pressure, and assume an active triangle soil wedge running from the base of the retaining wall to the surface.
- The soil behind the wall behaves as a rigid body, so accelerations are uniform at the interface between wall and soil, and thus they ignore wave propagation phenomena and their oscillatory nature, being thus unable to provide the actual distribution of pressures, just an estimate of the resultant force. This issue is the more apparent the taller the wall.
- Finally, it is impossible accommodate wall flexibility locally into the framework: either the wall moves as a rigid body or it remains completely still.

Moreover, there is a lack of consensus both on how to define the earthquake acceleration that is to added to gravity and how to consider heterogeneous backfills. In spite of these issues, these methods enjoy wide use to this day and seem to provide satisfactory design up to PGA 0.4 g [CMS16].

5.1.2 Approaches based on Elasticity

The only mathematically rigorous solution was obtained by Wood [Woo73], during the course of his graduate studied at Caltech under Housner's supervision. He considered a 2D finite stratum of soil on rigid bedrock confined between walls deforming under linear-elastic plane-strain conditions, and argued that the solution would resemble the one corresponding to a laterally semi-infinite soil stratum when the distance between walls was large enough. Nevertheless, this solution's mathematical "decorum" is overshadowed by being unintuitive (the mathematical expressions do not lend themselves to straightforward physical interpretation) and also troublesome to evaluate numerically.

Simplified models for one-wall systems have been developed throughout the years in order to circumvent this issue. Most of them rely on either proposing a kind of, what, following Verruijt [Ver96], we refer as *confined* elastodynamic solutions, wherein a displacement component or, as we will see, a stress component is neglected. Examples of the first have been successfully implemented in elastostatics [Wes38] and elastodynamics [Bar80].

The first attempt to consider a one-wall system directly trace back to the work by Matsuo and Ohara [MO60]. They assumed a *confined solution* in which no vertical displacement develops anywhere in the soil domain, not even at regions close to the wall. This solution happened to be unbounded in the incompressible-material limit.

Around the same time as Wood developed his exact solution, Scott [Sco73] proposed an innovative approach. Instead of trying to solve the equilibrium equations, the soil surrounding the wall is substituted by massless springs per unit of length of area (which are, potentially, a function of the frequency of the base-imposed excitation) that connect it to the far-field, which deforms as a 1D soil column ("shear beam"). The analytical solution can be easily obtained, as the stresses at the soil-wall interface arise from the difference between displacements in each region times the spring constant. Despite of its simplicity, or rather owing to it, this model does account for either the actual deformation mechanisms in the soil as shearing in the soil or potential dynamic amplification.

Some alternative one-wall models were provided later, e.g. Arias [ASO81] extended Scott's model discretization the soil domain as a web of masses connected by springs, but they failed to provide much-needed insight into the influence of relevant parameters, as wall flexibility or alteration of soil stiffness with depth,

The classic solutions for the one-wall case are due to Veletsos and Younan [VY94a; VY94b]. In the first, they assumed that no normal vertical stress develops anywhere in the soil in order to simplify and subsequently solve the equations of motion, so a solution for the displacement field, over the whole domain, could be retrieved. This pivotal assumption seems to be disproved by comparison to numerical simulations (where it is readily acknowledged that all the entries of the stress tensor are of the some order of magnitude in the wall surroundings). Additionally, satisfying vertical equilibrium and the boundary condition $\tau_{xy}|_w = 0$ is not possible due to the introduction of this severe simplification.
In the second, [VY94a], a substantial improvement on Scott's model 1973 was presented. It was assumed that the soil stratum behaves as an elastically-supported, semi-infinite horizontal visco-elastic bar with distributed mass and that the horizontal gradient of vertical displacements in the calculation of shear stresses is negligible, and thus a solution for the medium impedance was derived, so the stress field on the wall can be related to the displacement field in the far-field (1D soil column).
Later [YV00]), their analysis was refined to consider different wall typologies, yet the foregoing simplifications were kept. Nevertheless, this work became the first one in attempting to include the effect on wall flexibility on the magnitude and distribution of pressures.

In spite of their simplifications, the models predicts numerical simulations outcome satisfactorily and agree well with Wood's "exact" solution.

A more detailed summary of these and other previous studies, until 2011, was provided by [WS16]. State-of-the-art models, as those proposed by Klokinas and collaborators [KLM12], later used in the already-mentioned "kinematic framework" [BMS15], have been directly influenced by the Veletsos-Younan's 1994 landmark papers.

It is incumbent to note that all the aforementioned models rely only on the mechanical equilibrium equations (e.g. linear momentum balance) to study the problem at hand, bypassing any restriction that could be derived from energetic considerations. Moreover, requirements deriving from boundary conditions was sidestepped assuming that, in order to obtain simple engineering solutions, they had to be discounted.

In summary, there are a number of published solutions available but we shall show that, due to the pivotal assumptions they introduce, they miss some of the phenomena in the problem, as now it can be readily acknowledged from the exact solution derived in section 4.3.2.

5.2 Justification for the simplified model

A more detailed survey, including discussion, is provided by [SMC12], and a more recent one by [KL19]. One should recognize that the two techniques seem to deliver contradictory results/design recommendations, which, besides, are at times difficult to reconcile with experiments [WS16; Hus+16b].

The adequacy of a simpler, more amenable yet still insightful manner of tackling the problem other than dealing at once with the exact solution was put in full display in the previous chapter.

The proposed approach is directly based on the insight derived from section 4.3.3. This consisted of using the qualitative behavior of the displacement field to simplify the equations of motion, eqs. (2.27a) and (2.27b), to then derive a proxy model from these simplified equations. The main underpinning under this simplified model is the introduction of a new compressibility factor in the spirit of the one by Veletsos' [VY94b], called κ, which allows for simpler treatment of the equilibrium equations by decoupling the horizontal equilibrium from gradients of vertical displacement. The value of this compressibility factor is obtained upon imposition of one of the conservation laws mentioned in section 2.5, namely $\hat{\mathrm{J}}_x = 0$. This will be shown to work swimmingly for the quasi-static case and in the dynamic regime, although in the latter case the expression is more convoluted and requires evaluating sums of modal contributions.

The complete derivations, including commentary, can be found in Appendix D.

A suite of comparisons between the simplified and the exact solution and to other published aproximations will be pursued at the end of the chapter.

5.2.1 Concerning the horizontal displacement

Referring to mechanical equilibrium: according to the previous arguments, the zeroth-order equilibrium very far from the wall (that is, when $\Delta x \sim \ell_s$ or equivalently $x/H \gg 1$), comes given by eq. (4.21). Conversely, the zeroth-order equilibrium very close to the smooth and rigid wall (that is, when $\xi \to 0$ or $x/H \ll 1$), is defined by the system of eq. (4.32). Note that, in both limits, $x/H \ll 1$ and $x/H \gg 1$,

horizontal equilibrium decouples from vertical, in both approximations.

Thus, let us put forward a simplified model whose horizontal equilibrium is given by

$$c^2\frac{\partial^2\tilde{u}}{\partial\xi^2}+\frac{\partial^2\tilde{u}}{\partial\eta^2}-r^2\frac{\partial^2\tilde{u}}{\partial t^2}=e^{i\tau}\,. \tag{5.1}$$

Such a model is "leading-order equivalent" to the original one s it yields the same first-approximation behavior in both aforesaid limits, as long as the boundary conditions are not amended. The solution of this equation, provided boundary conditions are satisfied, could be expected to deliver a horizontal displacement evolution with the similar limit behavior as the original model.

Nevertheless, this model would return unphysical results as $\nu\longrightarrow 1/2$ (incompressible material limit): the horizontal displacement would tend to zero uniformly everywhere in the incomprenssibility limit. Observe that this problem is the same that was reported by Matsuo and Ohara [MO60]. Additionally, eq. (2.49) would not be satisfied. The issue arises from the on-the-wall equilibrium when only the first-order approximation is considered, hence, in order to correct it, more terms should be taken into account, but the equation coupling would reappear.

Instead of adding extra terms, let us modify eq. (5.1): let us change the parameter c that appears in by $1/\kappa$, a new compressibility factor, in the hope that the issue leading-order behavior is corrected without the coupling returning. Once the approximated displacement field is found in terms of κ, it remains the open question of how to find its actual value. We posit that fixing κ so as to render the simplified displacement in agreement to eq. (2.51) increases the fidelity of the simplified model, and hence it has to yield a proper approximation of the actual response that we can survey from the exact solution. One could wonder if this parameter derives from quasi-static energy balance and it does not change when considering dynamic effects. We shall show the shortcomings of such an assumption later.

Summarizing, consider the following equation in lieu of eq. (5.1):

$$\frac{1}{\kappa^2}\frac{\partial^2\tilde{u}}{\partial\xi^2}+\frac{\partial^2\tilde{u}}{\partial\eta^2}-r^2\frac{\partial^2\tilde{u}}{\partial t^2}=e^{i\tau}\,. \tag{5.2}$$

When solving this equation, the eigenfunction expansion corresponding to the infinite stratum will be used. This will entail a failure in meeting boundary conditions on the upper free edge of the stratum, except at the far-field and on the wall. There

are alternative approaches that would deliver better characterization of the displacement field, these are sidelined as is deemed unfitting given our final goal is obtaining resultant forces on the wall.

5.2.2 Concerning the vertical displacement

As for the second simplification: when $x/H \ll 1$, the vertical equilibrium equation, eq. (4.32b), is left unchanged, but the wall smoothness and rigidity entailed

$$\left.\frac{\partial \tilde{v}}{\partial \xi}\right|_{\xi=0} = \left.\frac{\partial^3 \tilde{v}}{\partial \xi^3}\right|_{\xi=0} = \left.\frac{\partial^5 \tilde{v}}{\partial \xi^5}\right|_{\xi=0} = \ldots = 0\,, \tag{5.3}$$

as it was obtained while discussing section 4.3.3; this does not require even derivatives being also equal to zero, but it does suggest that the vertical displacement behaves as, for instance, $\cosh(\xi)$ as $\xi \to 0$ (very close to the wall). Hence, let us assume that the vertical displacement $\tilde{v}$ scales as such in a local neighborhood very close to the wall.

If the horizontal displacement was given, the term $-(c^2-1)\partial^2\tilde{u}/\partial\eta\partial\xi$ in eq. (4.32b) follows directly and eq. (4.32a) can be solved as a forced wave equation where $\tilde{v}$ is the only unknown.

5.2.3 Heuristics and outcome of simplified approach

Summarizing, the heuristic approach being proposed consists of:

1) Solving the forced wave equation for the horizontal displacement, eq. (5.2), subjected to the rigidity condition on the wall.

2) Once the horizontal displacement evolution is known, moving to solve the approximate vertical equilibrium on the wall, eq. (4.32b), subjected to boundary conditions eq. (4.25b) and eq. (4.25d), exploiting any simplification deduced from the analysis of the on-the-wall behavior, eq. (5.3). At this point the displacement field is defined up to an unknown parameter, κ.

3) Finding the earth thrust on the wall and other variables, as functions of the unknown parameter κ.

4) Using the displacement field in $\mathrm{J}_x = 0$, eq. (4.38), find κ from this identity. This effectively closes the loop and the solution is wholly defined.

By fulfilling this heuristics, the earth thrust and the overturning moment are retrieved:

$$\frac{Q}{\rho \ddot{X}_g H^2} = \kappa \left[(c^2-2)\left(\bar{A}\cos(r_c) + \bar{B}\sin(r_c)\right) + \sum_{n=1}^{\infty} c^2 \tilde{u}_n \frac{\sqrt{k_n^2 - r^2}}{k_n} \right], \tag{5.4}$$

$$\frac{M_b}{\rho \ddot{X}_g H^3} = \kappa \Bigg[(c^2-2)\left(\cos(r_c)\left(\bar{A} + \frac{\bar{B}}{r_c}\right) + \sin(r_c)\left(\bar{B} - \frac{\bar{A}}{r_c}\right)\right) + \\ + \sum_{n=1}^{\infty} \frac{(-1)^{n+1}}{k_n}\left(c^2 \tilde{u}_n \frac{\sqrt{k_n^2 - r^2}}{k_n} - (c^2-2)\bar{C}_n \right) \Bigg], \tag{5.5}$$

where the value of the parameters that appear in the previous results are given by

$$\tilde{u}_n = -\frac{2}{k_n(k_n^2 - r^2)}, \tag{5.6a}$$

$$\bar{C}_n = \frac{(c^2-1)}{c^2} \frac{\sqrt{k_n^2 - r^2}}{k_n^2 - (r/c)^2} k_n \tilde{u}_n, \tag{5.6b}$$

$$\bar{A} = -\sum_{n=0}^{\infty} \bar{C}_n \tag{5.6c}$$

$$\bar{B} = \bar{A}\tan(r_c) + \sum_{n=1}^{\infty} \frac{\bar{C}_n (-1)^{n+1} k_n}{r_c \cos(r_c)} \left(1 - \left(\frac{c^2-2}{c^2-1}\right)\frac{(k_n^2 - (r/c)^2)}{k_n^2}\right), \tag{5.6d}$$

and $r = \varpi H/c_s$, $r_c = \varpi H/c_p$, $c = c_p/c_s$, $k_n = (2n-1)\pi/2$, with $n = 1, 2, 3, \ldots$ up to the number of modes one wanted to take into consideration.

To overhaul the derivation of the previous results, see Appendix D. There one can also find results corresponding to the low-frequency / long-wavelength limit of the solution. It is obtained for this regime that

$$\frac{Q^{qs}}{\rho \ddot{X}_g H^2} = -\kappa(\nu)\left[\left(\frac{2-\nu}{1-\nu}\right)\frac{14A}{\pi^3} + \left(\frac{\nu}{1-\nu}\right)\frac{8G}{\pi^2}\right], \tag{5.7}$$

$$\frac{M_b^{qs}}{\rho \ddot{X}_g H^3} = -2\kappa\left[\left(\frac{2-\nu}{1-\nu}\right)\frac{16}{\pi^4} + \left(\frac{\nu}{1-\nu}\right)\frac{2G}{\pi^2}\right], \tag{5.8}$$

$$\mathsf{e}^{qs} = \frac{M_b^{qs}}{HQ^{qs}} = \frac{16(2-\nu) + 2G\pi^2\nu}{7\zeta(3)\pi(2-\nu) + 4G\pi^2\nu}. \tag{5.9}$$

A is the Apery's constant (≈ 1.202), and G is the Catalan's constant (≈ 0.916). Note that the eccentricity of the thrust with respect to the wall base does not depend on κ.

The way the problem was chosen to be tackled did not use the concept of impedance at any point. Our analysis shows (see Appendix D) that the definition of impedances

does not happen in a forward manner in the quasi-static case, and that it is completely unframeable in such terms in the dynamic regime.

Recall that the quasi-static impedances are defined by

$$\sigma_{xx}|_w(y) = \sum_{n=1}^{\infty} K_n u_n|_{ff}(y)\,. \tag{5.10}$$

Thus, based on eq. (5.7), one can define

$$K_n^{qs} = \kappa k_n \Big(\frac{(3c^2-2)}{c^2} + \frac{(c^2-2)}{c^2}\frac{8G}{\pi^2}k_n \Big)\frac{\mu}{H}\,, \tag{5.11}$$

which would yield the same thrust as eq. (5.7).

Note that κ appears in its expression, which vehemently states that the boundary conditions on the wall have direct influence on the impedance values. This result suggests that the impedance is a parameter which is very difficult to bring into the problem unless they are defined a priori. It does not "spring" naturally from the equations and requires a fair deal of manipulation to bring it to stage, and once this happened, it seems to contradict our previous intuitions.
Overall, the resolution of this parameter not representing any kind of fundamental soil parameter, as re-stated recently by [Dur+18], is bolstered.

The explicit form κ still lingers. As mentioned earlier, a compact form of κ derived from the dynamic condition eq. (2.49) is elusive. For this reason, only the component associated to the fundamental mode will be considered in $\kappa(\nu, r)$ as shown. Nevertheless, when considering the quasi-static regime one can sum up the contribution of all the modes and find a compact closed-form expression for $\kappa(\nu)$. The quasi-static value of κ (squared, actual value corresponds to the positive root) is:

$$\kappa(\nu)^2 = \frac{1-\nu}{(\frac{192G^2}{\pi^4}-1)\nu + 96\frac{G^2}{\pi^4}(\frac{7A}{2\pi G}-1)+\frac{3}{2}} \tag{5.12}$$

whereas the dynamic one is

$$\kappa(\nu, r)^2 = \\ c^2 - \frac{2r^3}{r-\tan(r)}\sum_{n=1}^{\infty}\left[\frac{(c^2k_n - r^2)\bar{C}_n^2}{4} + \frac{c\,r\left(\frac{(\bar{A}^2-\bar{B}^2)\sin(2r_c)}{2} + 2\bar{B}\bar{C}_n + 2\bar{A}\bar{B}\sin^2(r_c)\right)}{2}\right]. \tag{5.13}$$

In order to gauge the model's accuracy, or lack thereof, we perform a suite of comparison to the exact solution derived in section 4.3.2.

5.2.3.1 Quasi-static results

First, we shall compare results concerning the low-frequency / long-wavelength regime. As a starting point let us use the same parameter that was used in section 4.3 to start the verification the simplified model, that is, the vertical displacement at the top of the wall, labeled v_{top}.

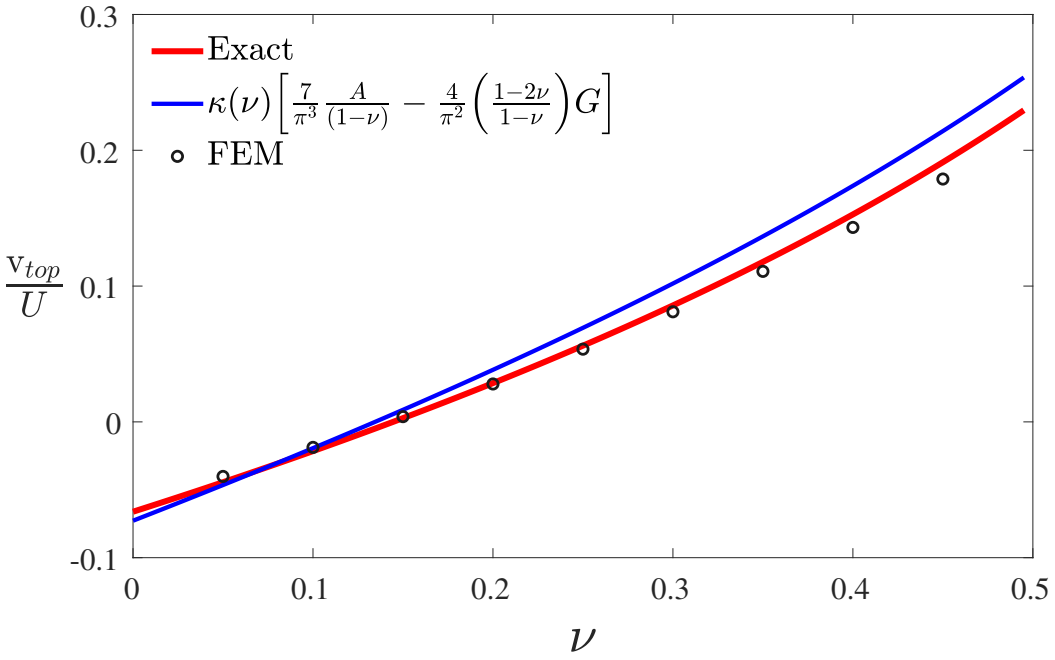

Figure 5.1: Comparison of quasi-static vertical displacement at the top of the wall: eq. (4.15) (Exact), model outcome and *Abaqus* (FEM)

The finite elements solution and the exact solution agree very well. The simplified model displays the same qualitative trend, even though it yields slightly larger values for almost-incompressible soils.

Once the vertical displacement has been considered, let us move forward in identical manner and consider the earth thrust. First, we would like to verify the thrust in the simplified model, not only against the exact quasi-static ($\Pi'_{14} \ll 1$) as a function of Poisson's ratio but also against Wood's exact solution for the two-wall system (which was used as the exact solution for comparison purposes until now), and, for the sake of completeness to FEM results.

At every instance, the thrust displays the same qualitative and quantitative features. All the solutions resemble each other.

The adjustment between exact quasi-static thrust and our new estimate is as tight as

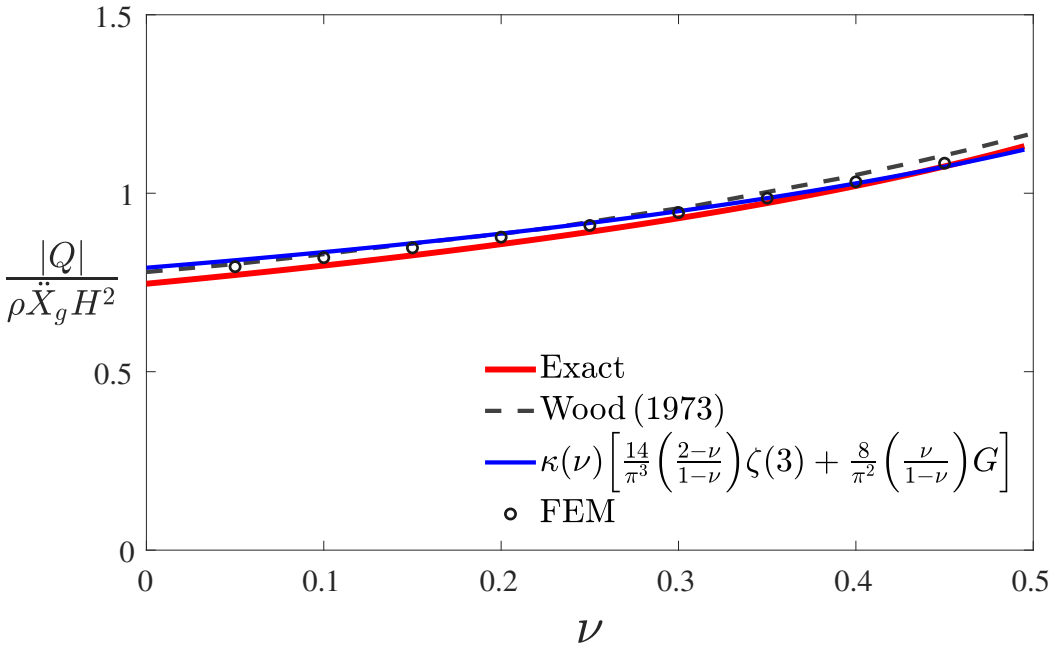

Figure 5.2: Comparison of quasi-static earth thrust: eq. (4.14) (Exact), exact solution for two-wall system (Wood (1973)), model outcome and *Abaqus* (FEM)

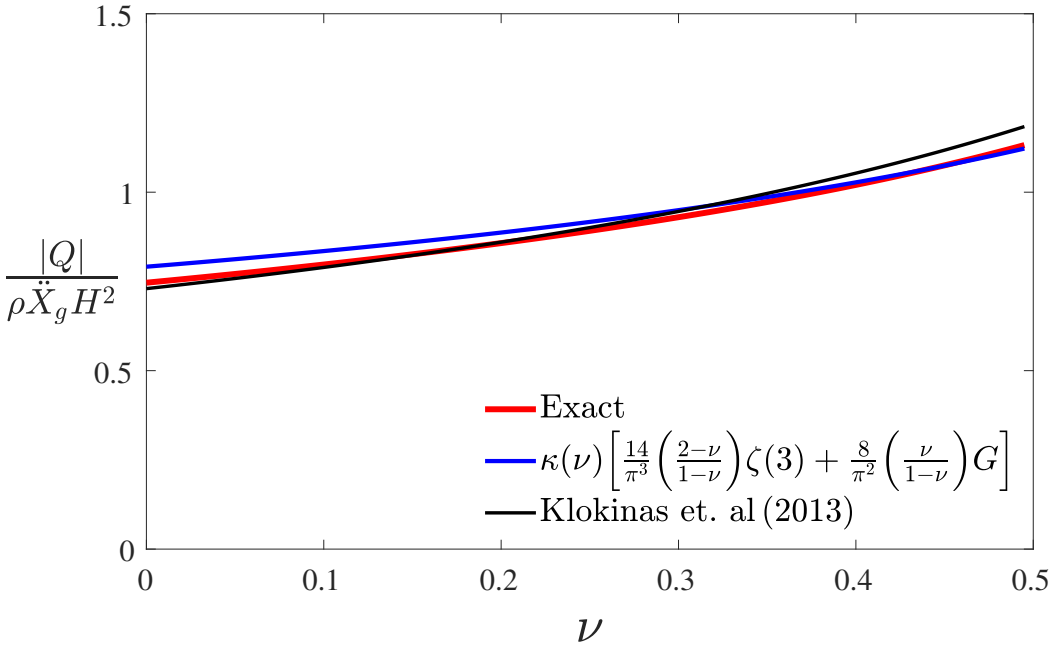

Figure 5.3: Comparison of quasi-static earth thrust: eq. (4.14) (Exact), model outcome and result in [KLM12] using sinusoidal shape.

the previous model [KLM12]. This result entails that the impedances in eq. (5.11) differ very little from those used in [KLM12] and, by extension, in [VY94a].

5.2.3.2 Dynamic results

A comparison between the dynamic results that the new model yields proceeds.

In first place, fig. 5.4 displays a comparison for the thrust ($\nu = 1/3$), including previour work [KLM12]. We acknowledge how using the parameter derived from the fully-dynamic J integral improves the agreement towards the exact solution.

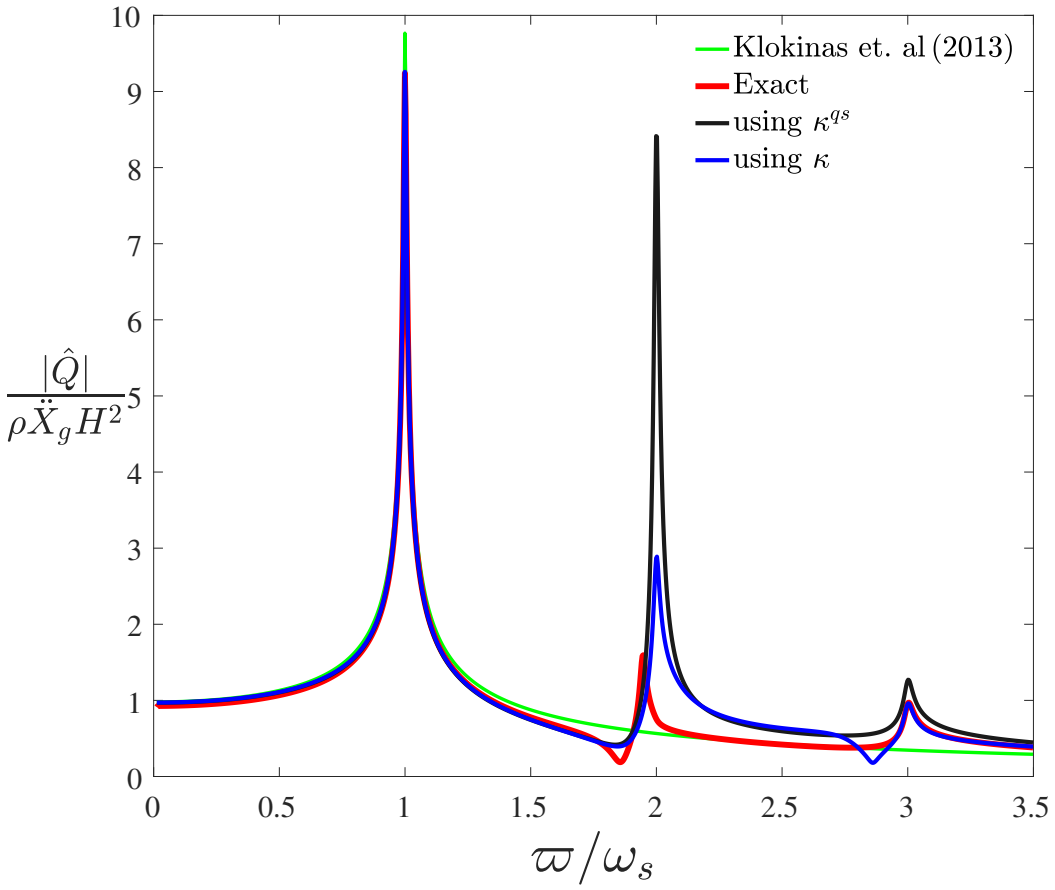

Figure 5.4: Comparison of dynamic earth thrust: eq. (4.14) (Exact), model outcome using $\kappa^{qs}(\nu)$ and $\kappa(\nu, \varpi)$ ($\nu = 1/3$)

Thrust for different values of damping and another Poisson's ratio ($\nu = 0.1$ in this case) are contained in fig. 5.5. Not only the fit of the simplified model to the exact solution is good, but also is better than the previous state-of-the-art model [KLM12], which misses the dip at ω_p altogether.

Finally, an comparison for $\hat{\mathrm{v}}_{top}$ is included for completeness sake ($\nu = 1/3$). Here, we also acknowledge how using $\kappa(r, \nu)$ instead of $\kappa^{qs}(\nu)$ improves the agreement between exact solution and model at the critical second resonance.

A comparison between $\kappa(r,\nu)$ and $\kappa^{qs}(\nu)$ that helps explain the previous results is presented in fig. 5.7.

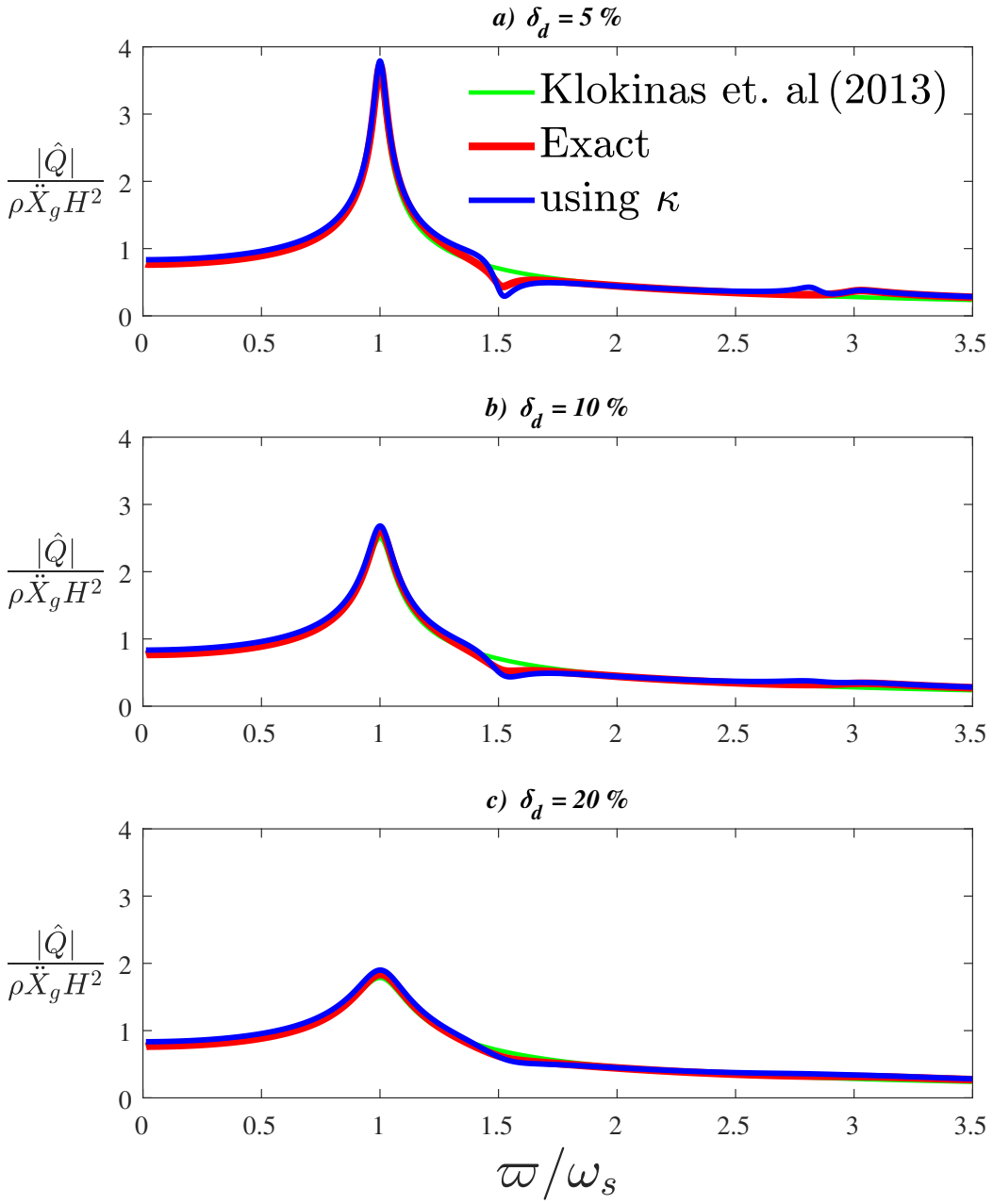

Figure 5.5: Comparison of dynamic earth thrust: eq. (4.14) (Exact), model outcome using $\kappa^{qs}(\nu)$ and $\kappa(\nu,\varpi)$ (ν = 0.1)

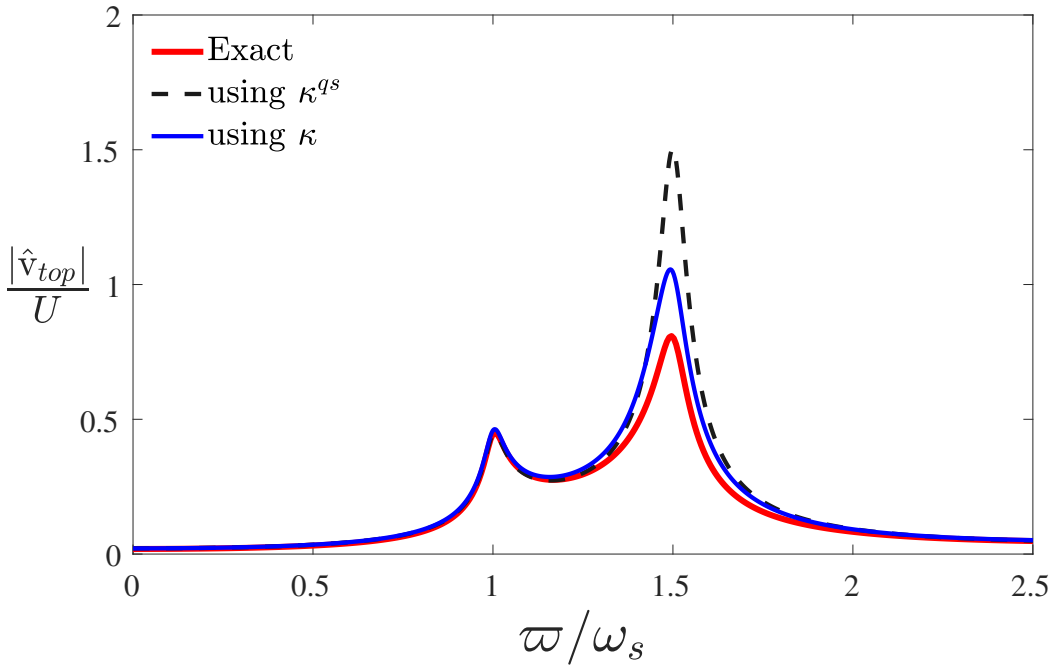

Figure 5.6: Comparison of dynamic vertical displacement at the top of the wall: eq. (4.14) (Exact), model outcome using $\kappa^{qs}(\nu)$ and $\kappa(\nu, \varpi)$

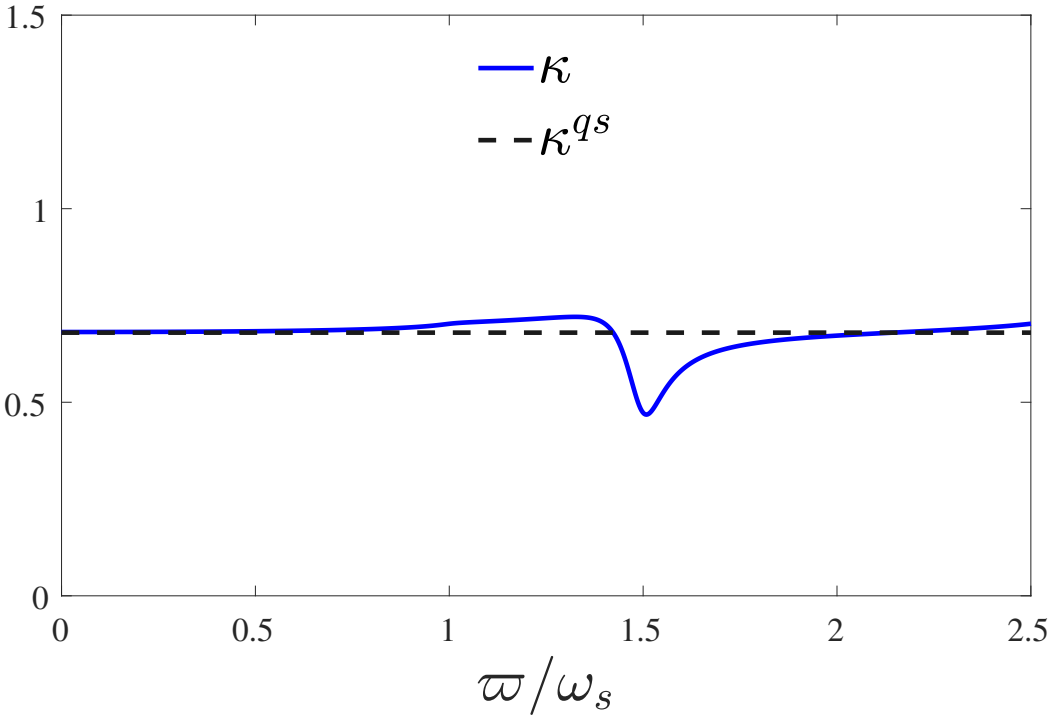

Figure 5.7: Comparison of dynamic $\kappa(\nu, \varpi)$ and quasi-static $\kappa^{qs}(\nu)$ compressibility factors

Chapter 6

SOIL-STRUCTURE KINEMATIC INTERACTION AS AN INSTANTIATION OF CONFIGURATIONAL FORCES

In this last chapter that culminates our thesis work we shall spell out a novel conceptualization of the a consequential phenomenon in SSI: *kinematic interaction*.

- We shall first present and motivate the subject in a succint introduction.
- The identities that the conservation laws expressed by the PII (balance of configurational forces) yield for the case of strip footing are presented and interpreted.
- Base motion filtering is analyzed in terms of balance of configurational forces between near-field and far-field. An approximation for the long-wavelenth regime is obtained from the balance, assuming other further simplifications, and compared to recent results [CMV17].

6.1 Introduction

We revisit the traditional interpretation of kinematic interaction to later provide a new one in terms of configurational forces.

6.1.1 The customary framework

The moniker *kinematic interaction* was introduced by Prof. E. Kausel [Kau76] and Prof. Whitman [SWL77], and since then, it has made its way into common parlance among scholars interested in SSI.

The phenomon itself was conclusively demonstrated by Housner, who, in a prominent paper [Hou57b], subjected various records of seismic response of the Hollywood Storage Building *along different directions* to scrutiny. It was concluded that wavefiled propagating along the foundation long direction experienced significant changes, whereas the one propagating along the short direction did not. Such a dichotomy, Houser resolved, must owe to the inability of the stiff foundation to "accommodate" deformations in the ground whose wavelength is similar or shorter than the dimensions of the foundation.

The importance of Housner's realization lays in the need for understanding how waves elicited by an earthquake interact with structures so that they can be designed and appraised properly. It is therefore unsurprising that the celebrated three-step method [KR74], which puts forward an alternative to avoid having to carry out dynamic simulations including a large chunk of the soil domain, considers the evaluation of kinematic interaction as its first step aimed to answering the question how the displacement field is affected by the inclusion of a rigid interface that mimics the presence of a buried structure.

Researchers at the Massachusetts Institute of Technology (MIT) [EMR77] gathered numerical results that furnished, for the first time, "transfer" functions relating the far field response to the displacement and and rotation of an embedded strip foundation. Luco and Mita [ML89; LM87], Veletsos and Wei [VW71], among others, have provided useful simulation results that provide foundation input motion for a number of soil parameters (including layering) and foundation parameters (including different shapes and embedment ratios).

There has been a number of scholars occupied with this problem since the 70's, and a bevy of simplified models have been devoted to comprehend its inner workings. For instance, the one proposed by Scanlan [Sca76] captures beautifully and explains some features in three dimensions, and has inspired many further explorations.

6.1.2 From the viewpoint of configurational forces

In section 1.2.2, we intended to motivate the concept of configurational forces by means of the classic examples of cracks and dislocations. In both cases, we observe that there is a region within the material around a "defect" or "inhomogeneity" that moves with respect to the body bulk it is immersed in. Let us, once again, reiterate the equivalence among these scenarios and the one of a rigid excavation carved out from the body free surface.

Picture a seismic event jolting the soil domain. A direct comparison of equivalent soil volumes in the different locations would reveal that there exists a relative displacement between near field and far field. This split arises from the presence of a superimposed field to the one we would find at the far-field, the so-called scattered field produced by the geometric irregularity. This is a customary interpretation given by SSI theory to this scenario, which also involves some rather specific terminology as base filtering, slab averaging and others.

We would like to put forward an alternative, yet equivalent, description: the ex-

cavation, seen as an inclusion inside the otherwise homogeneneous system, elicits configurational forces in the material that cause the region of soil around it to move relatively to the homogeneous ("inclusionless") regions of the body. We shall demonstrate how PIIs provide a better grasp on what is going on, as these establish a quantitative relation between the well-understood response in the far-field and at the near-field, unbeknownst to us.

One remarkable advantage of this framework is allowing a crystal-clear separation of effects purely due to the presence of the geometric discontinuity from those due, primarily, to the dynamic response of the foundation and the superstructure. Another advantage is providing direct relation between the parameters involved, which can help gauging the influence of "knotty" features, e.g., contact conditions between soil and foundation or foundation geometry.

In summary, the aim of this chapter is to explore what the path-independent integrals mean for kinematic interaction. The issue at hand is synthesized mathematically through a boundary value problem with mixed boundary conditions which, moreover, is defined over a domain with a convoluted boundary. For the most part, this has been assessed trough numerical results and simplified models. Instead, this alternative framework, at whose core the conservation laws, as seen in section 2.5, lay, yields, first, a general exact[1] set of relations connecting quantitatively the response of the far-field to the one of the excavation and the near field through balance of configurational forces are obtained. Second, once these identities are set in place, they can be simplified in order to derive a compact model to compare with the classic functions for *foundation input motion* provided by Elsabee and Morray [EMR77].

6.2 Identities to evaluate foundation input motion

We will study the response of a rigid excavation within a plane-strain homogeneous half-space subjected to SH waves, thence leaving out the possibility of a bedrock. The geometry of the excavation is defined by the height at the flanks, h, and its total in-plane width, W, see fig. 6.1.

Notice that, under these circumstances, the system is alike the one discussed in section 4.2, hence the system can represent a massless rigid strip footing as well as a water reservoir, with a few minor adjustments as having to take the limit $\Pi_1 \gg \infty$, so one must define $\Pi''_{14} = \Pi'_{14}/\Pi_1 = \varpi h/c_s$ incidentally, and ignoring hysteretic

[1] Exact in the sense of involving no simplifications within the scheme of steady-state plane-strain elastodynamics

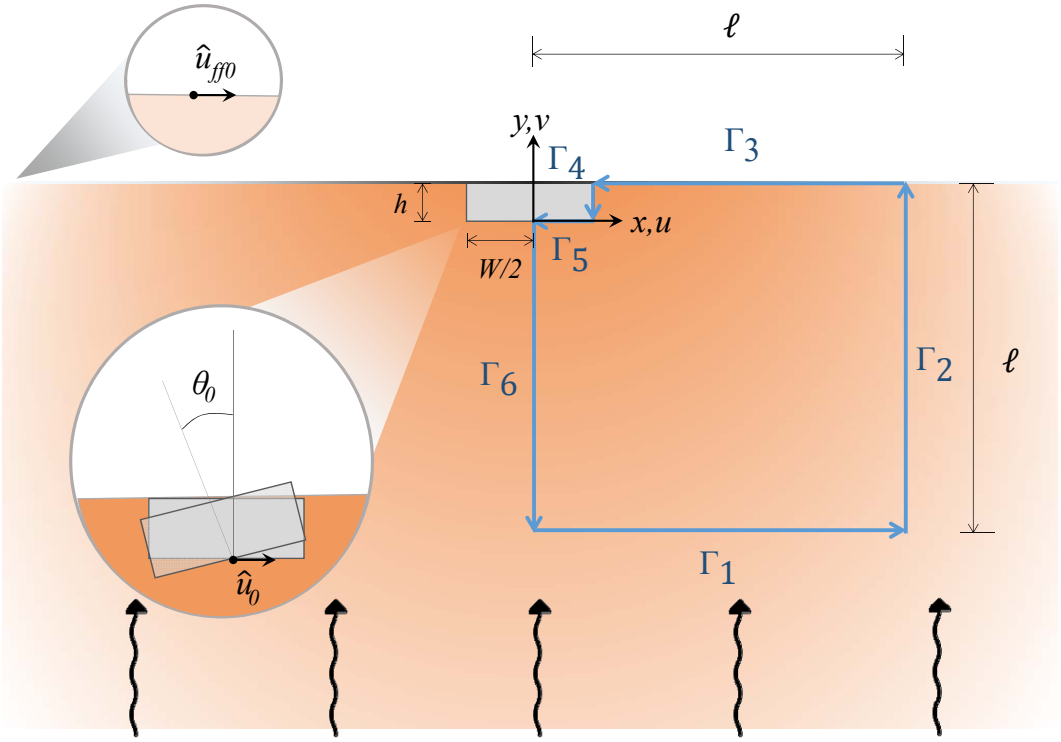

Figure 6.1: Scheme of the problem to be considered including the contour used to evaluate conservation laws

damping. Hence Π_7 vanishes and the new Π''_{14} replaces Π'_{14}, but see how prior conclusions on governing dimensionless groups extend to the current scenario. In this scenario, our dimensional analysis is equivalent to the one carried out by Conti and coworkers [CMV17]. In summary, we may say, for instance,

$$\frac{\theta_0 h}{\hat{u}_{ff0}} = I_\theta\left(\Pi_2, \Pi_6, \Pi''_{14}\right) = I_\theta\left(\frac{W}{h}, \nu, \frac{\varpi h}{c_s}\right), \tag{6.1}$$

where, recycling Conti's notation, $\hat{u}_{ff0}$ is the displacement at the free surface in the far-field and θ_0 is the rotation for foundation input motion.

Before going any further, keep in mind this an antisymmetric problem, composed by a symmetric geometry excited by an antisymmetric load. This fact will be summoned over and over as we study and simplify the contributions of different portions of the contour.

The system is considered to be excited by a harmonic wave, and to be in steady-state. The governing equation is eq. (2.37). The coordinate system origin is located at the middle point of the excavation base (over the axis of geometric symmetry, see fig. 6.1). We shall use the contour $\Gamma = \Gamma_1 \cup \Gamma_2 \cup \Gamma_3 \cup \Gamma_4 \cup \Gamma_5 \cup \Gamma_6$ in fig. 6.1 to

evaluate the integrals; the length ℓ can be deemed finite at first, yet it will tend to infinite once the proper argumentation has been discussed. Extra attention must be drawn to considering the displacement field at each contour accordingly.

6.2.1 Forthright simplifications of the displacement field

Before moving to evaluate the conservation laws on the contour, we shall discuss straightforward simplifications that boundary conditions, antisymmetry, and rigidity of the inclusion interface grant from the start.

6.2.1.1 Displacements at the far field

The displacement field at the far field corresponds to unidimensional wave propagation over at the subspace, as studied in section 3.2, and thus the displacement field is made up solely by horizontal displacement taking value at the top $\hat{u}_{ff}(y = h) = \hat{u}_0$ and depth evolution given by $\cos(\varpi(y - h)/c_s)$.

6.2.1.2 Displacements at the free surface

The displacement field is unknown, but the traction-free boundary condition imposes $\hat{\tau}_{xy}|_{y=h} = \hat{\sigma}_{yy}|_{y=h} = 0$.

6.2.1.3 Displacements over the axis of geometric symmetry

This is also the antisymmetry axis. Therein the vertical displacement is null, $\hat{v}|_{x=0} = 0$ and hence $\partial\hat{v}/\partial y|_{x=0} = 0$, whereas the horizontal displacement attains an extremum (minimum magnitude), and thus $\partial\hat{u}/\partial x|_{x=0} = 0$. Owing to these vanishing gradients, there are no normal stresses over axis. About the other gradients, clearly $\partial\hat{u}/\partial y|_{x=0} \neq 0$ and $\partial\hat{v}/\partial x|_{x=0} \neq 0$ either, hence the stress state is compounded solely by shearing.

6.2.1.4 Displacements in the excavation

The displacement field over the rigid excavation can be defined by three parameters: a horizontal displacement $\hat{u}_0$, a vertical displacement $\hat{v}_0$ and a rotation θ_0, measured with respect to the middle point of the base, which happens to be also the origin of the coordinate system. Hence, granting small displacements and rotations, the

displacement of the walls are

$$\hat{u} = \hat{u}_0 - \theta_0 y\,, \tag{6.2a}$$

$$\hat{v} = \hat{v}_{FIM} \pm \theta_0 \frac{W}{2}\,, \tag{6.2b}$$

where the ± sign depends on considering the right wall (+) or the left one (−). The displacements of the base are

$$\hat{u} = \hat{u}_0\,, \tag{6.2c}$$

$$\hat{v} = \hat{v}_{FIM} \pm x\theta_0\,. \tag{6.2d}$$

Since the problem is antisymmetric, $\hat{v}_0 = 0$, therefore the only vertical displacement must arise from rotation along the middle point of the base, as it is the only way that vertical displacements can be rendered agreeable to the antisymmetry conditions. In summary, at the wall

$$\hat{u} = \hat{u}_0 - \theta_0 y\,, \tag{6.3a}$$

$$\hat{v} = \pm\theta_0 \frac{W}{2}\,, \tag{6.3b}$$

and that of the base

$$\hat{u} = \hat{u}_0\,, \tag{6.4a}$$

$$\hat{v} = \theta_0 x\,. \tag{6.4b}$$

See that some gradients are still unknown, namely

$$\left.\frac{\partial \hat{u}}{\partial x}\right|_{x=W/2}, \quad \left.\frac{\partial \hat{v}}{\partial x}\right|_{x=W/2}, \quad \left.\frac{\partial \hat{u}}{\partial y}\right|_{x=0}, \quad \left.\frac{\partial \hat{v}}{\partial y}\right|_{x=0}. \tag{6.5}$$

These are the horizontal gradients on the wall and the vertical gradients at the base, which correspond, respectively, with $\hat{\sigma}_{xx}|_{x=W/2}$, $\hat{\tau}_{xy}|_{x=W/2}$, $\hat{\tau}_{xy}|_{y=0}$ and $\hat{\sigma}_{yy}|_{y=0}$.

6.2.2 A necessary note on modelization

We presuppose steady-state conditions. This assumptions deserves some discussion as it seems that the only way that can be formally introduced is on very specific intermediate-asymptotics scenario.

First of all, we presume steady-state harmonic excitation passing across Γ_1 on its way to the foundation and the free surface. By considering an adequate time span stretched as to assume that the first front has reached the free surface and the excavation and time long enough as to guarantee that steady-state conditions have

been attained there, yet at the same time short enough as for the reflected waves (or the scattered field for that matter) not to have time to reach and perturb the field at Γ_1. See how this argumentation in terms of time boils down to choosing a large enough value of ℓ in the contour.

Hence, we may assume that steady-state conditions exists at both the near-field and the far-field, but nothing has been said about the contours connecting them. Notwithstanding that steady-state conditions cannot be presumed at all points over these contour segments, the contribution of the portions undergoing transient change can be narrowed down if the contour length ℓ is chosen judiciously. When it comes to Γ_6, the inherent decay of the scattered field allows for a straightforward defintion of a region unaffected by it, and contribution from any reflection on the rigid interface can be belittled as much as wished by increasing ℓ sufficiently. Considering Γ_3, the wiggling excavation will behave as a source of surface waves; geometric spreading losses will be present in 3D analysis, but not in this 2D study, therefore one must exercise caution when arguing where the far-field starts (regardless where it does, Γ_3 can be lengthened as to contain "far-field-like" response predominately).

In summary, we shall presume steady-state conditions at all contours but Γ_3 and Γ_6. When it comes to considering these, an argument stemming from the conservation law $\hat{\mathrm{L}}_z$ shall be brought to bear.

6.2.3 Configurational force in horizontal direction: $\hat{\mathrm{J}}_x = 0$

Recall, eq. (2.49) boils down to a contour integral in the plane strain case, in particular $\hat{\mathrm{J}}_x = 0$ becomes

$$\hat{\mathrm{J}}_x = \int_\Gamma \left[(\hat{W} - \hat{T}) n_x - \hat{t}_i \hat{u}_{i,x} \right] dl = 0\,, \tag{6.6}$$

which in this case becomes

$$\begin{aligned} &\int_{\Gamma_2} \left[(\hat{W} - \hat{T}) \right]_{x\to\infty} dl + \int_{\Gamma_4} \left[-(\hat{W} - \hat{T} - \hat{\sigma}_{xx}\hat{u}_{,x} - \hat{\tau}_{xy}\hat{v}_{,x}) \right]_{x=W/2} dl + \\ &\int_{\Gamma_5} - \left[\hat{\sigma}_{yy}\hat{v}_{,x} \right]_{y=0} dl + \int_{\Gamma_6} \left[-(\hat{W} - \hat{T} - \hat{\tau}_{xy}\hat{v}_{,x}) \right]_{x=0} dl = 0\,. \end{aligned} \tag{6.7}$$

6.2.4 Configurational force in vertical direction: $\hat{\mathrm{J}}_y = 0$

Likewise,

$$\hat{\mathrm{J}}_y = \int_\Gamma \left[(\hat{W} - \hat{T}) n_x - \hat{t}_i \hat{u}_{i,y} \right] dl = 0\,, \tag{6.8}$$

becomes

$$\begin{aligned}&\int_{\Gamma_1} -\left[(\hat{W}-\hat{T}-\hat{\tau}_{xy}\hat{u}_{,y})\right]_{y\to-\infty} dl + \int_{\Gamma_3}\left[(\hat{W}-\hat{T})\right]_{y=h} dl\\ &+\int_{\Gamma_4}\left[\hat{\sigma}_{xx}\hat{u}_{,y}\right]_{x=W/2} dl + \int_{\Gamma_5}\left[(\hat{W}-\hat{T})-\hat{\sigma}_{yy}\hat{v}_{,y}-\hat{\tau}_{xy}\hat{u}_{,y}\right]_{y=0} dl = 0\,.\end{aligned} \tag{6.9}$$

6.2.5 Configurational torques: $\hat{\mathrm{L}}_z = 0$

Finally, we consider the balance of configurational torques using the same contour. The identity we will obtain has a different character, as geometric parameters (distances) enter the integrand directly. The conservation law in this case dictates

$$\begin{aligned}\hat{\mathrm{L}}_z(\Gamma) &= \int_\Gamma \epsilon_{zij}\left[(\hat{W}-\hat{T})x_j n_i + \hat{t}_i\hat{u}_j - \hat{t}_k\hat{u}_{k,i}x_j\right] dl\\ &= -\int_\Gamma \Big[(\hat{W}-\hat{T})(xn_y - yn_x) + \hat{t}_y\hat{u} - \hat{t}_x\hat{v}\\ &\qquad - \hat{t}_x(x\hat{u}_{,y} - y\hat{u}_{,x}) - \hat{t}_y(x\hat{v}_{,y} - y\hat{v}_{,x})\Big] dl = 0\,,\end{aligned} \tag{6.10}$$

yielding

$$\begin{aligned}&-\left[\hat{W}-\hat{T}-\hat{\tau}_{xy}\hat{u}_{,y}\right]_{y=-\ell}\frac{\ell^2}{2}\\ &+\int_{\Gamma_2}\left[(\hat{W}-\hat{T})(-y)+\hat{\tau}_{xy}\hat{u}\right]_{x=\ell} dl\\ &+\int_{\Gamma_3}\left[(\hat{W}-\hat{T})(x)\right]_{y=h} dl\\ &+\int_{\Gamma_4}\left[(\hat{W}-\hat{T}-\hat{\tau}_{xy}\hat{v}_{,x}-\hat{\sigma}_{xx}\hat{u}_{,x})(y)-\hat{\tau}_{xy}\hat{u}\right]_{x=W/2} dl\\ &+\int_{\Gamma_5}\left[(\hat{W}-\hat{T}-\hat{\tau}_{xy}u_{,y}-\hat{\sigma}_{yy}v_{,y})(x)+\hat{\sigma}_{yy}\hat{u}-\hat{\tau}_{xy}\hat{u}\right]_{y=0} dl\\ &+\int_{\Gamma_6}\left[(\hat{W}-\hat{T}-\hat{\tau}_{xy}\hat{v}_{,x})(y)-\hat{\tau}_{xy}\hat{u}\right]_{x=0} dl = 0\,.\end{aligned} \tag{6.11}$$

Now, let us interpret this result. Consider we were to take the limit as $\ell \to \infty$. The first term, the input from the impinging wave deep below, grows quadratically with the contour length. The two finite contours cannot keep up with this growth hence their contribution must be negligible in the limit. On the other hand, the rest of the contours do increase and so does include their contribution to the balance as they engulf more and more "far-field-like" domain as they stretch away from the excavation. There must be balance at *two separated levels*, the dominant in magnitude being the one involving contours whose length can be increased arbitrarily, and its

integrand also increases with length. Thus, the dominant part of eq. (6.11) must be

$$\begin{aligned}
&- \left[\hat{W} - \hat{T} - \hat{\tau}_{xy}\hat{u}_{,y}\right]_{y=-\ell} \frac{\ell^2}{2} \\
&+ \int_{\Gamma_2} \left[(\hat{W} - \hat{T})(-y) + \hat{\tau}_{xy}\hat{u}\right]_{x=\ell} dy \\
&+ \int_{\Gamma_3} \left[(\hat{W} - \hat{T})(x)\right]_{y=h} dx \\
&+ \int_{\Gamma_6} \left[(\hat{W} - \hat{T} - \hat{\tau}_{xy}\hat{v}_{,x})(y) - \hat{\tau}_{xy}\hat{u}\right]_{x=0} dy = 0\,,
\end{aligned} \tag{6.12}$$

and not just that: as the contours are lengthened, the ones over-the-axis and the free surface will resemble more and more its counterparts, as they can indefinite amount of "far-field-like" response. This means that their integrands, despite being unknown, must behave, for the most part, as if there was no perturbation whatsoever, and thus they effectively becomes the far field response. Hence, eq. (6.12):

$$\begin{aligned}
&- \left[\hat{W} - \hat{T} - \hat{\tau}_{xy}\hat{u}_{,y}\right]_{y=-\ell} \frac{\ell^2}{2} \\
&+ \int_{\Gamma_2} \left[(\hat{W} - \hat{T})(-y) + \hat{\tau}_{xy}\hat{u}\right]_{x=\ell} dy \\
&+ \int_{\Gamma_3} \left[(\hat{W} - \hat{T})(x)\right]_{y=h} dx \\
&+ \int_{\Gamma_6} \left[(\hat{W} - \hat{T} - \hat{\tau}_{xy}\hat{v}_{,x})(y) - \hat{\tau}_{xy}\hat{u}\right]_{x=0} dy = 0\,.
\end{aligned} \tag{6.13}$$

In conclusion, $\hat{\mathrm{L}}_z = 0$ suggests that if we take $\ell \to \infty$ in our contour, we may assume that the integrand in the regions Γ_3 and Γ_3 can be approximated by the one of Γ_1 and Γ_4, respectively.

See that if we include rigid bedrock at a finite depth the argumentation would change dramatically.

More sophisticated arguments concerning these two contribution magnitudes are not only possible but compulsory. Their absence herein is explained solely in terms of time limitations, a reason why they have to be laid out as future work.

6.2.6 Summary tables

The previous identities are deemed to more suitably presented by means of tables.

	$\hat{\mathrm{J}}_x = 0$	$\hat{\mathrm{J}}_y = 0$
Γ_1: bottom		$(\hat{W} - \hat{T} - \hat{\tau}_{xy}\hat{u}_{,y})$
Γ_2: far field	$(\hat{W} - \hat{T})$	
Γ_3: free surf.		$(\hat{W} - \hat{T})$
Γ_4: wall	$(\hat{W} - \hat{T} - \hat{\sigma}_{xx}\hat{u}_{,x} - \hat{\tau}_{xy}\hat{v}_{,x})$	$-\sigma_{xx}\hat{u}_{,y}$
Γ_5: base	$-\sigma_{yy}\hat{v}_{,x}$	$(\hat{W} - \hat{T} - \hat{\sigma}_{yy}\hat{v}_{,y} - \hat{\tau}_{xy}\hat{u}_{,y})$
Γ_6: axis	$(\hat{W} - \hat{T} - \hat{\tau}_{xy}\hat{v}_{,x})$	

Table 6.1: Summary of contributions to the PII

	$\hat{\mathrm{J}}_x = 0$	$\hat{\mathrm{J}}_y = 0$
Γ_1: bottom		$-\frac{1}{2}\left(\frac{\hat{\tau}_{xy}^2}{\mu} + \rho\varpi^2\hat{u}^2\right)$
Γ_2: far field	$\frac{1}{2}\left(\frac{\hat{\tau}_{xy}^2}{\mu} - \rho\varpi^2\hat{u}^2\right)$	
Γ_3: free surf.		$\frac{1}{2}\left(\frac{\hat{\sigma}_{xx}^2}{\lambda+2\mu} - \rho\varpi^2(\hat{u}^2 + \hat{v}^2)\right)$
Γ_4: wall	$-\frac{1}{2}\left(\frac{\hat{\sigma}_{xx}^2}{\lambda+2\mu} + \hat{\tau}_{xy}(\hat{v}_{,x} - \hat{u}_{,y}) + \rho\varpi^2(\hat{u}^2 + \hat{v}^2)\right)$	$-\sigma_{xx}\hat{u}_{,y}$
Γ_5: base	$-\sigma_{yy}\hat{v}_{,x}$	$-\frac{1}{2}\left(\frac{\hat{\sigma}_{yy}^2}{\lambda+2\mu} + \hat{\tau}_{xy}(\hat{u}_{,y} - \hat{v}_{,x}) + \rho\varpi^2(\hat{u}^2 + \hat{v}^2)\right)$
Γ_6: axis	$-\frac{1}{2}\left(\hat{\tau}_{xy}(\hat{v}_{,x} - \hat{u}_{,y}) + \rho\varpi^2\hat{u}^2\right)$	

Table 6.2: Summary of contributions to the PII, in terms of stresses

	$\hat{\mathrm{J}}_x = 0$	$\hat{\mathrm{J}}_y = 0$
Γ_1: bottom		$-\frac{1}{2}\left(\mu\hat{u}_{,y}^2 + \rho\varpi^2\hat{u}^2\right)$
Γ_2: far field	$\frac{1}{2}\left(\mu\hat{u}_{,y}^2 - \rho\varpi^2\hat{u}^2\right)$	
Γ_3: free surf.		$\frac{1}{2}\left((\lambda+2\mu)\hat{u}_{,x}^2 - \rho\varpi^2(\hat{u}^2+\hat{v}^2)\right)$
Γ_4: wall	$-\frac{1}{2}\Big((\lambda+2\mu)\hat{u}_{,x}^2 + \mu(\hat{v}_{,x}^2 - \theta_0^2) + \rho\varpi^2((\hat{u}_0 - \theta_0 y)^2 + (\theta_0 W/2)^2)\Big)$	$\theta_0(\lambda+2\mu)\hat{u}_{,x}$
Γ_5: base	$-\theta_0(\lambda+2\mu)\hat{u}_{,y}$	$-\frac{1}{2}\Big((\lambda+2\mu)\hat{v}_{,y}^2 + \mu(\hat{u}_{,y}^2 - \theta_0^2) + \rho\varpi^2(\hat{u}_0^2 + (\theta_0 x)^2)\Big)$
Γ_6: axis	$-\frac{1}{2}\left(\mu(\hat{v}_{,x}^2 - \hat{u}_{,y}^2) + \rho\varpi^2\hat{u}^2\right)$	

Table 6.3: Summary of contributions to the PII, in terms of displacements and displacement gradients

This last table allows for a quick count of unknowns:

- Concerning the excavation: $\hat{u}_0$ and $\hat{v}_0$ (rigid body movement), $\hat{u}_{,x}|_{x=W/2}$ and $\hat{v}_{,x}|_{x=W/2}$ (wall), $\hat{u}_{,y}|_{y=0}$ and $\hat{v}_{,y}|_{y=0}$ (base).
- On the free surface: $\hat{u}_{,x}|_{y=h}$, $\hat{u}$ and $\hat{v}$.
- Over the axis: $\hat{v}_{,x}|_{x=0}$, $\hat{u}_{,y}|_{x=0}$ and $\hat{u}|_{x=0}$.

The response of the bottom contour and the far-field have been argued to remain unperturbed and known. Hence, there are 12 unknowns: 6 concerning the excavation, 3 corresponding to the free surface, and 3 more corresponding to the displacement field over the axis.

6.2.7 A simplified model to comapare with classic results

A possible path forward:

- Assume that then displacement field over the axis is very similar to the one in the far-field, and thus it can be assumed to be equal to it at the each depth. This assumption is fitting in cases where the wavelength is not of the same order of magnitude as the geometric features of the structure. This removes three

unknowns directly, leaving 9: $\hat{u}_0$ and θ_0 (rigid body movement), $\hat{u}_{,x}|_{x=W/2}$ and $\hat{v}_{,x}|_{x=W/2}$ (excavation wall), $\hat{u}_{,y}|_{y=0}$ and $\hat{v}_{,y}|_{y=0}$ (excavation base), $\hat{u}_{,x}|_{y=h}$, $\hat{u}$ and $\hat{v}$ (free surface). See that this assumption also fixes $\hat{u}_0 = \hat{u}_{ff}(y = 0)$, as it now moves as the far-field at the corresponding depth. Therefore, only 8 unknowns remain in this case: θ_0 (rigid body movement), $\hat{u}_{,x}|_{x=W/2}$ and $\hat{v}_{,x}|_{x=W/2}$ (excavation wall), $\hat{u}_{,y}|_{y=0}$ and $\hat{v}_{,y}|_{y=0}$ (excavation base), $\hat{u}_{,x}|_{y=h}$, $\hat{u}$ and $\hat{v}$ (free surface).

- The contribution of the free surface is equivalent to perturbations introduced by the presence of the excavation in terms of Rayleigh waves. Since we can define the contour at our own discretion, let us lengthen it so much as to most of the segment to be oblivious to the presence of these waves, hence for most of the segment the contribution will be similar to the one in the far-field, that is, kinetic energy. Plainly, we propose the following replacement

$$\int_{\Gamma_3} \frac{1}{2} \left[\frac{\hat{\sigma}_{xx}^2}{\lambda + 2\mu} - \rho\varpi^2(\hat{u}^2 + \hat{v}^2) \right]_{y=h} dx \approx \int_{\Gamma_3} \frac{1}{2} \left[-\rho\varpi^2 \hat{u}_{ff}^2 \right]_{y=h} dx\,, \quad (6.14)$$

  what effectively removes the unknowns corresponding to the far-field.

- The previous two items are tantamount to bringing the insight we derived from the study of $\hat{\mathrm{L}}_z$, although for an excitation whose wavelengths were of the order of the geometrical features of the excavation the conclusions would have to be re-examined, as the scattering effects would certainly affect the contour contribution in the portions of the segments closer to the structure.

- If one assumed that soil was connected rigidly to the excavation contour analogously to how a slender beam connects to a clamped end (in contrast to a hinged end), one can venture that $\hat{v}_{,x}|_{x=W/2} \approx \theta_0$ and $\hat{u}_{,y}|_{y=0} \approx \theta_0$, that is, a certain continuity not only of displacement but also rotations. Now, θ_0 (rigid body movement), $\hat{u}_{,x}|_{x=W/2}$ (excavation wall), $\hat{v}_{,y}|_{y=0}$ (excavation base), thereby leaving 3 unknowns left for 2 equations. An equivalent count would be θ_0, $\hat{\sigma}_{xx}|_{x=W/2}$ and $\hat{\sigma}_{yy}|_{y=0}$. The same outcome can be obtained disregarding shear stresses, hence normal stresses assume the duty of restraining the displacement and rotation of the contour.

The table summary would simplify accordingly:

	$\hat{\mathrm{J}}_x = 0$	$\hat{\mathrm{J}}_y = 0$
Γ_1		$-\frac{1}{2}\left(\mu\hat{u}_{,y}^2 + \rho\varpi^2\hat{u}^2\right)$
Γ_2	$\frac{1}{2}\left(\mu\hat{u}_{,y}^2 - \rho\varpi^2\hat{u}^2\right)$	
Γ_3		$\frac{1}{2}\left(-\rho\varpi^2\hat{u}^2\right)$
Γ_4	$-\frac{1}{2}\Big((\lambda+2\mu)\hat{u}_{,x}{}^2 + \rho\varpi^2((\hat{u}_0 - \theta_0 y)^2 + (\theta_0 W/2)^2)\Big)$	$\theta_0(\lambda+2\mu)\hat{u}_{,x}$
Γ_5	$-\theta_0(\lambda+2\mu)\hat{v}_{,y}$	$-\frac{1}{2}\left((\lambda+2\mu)\hat{v}_{,y}{}^2 + \rho\varpi^2(\hat{u}_0^2 + (\theta_0 x)^2)\right)$
Γ_6	$\frac{1}{2}\left(\mu\hat{u}_{,y}^2 - \rho\varpi^2\hat{u}^2\right)$	

Table 6.4: Summary of simplified contributions to the PII, in terms of displacements and displacement gradients, unknowns highlighted in color.

or using stresses,

	$\hat{\mathrm{J}}_x = 0$	$\hat{\mathrm{J}}_y = 0$
Γ_1		$-\frac{1}{2}\left(\frac{\hat{\tau}_{xy}^2}{\mu} + \rho\varpi^2\hat{u}^2\right)$
Γ_2	$\frac{1}{2}\left(\frac{\hat{\tau}_{xy}^2}{\mu} - \rho\varpi^2\hat{u}^2\right)$	
Γ_3		$\frac{1}{2}\left(-\rho\varpi^2\hat{u}^2\right)$
Γ_4	$-\frac{1}{2}\left(\frac{\hat{\sigma}_{xx}{}^2}{\lambda+2\mu} + \rho\varpi^2((\hat{u}_0 - \theta_0 y)^2 + (\theta_0 W/2)^2)\right)$	$\theta_0\hat{\sigma}_{xx}$
Γ_5	$-\hat{\sigma}_{yy}\theta_0$	$-\frac{1}{2}\left(\frac{\hat{\sigma}_{yy}{}^2}{\lambda+2\mu} + \rho\varpi^2(\hat{u}_0^2 + (\theta_0 x)^2)\right)$
Γ_6	$-\frac{1}{2}\left(\frac{\hat{\tau}_{xy}^2}{\mu} - \rho\varpi^2\hat{u}^2\right)$	

Table 6.5: Summary of contributions to the PII, in terms of stresses, unknowns highlighted in color.

We end up with three unknowns for two equations. In particular, the normal stresses depend on the corresponding gradients, which are unknown and spell how the soil behaves as soon as it separates from the the excavation. If a Winkler-like

modelization of pressures was used, these become proportional to the displacements, instead of to the gradients. In other words:

Elasticity	Winkler model	
$\hat{\sigma}_{xx} = (\lambda + 2\mu)\hat{u}_{,x} + \lambda\hat{v}_{,y}$	$\hat{\sigma}_{xx} = K_x \Delta\hat{u}$	(6.15a)
$\hat{\sigma}_{yy} = (\lambda + 2\mu)\hat{v}_{,y} + \lambda\hat{u}_{,x}$	$\hat{\sigma}_{yy} = K_y \Delta\hat{v}$	(6.15b)

Using this model in the identities would trade two unknowns by two new ones, but if moreover we impose $K_x = K_y = K$, then the final count would be squared: two unknowns for two balance equations. In this case $\Delta\hat{v} = \hat{v}$ but $\Delta\hat{u} = \hat{u}_w - \hat{u}_{ff}(y) = \hat{u}_{ff}(0) - \hat{u}_{ff}(y)$, where $\hat{u}_w$ is the displacement of the excavation wall, thereby containing both the rigid body displacement and rotation. Let us update the table accordingly

	$\hat{\mathbf{J}}_x = 0$	$\hat{\mathbf{J}}_y = 0$
Γ_1		$-\frac{1}{2}\left(\frac{\hat{\tau}_{xy}^2}{\mu} + \rho\varpi^2\hat{u}^2\right)$
Γ_2	$\frac{1}{2}\left(\frac{\hat{\tau}_{xy}^2}{\mu} - \rho\varpi^2\hat{u}^2\right)$	
Γ_3		$\frac{1}{2}\left(-\rho\varpi^2\hat{u}^2\right)$
Γ_4	$-\frac{1}{2}\left(\frac{K^2(\hat{u}_0-\hat{u})^2}{\lambda+2\mu} + \rho\varpi^2((\hat{u}_0 - \theta_0 y)^2 + (\theta_0 W/2)^2)\right)$	$\theta_0 K(\hat{u}_0 - \hat{u})$
Γ_5	$-K{\theta_0}^2 x$	$-\frac{1}{2}\left(\frac{K^2(\theta_0 x)^2}{\lambda+2\mu} + \rho\varpi^2(\hat{u}_0^2 + (\theta_0 x)^2)\right)$
Γ_6	$-\frac{1}{2}\left(\frac{\hat{\tau}_{xy}^2}{\mu} - \rho\varpi^2\hat{u}^2\right)$	

Table 6.6: Summary of contributions to the PII, in terms of stresses, unknowns highlighted in color.

Hence, we end up with two unknowns and two equations which we can solve for these to obtain the input rotation.

6.2.7.1 Long-wavelength approximation to estimation foundation input motion

We can introduce a long-wavelength assumption to simplify the equations even further. By resorting to the following dimensionless variables

$$\tilde{K} = \frac{K\ h}{(\lambda + 2\mu)} \quad , \quad \tilde{\theta}_0 = \frac{\theta_0 h}{\hat{u}_{ff0}} \quad , \quad \tilde{B} = \frac{W/2}{h} \quad , \quad r = \frac{\varpi h}{c_s}, \tag{6.16}$$

the balance equations in table 6.6 boil down, for horizontal and vertical balance respectively, to

$$\begin{aligned} &- \tilde{B}^2 c^2 \tilde{\theta}_0^2 \tilde{K} + r^2 \left(\left(\tilde{B}^2 + \frac{1}{3} \right) \tilde{\theta}_0^2 - \tilde{\theta}_0 \cos(r) + \cos^2(r) \right) \\ &+ c^2 \tilde{K}^2 \left(\frac{\tilde{\theta}_0^2}{3} + \frac{2\tilde{\theta}_0}{r^2} - \frac{\tilde{\theta}_0 \left(r^2 + 2 \right) \cos(r)}{r^2} - \frac{3 \sin(2r)}{4r} + \frac{1}{2} \cos(2r) + 1 \right) \\ &- r \sin(r) \cos(r) = 0 \,, \end{aligned} \tag{6.17a}$$

$$\frac{\tilde{B}^3 \tilde{\theta}_0^2}{3} \left(c^2 \tilde{K}^2 + r^2 \right) + \tilde{B} r^2 \left(-1 + \cos^2(r) \right) - 2c^2 \tilde{\theta}_0 \tilde{K} \left(\frac{\tilde{\theta}_0}{2} + \frac{\sin(r)}{r} - \cos(r) \right) = 0 \,. \tag{6.17b}$$

The numerical solution of these equations to leading order in r (see Appendix E for more details) can be found in the corresponding *Mathematica* notebook. Let us compare to Conti et. al [CMV17]: after examination of results from numerical simulations, they proposed the following expression for $\hat{u}_0 / \hat{u}_{ff0}$:

$$\frac{\theta_0 h}{\hat{u}_{ff0}} = \frac{1 - \cos(r)}{1 + 1.7 (2B/h)^{1.62}} \,. \tag{6.18}$$

See fig. 6.2 for comparison between the latter and the results from solving eq. (6.17) to leading order.

One can acknowledge qualitative agreement between both, as well as also quantitative for lower values of $\varpi h / c_s$. The expected trend, less rotation as the aspect ratio decreases, which was already built into eq. (6.18), is also displayed by the simplified model, altough the reduction is not so acute. The disagreement between the two can be imputed on the assumptions that were introduced to reach a simplified model that could be solved (Winkler model, ignoring shear; in particular, the latter could be especially hurtful for low values of the aspect ratio and the restraining mechanism at the base is not properly accounted for) and also can be partially ascribed to not

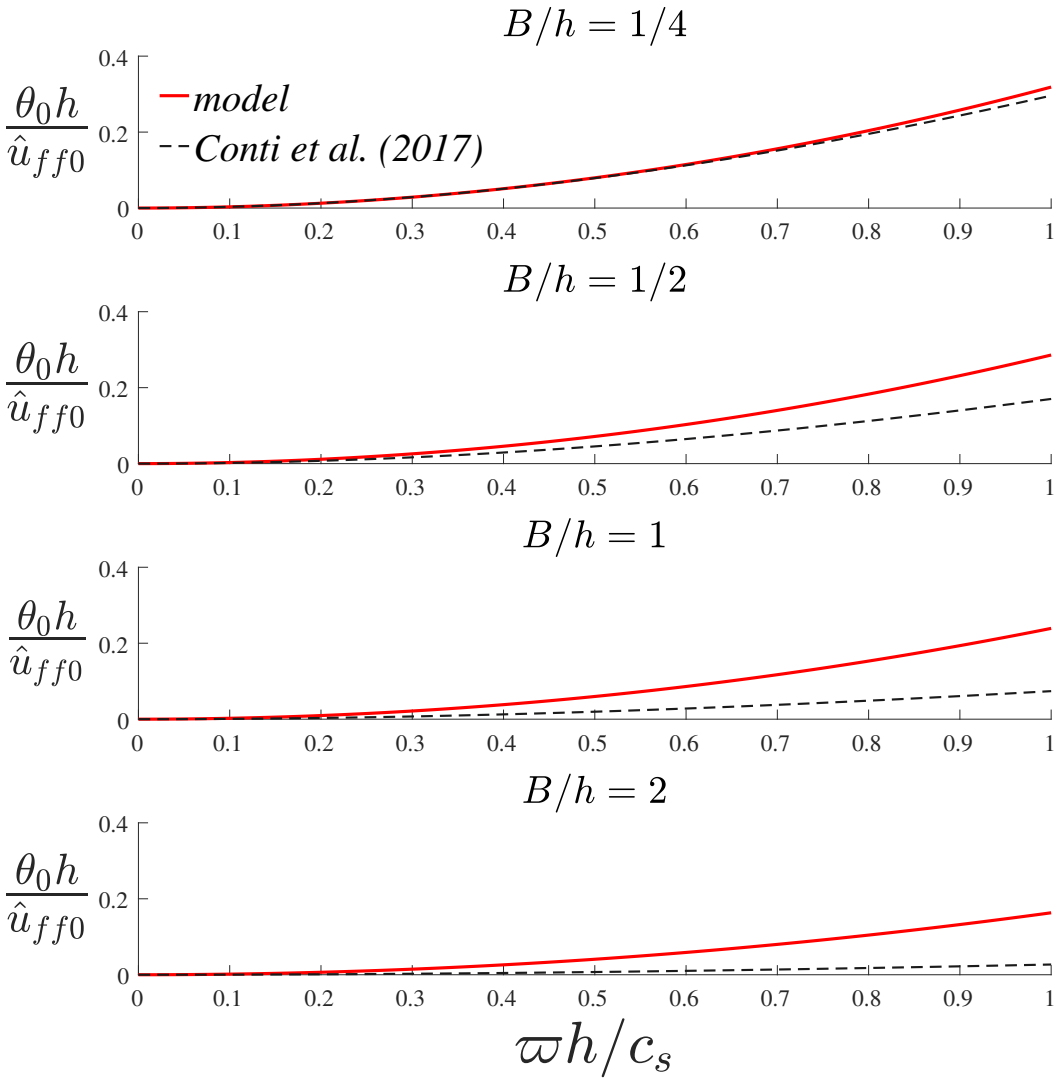

Figure 6.2: Comparison between expression provided by Conti and collaborators and the outcome of the proposed model for $\nu = 0.4$ and different values of aspect ratio

considering more terms in the perturbation series in terms of the parameter r: it could be the case that terms $O(r^3)$ gain more magnitude as the aspect ratio decreases.

In any event, one must point out that these results represent the first of their kind derived analytically from first principles (the path-independent integrals representing balance of configurational forces) without resorting to numerical simulations.

6.3 Conclusions

We have obtained, starting from fundamental principles, identities relating the far field motion to the foundation input motion. These have been simplified in order to

demonstrate its descriptive capacity and how it agrees to previous work, see fig. 6.2.

The main advantage of this new approach is that it can be easily adapted to consider more complex scenarios, from the 3D case to other foundation geometries, to potentially include the influence of soil heterogeneity. The possibilities moving forward are many.

Admittedly, the connection to wave scattering and dissipation has not been pursued thoroughly yet. This one must be as it completes the framing of the phenomenon in terms of *thermodynamic driving* forces.

This problem can be described as a *scattering problem* [WL78], whereas the inverse scenario of the loads applied over a foundation on a otherwise unperturbed soil is referred to as the *radiation problem*. Both can be framed and be related to configurational forces in natural fashion: if the displacement along a certain direction was unitary while the others are zero then the the corresponding configurational force acting on the foundation must relate the impedance along that direction. This opens a promising research path.

Chapter 7

CONCLUSIONS AND OUTLOOK

Main results

Chapters 5 and 6 represent the core of this text. Within them, we have shown how problems in SSI naturally fit in the scheme of balance of configurational forces presented in terms of the path-independent integrals outlined by Rice, Knowles, and other distinguided scholars.

In Chapter 5 we have exemplified how how these balance identities can be summoned to provide extra information sometimes necessary to enhance the fidelity of simplified models.

In Chapter 6 we have taken the phenomenon referred to as soil-structure kinematic interaction holistically and we have squared it in the general theory of configurational forces. This alternative conceptualization provided a first *tour de force* in the form of simplified expressions to obtain insight in the phenomenon of base motion filtering that had to be derived numerical experiments before.

A brief undertaking in Chapter 4, connected to the results Chapter 6, allow us to establish a relation (an inequality) between force on a contour (the earth thrust) and configurational force (the value of J_x) on the same segment. Using this approach we gained some, admittedly limited for now, understanding on the behavior of a system difficult to analyze by traditional means. More importantly, we have demonstrated the possibility of bounding classic force with a configurational force that can be estimated based on remote conditions (the far-field response), a promising technique that may yield relevant results in other situations where the main concern is gauging the magnitude of a force.

These, we believe, are but the first examples of a list of problems in geotechnical engineering that can be assessed in light of this new wherewithal.

Secondary results

In Chapter 4, we have demonstrated that the so-called Younan-Veletsos problem admits an exact steady-state solution in wavenunber space that can be expressed by means of elementary functions, and that current simplified models do not capture some features of this exact solution.

Another area we have made contributions to is 1D Site Response. Within Chapter 3 we have proposed a rather general characterization of high-frequency / long-wavelength response of inhomogeneous soil deposits with continuous variations of mechanical properties. In addition, approximate expressions to characterize the amplitude of the fundamental resonance mode of inhomogeneous soils with common variation of mechanical properties have been derived.

Finally, we hope that the Dimensional Analysis presented in section 4.2 may help guiding thoughtful studies concerning the betterment of understanding and our design procedures for underground structures in general and reservoirs in particular, by providing a holistic view of the problem and unveiling the relative importance of the parameters involved in it.

Outlook

The elephant in the room has gone unmentioned until this moment: the free surface we have encountered in these problems itself also represents a discontinuity in the otherwise continuous body. This opens the possibility of studying surface waves in terms of configurational forces too.

Other avenues of promising research, stemming from the work contained in this text and complementing it:

- Insofar applications of PII to SSI concerns, a bevy of potential application are open. The most obvious one is aiding the definition of foundation impedances [Gaz91]. Needless to say that the problem studied in section 4.4 requires further considerations in order to extend it to the fully dynamic setting and general geometry, and other PII as the L-integral may provide critical assessment of the rocking phenomenon. Given that the PII derive from elemental energetic (i.e. variational) considerations, similar PIIs may also exist in scenarios where the material response is more complex, for examples, if plasticity considerations are added. In such cases the PII may provide useful identities that could be guide analysis, simplified models or, even maybe, a new paradigm based on finding bounds for specific quantities, as we did for the thrust in section 4.4. Yet more options would be adding either spatially changing loading or more complex geometries or soil profiles, since the PIIs seem well-equipped to account for all these factors. The Boundary Integral Equation (BIE) formulation [ZA89] may also be used to relate complex scenarios to simplified ones.

- The exact solution of the Younan-Veletsos problem, section 4.3.2, can potentially be generalized to the case of flexible wall, what would provide new insight on the relation between wall stiffness and seismic earth pressures to confirm the insight obtained by Veletsos and Younan through simplified models and simulations [YV00]. Moreover, other wall boundary conditions, e.g. "bonded wall", may be fitted within the same method we have used to solve the problem. Less ambitious avenue would be considering poroelasticity, which has already received some attention from the Fracture Mechanics community.

- Results presented in section 2.6 should be generalized to scenarios wherein radiational damping is present in order to complete framework presented in this thesis. The methodology presented in section 3.3.3 to deal with the fundamental resonance mode may be extended to the non-linear regime.

BIBLIOGRAPHY

[Abr37] VM Abramov. "The Problem of the Contact of an Elastic Half Space With an Absolutely Rigid Base for the Determination of the Frictional Force". In: *Doklady*. 1937.

[AGM82] Jan D Achenbach, Arthur K Gautesen, and Harry McMaken. "Ray methods for waves in elastic solids: with applications to scattering by cracks". In: (1982).

[AK90] Rohan Abeyaratne and James K Knowles. "On the driving traction acting on a surface of strain discontinuity in a continuum". In: *Journal of the Mechanics and Physics of Solids* 38.3 (1990), pp. 345–360.

[AK93] Rohan Abeyaratne and James K Knowles. "A continuum model of a thermoelastic solid capable of undergoing phase transitions". In: *Journal of the Mechanics and Physics of Solids* 41.3 (1993), pp. 541–571.

[Ana+08] Ioannis Anastasopoulos et al. "Design of bridges against large tectonic deformation". In: *Earthquake Engineering and Engineering Vibration* 7.4 (2008), pp. 345–368.

[AP02] H Afra and A Pecker. "Calculation of free field response spectrum of a non-homogeneous soil deposit from bed rock response spectrum". In: *Soil Dynamics and Earthquake Engineering* 22.2 (2002), pp. 157–165.

[AR02] Keiiti Aki and Paul G Richards. *Quantitative seismology*. 2002.

[ASO81] A Arias, FJ Sanchez-Sesma, and E Ovando-Shelley. "A simplified elastic model for seismic analysis of earth-retaining structures with limited displacements". In: (1981).

[Bar80] FBJ Barends. "Dynamics of elastic plates on a flexible subsoil". In: *LGM-Mededelingen* 21 (1980), pp. 127–134.

[Ben90] Lee Benuska. "Ground motion, Loma Prieta earthquake Reconnaissance Report". In: *Earthquake Spectra* 6 (1990), pp. 25–80.

[BMS15] Scott J Brandenberg, George Mylonakis, and Jonathan P Stewart. "Kinematic framework for evaluating seismic earth pressures on retaining walls". In: *Journal of Geotechnical and Geoenvironmental Engineering* 141.7 (2015), p. 04015031.

[BO13] Carl M Bender and Steven A Orszag. *Advanced mathematical methods for scientists and engineers I: Asymptotic methods and perturbation theory*. Springer Science & Business Media, 2013.

[Bou85] Joseph Boussinesq. *Application des potentiels à l'étude de l'équilibre et du mouvement des solides élastiques*. Gauthier-Villars, Imprimeur-Libraire, 1885.

[BR16] Roberto Ballarini and Gianni Royer-Carfagni. "A Newtonian interpretation of configurational forces on dislocations and cracks". In: *Journal of the Mechanics and Physics of Solids* 95 (2016), pp. 602–620.

[BR73] Bernard Budiansky and JR Rice. "Conservation laws and energy-release rates". In: *Journal of applied mechanics* 40.1 (1973), pp. 201–203.

[BSS09] Building Seismic Safety Council (BSSC). *NEHRP Recommended Seismic Provisions for New Buildings and Other Structures (FEMA P-750)*. 2009.

[Bye98] Nina Byers. "E. Noether's discovery of the deep connection between symmetries and conservation laws". In: *arXiv preprint physics/9807044* (1998).

[Cer82] Valentino Cerruti. *Ricerche intorno all'equilibrio de'corpi elastici isotropi: memoria*. Coi tipi del Salviucci, 1882.

[Che67] GP Cherepanov. "Crack propagation in a continuum". In: *Prikl. Mat. Mekh* 31.3 (1967), pp. 476–488.

[Cle90] Maxwell J Clerk. "On a Method of Making a Direct Comparison of Electrostatic with Electromagnetic Force; with a Note on the Electromagnetic Theory of Light, WD Niven, ed". In: *The Scientific Papers of James Clerk Maxwell* 2 (1890).

[CMS16] Gabriel Candia, Roozbeh Geraili Mikola, and Nicholas Sitar. "Seismic response of retaining walls with cohesive backfill: Centrifuge model studies". In: *Soil Dynamics and Earthquake Engineering* 90 (2016), pp. 411–419.

[CMV17] Riccardo Conti, Marco Morigi, and Giulia MB Viggiani. "Filtering effect induced by rigid massless embedded foundations". In: *Bulletin of Earthquake Engineering* 15.3 (2017), pp. 1019–1035.

[Cou73] Charles Augustin Coulomb. "Essai sur une application des regles de maximis et minimis a quelques problemes de statique relatifs a l'architecture (essay on maximums and minimums of rules to some static problems relating to architecture)". In: (1973).

[CP92] RW Clough and J Penzien. *Dynamics of Structures*. 2nd York, 1992.

[CS77] Francis HK Chen and Richard T Shield. "Conservation laws in elasticity of the J-integral type". In: *Zeitschrift fuer angewandte Mathematik und Physik* 28.1 (1977), pp. 1–22.

[Dav03a] Craig A Davis. “Lateral seismic pressures for design of rigid underground lifeline structures”. In: *Advancing Mitigation Technologies and Disaster Response for Lifeline Systems*. 2003, pp. 1001–1010.

[Dav03b] Craig Alan Davis. “Study of near-source earthquake effects on flexible buried pipes.” In: (2003).

[Den87] Jacob Pieter Den Hartog. *Advanced strength of materials*. Courier Corporation, 1987.

[DG85] Panos Dakoulas and George Gazetas. “A class of inhomogeneous shear models for seismic response of dams and embankments”. In: *International Journal of Soil Dynamics and Earthquake Engineering* 4.4 (1985), pp. 166–182.

[DM89] José Domınguez and Fernando Medina. “Boundary elements for the analysis of the seismic response of dams including dam-water-foundation interaction effects. II”. In: *Engineering Analysis with Boundary Elements* 6.3 (1989), pp. 158–163.

[DR78a] José Dominguez and JM Roesset. “Dynamic stiffness of rectangular foundations”. In: *Nasa Sti/recon Technical Report N* 79 (1978).

[DR78b] José Dominguez and JM Roesset. *Response of embedded foundations to travelling waves*. Massachusetts Institute of Technology, Department of Civil Engineering . . ., 1978.

[Dur+18] Maria Giovanna Durante et al. “Winkler Stiffness Intensity for Flexible Walls Retaining Inhomogeneous Soil”. In: *Geotechnical Earthquake Engineering and Soil Dynamics V*. 2018.

[DV87] Ricardo Dobry and Mladen Vucetic. “Dynamic properties and seismic response of soft clay deposits”. In: Department of Civil Engineering, Rensselaer Polytechnic Institute. 1987.

[DWV71] Ricardo Dobry, Robert V Whitman, and José Manuel Roesset Vinuesa. *Soil properties and the one-dimensional theory of earthquake amplification*. MIT Department of Civil Engineering, Inter-American Program, 1971.

[EMR77] Farid Elsabee, Joseph Parker Morray, and Jose M Roesset. *Dynamic behavior of embedded foundations*. Massachusetts Institute of Technology, Department of Civil Engineering . . ., 1977.

[Esh56] JD Eshelby. “The continuum theory of lattice defects”. In: *Solid state physics*. Vol. 3. Elsevier, 1956, pp. 79–144.

[Esm16] Elnaz Esmaeilzadeh Seylabi. “Reduced order modeling of soil structure interaction problems”. PhD thesis. UCLA, 2016.

[Fle76] Donnie C Fletcher. “Conservation laws in linear elastodynamics”. In: *Archive for Rational Mechanics and Analysis* 60.4 (1976), pp. 329–353.

[Fre98] L Ben Freund. *Dynamic fracture mechanics*. Cambridge university press, 1998.

[Fur+11] Takashi Furumura et al. “Strong ground motions from the 2011 off-the Pacific-Coast-of-Tohoku, Japan (Mw= 9.0) earthquake obtained from a dense nationwide seismic network”. In: *Landslides* 8.3 (2011), p. 333.

[GAG19] Evangelia Garini, Ioannis Anastasopoulos, and George Gazetas. “Soil, basin and soil–building–soil interaction effects on motions of Mexico City during seven earthquakes”. In: *Géotechnique* (2019), pp. 1–27.

[Gaz82] George Gazetas. “Vibrational characteristics of soil deposits with variable wave velocity”. In: *International journal for numerical and analytical methods in Geomechanics* 6.1 (1982), pp. 1–20.

[Gaz87] George Gazetas. “Seismic response of earth dams: some recent developments”. In: *Soil dynamics and earthquake engineering* 6.1 (1987), pp. 2–47.

[Gaz91] George Gazetas. “Foundation vibrations”. In: *Foundation engineering handbook*. Springer, 1991, pp. 553–593.

[Gib74] RE Gibson. “The analytical method in soil mechanics”. In: *Geotechnique* 24.2 (1974), pp. 115–140.

[GM11] Christos Giarlelis and George Mylonakis. “Interpretation of dynamic retaining wall model tests in light of elastic and plastic solutions”. In: *Soil Dynamics and Earthquake Engineering* 31.1 (2011), pp. 16–24.

[GS91] George Gazetas and Kenneth H Stokoe. “Free vibration of embedded foundations: theory versus experiment”. In: *Journal of geotechnical engineering* 117.9 (1991), pp. 1382–1401.

[GSA19] Joaquin Garcia-Suarez, Elnaz Seylabi, and Domniki Asimaki. “Seismic harmonic response of inhomogeneous soil: scaling analysis”. In: *Géotechnique* (accepted, 2019).

[Gün62] Wilhelm Günther. “Über einige randintegrale der elastomechanik”. In: *Abh. Braunschw. Wiss. Ges* 14.53-72 (1962), p. 176.

[Gur76] Morton E Gurtin. “On a path-independent integral for elastodynamics”. In: *International Journal of Fracture* 12.4 (1976), pp. 643–644.

[Har+14] Alek Harounian et al. “Beyond Code-Based Design: Use of Advanced Numerical Modeling to Support Design of Los Angeles’s Headworks Reservoir”. In: *Geo-Congress 2014: Geo-characterization and Modeling for Sustainability*. 2014, pp. 3044–3053.

[Has+01] Youssef MA Hashash et al. “Seismic design and analysis of underground structures”. In: *Tunnelling and underground space technology* 16.4 (2001), pp. 247–293.

[HD72] Bobby O Hardin and Vincent P Drnevich. “Shear modulus and damping in soils: measurement and parameter effects”. In: *Journal of Soil Mechanics & Foundations Div* 98.sm6 (1972).

[HH59] George William Housner and Donald E Hudson. *Applied mechanics: dynamics*. Vol. 1. Van Nostrand, 1959.

[Hol41] DL Holl. “Stress transmission in earths”. In: *Highway Research Board Proceedings*. Vol. 20. 1941.

[Hor13] H.G. Hornung. *Dimensional Analysis: Examples of the Use of Symmetry*. Dover Books on Physics. Dover Publications, 2013.

[Hou57a] George W Housner. “Dynamic pressures on accelerated fluid containers”. In: *Bulletin of the seismological society of America* 47.1 (1957), pp. 15–35.

[Hou57b] George W Housner. “Interaction of building and ground during an earthquake”. In: *Bulletin of the Seismological Society of America* 47.3 (1957), pp. 179–186.

[Hud+14] Martin B Hudson et al. “Seismic Resilience Design for a Concrete Box Reservoir”. In: *International Efforts in Lifeline Earthquake Engineering*. 2014, pp. 137–144.

[Hus+16a] A Hushmand et al. “Seismic performance of underground reservoir structures: insight from centrifuge modeling on the influence of backfill soil type and geometry”. In: *Journal of Geotechnical and Geoenvironmental Engineering* 142.11 (2016), p. 04016058.

[Hus+16b] A Hushmand et al. “Seismic performance of underground reservoir structures: insight from centrifuge modeling on the influence of structure stiffness”. In: *Journal of Geotechnical and Geoenvironmental Engineering* 142.7 (2016), p. 04016020.

[ITN05] S Iai, T Tobita, and T Nakahara. “Generalised scaling relations for dynamic centrifuge tests”. In: *Geotechnique* 55.5 (2005), pp. 355–362.

[IZ93] Isao Ishibashi and Xinjian Zhang. “Unified dynamic shear moduli and damping ratios of sand and clay”. In: *Soils and foundations* 33.1 (1993), pp. 182–191.

[JE18] C Jeong and E Esmaeilzadeh Seylabi. “Seismic input motion identification in a heterogeneous halfspace”. In: *Journal of Engineering Mechanics* 144.8 (2018), p. 04018070.

[Joh82] KL Johnson. “One hundred years of Hertz contact”. In: *Proceedings of the Institution of Mechanical Engineers* 196.1 (1982), pp. 363–378.

[Kak+15] James Kaklamanos et al. “Comparison of 1D linear, equivalent-linear, and nonlinear site response models at six KiK-net validation sites”. In: *Soil Dynamics and Earthquake Engineering* 69 (2015), pp. 207–219.

[Kau06] Eduardo Kausel. *Fundamental solutions in elastodynamics: a compendium*. Cambridge University Press, 2006.

[Kau10] Eduardo Kausel. “Early history of soil–structure interaction”. In: *Soil Dynamics and Earthquake Engineering* 30.9 (2010), pp. 822–832.

[Kau13] Eduardo Kausel. “On the frequencies of inhomogeneous soil strata: Dobry’s paradox”. In: *Soil Dynamics and Earthquake Engineering* 47 (2013), pp. 38–40.

[Kau76] E Kausel. “Dynamic soil-structure interaction of nuclear power plant structure, Course on Soil Dynamics for Earthquake Design, International Centre for Computer Aided Design, S”. In: *Margherita, Italy* (1976).

[KC74] MK Kassir and MF Chuaprasert. “A rigid punch in contact with a nonhomogeneous elastic solid”. In: *Journal of Applied Mechanics* 41.4 (1974), pp. 1019–1024.

[KL19] Lohrasb Keykhosropour and Anne Lemnitzer. “Experimental studies of seismic soil pressures on vertical flexible, underground structures and analytical comparisons”. In: *Soil Dynamics and Earthquake Engineering* 118 (2019), pp. 166–178.

[KLM12] Panos Kloukinas, Miltiadis Langousis, and George Mylonakis. “Simple Wave Solution for Seismic Earth Pressures on Non-Yielding Walls”. In: 138 (Mar. 2012), pp. 1514–1519.

[KO90] Yu A Kravtsov and Yu I Orlov. “Geometrical optics of inhomogeneous media”. In: *Geometrical Optics of Inhomogeneous Media by Yu. A. Kravtsov, Yu. I. Orlov Berlin, GR: Springer-Verlag, 1990* (1990).

[KR74] E Kausel and JM Roesset. “Soil structure interaction problems for nuclear containment structures”. In: *Electric power and the civil engineer*. 1974.

[Kra96] Steven L Kramer. *Geotechnical earthquake engineering. in Prentice–Hall international series in civil engineering and engineering mechanics*. Prentice Hall Inc., Englewood Cliffs, New Jersey, 1996.

[KS72] James K Knowles and Eli Sternberg. “On a class of conservation laws in linearized and finite elastostatics”. In: *Archive for rational mechanics and analysis* 44.3 (1972), pp. 187–211.

[Kur13] R. Kurth. *Dimensional Analysis and Group Theory in Astrophysics*. Elsevier Science, 2013. ISBN: 9781483280202. URL: https://books.google.com/books?id=iaFGBQAAQBAJ.

[Lan51] Henry Louis Langhaar. *Dimensional analysis and theory of models*. Vol. 2. Wiley New York, 1951.

[LM87] JE Luco and Akira Mita. "Response of a circular foundation on a uniform half-space to elastic waves". In: *Earthquake engineering & structural dynamics* 15.1 (1987), pp. 105–118.

[Lov13] Augustus Edward Hough Love. *A treatise on the mathematical theory of elasticity*. Cambridge university press, 2013.

[Lov29] Augustus Edward Hough Love. "IX. The stress produced in a semi-infinite solid by pressure on part of the boundary". In: *Philosophical Transactions of the Royal Society of London. Series A, Containing Papers of a Mathematical or Physical Character* 228.659-669 (1929), pp. 377–420.

[Lub08] Jacob Lubliner. *Plasticity theory*. Courier Corporation, 2008.

[Lub18] Vlado A Lubarda. "Dislocation Burgers vector and the Peach–Koehler force: a review". In: *Journal of Materials Research and Technology* (2018).

[LW72] JE Luco and RA Westmann. "Dynamic response of a rigid footing bonded to an elastic half space". In: *Journal of Applied Mechanics* 39.2 (1972), pp. 527–534.

[Mau13] Gérard A Maugin. "Continuum mechanics through the twentieth century". In: *Springer, Berlin. doi* 10 (2013), pp. 978–94.

[Mau16] Gérard A Maugin. *Configurational forces: thermomechanics, physics, mathematics, and numerics*. Chapman and Hall/CRC, 2016.

[MD89] Fernando Medina and José Domınguez. "Boundary elements for the analysis of the seismic response of dams including dam-water-foundation interaction effects. I". In: *Engineering Analysis with Boundary Elements* 6.3 (1989), pp. 152–157.

[MH54] Richard George Merritt and George William Housner. "Effect of foundation compliance on earthquake stresses in multistory buildings". In: *Bulletin of the Seismological Society of America* 44.4 (1954), pp. 551–569.

[Mik12] Julius Miklowitz. *The theory of elastic waves and waveguides*. Vol. 22. Elsevier, 2012.

[MKP07] George Mylonakis, Panos Kloukinas, and Costas Papantonopoulos. “An alternative to the Mononobe–Okabe equations for seismic earth pressures”. In: *Soil Dynamics and Earthquake Engineering* 27.10 (2007), pp. 957–969.

[ML89] Akira Mita and J Enrique Luco. “Impedance functions and input motions for embedded square foundations”. In: *Journal of geotechnical engineering* 115.4 (1989), pp. 491–503.

[MO60] H Matsuo and Sukeo Ohara. “Lateral earth pressure and stability of quay walls during earthquakes”. In: *Proceedings of the Second World Conference on Earthquake Engineering*. Vol. 1. Science Council of Japan Tokyo-Kyoto, Japan. 1960, pp. 165–181.

[MRP13] George E Mylonakis, Emmanouil Rovithis, and Haralambos Parashakis. “1D harmonic response of layered inhomogeneous soil: exact and approximate analytical solutions”. In: *Computational Methods in Earthquake Engineering*. Springer, 2013, pp. 1–32.

[Mus13] Nikolaı Ivanovich Muskhelishvili. *Some basic problems of the mathematical theory of elasticity*. Springer Science & Business Media, 2013.

[Nil73] Fred Nilsson. “A path-independent integral for transient crack problems”. In: *International Journal of Solids and Structures* 9.9 (1973), pp. 1107–1115.

[NIS12] N NIST. “Soil-Structure-Interaction for Building Structures (NIST GCR 12-917-21)”. In: *National Institute of Standards and Technology, Gaithersburg, MD* 20899 (2012).

[Oka+04] Yoshimitsu Okada et al. “Recent progress of seismic observation networks in Japan—Hi-net, F-net, K-NET and KiK-net—”. In: *Earth, Planets and Space* 56.8 (2004), pp. xv–xxviii.

[Oka24] Saburo Okabe. “General theory on earth pressure and seismic stability of retaining wall and dam”. In: *J. of the Japan Society of Civil Engrg* 10.6 (1924), pp. 1277–1323.

[PD74] Harry George Poulos and Edward Hughesdon Davis. *Elastic solutions for soil and rock mechanics*. BOOK. John Wiley, 1974.

[Ric68] James R Rice. “A path independent integral and the approximate analysis of strain concentration by notches and cracks”. In: *Journal of applied mechanics* 35.2 (1968), pp. 379–386.

[Ric85] James R Rice. “Conserved integrals and energetic forces”. In: *Fundamentals of deformation and fracture* (1985), pp. 33–56.

[Roe77] JM Roesset. “Soil amplification of earthquakes”. In: *Numerical methods in geotechnical engineering* (1977), pp. 639–682.

[RPM11] EN Rovithis, H Parashakis, and GE Mylonakis. "1D harmonic response of layered inhomogeneous soil: Analytical investigation". In: *Soil Dynamics and Earthquake Engineering* 31.7 (2011), pp. 879–890.

[RS05] Antonio Barrero Ripoll and Miguel Pérez-Saborid Sánchez-Pastor. *Fundamentos y Aplicaciones de la Mecánica de Fluidos*. McGraw-Hill, 2005.

[RS50] William T Read and W Shockley. "Dislocation models of crystal grain boundaries". In: *Physical review* 78.3 (1950), p. 275.

[San59] J Lyell Sanders. *On the Griffith-Irwin fracture theory*. Citeseer, 1959.

[Sar94] SK Sarma. "Analytical solution to the seismic response of visco-elastic soil layers". In: *Geotechnique* 44.2 (1994), pp. 265–275.

[Sca76] RH Scanlan. "Seismic wave effects on soil-structure interaction". In: *Earthquake Engineering & Structural Dynamics* 4.4 (1976), pp. 379–388.

[Sco73] RF Scott. "Earthquake-induced pressures on retaining walls". In: *Proceedings of the 5th World Conference on Earthquake Engineering*. Vol. 2. 1973, pp. 1611–1620.

[See70] H Seed. "Design of earth retaining structures for dynamic loads". In: *ASCE Specialty Conf.-Lateral Stress in the Ground and Design of Earth Retaining Structures, 1970*. 1970.

[Sey+18] E Esmaeilzadeh Seylabi et al. "Seismic response of buried reservoir structures: a comparison of numerical simulations with centrifuge experiments". In: *Soil Dynamics and Earthquake Engineering* 109 (2018), pp. 89–101.

[Sim10] Dassault Systemes Simulia. "Abaqus analysis user's manual". In: *Dassault Systemes, Pawtucket, USA* (2010).

[SM05] T Sahaphol and S Miura. "Shear moduli of volcanic soils". In: *Soil Dynamics and Earthquake Engineering* 25.2 (2005), pp. 157–165.

[SMC12] Nicholas Sitar, Roozbeh Geraili Mikola, and Gabriel Candia. "Seismically induced lateral earth pressures on retaining structures and basement walls". In: *Geotechnical Engineering State of the Art and Practice: Keynote Lectures from GeoCongress 2012*. 2012, pp. 335–358.

[SP09] JF Semblat and A Pecker. "Waves and vibrations in soils". In: *Earthquakes, traffic, shocks* (2009).

[SRW72] Mauricio A Sarrazin, Jose M Roesset, and Robert V Whitman. "Dynamic soil-structure interaction". In: *Journal of the Structural Division* 98.st 7 (1972).

[Str15] John William Strutt. “Deep water waves, progressive or stationary, to the third order of approximation”. In: *Proceedings of the Royal Society of London. Series A, Containing Papers of a Mathematical and Physical Character* 91.629 (1915), pp. 345–353.

[SWL77] H Bolton Seed, Robert V Whitman, and John Lysmer. “Soil-structure interaction effects in the design of nuclear power plants”. In: *Structural and geotechnical mechanics, a volume honouring, Prentice Hall, Englewood Cliffs* (1977).

[SZ90] RS Steedman and X Zeng. “The influence of phase on the calculation of pseudo-static earth pressure on a retaining wall”. In: *Geotechnique* 40.1 (1990), pp. 103–112.

[Ter16] Kwan-ichi Terazawa. “On the elastic equilibrium of a semi-infinite solid under given boundary conditions”. In: *Journal of the College of Science* (1916), pp. 14–24.

[TG04] Thaleia Travasarou and George Gazetas. “On the linear seismic response of soils with modulus varying as a power of depth: the maliakos marine clay”. In: *Soils and foundations* 44.5 (2004), pp. 85–93.

[Tow96] Ikuo Towhata. “Seismic wave propagation in elastic soil with continuous variation of shear modulus in the vertical direction”. In: *Soils and Foundations* 36.1 (1996), pp. 61–72.

[Ver96] Arnold Verruijt. *Soil dynamics*. Technische Universiteit, Faculteit Civiele Techniek, 1996.

[Vre13] Christos Vrettos. “Dynamic response of soil deposits to vertical SH waves for different rigidity depth-gradients”. In: *Soil Dynamics and Earthquake Engineering* 47 (2013), pp. 41–50.

[Vre90] Ch Vrettos. “Dispersive SH-surface waves in soil deposits of variable shear modulus”. In: *Soil Dynamics and Earthquake Engineering* 9.5 (1990), pp. 255–264.

[VW71] Anestis Stavrou Veletsos and Yau T Wei. “Lateral and rocking vibration of footings”. In: *Journal of Soil Mechanics & Foundations Div* (1971).

[VY94a] Anestis S Veletsos and Adel H Younan. “Dynamic modeling and response of soil-wall systems”. In: *Journal of Geotechnical Engineering* 120.12 (1994), pp. 2155–2179.

[VY94b] AS Veletsos and AH Younan. “Dynamic soil pressures on rigid vertical walls”. In: *Earthquake engineering & structural dynamics* 23.3 (1994), pp. 275–301.

[Wei12] Hans F Weinberger. *A first course in partial differential equations: with complex variables and transform methods*. Courier Corporation, 2012.

[Wes38] HM Westergaard. "A problem of elasticity suggested by a problem in soil mechanics: soft material reinforced by numerous strong horizontal sheets". In: *Contributions to the mechanics of solids, Stephen Timoshenko 60th anniversary volume* (1938), pp. 268–277.

[Wil52] ML Williams. "Stress singularities resulting from various boundary conditions in angular corners of plates in extension". In: *Journal of applied mechanics* 19.4 (1952), pp. 526–528.

[WL78] HL Wong and JE Luco. "Dynamic response of rectangular foundations to obliquely incident seismic waves". In: *Earthquake Engineering & Structural Dynamics* 6.1 (1978), pp. 3–16.

[Wol00] Stephen Wolfram. *The mathematica book*. Vol. 4. Cambridge University Press Cambridge, 2000.

[Wol85] John P Wolf. *Soil-structure interaction*. Prentice Hall Inc., Englewood Cliffs, New Jersey, 1985.

[Woo14] David Muir Wood. *Geotechnical modelling*. CRC press, 2014.

[Woo73] John H Wood. "Earthquake-induced soil pressures on structures". In: (1973).

[WS16] Nathaniel Wagner and Nicholas Sitar. "On seismic response of stiff and flexible retaining structures". In: *Soil Dynamics and Earthquake Engineering* 91 (2016), pp. 284–293.

[YB95] JS Yang and RC Batra. "Conservation laws in linear piezoelectricity". In: *Engineering Fracture Mechanics* 51.6 (1995), pp. 1041–1048.

[YV00] AH Younan and Anestis Stavrou Veletsos. "Dynamic response of flexible retaining walls". In: *Earthquake engineering & structural dynamics* 29.12 (2000), pp. 1815–1844.

[ZA89] Ch Zhang and Jan Drewes Achenbach. "A new boundary integral equation formulation for elastodynamic and elastostatic crack analysis". In: *ASME J. Appl. Mech* 56 (1989), pp. 284–290.

[Zha90] Ch Zhang. "On some conservation laws in transient elastodynamics". In: *Acta Mechanica* 83.3 (1990), pp. 187–193.

[Zha97] JX Zhao. "MODAL ANALYSIS OF SOFT-SOIL SITES INCLUDING RADIATION DAMPING". In: *Earthquake engineering & structural dynamics* 26.1 (1997), pp. 93–113.

[Zlo12] M. Zlokarnik. *Dimensional Analysis and Scale-up in Chemical Engineering*. Springer Berlin Heidelberg, 2012. ISBN: 9783642766732. URL: https://books.google.com/books?id=M6zoCAAAQBAJ.

Appendix A

DERIVATIONS FOR CHAPTER II

A.1 Direct proof of path-independent integrals for steady-state dynamics

We aim to:

- Present a proof for the validity of the expression for the dynamic J and L integrals, in terms of steady-state amplitudes, presented in the body of section 2.5.
- From the dynamic equations, justify the re-formulation of the integrals in terms of relative displacements and prove the expressions given section 2.5.
- Finally, proceed to carve out a particular expression valid for low-frequencies / long-wavelengths from the general case of path-independent integrals expressed in terms of relative displacements.

A.1.1 J integral

For a direct proof of J, first, take eq. (2.49) after applying the divergence theorem

$$\hat{\mathrm{J}}_i = \int_\Omega \left[(\hat{W} - \hat{T})_{,i} - (\hat{\sigma}_{jk}\hat{u}_{j,i})_{,k} \right] \, dV = 0 \,, \tag{A.1}$$

and proceed to analyze the integrand,

$$(\hat{W} - \hat{T})_{,i} - (\hat{\sigma}_{jk}\hat{u}_{j,i})_{,k} = (\hat{W}_{,i} - \hat{T}_{,i}) - (\hat{\sigma}_{kj,k}\hat{u}_{j,i} + \hat{\sigma}_{jk}\hat{u}_{j,ik}) =$$

using the definitions (2.48) and (2.47)

$$= (\hat{\sigma}_{kj}\hat{u}_{k,ji} - \rho\hat{u}_k\hat{u}_{k,i}) - (\hat{\sigma}_{jk,k}\hat{u}_{j,i} + \hat{\sigma}_{jk}\hat{u}_{j,ik}) =$$

use eq. (2.46) to transform the first term of the second parenthesis,

$$= (\hat{\sigma}_{kj}\hat{u}_{k,ji} - \rho\hat{u}_k\hat{u}_{k,i}) - (-\rho\hat{u}_j\hat{u}_{i,jk} + \hat{\sigma}_{jk}\hat{u}_{j,i}) =$$

by noting that in the first term of the first parenthesis both k and j are summation indices, let us swap labels,

$$= (\hat{\sigma}_{jk}\hat{u}_{j,ki} - \rho\hat{u}_k\hat{u}_{k,i}) - (-\rho\hat{u}_j\hat{u}_{i,jk} + \hat{\sigma}_{jk}\hat{u}_{j,ik}) =$$

noticing that for the cross-derivatives it holds $\hat{u}_{j,ki} = \hat{u}_{j,ik}$, one obtains the final result

$$= (\hat{\sigma}_{jk}\hat{u}_{j,ik} - \rho\hat{u}_k\hat{u}_{k,i}) - (-\rho\hat{u}_j\hat{u}_{i,jk} + \hat{\sigma}_{jk}\hat{u}_{j,ik}) = 0 \,. \tag{A.2}$$

A.1.2 L integral

The proof for eq. (2.50) is a bit lengthier. Start from applying the divergence theorem in the same fashion as above, and move to analyzing the integrand again:

$$\epsilon_{kji}\left[\left((\hat{W}-\hat{T})x_k\right)_{,j}-\left(\hat{\sigma}_{pl}\hat{u}_{p,j}x_k\right)_{,l}+\left(\hat{\sigma}_{lj}\hat{u}_k\right)_{,l}\right]=$$

$$\epsilon_{kji}\left[(\hat{W}-\hat{T})_{,j}x_k+(\hat{W}-\hat{T})\delta_{kj}-\left(\hat{\sigma}_{pl}\hat{u}_{p,j}x_k\right)_{,l}+\left(\hat{\sigma}_{lj}\hat{u}_k\right)_{,l}\right]=$$

recall $\epsilon_{kji}\delta_{kj}=\epsilon_{kki}=0$, and thus the second addend vanishes

$$\epsilon_{kji}\left[(\hat{W}-\hat{T})_{,j}x_k-\hat{\sigma}_{pk}\hat{u}_{p,j}-\left(\hat{\sigma}_{pl}\hat{u}_{p,j}\right)_{,l}x_k+\hat{\sigma}_{lj,l}\hat{u}_k+\hat{\sigma}_{lj}\hat{u}_{k,l}\right]=$$

the first and third addend balance each other, as shown in eq. (A.2)

$$\epsilon_{kji}\left[-\hat{\sigma}_{pk}\hat{u}_{p,j}+\hat{\sigma}_{lj,l}\hat{u}_k+\hat{\sigma}_{lj}\hat{u}_{k,l}\right]=\epsilon_{kji}\left(\hat{\sigma}_{lj}\hat{u}_{k,l}-\hat{\sigma}_{pk}\hat{u}_{p,j}\right)+\epsilon_{kji}\hat{\sigma}_{lj,l}\hat{u}_k=$$

as demonstrated in [KS72], the first addend vanishes if the material is isotropic; moreover, apply eq. (2.46) to the other addend to finally obtain

$$=-\epsilon_{kji}\rho\varpi^2\hat{u}_j\hat{u}_k=-\rho\varpi^2\hat{\boldsymbol{u}}\wedge\hat{\boldsymbol{u}}=0\,, \tag{A.3}$$

the last result owing to the vector being parallel to itself.

A.2 Derivation of integrals in terms of relative displacements

Next, we introduce the substitution $\hat{u}_i\longrightarrow\hat{u}_i+X_i$ in the previous conservation laws. Recall that X_i are constants, and do not depend on space.

A.2.1 J integral

Let us begin by eq. (2.49):

$$\begin{aligned}\hat{\mathrm{J}}_i&=\int_{\partial\Omega}\left[\left(\hat{W}-\frac{\rho\varpi^2}{2}(\hat{u}_l+X_l)(\hat{u}_l+X_l)\right)n_i-\hat{t}_j\hat{u}_{i,j}\right]dS\\&=\int_{\partial\Omega}\left[\left(\hat{W}-\frac{\rho\varpi^2}{2}(\hat{u}_k\hat{u}_l+2X_l\hat{u}_l+X_lX_l)\right)n_i-\hat{t}_j\hat{u}_{i,j}\right]dS\\&=\int_{\partial\Omega}\left[\left(\hat{W}-\frac{\rho\varpi^2}{2}(\hat{u}_l\hat{u}_l+2X_l\hat{u}_l+X_lX_l)\right)n_i-\hat{t}_j\hat{u}_{i,j}\right]dS\end{aligned}$$

define $-\varpi^2X_l\equiv\ddot{X}_l$ and $-\varpi^2X_lX_l=(\mathrm{i}\varpi X_l)(\mathrm{i}\varpi X_l)\equiv\dot{X}_l\dot{X}_l$

$$=\int_{\partial\Omega}\left[\left(\hat{W}-\frac{\rho\varpi^2}{2}\hat{u}_l\hat{u}_l+\rho\ddot{X}_k\hat{u}_k\right)n_i-\hat{t}_j\hat{u}_{i,j}\right]dS+\frac{\dot{X}_l\dot{X}_l}{2}\int_{\partial\Omega}n_i dS\,.$$

The second integral vanishes (this can be seen either by applying physical intuition, the normals cancelling over the surface, or through application of the divergence theorem)

$$=\int_{\partial\Omega}\left[\left(\hat{W}-\frac{\rho\varpi^2}{2}\hat{u}_l\hat{u}_l+\rho\ddot{X}_k\hat{u}_k\right)n_i-\hat{t}_j\hat{u}_{i,j}\right]dS=0\,. \tag{A.4}$$

Note that the same conservation law, for the isotropic, would have been obtained from Cauchy-Navier equations of linear materials (anisotropic or isotropic).

A.2.2 L integral

Likewise, for eq. (2.50):

$$\hat{\mathrm{L}}_i = \int_{\partial\widehat{\Omega}} \epsilon_{kji}\left[\frac{1}{2}\left(\hat{\sigma}_{kj}u_{(k,j)} - \rho\varpi^2(\hat{u}_l + X_l)(\hat{u}_l + X_l)\right)x_k n_j + \hat{t}_j(\hat{u}_k + X_k) - \hat{t}_p\hat{u}_{p,j}x_k\right]dS$$

use the same definitions as in the previous case to obtain

$$= \int_{\partial\widehat{\Omega}} \epsilon_{kji}\left[\frac{1}{2}\left(\hat{\sigma}_{kj}u_{(k,j)} - \rho\varpi^2\hat{u}_l\hat{u}_l + 2\rho\ddot{X}_l\hat{u}_l\right)x_k n_j + \hat{t}_j\hat{u}_k + \hat{t}_j X_k - \hat{t}_p\hat{u}_{p,j}x_k\right]dS$$
$$+ \dot{X}_l\dot{X}_l\epsilon_{kji}\int_{\partial\widehat{\Omega}}\left(x_k n_j\right)dS$$

apply divergence theorem to the second integral

$$= \int_{\partial\widehat{\Omega}} \epsilon_{kji}\left[\frac{1}{2}\left(\hat{\sigma}_{kj}u_{(k,j)} - \rho\varpi^2\hat{u}_l\hat{u}_l + 2\rho\ddot{X}_l\hat{u}_l\right)x_k n_j + \hat{t}_j\hat{u}_k + \hat{t}_j X_k - \hat{t}_p\hat{u}_{p,j}x_k\right]dS$$
$$+ \dot{X}_l\dot{X}_l\epsilon_{kji}\delta_{kj}\int_{\widehat{\Omega}} dV$$

and note $\epsilon_{kji}\delta_{kj} = \epsilon_{kki} = 0$, and thus the second integral vanishes, leaving just

$$= \int_{\partial\widehat{\Omega}} \epsilon_{kji}\left[\frac{1}{2}\left(\hat{\sigma}_{kj}u_{(k,j)} - \rho\varpi^2\hat{u}_l\hat{u}_l + 2\rho\ddot{X}_l\hat{u}_l\right)x_k n_j + \hat{t}_j(\hat{u}_k + X_k) - \hat{t}_p\hat{u}_{p,j}x_k\right]dS$$
$$= 0. \tag{A.5}$$

Hence, these steady-state dynamic J and L integrals can be expressed in terms of relative displacements as

$$\hat{\mathrm{J}}_i = \int_{\partial\Omega}\left[\left(\hat{W} - \hat{T}\right)n_i + \rho\ddot{X}_k\hat{u}_k n_i z - \hat{t}_j\hat{u}_{i,j}\right]dS = 0\,, \tag{A.6}$$

$$\hat{\mathrm{L}}_i = \int_{\partial\widehat{\Omega}}\epsilon_{kji}\left[\left(\hat{W} - \hat{T} + \rho\ddot{X}_l\hat{u}_l\right)x_k n_j + \hat{t}_j(\hat{u}_k + X_k) - \hat{t}_p\hat{u}_{p,j}x_k\right]dS = 0\,, \tag{A.7}$$

where, $\hat{T}$ must be understood as the "kinetic energy of relative displacements" (it does not contain any contribution from X_i).

These new expressions are not proved as they are equivalent to the ones in the previous section.

A.3 Derivation of the quasi-static approximation from steady-state dynamics

Finally, the quasi-static equivalents can formally be obtained from these. Recall eq. (3.10) and attempt a similar, more general, procedure with an expansion for

u_i/X_g, where the terms order zero are assumed to be known and be independent of space and X_g is taken as to represent a characteristic displacement in the problem, as

$$\frac{\hat{u}_i(x,y)}{X_g} = \tilde{u}_{i_0} + r^2\tilde{u}_{i_1}(\xi,\eta) + O(r^4) \quad \text{as} \quad r = \frac{\varpi H}{c_s} \to 0\,, \tag{A.8}$$

and see how it follows that $|\hat{\varepsilon}_{ij}| \sim X_g/H$ and $|\hat{\sigma}_{ij}| \sim \mu X_g/H$; therefore (hereafter we shall introduce brackets with a sub-index around some terms to indicate corresponding term of the expansion)

$$\frac{\hat{\varepsilon}_{ij}(x,y)}{X_g/H} = r^2[\tilde{\varepsilon}_{ij}]_1(\xi,\eta) + O(r^4) \quad \text{as} \quad r = \frac{\varpi H}{c_s} \to 0\,, \tag{A.9}$$

$$\frac{\hat{\sigma}_{ij}(x,y)}{\mu X_g/H} = r^2[\tilde{\sigma}_{ij}]_1(\xi,\eta) + O(r^4) \quad \text{as} \quad r = \frac{\varpi H}{c_s} \to 0\,, \tag{A.10}$$

$$\frac{\hat{W}(x,y)}{\mu(X_g/H)^2} = r^4[\tilde{W}]_1(\xi,\eta) + O(r^6) \quad \text{as} \quad r = \frac{\varpi H}{c_s} \to 0\,. \tag{A.11}$$

A.3.1 J integral

Start by eq. (2.49) (not by eq. (A.6); it is feasible, yet more cumbersome) in dimensionless form and making the substitution (note that we shall introduce a characteristic length in order to express the differential surface in dimensionless form)

$$\begin{aligned}
\hat{\mathrm{J}}_i &= \int_{\partial\Omega}\left(\frac{1}{2}\left(2\hat{W} - \rho\varpi^2\hat{u}_k\hat{u}_k\right)n_i - \hat{\sigma}_{jk}\hat{u}_{i,j}n_k\right)dS \\
&= \mu\left(\frac{X_g}{H}\right)^2 H^2\int_{\partial\Omega}\left(\frac{1}{2}\left(2\tilde{W} - r^2\tilde{u}_k\tilde{u}_k\right)n_i - \tilde{\sigma}_{jk}\tilde{u}_{i,j}n_k\right)d\tilde{S} \\
&= \mu\left(\frac{X_g}{H}\right)^2 H^2\int_{\partial\Omega}\left(\frac{1}{2}\Big(2r^4[\tilde{W}]_1 + O(r^6)\right. \\
&\qquad\qquad - r^2\big(\tilde{u}_{k_0} + r^2\tilde{u}_{k_1} + O(r^4)\big)\big(\tilde{u}_{k_0} + r^2\tilde{u}_{k_1} + O(r^4)\big)\Big)n_i \\
&\qquad\qquad \left. - r^4[\tilde{\sigma}_{jk}\tilde{u}_{i,j}]_1 n_k + O(r^6)\right)d\tilde{S} = \\
&= \mu\left(\frac{X_g}{H}\right)^2 H^2 r^4\int_{\partial\Omega}\left([\tilde{W}]_1\,n_i - \tilde{u}_{k_0}\tilde{u}_{k_1}\,n_i - [\tilde{\sigma}_{jk}\tilde{u}_{i,j}]_1 n_k\right)d\tilde{S} \\
&\quad + \mu\left(\frac{X_g}{H}\right)^2 H^2 r^2\tilde{u}_{k_0}\tilde{u}_{k_0}\int_{\partial\Omega} n_i d\tilde{S} + O(r^6) =
\end{aligned}$$

upon application of the divergence theorem, it is clear the second integral vanishes, leaving

$$= \mu\left(\frac{X_g}{H}\right)^2 H^2 r^4\int_{\partial\Omega}\left([\tilde{W}]_1\,n_i - \tilde{u}_{k_0}\tilde{u}_{k_1}\,n_i - [\tilde{\sigma}_{jk}\tilde{u}_{i,j}]_1 n_k\right)d\tilde{S} + O(r^6) =$$

by noting that $\mu(X_g/H)^2 r^4 = \mu(H/\ell_s)^2 = -\rho\ddot{X}_g U$ and realizing $\ddot{X}_k = \tilde{u}_{k_0}\ddot{X}_g$, the last integral can be given in dimensional variables

$$= \int_{\partial\Omega} \left(\hat{W}\, n_i + \rho\ddot{X}_k \hat{u}_k n_i - \hat{\sigma}_{jk}\hat{u}_{i,j} n_k \right) dS + O(r^6) = 0\,. \tag{A.12}$$

The ratio between the integral and the other terms is $O(r^2)$, and thus, if $r \ll 1$, we can neglect the higher-order terms in the integral and take

$$\hat{\mathfrak{J}}_i = \int_{\partial\Omega} \left(\hat{W}\, n_i + \rho\ddot{X}_k \hat{u}_k n_i - \hat{t}_j \hat{u}_{i,j} \right) dS = 0\,, \tag{A.13}$$

see that the same result would have been obtained had we ignored the kinetic energy in eq. (A.6), as this addend contributes terms $O(r^6)$.

A.3.2 L integral

One can proceed in the very same fashion with eq. (2.50), the only term that requires extra attention is the one associated with work of tractions on the surface, as it seems to have a different scaling with respect to r than the rest. Let us stop for a moment to consider it carefully. We begin by expressing the surface integral as a volumen integral by sake of the divergence theorem:

$$\begin{aligned}
\epsilon_{kji} \int_{\partial\widehat{\Omega}} \hat{t}_j \hat{u}_k dS &= \epsilon_{kji} \int_{\partial\widehat{\Omega}} \hat{\sigma}_{jl} n_l \hat{u}_k dS = \epsilon_{kji} \int_{\widehat{\Omega}} \left(\hat{\sigma}_{jl}\hat{u}_k \right)_{,l} dV \\
&= \epsilon_{kji} \int_{\widehat{\Omega}} \hat{\sigma}_{jl,l}\hat{u}_k dV + \epsilon_{kji} \int_{\widehat{\Omega}} \hat{\sigma}_{jl}\hat{u}_{k,l} dV
\end{aligned}$$

apply equilibrium in the first integral

$$= -\epsilon_{kji} \int_{\widehat{\Omega}} \rho\varpi^2 \hat{u}_j \hat{u}_k dV + \epsilon_{kji} \int_{\widehat{\Omega}} \hat{\sigma}_{jl}\hat{u}_{k,l} dV$$

the first integral vanishes as $\hat{\boldsymbol{u}} \wedge \hat{\boldsymbol{u}} = 0$

$$= \epsilon_{kji} \int_{\widehat{\Omega}} \underbrace{\hat{\sigma}_{jl}}_{O(r^2)} \underbrace{\hat{u}_{k,l}}_{O(r^2)} dV\,,$$

thus this integral only contains $O(r^4)$ terms, and thus it can be used right away in the quasi-static approximation. Thus, also for the L-integral, the result is equivalent to remove the contribution of the kinetic energy from eq. (A.7), as this addend contributes terms $O(r^6)$.

When deciding if using or not these low-frequent approximations, recall that they entail errors $O(r^2)$.

Appendix B

DERIVATIONS FOR CHAPTER III

B.1 Proof of equivalence of approach in terms of normal modes

Herein we demonstrate in what way eq. (3.7) and eq. (3.4) are equivalent.

From eq. (3.4) the relative displacement is found just from subtracting the base displacement, then simply project it onto $\sin(k_n\eta)$ and operate:

$$u = u_t - X_g e^{i\varpi t} = X_g e^{i\varpi t}\left[\frac{\cos(r(1-\eta))}{\cos(r)} - 1\right]$$

note that 1 can not be perfecly projected onto $\sin(k_n\eta)$, then

$$\begin{aligned}
&\sim X_g e^{i\varpi t}\sum_{n=1}^{\infty}\left[\frac{2\cos(r)}{k_n(1-r_n^2)\cos(r)} - \frac{2}{k_n}\right]\sin(k_n\eta)\\
&= X_g e^{i\varpi t}\sum_{n=1}^{\infty}\left[\frac{2}{k_n(1-r_n^2)} - \frac{2}{k_n}\right]\sin(k_n\eta)\\
&= X_g e^{i\varpi t}\sum_{n=1}^{\infty}\frac{2r_n^2}{k_n(1-r_n^2)}\sin(k_n\eta)
\end{aligned}$$

substitute $r_n = r/k_n = \varpi H/k_n c_s$,

$$\begin{aligned}
&= X_g e^{i\varpi t}\sum_{n=1}^{\infty}\frac{2}{k_n}\frac{\left(\frac{\varpi}{k_n c_s/H}\right)^2}{1-r_n^2}\sin(k_n\eta)\\
&= e^{i\varpi t}\underbrace{X_g\varpi^2}_{-\ddot{X}_g}\frac{H^2}{c_s^2}\sum_{n=1}^{\infty}\frac{2}{k_n^3\left(1-r_n^2\right)}\sin(k_n\eta)\\
&= -Ue^{i\varpi t}\sum_{n=1}^{\infty}\frac{2}{k_n^3\left(1-r_n^2\right)}\sin(k_n\eta)\,, \qquad \text{(B.1)}
\end{aligned}$$

so both steady-state solutions are equivalent in the L^2-sense, yet not point-wise.

The free vibration (transient part) since it represents a movement with respect to the base, is necessarily the same, so it is deemed not to require proof.

B.2 WKB application to steady-state dynamic response of soil deposits on rigid bedrock

As it was mentioned in the body of the chapter, introducing the ansatz eq. (3.29) into eq. (3.28b) yields

$$\epsilon^2 \left[\frac{1}{\delta^2} \left(\sum_{n=0}^{\infty} \delta^n S_n'(\eta) \right)^2 + \frac{1}{\delta} \left(\sum_{n=0}^{\infty} \delta^n (S_n''(\eta) + 2m(\eta) S_n'(\eta)) \right) \right] + q(\eta) = 0 \,, \tag{B.2}$$

to leading order ($n = 0$):

$$\frac{\varepsilon^2}{\delta^2} S_0'^2(\eta) + \frac{\varepsilon^2}{\delta} \left[2S_0'(\eta) S_1'(\eta) + S_0''(\eta) + 2m(\eta) S_0'(\eta) \right] + q(\eta) = 0 \,, \tag{B.3}$$

in the limit $\delta \to 0$, dominant balance imposes $\delta \sim \epsilon$, and therefore

$$\frac{\varepsilon^2}{\delta^2} S_0'^2(\eta) + q(\eta) = S'^2_0(\eta) + q(\eta) = 0 \,, \tag{B.4}$$

for such a limit. Then, by simple integration of eq. (B.4))

$$S_0(\eta) = \int_1^{\eta} \sqrt{-q(\eta')} d\eta' = \pm i \int_1^{\eta} \sqrt{q(\eta')} d\eta' \,, \tag{B.5}$$

where η' represents a dummy integration variable.

Note also that eq. (3.29) turns into

$$\tilde{u}(\eta) \sim \exp\left(\frac{1}{\epsilon} \sum_{n=0}^{\infty} \epsilon^n S_n(\eta) \right) , \tag{B.6a}$$

and recalling that $r = 1/\epsilon$

$$\tilde{u}(\eta) \sim \exp\left(r \sum_{n=0}^{\infty} \frac{S_n(\eta)}{r^n} \right) = \exp\left(r S_0(\eta) + S_1(\eta) + \frac{S_2(\eta)}{r} + \dots \right) . \tag{B.6b}$$

Thus, utilize appendix B.2 to find the first order approximation

$$\tilde{u}(\eta) = A \exp\left(ir \int_1^{\eta} \sqrt{q(\eta')} d\eta' \right) + B \exp\left(-ir \int_1^{\eta} \sqrt{q(\eta')} d\eta' \right) , \tag{B.7}$$

which, after imposing boundary conditions to find A, B boils down to

$$\tilde{u}(\eta) = \frac{\cos\left(r \int_{\eta}^{1} \sqrt{q(\eta')} d\eta' \right)}{\cos\left(r \int_0^1 \sqrt{q(\eta')} d\eta' \right)} \,. \tag{B.8}$$

We could undo the non-dimensionalization at this point, but let us find the base-to-surface amplification, A, first, and then do so:

$$A(\varpi) = \frac{u(y=H)}{X_g} = \tilde{u}(\eta=1) = \frac{1}{\cos\left(r\int_0^1 \sqrt{q(\eta')}d\eta'\right)} =$$

now remove dimensionless variables and parameters, in particular, take into account that $\sqrt{q(\eta)} = 1/f(\eta) = 1/(V_s(y)/V_{base})$

$$= \frac{1}{\cos\left(r\int_0^1 \frac{d\eta'}{f(\eta')}\right)} = \frac{1}{\cos\left(\varpi\int_0^H \frac{dy}{V_s(y)}\right)} = \frac{1}{\cos\left(\frac{\varpi H}{V_{s,eq}}\right)}\,, \tag{B.9}$$

where

$$V_{s,eq} = H\left(\int_0^H \frac{dy}{V_s(y)}\right)^{-1}\,, \tag{B.10}$$

happens to be the harmonic mean of the function $V_s(y)$ in the interval $[0, H]$. An estimation of the error in using this approximation remains a task to tackle.

This is the part of the recursion concerning ϵ^0 (*geometrical optics solution*). Now we can proceed to find the next term in the approximation, ϵ^1:

$$2S_0'(\eta)S_1'(\eta) + S_0''(\eta) + 2m(\eta)S_0'(\eta) = 0\,, \tag{B.11a}$$

$$2S_1'(\eta) + \frac{S_0''(\eta)}{S_0'(\eta)} + 2m(\eta) = 0\,, \tag{B.11b}$$

recall $m(\eta) = f'(\eta)/f(\eta)$, and then integrate (let C be a constant):

$$2S_1(\eta) + \ln(S_0'(\eta)) + 2\ln f(\eta) = C\,, \tag{B.11c}$$

$$2S_1(\eta) + \ln(S_0'(\eta)f^2(\eta)) = C\,, \tag{B.11d}$$

see that, from eq. (B.4)), $S_0'(\eta) = \sqrt{-q(x)} = i/f(\eta)$

$$2S_1(\eta) + \ln(i) + \ln(f(\eta)) = C\,, \tag{B.11e}$$

$$2S_1(\eta) + i\frac{\pi}{2} + \ln(f(\eta)) = C\,, \tag{B.11f}$$

$$S_1(\eta) = \frac{C}{2} - i\frac{\pi}{4} + \ln(f(\eta)^{-1/2})\,. \tag{B.11g}$$

Thus, adding this new term into eq. (B.6b)) yields

$$\tilde{u}(\eta) = f(\eta)^{-1/2}\frac{\cos\left(r\int_\eta^1 \sqrt{q(\eta')}d\eta'\right)}{\cos\left(r\int_0^1 \sqrt{q(\eta')}d\eta'\right)}\,, \tag{B.12}$$

and hence the amplification

$$A(\varpi) = \frac{f(1)^{-1/2}}{\cos\left(\frac{\varpi H}{c_{s,eq}}\right)}\,. \tag{B.13}$$

This solution corresponds to the so-called *physical optics solution*.

Let us obtain one more term of the solution. So far we have $S_0' = \sqrt{-q(\eta)}$ and $S_1' = -f'(\eta)/2f(\eta)$. We are going to need also $S_1'' = -[f''(\eta)/f(\eta) - (f'(\eta)/f(\eta))^2]/2$. Then, take the next power, ϵ^2:

$$2S_0'(\eta)S_2'(\eta) + \left(S_1'(\eta)\right)^2 + S_1''(\eta) + 2m(\eta)S_1'(\eta) = 0\,, \tag{B.14a}$$

$$2S_0'(\eta)S_2'(\eta) + \left(-\frac{1}{2}\frac{f'(\eta)}{f(\eta)}\right)^2 - \frac{1}{2}\left(\frac{f''(\eta)}{f(\eta)} - \left(\frac{f'(\eta)}{f(\eta)}\right)^2\right) + \\ + 2\frac{f'(\eta)}{f(\eta)}\left(-\frac{1}{2}\frac{f'(\eta)}{f(\eta)}\right) = 0\,, \tag{B.14b}$$

$$2S_0'(\eta)S_2'(\eta) + \frac{1}{4}\left(\frac{f'(\eta)}{f(\eta)}\right)^2 + \frac{1}{2}\left(\frac{f'(\eta)}{f(\eta)}\right)^2 - \frac{1}{2}\frac{f''(\eta)}{f(\eta)} - \left(\frac{f'(\eta)}{f(\eta)}\right)^2 = 0\,, \tag{B.14c}$$

$$2S_0'(\eta)S_2'(\eta) - \frac{1}{4}\left(\frac{f'(\eta)}{f(\eta)}\right)^2 - \frac{1}{2}\frac{f''(\eta)}{f(\eta)} = 0\,, \tag{B.14d}$$

$$S_2'(\eta)\left(\frac{\pm 1}{f(\eta)}\right) = \frac{1}{4}\left(\frac{f'(\eta)}{f(\eta)}\right)^2 + \frac{1}{2}\frac{f''(\eta)}{f(\eta)}\,, \tag{B.14e}$$

$$\pm iS_2'(\eta) = \frac{1}{8}\frac{(f'(\eta))^2}{f(\eta)} + \frac{1}{4}f''(\eta)\,, \tag{B.14f}$$

$$S_2(\eta) = \pm i\left(\frac{1}{8}\int_0^\eta \frac{(f'(\eta))^2}{f(\eta)}d\eta + \frac{1}{4}\left(f'(\eta) - f'(0)\right)\right)\,. \tag{B.14g}$$

This coefficient does not attain a nice closed form as happened with the previous ones. From it, one could surmise that, should the series converge also around $r \sim 1$, the natural frequency, yet not the amplitude (as the coefficient is imaginary), at the first resonant peak do not only depend on the distribution of stiffness but also on its gradients.

Validity conditions

The approximation to be verified *all over the layer* it is necessary for the parameters to verify

$$r \gg \frac{\ln(f(\eta)^{-1/2})}{\int_0^\eta \frac{d\eta}{f(\eta)}}\,, \qquad \forall\eta \in [0,1] \quad \text{as} \quad r \to \infty\,. \tag{B.15}$$

Note that, however large the left-hand side, one can always define a high-enough frequency so that the inequality is verified.

Moreover, from a “small-parameter standpoint", eq. (3.32) is always valid for as long as $f'(\eta)/f(\eta)$ is not as large as to compensate the presence of the small parameter ϵ in eq. (3.28b)): in mathematical terms, it must be verified that

$$\epsilon^2 \left| \frac{f'(\eta)}{f(\eta)} \right| \ll 1 \tag{B.16a}$$

or inverting ϵ

$$\left| \frac{f'(\eta)}{f(\eta)} \right| \ll r^2 \,. \tag{B.16b}$$

See that this local condition does not when there are either sudden jumps in the velocity profile, as it happens in those cases $f'(\eta) \to \infty$, viz. when the gradient is large (potentially infinite), or complementarily when the derivative at some point cannot be defined (when for example the profile presents a kink). Nevertheless, as long as the gradient, and hence the velocities, remains bounded there is always a sufficiently high frequency at which point the approximation starts being valid. It is interesting to note that the sign of $f'(\eta)$ does not affect the result, for the approximation to be adequate only the magnitude of the gradient does matter while its sign is irrelevant, so the result holds if the velocity profile is globally or locally increasing or decreasing.

Generalization

An even-more-general result can be obtained: using this small parameters framework one can show that actually a similar result holds even for the case wherein both stiffness and density change across the layer.

Suppose $\rho = \rho_{base} h(\eta)$, whereas $\mu = \mu_{base} j(\eta)$, where both $j(\eta)$ and $j(\eta)$ are positive and bounded functions in the interval and also belong in $C^1([0,1])$. The corresponding counterpart of eq. (3.28a) is

$$\epsilon^2 \frac{d^2 \tilde{u}_t}{d\eta^2} + \epsilon^2 \frac{j'(\eta)}{j(\eta)} \frac{d\tilde{u}_t}{d\eta} + \frac{h(\eta)}{j(\eta)} \tilde{u}_t = 0 \,, \tag{B.17}$$

thus redefining $m(\eta) = j'(\eta)/2j(\eta)$ and $q(\eta) = h(\eta)/j(\eta)$ yields a new eq. (3.28b) again, which, repeating the procedure,

$$A(\varpi) = \frac{\left(\frac{\rho_{top}\mu_{top}}{\rho_{base}\mu_{base}} \right)^{1/4}}{\cos\left(\frac{\varpi H}{c_{s,eq}} \right)} \,, \tag{B.18}$$

where $c_{s,eq}$ is still given by the harmonic mean of the point-wise defined shear-wave velocity distribution, as originally given by $f(\eta) = \sqrt{\mu(\eta)/\rho(\eta)}$.

Appendix C

DERIVATIONS FOR CHAPTER IV

C.1 Exact solution of Younan-Veletsos problem

A detailed, step-by-step derivation of the main result in section 4.3 follows.

C.1.1 Presentation of the problem: total displacements

An scheme of the original system can be found in fig. 4.2.

Let us re-state the problem: consider a semi-infinite soft-soil layer, resting on rigid bedrock and bounded to the left by a rigid (thus it moves with the bedrock base) and smooth wall (thus no shear stresses develop at the soil-wall interface). The excitation of the system is an imposed time-varying displacement at the base $\mathcal{X}_g(t)$, which is supposed to be known and which cannot be affected by wave reflections. Find the displacement field.

Recall that the assumption introduced by the Younan and Veletsos prevented considerations of wall smoothness, as the shear stress comes constrained by their pivotal assumption: no σ_{yy} stress developing anywhere.

Assuming that the soil behaves as a homogeneous, density ρ, isotropic linear-elastic solid (characterized by Lamé parameters μ, shear modulus, and λ), undergoing small deformations, the equations that govern the material response are the so-called Cauchy-Navier equations:

$$(\lambda + 2\mu)\frac{\partial^2 u_t}{\partial x^2} + (\lambda + \mu)\frac{\partial^2 v_t}{\partial x \partial y} + \mu\frac{\partial^2 u_t}{\partial y^2} = \rho\frac{\partial^2 u_t}{\partial t^2} \tag{C.1a}$$

$$(\lambda + 2\mu)\frac{\partial^2 v_t}{\partial y^2} + (\lambda + \mu)\frac{\partial^2 u_t}{\partial x \partial y} + \mu\frac{\partial^2 v_t}{\partial x^2} = \rho\frac{\partial^2 v_t}{\partial t^2} \tag{C.1b}$$

subjected to the following boundary conditions: At $y = 0$

$$u_t(x, y = 0, t) = \mathcal{X}_g(t) \qquad v_t(x, y = 0, t) = 0\,, \tag{C.2a}$$

and at $y = H$

$$\tau_{xy}(x, y = H, t) = 0 \qquad \sigma_{yy}(x, y = H, t) = 0 \tag{C.2b}$$

and at $x = 0$

$$\tau_{xy}(x = 0, y, t) = 0 \qquad u_t(x = 0, y, t) = \mathcal{X}_g(t)\,. \tag{C.2c}$$

C.1.2 Introducing relative displacements

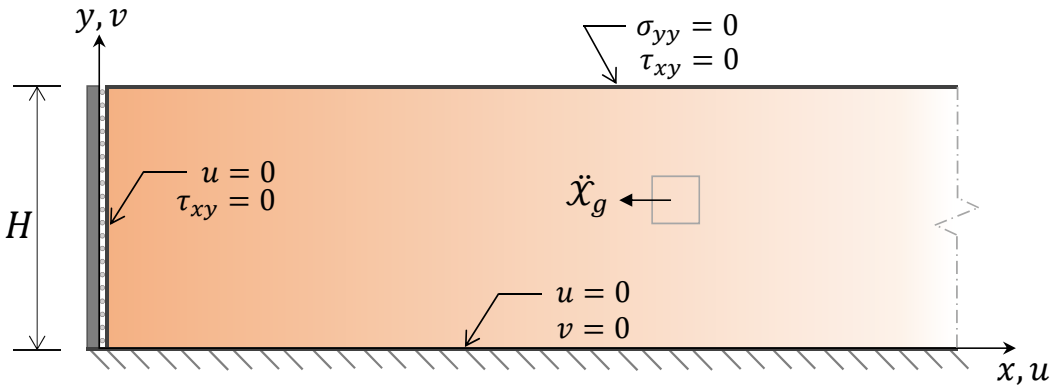

Figure C.1: System re-framed in terms of relative displacements

Both u_t and v_t represent total displacements, measure with respect to some unmoved reference. For this particular problem, it turned out to be very useful to work with relative displacements rather. Thus, let us apply a change of variable $u_t(x,y,t) = u(x,y,t) + \mathcal{X}_g(t)$, $v_t(x,y,t) = v(x,y,t)$ to Eqs.(C.1) in order to obtain the equations of motion in terms of relative displacements

$$(\lambda+2\mu)\frac{\partial^2 u}{\partial x^2} + (\lambda+\mu)\frac{\partial^2 v}{\partial x \partial y} + \mu\frac{\partial^2 u}{\partial y^2} = \rho\frac{\partial^2 u}{\partial t^2} + \rho\ddot{\mathcal{X}}_g(t) \tag{C.3a}$$

$$(\lambda+2\mu)\frac{\partial^2 v}{\partial y^2} + (\lambda+\mu)\frac{\partial^2 u}{\partial x \partial y} + \mu\frac{\partial^2 v}{\partial x^2} = \rho\frac{\partial^2 v}{\partial t^2} \tag{C.3b}$$

as for eq. (C.2a)):

$$u(x, y=0, t) = 0 \qquad v(x, y=0, t) = 0\,, \tag{C.4a}$$

whereas eq. (C.2b)) does not change insofar the stresses do not depend on the displacements themselves but on their spatial gradients:

$$\tau_{xy}(x, y=H, t) = 0 \qquad \sigma_{yy}(x, y=H, t) = 0\,. \tag{C.4b}$$

Similarly eq. (C.2b)) becomes

$$\tau_{xy}(x=0, y, t) = 0 \qquad u(x=0, y, t) = 0 \tag{C.4c}$$

Note that the original problem can be classified as “unforced wave propagation with inhomogeneous mixed boundary conditions", while this modified one corresponds to “forced wave propagation (because now there is an external body force, $\rho\ddot{\mathcal{X}}_g$) with homogeneous mixed boundary conditions".

Purposefully, nothing has been said about initial conditions since we shall focus on steady-state response in frequency domain. Considering a transient regime governed

by the initial conditions can be easily done by appealing to Laplace's transform in time. This path could be pursued, but it is unnecessary if the goal is obtaining transfer functions in frequency domain.

C.2 Dealing with the time domain

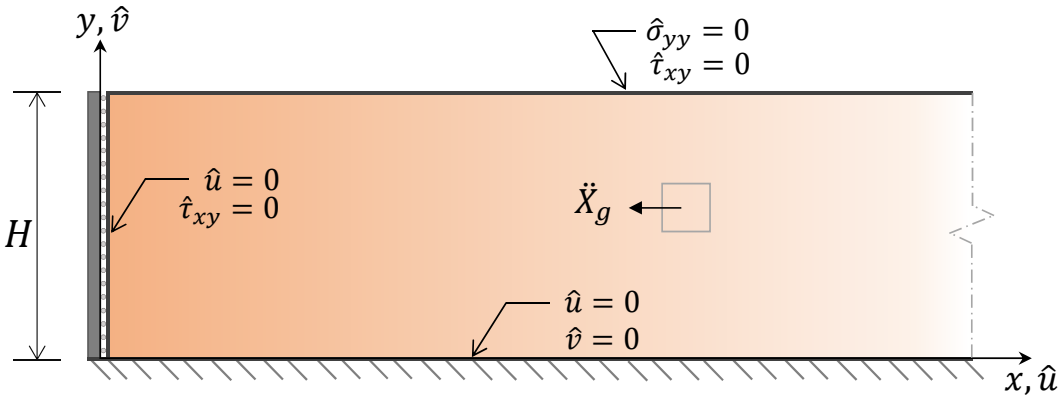

Figure C.2: System after assuming harmonic excitation and response

The assumption of steady-state regime would enable us to take Fourier transform in time, as we could disregard the initial conditions. The actual issue with using Fourier transform at this point is having to deal with the normalization factor at the transform and anti-transform.

One of our main concerns is finding the transfer function for the earth thrust on the wall, therefore a more-convenient, equivalent way of proceeding is assuming a harmonic decomposition of both the load and the response and, invoking superposition, to focus to one sole harmonic. In summary, this means assuming $u = \hat{u}e^{i\varpi t}$, $v = \hat{v}e^{i\varpi t}$ as well as $\ddot{X}_g = \ddot{X}_g e^{i\varpi t}$, where ϖ can be any certain excitation frequency and $\hat{u}$, $\hat{v}$ must be understood as complex numbers. Introducing these changes into eq. (C.3)) yields

$$(\lambda + 2\mu)\frac{\partial^2 \hat{u}}{\partial x^2} + (\lambda + \mu)\frac{\partial^2 v}{\partial x \partial y} + \mu\frac{\partial^2 \hat{u}}{\partial y^2} + \rho\varpi^2\hat{u} = \rho\ddot{X}_g(t)\,, \tag{C.5a}$$

$$(\lambda + 2\mu)\frac{\partial^2 \hat{v}}{\partial y^2} + (\lambda + \mu)\frac{\partial^2 \hat{u}}{\partial x \partial y} + \mu\frac{\partial^2 \hat{v}}{\partial x^2} + \rho\varpi^2\hat{v} = 0\,, \tag{C.5b}$$

with boundary conditions:

$$\hat{u}(x, y = 0) = 0 \qquad \hat{v}(x, y = 0) = 0\,, \tag{C.6a}$$

$$\hat{\tau}_{xy}(x, y = H) = 0 \qquad \hat{\sigma}_{yy}(x, y = H) = 0\,, \tag{C.6b}$$

$$\hat{\tau}_{xy}(x = 0, y) = 0 \qquad \hat{u}(x = 0, y) = 0\,. \tag{C.6c}$$

C.3 Nondimensionalization and key symmetry argument

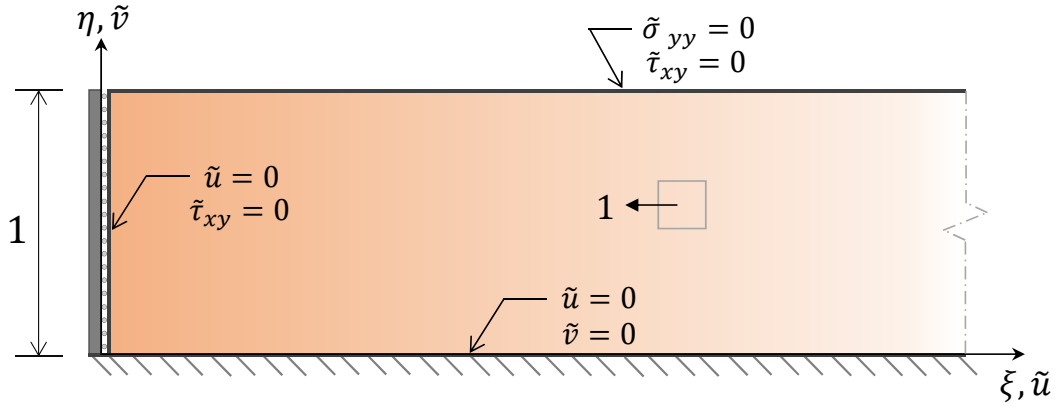

Figure C.3: System after non-dimensionalization

Working with dimensionless equations eases keeping track of the parameters of the problem and partially relieves the burden of algebraic manipulations. Nevertheless, this step is optional and does not bear any significance within the solving procedure. For the purpose of writing the last equations in dimensionless form, the following dimensionless variables and parameters are introduced:

$$\xi = x/H \qquad \text{(dimensionless horizontal coordinate)}, \tag{C.7a}$$

$$\eta = y/H \qquad \text{(dimensionless vertical coordinate)}, \tag{C.7b}$$

$$\tilde{u} = \frac{\hat{u}}{\rho \ddot{X}_g H^2/\mu} \qquad \text{(dimensionless horizontal coordinate)}, \tag{C.7c}$$

$$\tilde{v} = \frac{\hat{v}}{\rho \ddot{X}_g H^2/\mu} \qquad \text{(dimensionless horizonta coordinate)}, \tag{C.7d}$$

$$r = \frac{\varpi}{c_s/H} \qquad \text{(dimensionless external frequency)}, \tag{C.7e}$$

$$c = \sqrt{\frac{\lambda + 2\mu}{\mu}} = \sqrt{\frac{2(1-\nu)}{1-2\nu}}\,. \tag{C.7f}$$

where also $c = c(\nu) = c_s/c_p$, the ratio between P-wave and S-wave propagation velocities, (which, in the case of isotropic linear-elastic solid, is a function of Poisson's ratio ν solely) has been introduced in the main body of the thesis.

Once again, use this change of variables to turn the equations of motion into

$$c^2 \frac{\partial^2 \tilde{u}}{\partial \xi^2} + (c^2 - 1)\frac{\partial^2 \tilde{v}}{\partial \xi \eta} + \frac{\partial^2 \tilde{u}}{\partial \eta^2} + r^2 \tilde{u} = 1\,, \tag{C.8a}$$

$$c^2 \frac{\partial^2 \tilde{v}}{\partial \eta^2} + (c^2 - 1)\frac{\partial^2 \tilde{u}}{\partial \xi \eta} + \frac{\partial^2 \tilde{v}}{\partial \xi^2} + r^2 \tilde{v} = 0\,, \tag{C.8b}$$

subject to the boundary conditions at $\eta = 0$:

$$\tilde{u}(\xi, \eta = 0) = 0 \quad \tilde{v}(\xi, \eta = 0) = 0\,, \tag{C.9a}$$

at $\eta = 1$

$$\tau_{xy}(\xi, \eta = 1) = 0 \rightarrow \frac{\partial \tilde{u}}{\partial \eta}\bigg|_{\eta=1} + \frac{\partial \tilde{v}}{\partial \xi}\bigg|_{\eta=1} = 0\,, \tag{C.9b}$$

$$\sigma_{yy}(\xi, \eta = 1) = 0 \rightarrow c^2 \frac{\partial \tilde{v}}{\partial \eta}\bigg|_{\eta=1} + (c^2 - 2)\frac{\partial \tilde{u}}{\partial \xi}\bigg|_{\eta=1} = 0\,, \tag{C.9c}$$

at $\xi = 0$ (smooth, rigid wall)

$$\tilde{u}(\xi = 0, \eta) = 0\,, \tag{C.9d}$$

$$\tau_{xy}(\xi = 0, \eta) = 0 \rightarrow \frac{\partial \tilde{u}}{\partial \eta}\bigg|_{\xi=0} + \frac{\partial \tilde{v}}{\partial \xi}\bigg|_{\xi=0} = \frac{\partial \tilde{v}}{\partial \xi}\bigg|_{\xi=0} = 0\,. \tag{C.9e}$$

At this very moment we move to consider the how to deal with the unboundedness of the horizontal coordinate. Since $x \in [0, +\infty)$, an approach based on applying Laplace's transform on displacements may seem on point at first, however opting for this approach requires knowledge of both the value of the displacement and its first derivative at the wall, what is not the case: the value of $\tilde{u}$ is known yet $\partial\tilde{u}/\partial\xi$ is not, and conversely $\partial\tilde{v}/\partial\xi$ it is known while $\tilde{v}$ is not. Thus, applying Laplace's transform would be entering a cul-de-sac. Nevertheless, the conditions seem ideal to apply Fourier sine transform and Fourier cosine transform, yet this option appears confusing as it would require using different transforms for each displacement component.

The fitting approach for this specific problem is appealing to symmetry and then applying the classic Fourier Transform. The symmetry argument reads: this type of wall, in our formulation in terms of relative displacement, amounts to applying a symmetry condition on a infinite layer wherein the body force suddenly changes sign at $\xi = 0$.

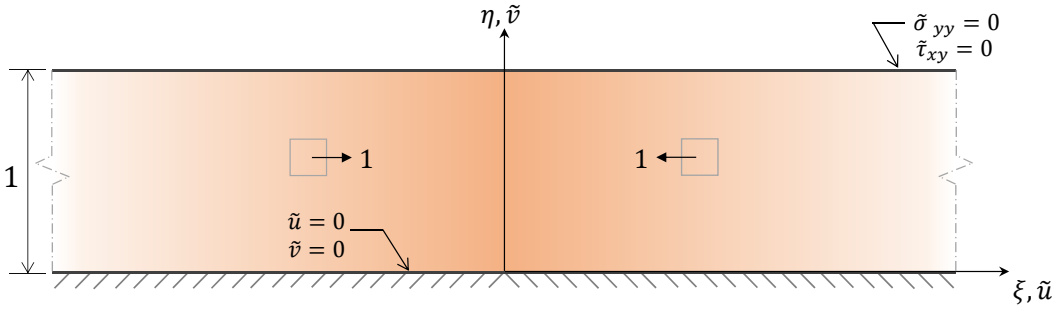

Figure C.4: Nondimensional system after applying symmetry argument

Thus, in lieu of the semi-infinite soil strip domain, let us consider a infinite domain where at $\xi = 0$ there is a discontinuity in the "loading", that is, the external body force, originally simply -1 defined over $x \geq 0$, now follows minus the sign function, $-\operatorname{sign}(\xi) = 2\theta_0(\xi) - 1$ defined over $x \in \mathbb{R}$, where $\theta_0(\xi)$ is the Heaviside function centered at $\xi = 0$.

Hence, the system that will finally be solved is governed by the following equations and boundary conditions:

$$c^2\frac{\partial^2\tilde{u}}{\partial\xi^2} + (c^2-1)\frac{\partial^2\tilde{v}}{\partial\xi\eta} + \frac{\partial^2\tilde{u}}{\partial\eta^2} + r^2\tilde{u} = -\operatorname{sign}(\xi)\,, \tag{C.10a}$$

$$c^2\frac{\partial^2\tilde{v}}{\partial\eta^2} + (c^2-1)\frac{\partial^2\tilde{u}}{\partial\xi\eta} + \frac{\partial^2\tilde{v}}{\partial\xi^2} + r^2\tilde{v} = 0\,, \tag{C.10b}$$

subject to the boundary conditions at $\eta = 0$:

$$\tilde{u}(\xi,\eta=0) = 0 \quad \tilde{v}(\xi,\eta=0) = 0\,, \tag{C.11a}$$

at $\eta = 1$:

$$\tau_{xy}(\xi,\eta=1) = 0 \rightarrow \frac{\partial\tilde{u}}{\partial\eta}\bigg|_{\eta=1} + \frac{\partial\tilde{v}}{\partial\xi}\bigg|_{\eta=1} = 0\,, \tag{C.11b}$$

$$\sigma_{yy}(\xi,\eta=1) = 0 \rightarrow c^2\frac{\partial\tilde{v}}{\partial\eta}\bigg|_{\eta=1} + (c^2-2)\frac{\partial\tilde{u}}{\partial\xi}\bigg|_{\eta=1} = 0\,. \tag{C.11c}$$

At this point, we can go in for the kill. Resort to Fourier Transform to define the amplitudes of the displacement field in wavenumber space:

$$\mathcal{F}[\tilde{u}] = \frac{1}{\sqrt{2\pi}}\int_{-\infty}^{+\infty}\tilde{u}e^{ik\xi}d\xi = U\,, \tag{C.12}$$

$$\mathcal{F}[\tilde{v}] = \frac{1}{\sqrt{2\pi}}\int_{-\infty}^{+\infty}\tilde{v}e^{ik\xi}d\xi = V\,, \tag{C.13}$$

wherein k represents a dimensionless wavenumber, related to the physical wavenumber, call it k, by $\mathrm{k} = kH$, where H still represents the wall height.

$$-c^2k^2U + ik(c^2-1)\frac{\partial V}{\partial\eta} + \frac{\partial^2U}{\partial\eta^2} + r^2U = \sqrt{\frac{2}{\pi}}\frac{i}{k}\,, \tag{C.14a}$$

$$c^2\frac{\partial^2V}{\partial\eta^2} + ik(c^2-1)\frac{\partial U}{\partial\eta} - k^2V + r^2V = 0\,, \tag{C.14b}$$

or more condensed:

$$ik(c^2-1)\frac{\partial V}{\partial\eta} + \frac{\partial^2U}{\partial\eta^2} + (r^2-c^2k^2)U - \sqrt{\frac{2}{\pi}}\frac{i}{k} = 0\,, \tag{C.15a}$$

$$c^2\frac{\partial^2V}{\partial\eta^2} + ik(c^2-1)\frac{\partial U}{\partial\eta} + (r^2-k^2)V = 0\,, \tag{C.15b}$$

subject to boundary conditions. These are, at $\eta = 0$:

$$U(0) = 0 \quad V(0) = 0\,, \tag{C.16a}$$

at $\eta = 1$:

$$\tau_{xy} = 0 \rightarrow \frac{\partial U}{\partial \eta}\Big|_{\eta=1} + ikV = 0\,, \tag{C.16b}$$

$$\sigma_{yy} = 0 \rightarrow c^2 \frac{\partial V}{\partial \eta}\Big|_{\eta=1} + ik(c^2 - 2)U = 0\,, \tag{C.16c}$$

what represents the problem in the original vertical (nondimensional) variable and in wavenumber (k) domain.

The system of equation can be even more condensed by introducing $\mathcal{V} = \partial V/\partial\eta$, $\mathcal{U} = \partial U/\partial\eta = \partial(U - (k(r^2 - c^2k^2))^{-1})/\partial\eta$ as extra variables, and thus

$$\frac{\partial \mathcal{U}}{\partial \eta} = ik(1 - c^2)\mathcal{V} + (c^2k^2 - r^2)\left(U + \sqrt{\frac{2}{\pi}}\frac{i}{k(c^2k^2 - r^2)}\right), \tag{C.17a}$$

$$\frac{\partial}{\partial \eta}\left(U + \sqrt{\frac{2}{\pi}}\frac{i}{k(c^2k^2 - r^2)}\right) = \mathcal{U}\,, \tag{C.17b}$$

$$\frac{\partial \mathcal{V}}{\partial \eta} = ik\frac{(1 - c^2)}{c^2}\mathcal{U} + \frac{(k^2 - r^2)}{c^2}V\,, \tag{C.17c}$$

$$\frac{\partial V}{\partial \eta} = \mathcal{V}\,, \tag{C.17d}$$

subject to the boundary conditions: at $\eta = 0$

$$U(0) = 0 \quad V(0) = 0\,, \tag{C.18a}$$

at $\eta = 1$

$$\mathcal{U}(1) = -ikV(1)\,, \tag{C.18b}$$

$$c^2\mathcal{V}(1) = -ik(c^2 - 2)U(1)\,, \tag{C.18c}$$

introduce a vector of unknowns,

$$\boldsymbol{X} = \left[\mathcal{U} \quad U + \sqrt{\frac{2}{\pi}}\frac{i}{k(c^2k^2 - r^2)} \quad \mathcal{V} \quad V\right]^\top, \tag{C.19}$$

thus the Eqs.(C.17) can be written simply as

$$\boldsymbol{X}' = \boldsymbol{D}\boldsymbol{X}\,, \tag{C.20}$$

where

$$\boldsymbol{D} = \begin{bmatrix} 0 & (c^2k^2 - r^2) & ik(1-c^2) & 0 \\ 1 & 0 & 0 & 0 \\ ik\frac{(1-c^2)}{c^2} & 0 & 0 & \frac{(k^2-r^2)}{c^2} \\ 0 & 0 & 1 & 0 \end{bmatrix} \tag{C.21}$$

the eigenvalues of this matrix are

$$\lambda_1 = -\sqrt{k^2 - r^2}, \quad \lambda_2 = \sqrt{k^2 - r^2}, \quad \lambda_3 = -\sqrt{k^2 - (r/c)^2}, \quad \lambda_4 = \sqrt{k^2 - (r/c)^2}, \tag{C.22}$$

each of these solution corresponds to S-waves (first two solutions) and P-waves (last two solutions) propagating within this infinite stratum.

The eigenvectors (normalized to 1 in the fourth entry) are

$$\boldsymbol{\varphi}_1 = \begin{bmatrix} i\frac{(k^2-r^2)}{k} \\ -i\frac{(\sqrt{k^2-r^2})}{k} \\ -\sqrt{k^2 - r^2} \\ 1 \end{bmatrix}, \quad \boldsymbol{\varphi}_2 = \begin{bmatrix} i\frac{(k^2-r^2)}{k} \\ i\frac{(\sqrt{k^2-r^2})}{k} \\ \sqrt{k^2 - r^2} \\ 1 \end{bmatrix},$$

$$\boldsymbol{\varphi}_3 = \begin{bmatrix} ik \\ -i\frac{k}{\sqrt{k^2-(r/c)^2}} \\ -\sqrt{k^2 - (r/c)^2} \\ 1 \end{bmatrix}, \quad \boldsymbol{\varphi}_4 = \begin{bmatrix} ik \\ i\frac{k}{\sqrt{k^2-(r/c)^2}} \\ \sqrt{k^2 - (r/c)^2} \\ 1 \end{bmatrix}, \tag{C.23}$$

thus the solution must be

$$\boldsymbol{X} = \begin{bmatrix} \mathcal{U} \\ U + \sqrt{\frac{2}{\pi}}\frac{i}{k(c^2k^2-r^2)} \\ \mathcal{V} \\ V \end{bmatrix} = A \begin{bmatrix} i\frac{(k^2-r^2)}{k} \\ -i\frac{(\sqrt{k^2-r^2})}{k} \\ -\sqrt{k^2 - r^2} \\ 1 \end{bmatrix} e^{-(\sqrt{k^2-r^2})\eta} + B \begin{bmatrix} i\frac{(k^2-r^2)}{k} \\ i\frac{(\sqrt{k^2-r^2})}{k} \\ \sqrt{k^2 - r^2} \\ 1 \end{bmatrix} e^{(\sqrt{k^2-r^2})\eta}$$

$$+C \begin{bmatrix} ik \\ -i\frac{k}{\sqrt{k^2-(r/c)^2}} \\ -\sqrt{k^2 - (r/c)^2} \\ 1 \end{bmatrix} e^{-(\sqrt{k^2-\left(\frac{r}{c}\right)^2})\eta} + D \begin{bmatrix} ik \\ i\frac{k}{\sqrt{k^2-\left(\frac{r}{c}\right)^2}} \\ \sqrt{k^2 - (r/c)^2} \\ 1 \end{bmatrix} e^{(\sqrt{k^2-(r/c)^2})\eta}, \tag{C.24}$$

introducing the following shorthands $\alpha = \sqrt{k^2 - r^2}$ and $\beta = \sqrt{k^2 - (r/c)^2}$:

$$\boldsymbol{X} = \begin{bmatrix} \mathcal{U} \\ U + \sqrt{\frac{2}{\pi}} \frac{i}{c^2 k \beta^2} \\ \mathcal{V} \\ V \end{bmatrix} = A \begin{bmatrix} i\frac{\alpha^2}{k} \\ -i\frac{\alpha}{k} \\ -\alpha \\ 1 \end{bmatrix} e^{-\alpha\eta} + B \begin{bmatrix} i\frac{\alpha^2}{k} \\ i\frac{\alpha}{k} \\ \alpha \\ 1 \end{bmatrix} e^{\alpha\eta} + \\ + C \begin{bmatrix} ik \\ -i\frac{k}{\beta} \\ -\beta \\ 1 \end{bmatrix} e^{-\beta\eta} + D \begin{bmatrix} ik \\ i\frac{k}{\beta} \\ \beta \\ 1 \end{bmatrix} e^{\beta\eta}, \tag{C.25}$$

where A, B, C, and D are constants (which nevertheless depend on the parameter k) to be determined from the boundary conditions, which, yet again, we move to consider, starting from the easiest ones, $V(0) = 0$ and $U(0) = 0$:

$$V(0) = A + B + C + D = 0, \tag{C.26}$$

$$U(0) = \frac{i\alpha}{k}(B - A) + \frac{ik}{\beta}(D - C) - \sqrt{\frac{2}{\pi}} \frac{i}{c^2 k \beta^2} = 0, \tag{C.27}$$

followed by the most convoluted conditions at $\eta = 1$, $\tau_{xy} = 0$:

$$\mathcal{U}(1) + ikV(1) = 0 \rightarrow \frac{i\alpha^2}{k}(Ae^{-\alpha} + Be^{\alpha}) + ik(Ce^{-\beta} + De^{\beta}) + \\ ik(Ae^{-\alpha} + Be^{\alpha}) + ik(Ce^{-\beta} + De^{\beta}) = 0, \tag{C.28a}$$

$$\left(k + \frac{\alpha^2}{k}\right)(Ae^{-\alpha} + Be^{\alpha}) + 2k(Ce^{-\beta} + De^{\beta}) = 0. \tag{C.28b}$$

And $\sigma_{yy} = 0$ (note that we are summing and subtracting some terms to have entries of $\boldsymbol{X}$ appearing):

$$c^2\mathcal{V}(1) + ik(c^2 - 2)\left(U(1) \pm \sqrt{\frac{2}{\pi}} \frac{i}{c^2 k \beta^2}\right) = 0, \tag{C.29a}$$

$$c^2\mathcal{V}(1) + ik(c^2 - 2)\left(U(1) + \sqrt{\frac{2}{\pi}} \frac{i}{c^2 k \beta^2}\right) = -\sqrt{\frac{2}{\pi}} \frac{(c^2 - 2)}{c^2 \beta^2} = \\ = c^2\alpha(Be^{\alpha} - Ae^{-\alpha}) + c^2\beta(De^{\beta} - Ce^{-\beta}) \\ - (c^2 - 2)\alpha(Be^{\alpha} - Ae^{-\alpha}) - (c^2 - 2)\frac{k^2}{\beta}(De^{\beta} - Ce^{-\beta}) = \\ = 2\alpha(Be^{\alpha} - Ae^{-\alpha}) + \left(\frac{c^2(\beta^2 - k^2) + 2k^2}{\beta}\right)(De^{\beta} - Ce^{-\beta}). \tag{C.29b}$$

Recast these conditions in matrix form:

$$\begin{bmatrix} 1 & 1 & 1 & 1 \\ -\frac{i\alpha}{k} & \frac{i\alpha}{k} & -\frac{ik}{\beta} & \frac{ik}{\beta} \\ \left(k+\frac{\alpha^2}{k}\right)e^{-\alpha} & \left(k+\frac{\alpha^2}{k}\right)e^{\alpha} & 2ke^{-\beta} & 2ke^{\beta} \\ -2\alpha e^{-\alpha} & 2\alpha e^{\alpha} & -\left(\frac{c^2(\beta^2-k^2)+2k^2}{\beta}\right)e^{-\beta} & \left(\frac{c^2(\beta^2-k^2)+2k^2}{\beta}\right)e^{\beta} \end{bmatrix} \begin{bmatrix} A \\ B \\ C \\ D \end{bmatrix}$$

$$= \begin{bmatrix} 0 \\ \sqrt{\frac{2}{\pi}}\frac{i}{c^2k\beta^2} \\ 0 \\ -\sqrt{\frac{2}{\pi}}\frac{(c^2-2)}{c^2\beta^2} \end{bmatrix}. \tag{C.30}$$

The value of the constants is found after solving (inverting) this linear system. The actual expressions are computed by recourse to Mathematica. The expressions are frankly overwhelmingly convoluted, and so long that cannot fit in one lanscape page. At the end of the document I include the expression of A, as much as it fits!

Once these coefficients have been computed, the solution in frequency-wavenumber domain has been finally attained. One can then move to calculate, for instance, the vertical displacement at the top of the wall, $\tilde{v}(\eta = 1) = \tilde{v}_{top}$, by inverting the transform:

$$\tilde{v}_{top} = \tilde{v}(\eta = 1, \xi = 0) = F^{-1}[V]_{\eta=1,\xi=0} = \frac{1}{\sqrt{2\pi}} \int_{-\infty}^{+\infty} \left[V e^{-ik\xi} \right]_{\eta=1,\xi=0} dk \tag{C.31}$$

recall $V = Ae^{-\alpha\eta} + Be^{\alpha\eta} + Ce^{-\beta\eta} + De^{\beta\eta}$:

$$= \frac{1}{\sqrt{2\pi}} \int_{-\infty}^{+\infty} \left[Ae^{-\alpha} + Be^{\alpha} + Ce^{-\beta} + De^{\beta} \right] dk \,. \tag{C.32}$$

Inverting this integral analytically seems to me virtually impossible: as there is no direct inversion, owing to the utmost complexity of the coefficients, one would have to resort to solving the interval by closing the contour over the imaginary axis and using residue calculus (Cauchy theorem of complex analysis); this would require dining the zeros of the denominator of the coefficients, which is also no less of a phenomenal task.

At least, one can try to approximate the integral numerically, as the coefficients are already in *Mathematica* [Wol00]. In order to approximate this integral numerically the integration has to be stopped at some point; the logical limit is $k = 10$, following the reasoning in section 4.3.3, which indicated that that the shortest wavelengths

present in the problem must be $\lambda \sim H$, and thus the highest dimensionless wavenumber must be $k \sim 1$, and thus ranging up to $k = 10$ must be enough as to include all of them.

Next, v_{top} is one of the pieces we need to calculate the thrust, by using dimensionless quantities one can write

$$\frac{Q}{\rho \ddot{X}_g H^2} = c^2 \int_0^1 \frac{\partial \tilde{u}}{\partial \xi}\Big|_w d\eta + (c^2 - 2)\tilde{v}_{top}\,, \tag{C.33}$$

so the second addend is ready and we shall focus now on the first one. First, see that

$$\tilde{u} = F^{-1}[U] = \frac{1}{\sqrt{2\pi}} \int_{-\infty}^{+\infty} U e^{-ik\xi} dk\,, \tag{C.34a}$$

thus

$$\frac{\partial \tilde{u}}{\partial \xi} = \frac{1}{\sqrt{2\pi}} \int_{-\infty}^{+\infty} ikU e^{-ik\xi} dk \rightarrow \tag{C.34b}$$

$$\frac{\partial \tilde{u}}{\partial \xi}\Big|_w = \frac{\partial \tilde{u}}{\partial \xi}\Big|_{\xi=0} = \frac{1}{\sqrt{2\pi}} \int_{-\infty}^{+\infty} ikU dk\,, \tag{C.34c}$$

where $U = -\sqrt{\frac{2}{\pi}} \frac{i}{c^2 k \beta^2} - \frac{i\alpha}{k}\left(Ae^{-\alpha\eta} - Be^{\alpha\eta}\right) - \frac{ik}{\beta}\left(Ce^{-\beta\eta} - De^{\beta\eta}\right)$

$$\int_0^1 \frac{\partial \tilde{u}}{\partial \xi}\Big|_w d\eta = \frac{1}{\sqrt{2\pi}} \int_{-\infty}^{+\infty} ik \left(\int_0^1 U d\eta \right) d\eta\,, \tag{C.34d}$$

then $\int_0^1 U d\eta = -\sqrt{\frac{2}{\pi}} \frac{i}{c^2 k \beta^2} + \frac{i}{k}\left[A(e^{-\alpha} - 1) + B(e^{\alpha} - 1)\right] + \frac{ik}{\beta^2}\left[C(e^{-\beta} - 1) + D(e^{\beta} - 1)\right]$, and hence

$$\int_0^1 \frac{\partial \tilde{u}}{\partial \xi}\Big|_w d\eta = \frac{1}{\sqrt{2\pi}} \int_{-\infty}^{+\infty} ik \Big(- \sqrt{\frac{2}{\pi}} \frac{i}{c^2 k \beta^2} + \frac{i}{k}\left[A(e^{-\alpha} - 1) + B(e^{\alpha} - 1)\right] + \frac{ik}{\beta^2}\left[C(e^{-\beta} - 1) + D(e^{\beta} - 1)\right] \Big) d\eta = \tag{C.35a}$$

$$= \frac{1}{\sqrt{2\pi}} \int_{-\infty}^{+\infty} \Big(\sqrt{\frac{2}{\pi}} \frac{1}{c^2 \beta^2} - \left[A(e^{-\alpha} - 1) - B(e^{\alpha} - 1)\right] - \left(\frac{k}{\beta}\right)^2 \left[C(e^{-\beta} - 1) + D(e^{\beta} - 1)\right] \Big) d\eta\,. \tag{C.35b}$$

Once both addends are ready, the final expression for the thrust can be obtained:

$$\frac{Q}{\rho \ddot{X}_g H^2} = \frac{1}{\sqrt{2\pi}} \int_{-\infty}^{+\infty} \left\{ \frac{\sqrt{2/\pi}}{\beta^2} + c^2(A + B) - 2(Ae^{-\alpha} + Be^{\alpha}) + \right.$$
$$\left. + \left[c^2 \left(1 - \left(\frac{k}{\beta}\right)^2 \right) - 2 \right] \left(Ce^{-\beta} + De^{\beta} \right) + \left(\frac{ck}{\beta}\right)^2 (C + D) \right\} dk\,. \tag{C.36}$$

C.3.1 Asymptotics

One can acknowledge that the wavenumber content is very localized around $k = 0$, adopting a gaussian-like shape. This suggests approximating the integral through Laplace's Method [BO13]. Let us illustrate this with v_{top}:

$$\begin{aligned}\tilde{v}_{top} &= \frac{1}{\sqrt{2\pi}}\int_{-\infty}^{+\infty} V_{top}dk = \frac{1}{\sqrt{2\pi}}\int_{-\infty}^{+\infty} \exp(\ln V_{top})dk \\ &\approx \frac{1}{\sqrt{2\pi}}\left(\sqrt{\frac{2\pi}{\left|\frac{\partial^2}{\partial k^2}(\ln V_{top})\right|_{k=0}}}\exp(\ln V_{top}|_{k=0})\right) \\ &= \sqrt{\frac{1}{\left|\frac{V''_{top}|_{k=0}}{V_{top}|_{k=0}}\right|}}V_{top}|_{k=0} = \sqrt{\left|\frac{V_{top}|_{k=0}}{V''_{top}|_{k=0}}\right|}V_{top}|_{k=0}\,.\end{aligned} \tag{C.37}$$

After evaluating this expression symbolycally on *Mathematica*, we acknowledge that it does not yield a clearer result than the original coefficients.

However, but we can still include one extra approximation: long-wavelength/quasi-static behavior. The alternative approach is taking the long-wavelength approximation before applying Laplace's Method (switching the order does not yield the same result). In this case, take $r \to 0$ and proceed to evaluate the approximation:

$$V_{top}|_{r=0} = \frac{5-2c^2}{3\sqrt{2\pi}c^2} + \frac{70-89c^2+24c^4}{20\sqrt{2\pi}c^4}k^2 + O(k^4) \tag{C.38}$$

thus

$$\tilde{v}^{qs}_{top} \approx \sqrt{\left|\frac{V_{top}|_{r=0,k=0}}{V''_{top}|_{r=0,k=0}}\right|}V_{top}|_{r=0,k=0} = \frac{5-2c^2}{3\sqrt{2\pi}c^2}\sqrt{\frac{10}{3}\left|\frac{c^2(5-2c^2)}{70-89c^2+24c^4}\right|}\,. \tag{C.39}$$

To verify this result, let us compare eq. (C.39) to eq. (4.15) and to eq. (D.26).

The method approach seem reasonable inasmuch v_{top} is concerned. Nevertheless, it does not provide a better result than the simplified model we have presented in the chapter 5.

C.4 The LADWP problems

Dr. C.A. Davis (LADWP) mentioned, in direct communication to the author, that a similar problem had been tackled by a student of Prof. Vincent Lee (USC). Even though we could not find a reference on such work, it is deemed an interesting problem in and of itself, and moreover, it can be easily solved by using results

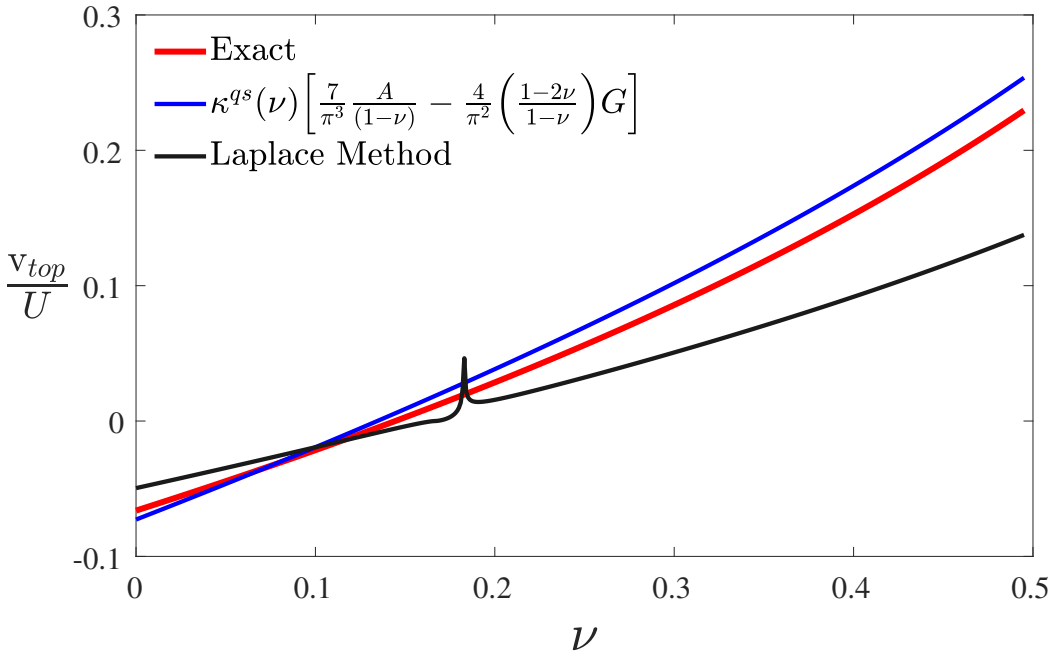

Figure C.5: Comparison for the quasi-static vertical displacement: exact, model and asymptotitc of exact solution

already derived for the exact solution and it may help visualizing some features of the response as the expressions of the coefficients are much simpler.

This can be considered as a special case of the Younan-Veletsos problem, in which $H \to \infty$, and therefore the wall does not see the base, just the free surface.

This case must be carefully interpreted: it does not represent the exact solution in the new scenario (the absence of the base requires abandoning any notion of relative displacement) but the steady state of the new problem corresponding to a harmonic excitation, but it does not represent an intermediate asymptotics scenario. In order to render it more coherent, we may remove the force altogether and simply perform an analysis of the types of waves that can be sustained is this configuration.
This problem simplifies the original one in such a way that makes dealing with the coefficients easier and permits straightforward physical interpretation that was refused in the first case. See that we are re-defining the vertical coordinate ($\eta \to 1-\eta$) to work in a more convenient frame. The extra constants can be absorbed in the constants A, B, C, and D.

Recall that Eq.(C.24) represents the most general solution of the steady-state wave propagation in the medium, provided there is a wall. Different instantiations of BCs would require just adapting the coefficients accordingly.

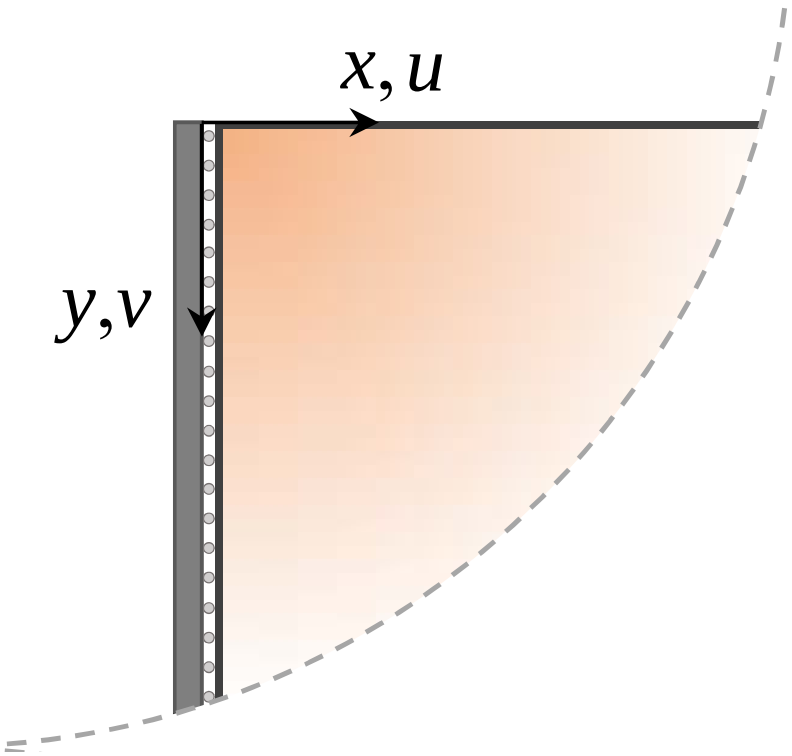

Figure C.6: Scheme of LADWP reduced problem I

Let us remove the body force:

$$\boldsymbol{X} = \begin{bmatrix} \mathcal{U} \\ U \\ \mathcal{V} \\ V \end{bmatrix} = A \begin{bmatrix} i\frac{\alpha^2}{k} \\ -i\frac{\alpha}{k} \\ -\alpha \\ 1 \end{bmatrix} e^{-\alpha\eta} + B \begin{bmatrix} i\frac{\alpha^2}{k} \\ i\frac{\alpha}{k} \\ \alpha \\ 1 \end{bmatrix} e^{\alpha\eta} + C \begin{bmatrix} ik \\ -i\frac{k}{\beta} \\ -\beta \\ 1 \end{bmatrix} e^{-\beta\eta} + D \begin{bmatrix} ik \\ i\frac{k}{\beta} \\ \beta \\ 1 \end{bmatrix} e^{\beta\eta} . \quad \text{(C.40)}$$

Next, we argue $B = D = 0$ since the surface waves at $\eta = 0$ must decay as we traverse the domain downward. Hence

$$\boldsymbol{X} = \begin{bmatrix} \mathcal{U} \\ U \\ \mathcal{V} \\ V \end{bmatrix} = A \begin{bmatrix} i\frac{\alpha^2}{k} \\ -i\frac{\alpha}{k} \\ -\alpha \\ 1 \end{bmatrix} e^{-\alpha\eta} + C \begin{bmatrix} ik \\ -i\frac{k}{\beta} \\ -\beta \\ 1 \end{bmatrix} e^{-\beta\eta} , \quad \text{(C.41)}$$

this automatically enforces ration boundary conditions. Finally, stress-free boundary conditions the top ($\eta = 0$) must be enforced. Thus, the linear system yielding the coefficients, (C.30), simplifies dramatically:

$$\begin{bmatrix} \left(k + \frac{\alpha^2}{k}\right) & 2k \\ 2\alpha & \left(\frac{c^2(\beta^2 - k^2) + 2k^2}{\beta}\right) \end{bmatrix} \begin{bmatrix} A \\ C \end{bmatrix} = \begin{bmatrix} 0 \\ \sqrt{\frac{2}{\pi}} \frac{(c^2-2)}{c^2\beta^2} \end{bmatrix} . \quad \text{(C.42)}$$

Hence the constants would be

$$A = -\frac{2\sqrt{\frac{2}{\pi}}(c^2-2)k^2}{c^2\beta\left\{(k^2+\alpha^2)^2-4k^2\alpha\beta\right\}} \tag{C.43a}$$

$$C = -\frac{(k^2+\alpha^2)}{2k^2}A \tag{C.43b}$$

the displacement solution would be

$$V = -\frac{\sqrt{\frac{2}{\pi}}(c^2-2)\left(2k^2e^{-\alpha\eta}-(k^2+\alpha^2)e^{-\beta\eta}\right)}{c^2\beta\left\{(k^2+\alpha^2)^2-4k^2\alpha\beta\right\}}, \tag{C.44a}$$

$$U = -\sqrt{\frac{2}{\pi}}\frac{i}{c^2k\beta^2} + \frac{i\sqrt{\frac{2}{\pi}}(c^2-2)k\left(\alpha\beta e^{-\alpha\eta}-(k^2+\alpha^2)e^{-\beta\eta}\right)}{c^2\beta^2\left\{(k^2+\alpha^2)^2-4k^2\alpha\beta\right\}}. \tag{C.44b}$$

If we were to invert these Fourier Transforms we would find that there is a component of P-waves and another one from R-waves, since the poles given by the equation

$$(k^2+\alpha^2)^2-4k^2\alpha\beta = 0, \tag{C.45}$$

corresponding to the S-wave velovity and the amplitude decays exponentially with depth. There is no response in terms of S-waves.

The complementary problem considers the lower corner of the soil-wall system. Incidentally, this configuration does have a physical meaning: it can be considered as an intermediate steady-state in which transient effects at the base have vanished, leaving only the effects of the forced vibration, and the information from the wave reflection at the free-surface has not reached this region yet.

The original frame of reference conveniently stays the same in this case. Again, the first argument is alike in the foregoing scenario: $B = D = 0$ as waves cannot grow exponentially into the bulk of the domain. In this case, the boundary conditions that we have to enforce correspond to the rigid base, and thus $V(0) = U(0) = 0$, which amounts to solving

$$\begin{bmatrix} 1 & 1 \\ -i\frac{\alpha}{k} & -i\frac{k}{\beta} \end{bmatrix}\begin{bmatrix} A \\ C \end{bmatrix} = \begin{bmatrix} 0 \\ 0 \end{bmatrix}. \tag{C.46}$$

In such a case the determinant yields

$$-\frac{k}{\beta}+\frac{\alpha}{k} = 0 \rightarrow k^2 = \alpha\beta. \tag{C.47}$$

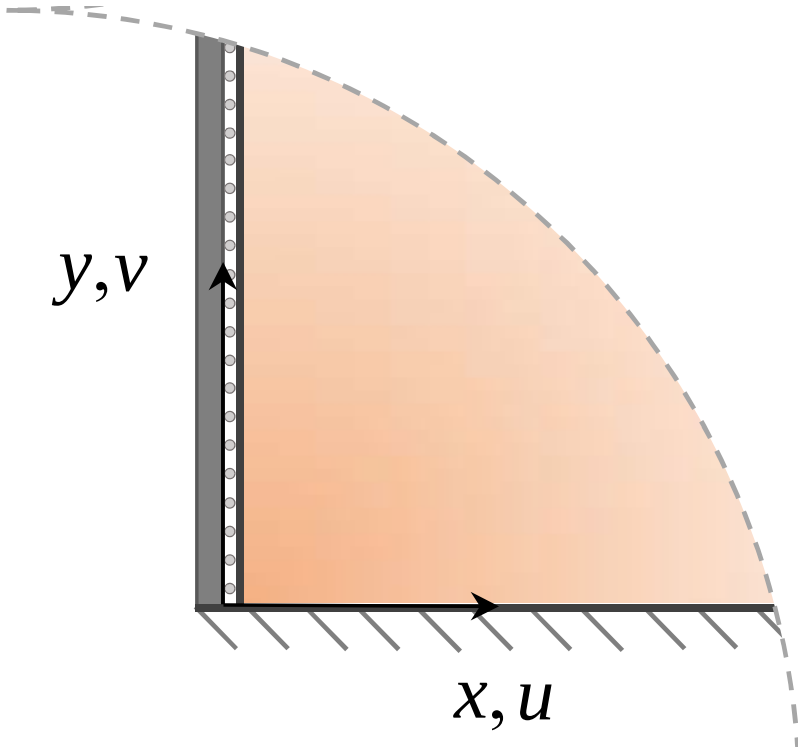

Figure C.7: Scheme of LADWP reduced problem II

Let us explore this condition

$$k^4 = (\alpha\beta)^2 = (k^2 - r^2)(k^2 - (r/c)^2) = k^4 - k^2(r^2 + (r/c)^2) + r^4/c^2\,, \tag{C.48}$$

which yields

$$r/k = \pm\sqrt{1 + c^2}\,. \tag{C.49}$$

Undoing the non-dimensionalziation, recall $r = \omega H/c_s$ and $k = \mathrm{k}H$,

$$\frac{\varpi}{\mathrm{k}c_s} = \sqrt{1 + c^2}\,, \tag{C.50}$$

then

$$\frac{\varpi}{\mathrm{k}} = \sqrt{c_s^2 + c_p^2}\,. \tag{C.51}$$

Should we solve the system considering the loading

$$\begin{bmatrix} 1 & 1 \\ -i\frac{\alpha}{k} & -i\frac{k}{\beta} \end{bmatrix} \begin{bmatrix} A \\ C \end{bmatrix} = \begin{bmatrix} 0 \\ \sqrt{\frac{2}{\pi}}\frac{i}{c^2 k\beta^2} \end{bmatrix}, \tag{C.52}$$

hence the values of the constants in this case are

$$C = -A = \frac{\sqrt{2/\pi}}{c^2 k\beta^2 \left(\frac{\alpha}{k} - \frac{k}{\beta}\right)}, \tag{C.53}$$

hence

$$V = \sqrt{\frac{2}{\pi}} \frac{\left(e^{-\beta\eta} - e^{-\alpha\eta}\right)}{c^2 k\beta^2 \left(\frac{\alpha}{k} - \frac{k}{\beta}\right)}, \tag{C.54}$$

$$U + \sqrt{\frac{2}{\pi}} \frac{i}{c^2 k\beta^2} = \sqrt{\frac{2}{\pi}} \frac{i}{c^2 k\beta^2 \left(\frac{\alpha}{k} - \frac{k}{\beta}\right)} \left(\frac{\alpha}{k} e^{-\alpha\eta} - \frac{k}{\beta} e^{-\beta\eta}\right). \tag{C.55}$$

Appendix D

DERIVATIONS FOR CHAPTER V

D.1 Derivation of simplified model

The preceding eq. (5.2) and eq. (4.32b) are the simplified equations for the non-dimensional displacement field, the first one for the horizontal displacement all along the domain and the second for the vertical displacement at the wall.

D.1.1 Quasi-static regime

Focus first on the case $\varpi/\omega_s \ll 1$ (low frequency) or, equivalently, $H/\lambda_s \ll 1$ (long-wavelength).

D.1.1.1 Horizontal displacement

Under the assumption of quasi-static loading, the aforementioned equations can be simplified taking $r^2 \to 0$ and τ can be taken as a parameter. For the sake of conciseness, the factor $e^{i\varpi\tau}$ will be substituted by 1, just to lighten the equations, yet please bear in mind that all the results and parameters, in reality, come multiplied by this exponential.

$$\frac{1}{\kappa^2}\frac{\partial^2\tilde{u}}{\partial\xi^2} + \frac{\partial^2\tilde{u}}{\partial\eta^2} = 1\,, \tag{D.1a}$$

$$c^2\frac{\partial^2\tilde{v}_w}{\partial\eta^2} = -(c^2-1)\frac{\partial^2\tilde{u}}{\partial\xi\partial\eta}\Big|_w\,. \tag{D.1b}$$

Let us begin by applying Fourier sine transform along x-direction:

$$-\frac{k^2}{\kappa^2}\mathcal{U} + \frac{d^2\mathcal{U}}{d\eta^2} = \sqrt{\frac{2}{\pi}}\frac{1}{k}\,, \tag{D.2}$$

where

$$\mathcal{U}(k,\eta) = \int_0^\infty \tilde{u}(\xi,\eta)\sin(k\xi)d\xi = \mathcal{F}_s[\tilde{u}(\xi,\eta)](k,\eta)\,. \tag{D.3}$$

Note that the transform is properly defined, even though apparently the resulting function is not integrable in the interval $[0,\infty)$, the earlier result can be obtained by means of an integrating factor $e^{-a\xi}$, taking the limit $a \to 0$ once the transform has been found.

Different approaches are plausible to deal with the variations in the vertical direction. Evidently, the use of the eigenfunctions corresponding to the far-field would preclude meeting the boundary condition $\tau_{xy}|_{top} = 0 \rightarrow \partial\tilde{v}/\partial\xi|_{top} = -\partial\tilde{u}/\partial\eta|_{top}$ since it would force $\partial v/\partial x|_{top} = 0$ all along the domain. Despite this, recall that only the vertical displacement *on the wall* is necessary to find the thrust, and on the rigid wall, certainly $\partial\tilde{u}/\partial\eta|_w = 0$, in particular, at the top; therefore, let us ignore the problems with using the $sin(k_n\eta)$ expansion and proceed keeping in mind that this issue is ancillary for the purpose of calculating the thrust. Thus:

$$\mathcal{U} = \sum_{n=1}^{\infty} \mathcal{U}_n(k) \sin\left((2n-1)\frac{\pi}{2}\eta\right) = \sum_{n=1}^{\infty} \mathcal{U}_n(k) \sin(k_n\eta)\,, \tag{D.4a}$$

$$1 \sim \sum_{n=1}^{\infty} \frac{2}{k_n} \sin(k_n\eta)\,. \tag{D.4b}$$

Note that the second series suffers from Gibbs pathology [Wei12], therefore it does not converge uniformly and the equality sign should not be used, instead *similar to* ($\sim$) is being used in its place. This behavior does not come as a surprise since a sine series is being used to expand an even function and, not to mention that a sine expansion is being used to attain a value $\neq 0$ at $\eta = 0$.

The appearance of Gibbs' phenomenon does not compromise the final results as the series is going to be integrated, what makes the issue vanish. A graphic demonstration of the phenomenon is displayed in the next figure.

Using Eqs.(D.4) in eq. (D.2)):

$$-\left(\frac{k^2}{\kappa^2} + k_n^2\right)\mathcal{U}_n = \sqrt{\frac{2}{\pi}}\frac{2}{k k_n} \rightarrow \mathcal{U}_n = -\sqrt{\frac{2}{\pi}}\frac{2}{k k_n(\frac{k^2}{\kappa^2} + k_n^2)}\,, \tag{D.5}$$

inverting the sine transform:

$$\tilde{u}_n(\xi) = -\frac{2}{k_n^3}(1 - e^{-\kappa k_n \xi}) \rightarrow \tilde{u} = -\sum_{n=1}^{\infty} \frac{2}{k_n^3}(1 - e^{-\kappa k_n \xi}) \sin(k_n\eta)\,. \tag{D.6}$$

If $\kappa = 1/c$, the model would deliver null displacement in the incompressible limit, a truly unphysical result. That is what would have happened if eq. (5.1) had been used in lieu of eq. (5.2), which was modified by virtue of introducing the compressibility factor κ to replace c.

Once the horizontal displacement has been estimated, proceed to find the vertical

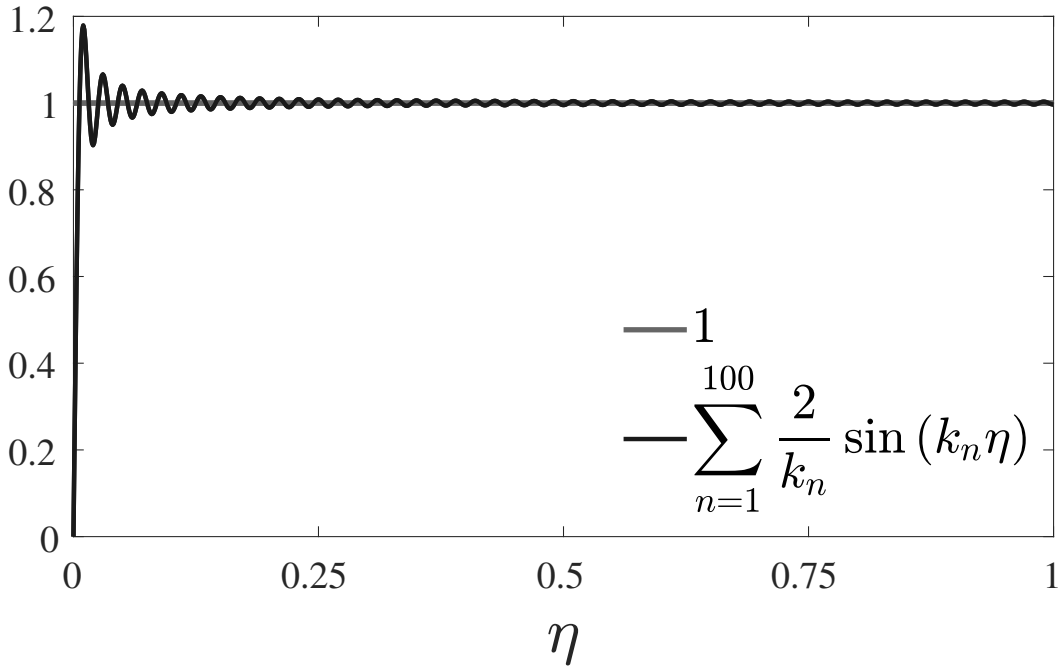

Figure D.1: Gibbs phenomenon observed when using $\sin(k_n\eta)$ to expand 1 in the interval $\eta \in [0, 1]$

displacement. Begin by computing the "forcing" term:

$$\begin{aligned}\frac{\partial^2 \tilde{u}}{\partial\xi\partial\eta}\Big|_w &= -\sum_{n=1}^{\infty} \frac{\partial^2}{\partial\xi\partial\eta}\Big[\frac{2}{k_n^3}(1 - e^{-\kappa k_n \xi})\sin(k_n\eta)\Big]_{\xi=0} \\ &= -\sum_{n=1}^{\infty} \frac{\partial^2}{\partial\xi\partial\eta}\Big[\frac{2}{k_n^3}(\kappa k_n \xi)\sin(k_n\eta)\Big]_{\xi=0}\end{aligned}$$

note that $(\kappa k_n \xi) \sim \sinh(\kappa k_n \xi)$ as $\xi \to 0$, and thus, as the limit is implicitly being taken, one can swap them

$$\begin{aligned}&= -\sum_{n=1}^{\infty} \frac{\partial^2}{\partial\xi\partial\eta}\Big[\frac{2}{k_n^3}\sinh(\kappa k_n \xi)\sin(k_n\eta)\Big]_{\xi=0} \\ &= -\sum_{n=1}^{\infty} \frac{\partial}{\partial\eta}\Big[\frac{2}{k_n^2}\cosh(\kappa k_n \xi)\sin(k_n\eta)\Big]_{\xi=0} \\ &= -2\kappa \sum_{n=1}^{\infty} \frac{\cos(k_n\eta)}{k_n}\,. \end{aligned} \tag{D.7}$$

This result does hint that $\tilde{v}$ can be understood to behave locally as $\cosh(\kappa k_n \xi)$ very close to the wall, and this would comply with the previous equation and the restrictions in eq. (5.3) imposed by the frictionless-rigid wall.

It is both relevant and interesting to realize that the previous sum can be expressed in closed form as a certain function (recall $k_n = (2n-1)\pi/2$):

$$\begin{aligned}
\sum_{n=1}^{\infty} \frac{\cos(k_n\eta)}{k_n} &= \frac{1}{2}\Big[\sum_{n=1}^{\infty} \frac{e^{ik_n\eta}}{k_n} + \sum_{n=1}^{\infty} \frac{e^{-ik_n\eta}}{k_n}\Big] \\
&= \frac{1}{\pi}\Big[\sum_{n=1}^{\infty} \frac{(e^{i\frac{\pi}{2}\eta})^{2n-1}}{2n-1} + \sum_{n=1}^{\infty} \frac{(e^{-i\frac{\pi}{2}\eta})^{2n-1}}{2n-1}\Big] \\
&= \frac{1}{\pi}\Big[\operatorname{arctanh}(e^{i\frac{\pi}{2}\eta}) + \operatorname{arctanh}(e^{-i\frac{\pi}{2}\eta})\Big] \\
&= \frac{1}{2\pi}\Big[\log\Big(\frac{1+e^{i\frac{\pi}{2}\eta}}{1-e^{i\frac{\pi}{2}\eta}}\Big) + \log\Big(\frac{1+e^{-i\frac{\pi}{2}\eta}}{1-e^{-i\frac{\pi}{2}\eta}}\Big)\Big] \\
&= \frac{1}{2\pi}\Big[\log\Big(\frac{(1+e^{i\frac{\pi}{2}\eta})(1+e^{-i\frac{\pi}{2}\eta})}{(1-e^{i\frac{\pi}{2}\eta})(1-e^{-i\frac{\pi}{2}\eta})}\Big)\Big] \\
&= \frac{1}{2\pi}\Big[\log\Bigg(\frac{(\frac{e^{i\frac{\pi}{4}\eta}+e^{-i\frac{\pi}{4}\eta}}{2})^2}{(\frac{e^{i\frac{\pi}{4}\eta}-e^{-i\frac{\pi}{4}\eta}}{2i})^2}\Bigg)\Big] \\
&= \frac{1}{\pi}\Big[\log\Big(\frac{1}{\tan(\frac{\pi}{4}\eta)}\Big)\Big] = -\frac{1}{\pi}\log\Big(\tan\Big(\frac{\pi}{4}\eta\Big)\Big) = g(\eta)\,. \qquad \text{(D.8)}
\end{aligned}$$

So the infinite sum converges to a specific function in $\eta \in [0,1]$, yet the function $g(\eta)$ itself diverges at $\eta \to 0$. The integral of its absolute value and the integral of itself squared are both finite, hence both $g(\eta) \in L^1([0,1])$ and $g(\eta) \in L^2([0,1])$.

Therefore, since $g(\eta) \in L^1([0,1])$, then $g_1(\eta) = \int_0^\eta f(\eta')d\eta' \in L^2([0,1])$ and $g_2(\eta) = \int_0^\eta g_1(\eta')d\eta' \in L^2([0,1])$ as well, by virtue of the Cauchy-Schwartz inequality. Thus, by integration over the sums:

$$\begin{aligned}
g_1(\eta) = \int_0^\eta g(\eta')d\eta' &= \int_0^\eta \sum_{n=1}^{\infty} \frac{\cos(k_n\eta')}{k_n} d\eta' = \\
&= \sum_{n=1}^{\infty} \frac{1}{k_n}\int_0^\eta \cos(k_n\eta')d\eta' = \sum_{n=1}^{\infty} \frac{\sin(k_n\eta)}{k_n^2} \qquad \text{(D.9a)} \\
g_2(\eta) = \int_0^\eta g_1(\eta')d\eta' &= \int_0^\eta \sum_{n=1}^{\infty} \frac{\sin(k_n\eta')}{k_n^2} d\eta' = \\
&= \sum_{n=1}^{\infty} \frac{1}{k_n^2}\int_0^\eta \sin(k_n\eta')d\eta' = \sum_{n=1}^{\infty} \frac{(1-\cos(k_n\eta))}{k_n^3}\,. \qquad \text{(D.9b)}
\end{aligned}$$

Furthermore, an approximation of $g(\eta)$ can be found by taking just the first two

terms of its series expansion around $\eta = 0$:

$$g(\eta) = -\frac{1}{\pi}\log\left(\tan\left(\frac{\pi}{4}\eta\right)\right) = -\left(\frac{\log(\frac{\pi}{4}\eta)}{\pi} + \frac{\pi}{48}\eta^2 + \frac{7\pi^3}{23040}\eta^4\right) + O(\eta^6)$$
$$= -\left(\frac{\log(\frac{\pi}{4}\eta)}{\pi} + \frac{\pi}{48}\eta^2\right) + O\left(\eta^4\right). \tag{D.10}$$

Then

$$g_1(\eta) = \sum_{n=1}^{\infty}\frac{\sin(k_n\eta)}{k_n^2} = \int_0^\eta g(\eta')d\eta' \approx \int_0^\eta -\left(\frac{\log(\frac{\pi}{4}\eta')}{\pi} + \frac{\pi}{48}\eta'^2\right)d\eta'$$
$$= \frac{[1-\log(\frac{\pi}{4}\eta)]\eta}{\pi} - \frac{\pi}{144}\eta^3, \tag{D.11a}$$
$$g_2(\eta) = \sum_{n=1}^{\infty}\frac{(1-\cos(k_n\eta))}{k_n^3} = \int_0^\eta g_1(\eta')d\eta'$$
$$\approx \int_0^\eta \left(\frac{[1-\log(\frac{\pi}{4}\eta')]\eta'}{\pi} - \frac{\pi'}{144}\eta'^3\right)d\eta'$$
$$= \frac{[3-2\log(\frac{\pi}{4}\eta)]\eta^2}{4\pi} - \frac{\pi}{576}\eta^4. \tag{D.11b}$$

D.1.1.2 Vertical displacement

Next, assume that

$$\tilde{v}_w(\eta) = \sum_{n=1}^{\infty}\tilde{v}_n\cosh(\kappa k_n\xi), \tag{D.12}$$

and also that the n-th addend is to balance the n-th term of the forcing

$$c^2\frac{\partial^2\tilde{v}_n}{\partial\eta^2} + \kappa^2 k_n^2\tilde{v}_n = -(c^2-1)\frac{\partial^2\tilde{u}_n}{\partial\xi\partial\eta}\Big|_w = 2\kappa(c^2-1)\frac{\cos(k_n\eta)}{k_n}. \tag{D.13}$$

The homogeneous solution is

$$\tilde{v}_w|_{hom}(\eta) = A_n\sin\left(\frac{\kappa}{c}k_n\eta\right) + B_n\cos\left(\frac{\kappa}{c}k_n\eta\right), \tag{D.14}$$

where A_n and B_n can be found by implementing the boundary conditions. The particular solution is of the form $\tilde{v}_w|_{par}(\eta) = C_n\cos(k_n\eta)$; clearly

$$C_n = -\frac{2\kappa(c^2-1)}{k_n^3(c^2-\kappa^2)}, \tag{D.15}$$

therefore

$$\tilde{v}_n(\eta) = -\frac{2\kappa(c^2-1)}{k_n^3(c^2-\kappa^2)}\cos(k_n\eta) + A_n\sin\left(\frac{\kappa}{c}k_n\eta\right) + B_n\cos\left(\frac{\kappa}{c}k_n\eta\right). \tag{D.16}$$

A further simplification can be attempted before continuing: consider that the ratio κ/c is small, $\kappa/c \ll 1$, and thus the following approximations are on point:

$$\frac{1}{c^2-\kappa^2} = \frac{1}{c^2}\frac{1}{1-(\frac{\kappa}{c})^2} = \frac{1}{c^2}\left(1+\left(\frac{\kappa}{c}\right)^2+O\left[\left(\frac{\kappa}{c}\right)^4\right]\right), \tag{D.17a}$$

$$\sin\left(\frac{\kappa}{c}k_n\eta\right) = \left(\frac{\kappa}{c}k_n\eta\right) - \frac{1}{6}\left(\frac{\kappa}{c}k_n\eta\right)^3 + O\left[\left(\frac{\kappa}{c}\right)^5\right], \tag{D.17b}$$

$$\cos\left(\frac{\kappa}{c}k_n\eta\right) = 1 - \frac{1}{2}\left(\frac{\kappa}{c}k_n\eta\right)^2 + O\left[\left(\frac{\kappa}{c}\right)^4\right], \tag{D.17c}$$

thus

$$\begin{aligned}\tilde{v}_n(\eta) &= -\frac{2\kappa(c^2-1)}{c^2}\cos(k_n\eta) + A_n\left(\frac{\kappa}{c}k_n\eta\right) + B_n(1) + O\left[\left(\frac{\kappa}{c}\right)^2\right] \\ &\approx -\frac{2\kappa(c^2-1)}{c^2}\cos(k_n\eta) + c_1\eta + c_2\,,\end{aligned} \tag{D.18}$$

as long as $\kappa/c \ll 1$. Using the latter expression simplifies the procedure of attaining an expression for the earth thrust without compromising accuracy, as it will be shown. Notice that the approximation entails

$$c^2\left|\frac{\partial^2\tilde{v}}{\partial\eta^2}\right| \ll \left|\frac{\partial^2\tilde{v}}{\partial\xi^2}\right|, \tag{D.19}$$

so the contribution of $\partial^2 v/\partial\xi^2$ can be ignored in eq. (D.13). The validity of this assumption is further commented once the actual value of κ is derived, see fig. D.3.

Move to enforce boundary conditions in order to find the values of the constants. Start by $\tilde{v}_n(0) = 0$:

$$\tilde{v}_n(0) = -\frac{2\kappa(c^2-1)}{c^2}\frac{1}{k_n^3} + c_1\eta + c_2 = 0 \rightarrow c_2 = \frac{2\kappa(c^2-1)}{c^2}\frac{1}{k_n^3}, \tag{D.20}$$

hence,

$$\tilde{v}_n(\eta) = \frac{2\kappa(c^2-1)}{c^2}\frac{(1-\cos(k_n\eta))}{k_n^3} + c_1\eta\,, \tag{D.21}$$

followed by $\sigma_{yy}|_{y=H} = 0$, what translates into

$$\begin{aligned}
\frac{\partial \tilde{v}_n}{\partial \eta}\Big|_{\eta=1} &= \frac{\partial}{\partial \eta}\Big[\frac{2\kappa(c^2-1)}{c^2}\frac{(1-\cos(k_n\eta))}{k_n^3} + c_1\eta\Big]_{\eta=1} \\
&= \frac{2\kappa(c^2-1)}{c^2}\frac{(-1)^{n+1}}{k_n^2} + c_1 \\
&= -\Big(\frac{c^2-2}{c^2}\Big)\frac{\partial \tilde{u}}{\partial \xi}\Big|_{\eta=1} \\
&= -\Big(\frac{c^2-2}{c^2}\Big)\frac{\partial}{\partial \xi}\Big[-\frac{2}{k_n^3}(1-e^{-\kappa k_n \xi})\underbrace{\sin(k_n)}_{(-1)^{n+1}}\Big]_{\xi=0} \\
&= \Big(\frac{c^2-2}{c^2}\Big)\frac{2\kappa}{k_n^2}(-1)^{n+1} = 2\kappa\Big(\frac{c^2-2}{c^2}\Big)\frac{(-1)^{n+1}}{k_n^2}\,,
\end{aligned} \tag{D.22}$$

therefore

$$c_1 = 2\kappa\Big(\frac{c^2-2}{c^2}\Big)\frac{(-1)^{n+1}}{k_n^2} - 2\kappa\frac{(c^2-1)}{c^2}\frac{(-1)^{n+1}}{k_n^2} = -\frac{2\kappa}{c^2}\frac{(-1)^{n+1}}{k_n^2}\,. \tag{D.23}$$

In conclusion,

$$\tilde{v}_n(\eta) = \frac{2\kappa}{c^2 k_n^3}\Big[(c^2-1)(1-\cos(k_n\eta)) - (-1)^{n+1}k_n\eta\Big]\,, \tag{D.24a}$$

$$\tilde{v}_w(\eta) = \sum_{n=1}^{\infty}\tilde{v}_n(\eta) = \sum_{n=1}^{\infty}\frac{2\kappa}{c^2 k_n^3}\Big[(c^2-1)(1-\cos(k_n\eta)) - (-1)^{n+1}k_n\eta\Big]\,. \tag{D.24b}$$

A compact approximation for the vertical displacement at the wall can be found by using eqs. (D.8), (D.11a) and (D.11b). Look at the expression that was derived before

$$\tilde{v}_w(\eta) = \sum_{n=1}^{\infty}\frac{2\kappa}{c^2 k_n^3}\Big[(c^2-1)(1-\cos(k_n\eta)) - (-1)^{n+1}k_n\eta\Big]$$

apply eq. (D.11a) and eq. (D.11b),

$$\simeq \frac{2\kappa}{c^2}\left[(c^2-1)\left(\frac{[3-2\log(\frac{\pi}{4}\eta)]\eta^2}{4\pi} - \frac{\pi}{576}\eta^4\right) - \frac{4G}{\pi^2}\eta\right]\,. \tag{D.25}$$

For the purpose of calculating the thrust (it will be shown) only $\tilde{v}(1)$ is required:

$$\tilde{v}_n(1) = \frac{2\kappa}{c^2 k_n^3}\Big[(c^2-1) - (-1)^{n+1}k_n\Big]\,, \tag{D.26a}$$

recalling that $k_n = (2n-1)\pi/2$, sum over all the modal contributions

$$\begin{aligned}
\tilde{v}_w(1) &= \kappa\Big(\sum_{n=1}^{\infty}\frac{16(c^2-1)}{c^2\pi^3(2n-1)^3} - \sum_{n=1}^{\infty}\frac{8(-1)^{n+1}}{c^2\pi^2(2n-1)^2}\Big)\\
&= \kappa\Big(\frac{16(c^2-1)}{c^2\pi^3}\sum_{n=1}^{\infty}\frac{1}{(2n-1)^3} - \frac{8}{c^2\pi^2}\sum_{n=1}^{\infty}\frac{(-1)^{n+1}}{(2n-1)^2}\Big)\\
&= \kappa\Big(\frac{16(c^2-1)}{c^2\pi^3}\frac{7\zeta(3)}{8} - \frac{8}{c^2\pi^2}G\Big)\\
&= \kappa\Big(\frac{14(c^2-1)}{c^2\pi^3}\zeta(3) - \frac{8}{c^2\pi^2}G\Big)\\
&= \kappa\Big(\frac{7}{\pi^3(1-\nu)}\zeta(3) - \frac{4(1-2\nu)}{\pi^2(1-\nu)}G\Big)\,.
\end{aligned} \tag{D.26b}$$

D.1.2 Earth thrust, overturning moment at the base and eccentricity

All the necessary pieces to estimate the thrust are put in place. Let us first find an expression for the non-dimensional thrust:

$$\begin{aligned}
\frac{Q}{\rho\ddot{X}_g H^2} &= \frac{1}{\rho\ddot{X}_g H^2}\Big[(\lambda+2\mu)\int_0^H \frac{\partial u}{\partial x}\Big|_w dy + \lambda v|_w(H)\Big]\\
&= (\lambda+2\mu)\underbrace{\frac{U}{\rho\ddot{X}_g H^2}}_{1/\mu}\int_0^1 \frac{\partial\tilde{u}}{\partial\xi}\Big|_w d\eta + \lambda\underbrace{\frac{U}{\rho\ddot{X}_g H^2}}_{1/\mu}\tilde{v}_w(1)\\
&\qquad\underbrace{\qquad\qquad}_{c^2} \qquad\qquad\qquad \underbrace{\qquad}_{c^2-2}\\
&= c^2\int_0^1 \frac{\partial\tilde{u}}{\partial\xi}\Big|_w d\eta + (c^2-2)\tilde{v}_w(1)\,.
\end{aligned} \tag{D.27}$$

$\tilde{v}_w(1)$ has already been computed, eq. (D.26)b), then move to compute the other addend:

$$\begin{aligned}
\int_0^1 \frac{\partial\tilde{u}}{\partial\xi}\Big|_w d\eta &= \int_0^1 \Big[-\sum_{n=1}^{\infty}\frac{2\kappa}{k_n^2}\sin(k_n\eta)\Big]d\eta = \sum_{n=1}^{\infty}\frac{2\kappa}{k_n^3}\Big[\cos(k_n\eta)\Big]_0^1\\
&= -\sum_{n=1}^{\infty}\frac{2\kappa}{k_n^3} = -\frac{16\kappa}{\pi^3}\sum_{n=1}^{\infty}\frac{1}{(2n-1)^3} = -\frac{16\kappa}{\pi^3}\frac{7\zeta(3)}{8} = -\frac{14\kappa}{\pi^3}\zeta(3)\,.
\end{aligned} \tag{D.28}$$

Thus (now that the substitutions are being made, therefore the super-index qs will be used to specify that the thrust corresponds to the low frequency approximation)

$$\begin{aligned}\frac{Q_x^{qs}}{\rho\ddot{X}_g H^2} &= c^2\int_0^1 \frac{\partial\tilde{u}}{\partial\xi}\Big|_w d\eta + (c^2-2)\tilde{v}_w(1)\\ &= c^2\kappa\Big[-\frac{14}{\pi^3}\zeta(3)\Big] + (c^2-2)\kappa\Big[\frac{14(c^2-1)}{c^2\pi^3}\zeta(3) - \frac{8}{c^2\pi^2}G\Big]\\ &= -\kappa\Big[\Big(\frac{3c^2-2}{c^2}\Big)\frac{14\zeta(3)}{\pi^3} + \Big(\frac{c^2-2}{c^2}\Big)\frac{8G}{\pi^2}\Big], \end{aligned} \tag{D.29a}$$

in terms of Poisson's ratio:

$$\frac{Q_x^{qs}}{\rho\ddot{X}_g H^2} = -\kappa\Big[\Big(\frac{2-\nu}{1-\nu}\Big)\frac{14\zeta(3)}{\pi^3} + \Big(\frac{\nu}{1-\nu}\Big)\frac{8G}{\pi^2}\Big]. \tag{D.29b}$$

Note that the expression between brackets is bounded for any value of Poisson's ratio, $\nu = 1/2$ included. Additionally, it is acknowledged that this would not happen if the contribution of the vertical displacement was not taken into account.

Each displacement contributions tend to infinity as $\nu \longrightarrow 1/2$, so their relative importance can not be directly understood. One can represent their relative contributions to $Q^{qs}/c^2\rho\ddot{X}_g H^2$, which happen to be always finite:

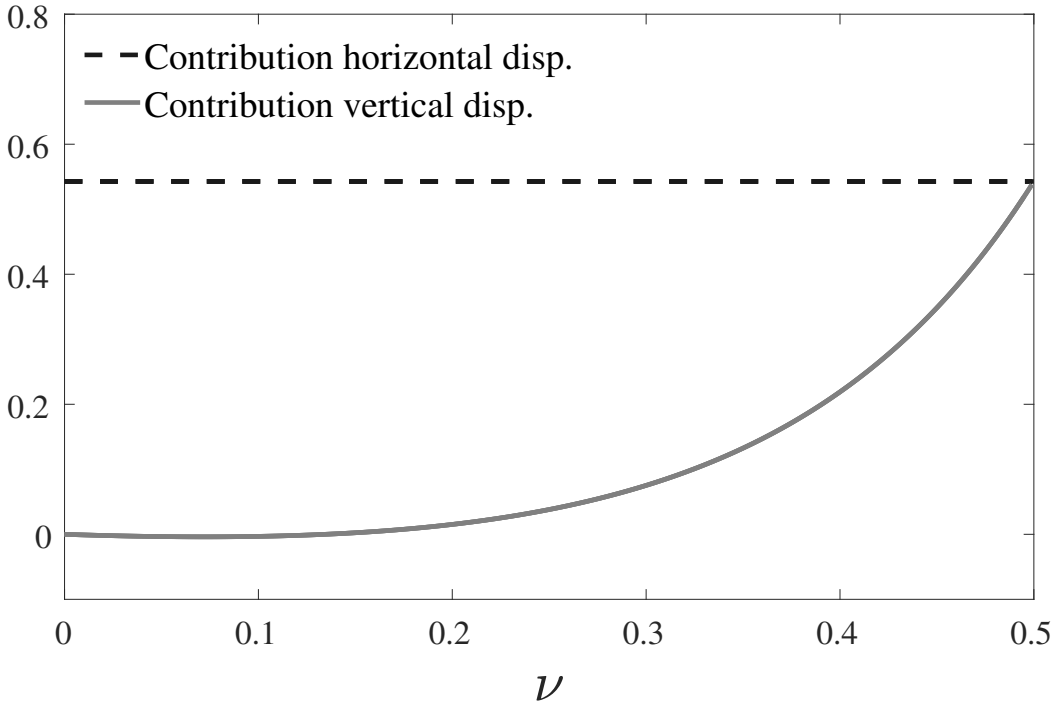

Figure D.2: Contribution to the quasi-static thrust of each addend in eq. (D.29b))

Fig.(D.2) reflects the contribution of the horizontal displacement gradient is constant and much greater than the one of the vertical displacement at the top of the wall, by

around one order of magnitude, except for values $\nu < 0.35$ (approximately), and in the limit, both attain similar value.

The value given for the incompressible limit case is

$$\lim_{\nu\to 1/2} \frac{Q_x^{qs}}{\rho \ddot{X}_g H^2} = -\frac{2\kappa_\infty}{\pi^3}(21\zeta(3) + 4\pi G)\,, \tag{D.30}$$

where $\kappa_\infty = \kappa(c \to \infty) = \kappa(\nu \to 1/2)$, whatever value it turns out to be.

A condition for obtaining a finite limit thrust can be given; assuming that the displacement field remains finite, the following condition must be met:

$$\int_0^1 \left.\frac{\partial \tilde{u}}{\partial \xi}\right|_w d\eta + \tilde{v}(1) = O(c^{-2}) \quad \text{as} \quad c \to \infty\,. \tag{D.31}$$

It is interesting that this condition is less restrictive than the conventional (2D) compressibility condition, that is nothing but volume conservation,

$$\lim_{\nu\to 1/2} \left(\frac{\partial \tilde{u}}{\partial \xi} + \frac{\partial \tilde{v}}{\partial \eta}\right) = 0\,. \tag{D.32}$$

It follows the calculation of the overturning moment at the base of the wall:

$$\begin{aligned}\frac{M_b}{\rho \ddot{X}_g H^3} = \int_0^1 \frac{\sigma_{xx}|_w}{\rho \ddot{X}_g H}\eta d\eta &= \int_0^1 \sum_{n=1}^{\infty} \left(c^2 \left.\frac{\partial \tilde{u}_n}{\partial \xi}\right|_w + (c^2-2)\left.\frac{\partial \tilde{v}_n}{\partial \eta}\right|_w\right)\eta d\eta \\ &= \sum_{n=1}^{\infty}\left(c^2 \int_0^1 \left.\frac{\partial \tilde{u}_n}{\partial \xi}\right|_w \eta d\eta + (c^2-2)\int_0^1 \left.\frac{\partial \tilde{v}_n}{\partial \eta}\right|_w \eta d\eta\right),\end{aligned} \tag{D.33}$$

evaluating the integrals

$$\int_0^1 \left.\frac{\partial \tilde{u}_n}{\partial \xi}\right|_w \eta d\eta = -\frac{2\kappa}{k_n^2}\int_0^1 \sin(k_n\eta)\eta d\eta = -\frac{2\kappa}{k_n^2}\frac{(-1)^{n+1}}{k_n^2} = -\frac{2\kappa(-1)^{n+1}}{k_n^4}\,, \tag{D.34a}$$

$$\begin{aligned}\int_0^1 \left.\frac{\partial \tilde{v}_n}{\partial \eta}\right|_w \eta d\eta &= \frac{2\kappa}{c^2 k_n^2}\int_0^1 \left[(c^2-1)\sin(k_n\eta) - (-1)^{n+1}\right]\eta d\eta \\ &= \frac{2\kappa}{c^2}\left[(c^2-1)\frac{(-1)^{n+1}}{k_n^4} + \frac{(-1)^{n+1}}{2k_n^2}\right],\end{aligned} \tag{D.34b}$$

thus

$$\begin{aligned}\frac{M_b^{qs}}{\rho\ddot{X}_g H^3} &= -2\kappa\sum_{n=0}^{\infty}\left[\left(c^2-\frac{(c^2-2)(c^2-1)}{c^2}\right)\frac{(-1)^{n+1}}{k_n^4}-\left(\frac{c^2-2}{c^2}\right)\frac{(-1)^{n+1}}{2k_n^2}\right]\\ &= -2\kappa\Big[\Big(\frac{3c^2-2}{c^2}\Big)\underbrace{\sum_{n=0}^{\infty}\frac{(-1)^{n+1}}{k_n^4}}_{=0.16244...\approx\frac{16}{\pi^4}}+\Big(\frac{c^2-2}{c^2}\Big)\underbrace{\sum_{n=0}^{\infty}\frac{(-1)^{n+1}}{2k_n^2}}_{=\frac{2}{\pi^2}G}\Big]\\ &\approx -2\kappa\Big[\Big(\frac{2-\nu}{1-\nu}\Big)\frac{16}{\pi^4}+\Big(\frac{\nu}{1-\nu}\Big)\frac{2G}{\pi^2}\Big]\,.\end{aligned}\tag{D.35}$$

Finally, note that the eccentricity of the thrust with respect to the wall base does not depend on κ:

$$\mathsf{e}^{qs}=\frac{M_b^{qs}}{HQ^{qs}}=\frac{\left(\frac{2-\nu}{1-\nu}\right)\frac{16}{\pi^4}+\left(\frac{\nu}{1-\nu}\right)\frac{2G}{\pi^2}}{\left(\frac{2-\nu}{1-\nu}\right)\frac{7\zeta(3)}{\pi^3}+\left(\frac{\nu}{1-\nu}\right)\frac{4G}{\pi^2}}=\frac{16(2-\nu)+2G\pi^2\nu}{7\zeta(3)\pi(2-\nu)+4G\pi^2\nu}\,.\tag{D.36}$$

The necessary algebraic manipulations as to obtain the quasi-static thrust are tedious yet not too burdensome, unlike in the dynamic case.

In order to simplify calculations, some shortcuts would be useful. In this spirit, the following variable is defined:

$$\tilde{Q}(\eta)=c^2\int_0^{\eta}\left.\frac{\partial\tilde{u}}{\partial\xi}\right|_w d\eta'+(c^2-2)\tilde{v}_w(\eta)\,,\tag{D.37}$$

where η' is a dummy integration variable; eq. (D.37) represents the contribution to the lateral thrust of the section running from the base up to a height ηH, therefore $\tilde{Q}(1)=Q/\rho\ddot{X}_g H^2$; using this definition both the moment at the base and the eccentricity can be expressed in compact form:

$$\frac{M_b}{\rho\ddot{X}_g H^3}=\tilde{Q}(1)-\int_0^1\tilde{Q}(\eta)d\eta\,,\tag{D.38a}$$

the prior expression follows fro integration by parts in the defintion of M_b, see eq. (D.33), and

$$\mathsf{e}=1-\int_0^1\frac{\tilde{Q}(\eta)}{\tilde{Q}(1)}d\eta\,.\tag{D.38b}$$

These expressions are completely general, so they will be used for the dynamic case.

D.1.3 Impedances

Recall that the quasi-static impedances are defined by

$$\sigma_{xx}|_w(y) = \sum_{n=1}^{\infty} K_n u_n|_{ff}(y)\,. \tag{D.39}$$

Their value can be obtained in this case from eq. (D.29b) :

$$\frac{\sigma_{xx}|_w}{\rho \ddot{X}_g H} = \sum_{n=1}^{\infty} c^2 \frac{\partial \tilde{u}_n}{\partial \xi} + (c^2-2)\frac{\partial \tilde{v}_n}{\partial \eta} \sim \sum_{n=1}^{\infty} u_n|_{ff} \underbrace{\left[\kappa k_n \left(\frac{(3c^2-2)}{c^2} + \frac{(c^2-2)}{c^2}\frac{8G}{\pi^2}k_n\right)\right]}_{\frac{K_n^{qs}}{\mu/H}}, \tag{D.40}$$

thus, in other words

$$K_n^{qs} = \kappa k_n \left(\frac{(3c^2-2)}{c^2} + \frac{(c^2-2)}{c^2}\frac{8G}{\pi^2}k_n\right)\frac{\mu}{H}, \tag{D.41}$$

note that a little "trick" had to be used in order to attain the result: it has been noted that

$$\frac{4G}{\pi^2} = \sum_{n=1}^{\infty} \frac{(-1)^{n+1}}{k_n^2} \sim \frac{4G}{\pi^2}\sum_{n=1}^{\infty}\frac{2}{k_n}\sin(k_n\eta), \tag{D.42}$$

since the constant can be understood as a function defined over the interval $[1,0]$ and expanded as a sine series ($\sim$ has to replace $=$ again since the expansion suffers from Gibbs pathology, see eq. (4.25), yet, again, this does not interfere with the final result, the thrust, for reasons previously mentioned). One can verify that this impedance would return the same thrust.

D.1.4 Evaluation of $\mathrm{J}_x = 0$ to find κ

The expression for the earth thrust was attained but there is a parameter that has not been specified yet, κ, that controls how rapidly the effects due to the wall vanish as the far-field is approached. This undetermined parameter shall be found so as to furnish the previous model coherent with the energy balance equivalence requirements. First, particularize the expression for $\mathrm{J}_x = 0$ for the frictionless-rigid wall case, eq. (2.53). Next, the right-hand side is evaluated using the quasi-static solution in the far-field, eq. (3.8):

$$\frac{c^2}{2}\left(\left\|\frac{\partial \tilde{u}}{\partial \xi}\Big|_w\right\|^2_{L^2([0,1])} - \left\|\frac{\partial \tilde{v}}{\partial \eta}\Big|_w\right\|^2_{L^2([0,1])}\right) = \frac{1}{6}\,. \tag{D.43}$$

As a sanity check, note that, passing the factor c^2 to the other member and taking the limit as $c \to \infty$ (equivalent to $\nu \to 1/2$), it follows that

$$\lim_{\nu\to 1/2}\left(\left\|\frac{\partial\tilde{u}}{\partial\xi}\Big|_w\right\|^2_{L^2([0,1])} - \left\|\frac{\partial\tilde{v}}{\partial\eta}\Big|_w\right\|^2_{L^2([0,1])}\right) = \lim_{\nu\to 1/2}\frac{1}{3c^2} = 0\,, \tag{D.44}$$

what is just a weaker version (or a consequence) of the classic incompressibility condition, eq. (D.32). The expressions for the gradients that were derived from the model are shown again:

$$\frac{\partial\tilde{u}_n}{\partial\xi}\Big|_{\xi=0} = -\frac{2\kappa}{k_n^2}\sin(k_n\eta)\,, \tag{D.45a}$$

$$\frac{\partial\tilde{v}_n}{\partial\eta} = \frac{2\kappa}{c^2k_n^2}\Big[(c^2-1)\sin(k_n\eta) - (-1)^{n+1}\Big]\,, \tag{D.45b}$$

observe that this displacement field (although they are defined properly only in the wall vicinity) does satisfy the incompressibility condition in the limit $c \to \infty$.

The evaluation of the norms is tackled next. The swapping of sums and integrals is allowed because the sums converge to functions in $L^2([0,1])$, as it has already been argued. First,

$$\begin{aligned}\left\|\frac{\partial\tilde{u}}{\partial\xi}\Big|_w\right\|^2_{L^2([0,1])} &= \int_0^1 \Big(\sum_{n=0}^{\infty}\frac{2\kappa}{k_n^2}\sin(k_n\eta)\Big)\Big(\sum_{m=0}^{\infty}\frac{2\kappa}{k_m^2}\sin(k_m\eta)\Big)d\eta \\ &= 4\kappa^2\int_0^1\Big(\sum_{n=0}^{\infty}\sum_{m=0}^{\infty}\frac{\sin(k_n\eta)\sin(k_m\eta)}{k_n^2k_m^2}\Big)d\eta \\ &= 4\kappa^2\sum_{n=0}^{\infty}\sum_{m=0}^{\infty}\frac{1}{k_n^2k_m^2}\int_0^1\sin(k_n\eta)\sin(k_m\eta)d\eta\,,\end{aligned}$$

recall that $\sin(k_n\eta)$ and $\sin(k_n\eta)$ are orthogonal, except for $n = m$:

$$= 4\kappa^2\sum_{n=0}^{\infty}\frac{1}{k_n^4}\underbrace{\int_0^1\sin^2(k_n\eta)d\eta}_{=1/2} = 2\kappa^2\sum_{n=0}^{\infty}\underbrace{\frac{1}{k_n^4}}_{=1/6} = \frac{\kappa^2}{3}\,, \tag{D.46}$$

the same result would have been obtained right away by invoking the Parseval's theorem [Wei12]. And for the other norm:

$$\begin{aligned}\left\|\frac{\partial\tilde{v}}{\partial\eta}\Big|_w\right\|^2_{L^2([0,1])} = \int_0^1 &\Big(\sum_{n=0}^{\infty}\frac{2\kappa}{c^2k_n^2}\Big[(c^2-1)\sin(k_n\eta) - (-1)^{n+1}\Big]\Big) \\ &\Big(\sum_{m=0}^{\infty}\frac{2\kappa}{c^2k_m^2}\Big[(c^2-1)\sin(k_m\eta) - (-1)^{m+1}\Big]\Big)d\eta =\end{aligned}$$

$$= \frac{4\kappa^2(c^2-1)^2}{c^4}\int_0^1 \Big(\sum_{n=0}^{\infty}\sum_{m=0}^{\infty}\frac{\sin(k_n\eta)\sin(k_m\eta)}{k_n^2k_m^2}\Big)d\eta$$
$$- \frac{4\kappa^2(c^2-1)}{c^4}\int_0^1 \Big(\sum_{n=0}^{\infty}\sum_{m=0}^{\infty}\frac{(-1)^{n+1}\sin(k_m\eta)}{k_n^2k_m^2}\Big)d\eta$$
$$- \frac{4\kappa^2(c^2-1)}{c^4}\int_0^1 \Big(\sum_{n=0}^{\infty}\sum_{m=0}^{\infty}\frac{\sin(k_n\eta)(-1)^{m+1}}{k_n^2k_m^2}\Big)d\eta$$
$$+ \frac{4\kappa^2}{c^4}\int_0^1 \Big(\sum_{n=0}^{\infty}\sum_{m=0}^{\infty}\frac{1}{k_n^2k_m^2}\Big)d\eta =$$

integral and sums can be swapped:

$$= \frac{4\kappa^2(c^2-1)^2}{c^4}\sum_{n=0}^{\infty}\sum_{m=0}^{\infty}\frac{1}{k_n^2k_m^2}\underbrace{\int_0^1 \sin(k_n\eta)\sin(k_m\eta)d\eta}_{=1/2\ (n=m)\text{ or }0\ (n\neq m)}$$
$$- \frac{4\kappa^2(c^2-1)}{c^4}\sum_{n=0}^{\infty}\sum_{m=0}^{\infty}\frac{(-1)^{n+1}}{k_n^2k_m^2}\underbrace{\int_0^1 \sin(k_m\eta)d\eta}_{=1/k_m}$$
$$- \frac{4\kappa^2(c^2-1)}{c^4}\sum_{n=0}^{\infty}\sum_{m=0}^{\infty}\frac{(-1)^{m+1}}{k_n^2k_m^2}\underbrace{\int_0^1 \sin(k_n\eta)d\eta}_{=1/k_n}$$
$$+ \frac{4\kappa^2}{c^4}\sum_{n=0}^{\infty}\sum_{m=0}^{\infty}\frac{(-1)^{n+1}(-1)^{n+1}}{k_n^2k_m^2}\underbrace{\int_0^1 d\eta}_{=1} =$$

recall the Fubini–Tonelli theorem to evaluate the double sums as iterated sums:

$$= \frac{4\kappa^2}{c^4}\Big[\frac{(c^2-1)^2}{2}\underbrace{\Big(\sum_{n=0}^{\infty}\frac{1}{k_n^4}\Big)}_{=1/6} - (c^2-1)\underbrace{\Big(\sum_{n=0}^{\infty}\frac{(-1)^{n+1}}{k_n^2}\Big)}_{=4G/\pi^2}\underbrace{\Big(\sum_{m=0}^{\infty}\frac{1}{k_m^3}\Big)}_{=7A/\pi^3}$$
$$- (c^2-1)\underbrace{\Big(\sum_{m=0}^{\infty}\frac{(-1)^{m+1}}{k_m^2}\Big)}_{=4G/\pi^2}\underbrace{\Big(\sum_{n=0}^{\infty}\frac{1}{k_n^3}\Big)}_{=7A/\pi^3} + \underbrace{\Big(\sum_{n=0}^{\infty}\frac{(-1)^{n+1}}{k_n^2}\Big)}_{=4G/\pi^2}\underbrace{\Big(\sum_{m=0}^{\infty}\frac{(-1)^{m+1}}{k_m^2}\Big)}_{=4G/\pi^2}\Big]$$
$$= \frac{4\kappa^2}{c^4}\Big[\frac{(c^2-1)^2}{12} - \frac{56(c^2-1)AG}{\pi^5} + \frac{64G^2}{\pi^4}\Big]$$
$$= \frac{\kappa^2}{c^4}\Big[\frac{(c^2-1)^2}{3} - \frac{224(c^2-1)AG}{\pi^5} + \frac{64G^2}{\pi^4}\Big], \tag{D.47}$$

thus

$$\left\| \frac{\partial \tilde{u}}{\partial \xi}\Big|_w \right\|^2_{L^2([0,1])} - \left\| \frac{\partial \tilde{v}}{\partial \eta}\Big|_w \right\|^2_{L^2([0,1])} = \frac{\kappa^2}{3} - \frac{\kappa^2}{c^4}\left[\frac{(c^2-1)^2}{3} - \frac{224(c^2-1)AG}{\pi^5} + \frac{64G^2}{\pi^4}\right] = \frac{1}{3c^2}\,. \tag{D.48}$$

Isolating κ from eq. (D.43):

$$\kappa = \frac{c}{\sqrt{(2c^2-1) + \frac{672AG}{\pi^5}(c^2-1) - \frac{192G^2}{\pi^4}}} = \sqrt{\frac{1-\nu}{(\frac{192G^2}{\pi^4}-1)\nu + 96\frac{G^2}{\pi^4}(\frac{7A}{2\pi G}-1) + \frac{3}{2}}}. \tag{D.49}$$

This value renders the model in agreement to the requirement imposed by $J_1 = 0$.

Note that, had the contribution of $\partial^2 v/\partial x^2$ not being ignored in the vertical equilibrium equation, a more complex expression for the displacement field would been attained, the norms would have not been evaluated easily and a simple expression for κ would have not been obtained. Recall that this approximation entailed some errors, which were estimated to be $O\left[(\kappa/c)^2\right]$. Given this comparison, it appears

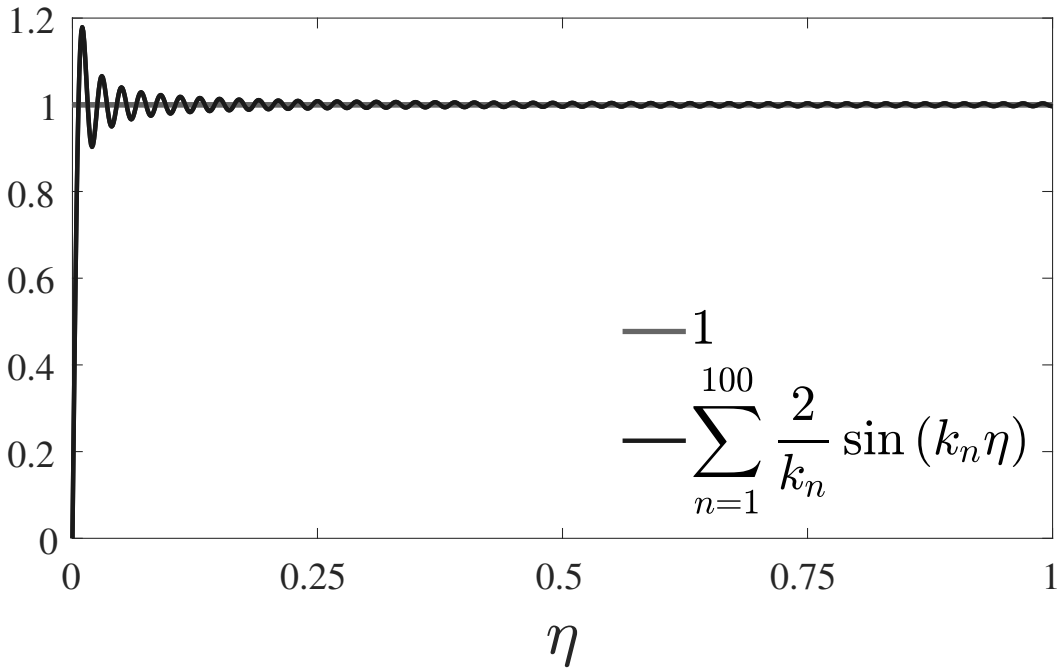

Figure D.3: Comparison of $\kappa^{qs}(\nu)$ and $c(\nu)$

logical to expect small errors along the whole range of values of ν, the smaller the higher ν is.

D.2 Dynamic Regime

Let us pass to consider the horizontal equilibrium in the dynamic setting.

D.2.1 Horizontal displacement

The equation to be solved first is eq. (5.2):

$$\frac{1}{\kappa^2}\frac{\partial^2\tilde{u}}{\partial\xi^2} + \frac{\partial^2\tilde{u}}{\partial\eta^2} - r^2\frac{\partial^2\tilde{u}}{\partial\tau^2} = e^{i\tau}\,. \tag{D.50}$$

Let us assume a harmonic evolution given by $e^{i\tau}$, hence redefine $\tilde{u}$ as just the amplitude

$$\frac{1}{\kappa^2}\frac{\partial^2\tilde{u}}{\partial\xi^2} + \frac{\partial^2\tilde{u}}{\partial\eta^2} + r^2\tilde{u} = 1\,. \tag{D.51}$$

Inspired by the quasi-static solution, eq. (D.6), try directly a solution of the form

$$\tilde{u} = \sum_{n=0}^{\infty}\tilde{u}_n(1 - e^{-\bar{\kappa}k_n\xi})\sin(k_n\eta)\,, \tag{D.52}$$

where now $\bar{\kappa}$ may contain other factors, as we shall see,

$$-k_n^2\left(\frac{\bar{\kappa}}{\kappa}\right)^2 e^{-\bar{\kappa}k_n\xi}\tilde{u}_n + k_n^2(1 - e^{-\bar{\kappa}k_n\xi})\tilde{u}_n - r^2(1 - e^{-\bar{\kappa}k_n\xi})\frac{\partial^2\tilde{u}_n}{\partial\tau^2} = \frac{2}{k_n} \tag{D.53}$$

terms with and without ξ-dependence can be gathered together, therefore

$$-k_n^2\left(\frac{\bar{\kappa}}{\kappa}\right)^2 - k_n^2 + r^2 = 0\,, \tag{D.54a}$$

$$-k_n^2\tilde{u}_n + r^2\tilde{u}_n = \frac{2}{k_n}\,, \tag{D.54b}$$

the first one can be used to retrieve the value of $\bar{\kappa}$ and the latter to get $\tilde{u}_n$:

$$\bar{\kappa} = \kappa\sqrt{1 - r_n^2} \tag{D.55}$$

$$\tilde{u}_n = \frac{2}{k_n^3(1 - r_n^2)} = \frac{2}{k_n(k_n^2 - r^2)}\,, \tag{D.56}$$

and hence

$$\tilde{u} = -\sum_{n=1}^{\infty}\frac{2}{k_n^3}\frac{(1 - e^{-\kappa k_n\sqrt{1-r_n^2}\xi})}{1 - r_n^2}\sin(k_n\eta) = \sum_{n=1}^{\infty}\tilde{u}_n(1 - e^{-\kappa k_n\sqrt{1-r_n^2}\xi})\sin(k_n\eta)\,. \tag{D.57}$$

D.2.2 Vertical displacement

The governing equation for the vertical displacement at the wall is eq. (4.32b), which corresponds to a forced wave equation. If we assume harmonic evolution and, again as in the quasi-static case, $\kappa \ll c$, it can be simplified into

$$c^2\frac{\partial^2\tilde{v}}{\partial\eta^2} + r^2\tilde{v} = -(c^2-1)\frac{\partial^2\tilde{u}}{\partial\eta\partial\xi}\Big|_{\xi=0}, \tag{D.58}$$

from this equation, one can readily acknowledge that the natural vibration of the vertical displacement, unlike the horizontal one, shall happen at natural frequencies corresponding to $r/c \sim \varpi H/cc_s = \varpi H/c_p$, that is, to frequencies based on the p-wave velocity, unlike those based on s-wave velocity that the horizontal displacement yielded; to conclude this aside: the resonance of the thrust with natural vibration associated to p-wave velocities originates in the vertical displacement, not in the horizontal one. The homogeneous solution is given by

$$c^2\frac{\partial^2\tilde{v}_w|_{hom}}{\partial\eta^2} + r^2\tilde{v}_w|_{hom} = 0 \rightarrow \tilde{v}_w|_{hom} = A\cos(r_c\eta) + B\sin(r_c\eta), \tag{D.59}$$

whereas the particular solution requires first to know the forcing:

$$\frac{\partial^2\tilde{u}}{\partial\eta\partial\xi}\Big|_{\xi=0} = \sum_{n=1}^{\infty} k_n^2\sqrt{1-r_n^2}\tilde{u}_n\cos(k_n\eta) = -\sum_{n=1}^{\infty}\frac{2\kappa}{k_n}\frac{\cos(k_n\eta)}{\sqrt{1-r_n^2}}, \tag{D.60}$$

thus the particular solution shall be $\tilde{v}_w|_{par} = C_n\cos(k_n\eta)$, where

$$C_n(-c^2k_n^2 + r^2) = -\kappa(c^2-1)k_n^2\sqrt{1-r_n^2}\tilde{u}_n \rightarrow C_n = \kappa\frac{(c^2-1)}{c^2}\frac{\sqrt{1-r_n^2}}{1-r_n^{\nu 2}}\tilde{u}_n\,. \tag{D.61}$$

In conclusion:

$$\tilde{v} = \sum_{n=1}^{\infty} C_n\cos(k_n\eta) + A\cos(r_c\eta) + B\sin(r_c\eta), \tag{D.62}$$

wherein the values of A, B must meet the boundary conditions. At the base, $\tilde{v}_w(0) = 0$:

$$A + \sum_{n=1}^{\infty} C_n = 0 \rightarrow A = -\sum_{n=1}^{\infty} C_n\,. \tag{D.63}$$

The boundary condition at the top ($\sigma_{yy}(\eta = 1) = 0$) yields B, yet through a relation more involved:

$$c^2\frac{\partial\tilde{v}_w}{\partial\eta}\Big|_{\eta=1} + (c^2-2)\frac{\partial\tilde{u}}{\partial\xi}\Big|_{\xi=0,\eta=1} = 0, \tag{D.64}$$

where

$$\frac{\partial \tilde{v}}{\partial \eta}\Big|_{\eta=1} = -\sum_{n=1}^{\infty} C_n k_n \sin(k_n) + r_c(-A\sin(r_c) + B\cos(r_c)) =$$

$$= r_c(B\cos(r_c) - A\sin(r_c)) - \sum_{n=1}^{\infty} C_n k_n (-1)^{n+1}\,, \tag{D.65}$$

$$-\frac{(c^2-2)}{c^2}\frac{\partial \tilde{u}}{\partial \xi}\Big|_{\eta=1} = -\frac{(c^2-2)}{c^2}\sum_{n=1}^{\infty} \kappa \tilde{u}_n (-1)^{n+1} k_n \sqrt{1-r_n^2}$$

$$= -\kappa\left(\frac{c^2-2}{c^2-1}\right)\sum_{n=1}^{\infty} C_n(1-r_n^{\nu 2}) k_n (-1)^{n+1}\,, \tag{D.66}$$

thus, combining into the equation and isolating B

$$B = A\tan(r_c) + \sum_{n=1}^{\infty} \frac{C_n(-1)^{n+1}k_n}{r_c\cos(r_c)}\left(1 - \left(\frac{c^2-2}{c^2-1}\right)(1-r_n^{\nu 2})\right)\,. \tag{D.67}$$

Once the constants have been defined, the vertical displacement is ready. One can verify that this solution boils down to the quasi-static one in the limit $r \to 0$.

Before moving to the next item, let us point out that the sum of all the C_n does not converge to any closed form value.

D.2.2.1 An equation for the dynamic thrust

An equation for the thrust could be derived so the "partial" thrust can be obtained from solving a PDE thereby the vertical displacement, as we detail next. Let us resort to the partial thrust as in eq. (D.37)), and realize that the vertical displacement can be written in terms of the vertical and the horizontal displacement:

$$\tilde{v}_w(\eta) = \frac{\tilde{Q}(\eta)}{(c^2-2)} - \frac{c^2}{(c^2-2)}\int_0^{\eta} \frac{\partial \tilde{u}}{\partial x}\Big|_w d\eta'\,, \tag{D.68}$$

substituting this expression in the vertical equilibrium equation:

$$c^2\frac{\partial^2 \tilde{v}_w}{\partial \eta^2} + r^2\tilde{v}_w(\eta) = c^2\frac{\partial^2}{\partial \eta^2}\Big[\frac{\tilde{Q}(\eta)}{(c^2-2)} - \frac{c^2}{(c^2-2)}\int_0^{\eta}\frac{\partial \tilde{u}}{\partial x}\Big|_w d\eta'\Big] \tag{D.69a}$$

$$+ r^2\Big[\frac{\tilde{Q}(\eta)}{(c^2-2)} - \frac{c^2}{(c^2-2)}\int_0^{\eta}\frac{\partial \tilde{u}}{\partial x}\Big|_w d\eta'\Big] =$$

$$= \frac{c^2}{(c^2-2)}\frac{\partial^2 \tilde{Q}}{\partial \eta^2} - \frac{r^2}{(c^2-2)}\frac{\partial^2 \tilde{Q}}{\partial \tau^2} \tag{D.69b}$$

$$- \frac{c^4}{(c^2-2)}\frac{\partial^2 \tilde{u}}{\partial \eta \partial \xi} - \frac{r^2c^2}{(c^2-2)}\int_0^{\eta}\frac{\partial \tilde{u}}{\partial x}\Big|_w d\eta' \tag{D.69c}$$

$$= -(c^2-1)c^2\frac{\partial^2 \tilde{u}}{\partial \eta \partial \xi}\,. \tag{D.69d}$$

Hence

$$\frac{\partial^2 \tilde{Q}}{\partial \eta^2} - \left(\frac{r}{c}\right)^2 \tilde{Q} = \frac{(3c^2-2)}{c^2}\frac{\partial^2 \tilde{u}}{\partial \eta \partial \xi} + r^2 \int_0^\eta \frac{\partial \tilde{u}}{\partial x}\Big|_w d\eta' \,, \tag{D.70}$$

since the horizontal displacement evolution is known at this point, eq. (D.57)), the forcing term can be explicitly stated:

$$\frac{(3c^2-2)}{c^2}\frac{\partial^2 \tilde{u}}{\partial \eta \partial \xi} + r^2 \int_0^\eta \frac{\partial \tilde{u}}{\partial \xi}\Big|_w d\eta' \tag{D.71}$$

$$= -\sum_{n=1}^{\infty} \frac{2\kappa}{k_n \sqrt{1-r_n^2}} \left[\left(\frac{3c^2-2}{c^2} - r_n^2 \right) \cos(k_n \eta) + r_n^2 \right] e^{i\tau} \,, \tag{D.72}$$

and the boundary conditions for the equation would be

$$\tilde{v}_w(\eta = 0) = 0 \qquad \rightarrow \tilde{Q}(\eta = 0) = 0 \tag{D.73a}$$

$$c^2 \frac{\partial \tilde{v}_w}{\partial \eta}\Big|_{top} = -(c^2-2)\frac{\partial \tilde{u}}{\partial \eta}\Big|_{top} \qquad \rightarrow \frac{\partial \tilde{Q}}{\partial \eta}\Big|_{top} = 4\left(\frac{c^2-1}{c^2}\right)\frac{\partial \tilde{u}}{\partial \eta}\Big|_{top} = 4\left(\frac{c^2-1}{c^2}\right)\sum_{n=1}^{\infty}\frac{2\kappa}{k_n^2}\frac{(-1)^{n+1}}{\sqrt{1-r_n^2}} \,. \tag{D.73b}$$

Having the problem re-expressed in terms of a differential equation for the thrust allows for simpler understanding of the thrust behavior in different regimes. For example, one could directly take the asymptotic for the low-frequency case (quasi-static behavior, $r \rightarrow 0$), high-frequency ($r \rightarrow \infty$), or incompressible material ($\nu \rightarrow 1/2$ or $c \rightarrow \infty$, note that in this particular case one would obtain $\tilde{Q} = O(r^{1/2})$, an unrealistic scaling unless κ introduces an extra term that compensates).

Observe that it can be derived from the equation for the thrust is that the "natural vibration" of the thrust happens at frequencies odd multiple of $\omega_p = c\omega_s$, that is, at the frequency of the shear beam modified with the P-wave velocity instead of S-wave.

D.2.3 Earth thrust, overturning moment at the base and eccentricity

Let us compute the partial thrust first. This can be achieved since we have the vertical and the horizontal displacement:

$$\tilde{Q}(\eta) = c^2 \int_0^\eta \frac{\partial \tilde{u}}{\partial \xi}\Big|_w d\xi + (c^2-2)\tilde{v}_w(\eta) \,, \tag{D.74}$$

on one hand

$$\int_0^\eta \left.\frac{\partial \tilde{u}}{\partial \xi}\right|_w d\xi = \sum_n^\infty \kappa \tilde{u}_n \sqrt{1-r_n^2}(1-\cos(k_n\eta)), \tag{D.75}$$

on the other hand, the vertical displacement is given by eq. (D.62), hence

$$\begin{aligned}\tilde{Q}(\eta) = \kappa &\left[\sum_{n=1}^\infty c^2 \tilde{u}_n \sqrt{1-r_n^2}(1-\cos(k_n\eta)) + (c^2-2)C_n\cos(k_n\eta)\right] \\ &+ (c^2-2)\left[A\cos(r_c\eta) + B\sin(r_c\eta)\right], \end{aligned}\tag{D.76}$$

recall that the values of u_n, C_n, A, B are already given above. Also, A, B depend on κ despite not being shown explicitly. Once eq. (D.76) is ready, recall eq. (D.37):

$$\frac{Q}{\rho \ddot{X}_g H^2} = \tilde{Q}(1) = \kappa\left((c^2-2)\left(\bar{A}\cos(r_c) + \bar{B}\sin(r_c)\right) + \sum_{n=1}^\infty c^2\tilde{u}_n\sqrt{1-r_n^2}\right), \tag{D.77}$$

where $\bar{A} = A/\kappa$ and $\bar{B} = B/\kappa$. For the moment, eq. (D.38a), we also need the integral of the partial thrust:

$$\begin{aligned}\int_0^1 \tilde{Q}(\eta)d\eta = \kappa &\left[\sum_{n=1}^\infty c^2\tilde{u}_n\sqrt{1-r_n^2}\left(1-\frac{(-1)^{n+1}}{k_n}\right) + (c^2-2)C_n\frac{(-1)^{n+1}}{k_n}\right] \\ &+ \frac{(c^2-2)}{r_c}\left[A\sin(r_c\eta) - B\cos(r_c\eta)\right], \end{aligned}\tag{D.78}$$

once both pieces are ready, substitute them into eq. (D.38a) to obtain

$$\begin{aligned}\frac{M_b}{\rho\ddot{X}_g H^3} &= \tilde{Q}(1) - \int_0^1 \tilde{Q}(\eta)d\eta = \\ &= \kappa\Bigg[(c^2-2)\left(\cos(r_c)\left(\bar{A}+\frac{\bar{B}}{r_c}\right) + \sin(r_c)\left(\bar{B}-\frac{\bar{A}}{r_c}\right)\right) + \\ &\qquad + \sum_{n=1}^\infty \frac{(-1)^{n+1}}{k_n}\left(c^2\tilde{u}_n\sqrt{1-r_n^2} - (c^2-2)\bar{C}_n\right)\Bigg]. \end{aligned}\tag{D.79}$$

The expression of the eccentricity follows from the one of the thrust and the moment and it will not be explicitly shown.

D.2.4 Evaluation of $\hat{\mathrm{J}}_1 = 0$ to find κ

It was found that, for the smooth-rigid wall, $\hat{\mathrm{J}}_x = 0$ reduces to

$$\begin{aligned}&\int_0^1 \left\{\frac{c^2}{2}\left[\left(\left.\frac{\partial\tilde{u}}{\partial\xi}\right|_w\right)^2 - \left(\left.\frac{\partial\tilde{v}}{\partial\eta}\right|_w\right)^2\right] + \frac{1}{2}r^2(\tilde{v}_w)^2\right\}d\eta \\ &= \int_0^1 \left\{\frac{1}{2}\left[\left(\left.\frac{\partial\tilde{u}}{\partial\eta}\right|_{ff}\right)^2 - r^2(\tilde{u}_{ff})^2\right] + \tilde{u}_{ff}\right\}d\eta\,. \end{aligned}\tag{D.80}$$

Using norm notation:

$$\frac{c^2}{2}\left(\left\|\left.\frac{\partial\tilde{u}}{\partial\xi}\right|_w\right\|^2_{L^2([0,1])} - \left\|\left.\frac{\partial\tilde{v}}{\partial\eta}\right|_w\right\|^2_{L^2([0,1])}\right) + \frac{r^2}{2}\left\|\tilde{v}_w\right\|^2_{L^2([0,1])} \tag{D.81}$$

$$= \frac{1}{2}\left(\left\|\left.\frac{\partial\tilde{u}}{\partial\eta}\right|_{ff}\right\|^2_{L^2([0,1])} - r^2\left\|\tilde{u}_{ff}\right\|^2_{L^2([0,1])}\right) + \left\langle 1, \tilde{u}|_{ff}\right\rangle_{L^2([0,1])}. \tag{D.82}$$

Calculating the right-hand side is no challenge as the far-field response comes in a compact, manageable closed form. Conversely, dealing with the norms associated to the left-hand side is no easy task, albeit one can compute some of these norms in closed forms by appealing to Parseval's theorem. Let us begin with the norm of horizontal gradient of horizontal displacement: consider, based on eq. (D.57), that its Fourier-coefficients are given by $\tilde{u}_n\sqrt{1-r_n^2}k_n$, then

$$\begin{aligned}\left\|\left.\frac{\partial\tilde{u}}{\partial\xi}\right|_w\right\|^2_{L^2([0,1])} &= \frac{\kappa^2}{2}\left(\sum_{n=1}^{\infty}(k_n\sqrt{1-r_n^2}\tilde{u}_n)^2\right) = \frac{\kappa^2}{2}\left(\sum_{n=1}^{\infty}(k_n^2-r^2)\tilde{u}_n^2\right)\\ &= \frac{\kappa^2}{2}\left(\sum_{n=1}^{\infty}k_n^2\tilde{u}_n^2 - r^2\sum_{n=1}^{\infty}\tilde{u}_n^2\right) = \kappa^2\left(\frac{\tan(r)-r}{r^3}\right).\end{aligned} \tag{D.83}$$

This nice convergence can also be found in some of the terms corresponding to the vertical displacements. In order to illustrate this, let us analyze the norm of the vertical displacement itself:

$$\begin{aligned}\left\|\tilde{v}_w\right\|^2_{L^2([0,1])} = \int_0^1 &\left(\sum_{n=1}^{\infty}C_n\cos(k_n\eta) + A\cos(r_c\eta) + B\sin(r_c\eta)\right)\\ &\left(\sum_{m=1}^{\infty}C_n\cos(k_n\eta) + A\cos(r_c\eta) + B\sin(r_c\eta)d\eta\right)d\eta =\\ = \frac{1}{2}\sum_{n=1}^{\infty}C_n^2 &+ A^2\left(\frac{1}{2}+\frac{\sin(r_c)}{4r_c}\right) + B^2\left(\frac{1}{2}-\frac{\sin(r_c)}{4r_c}\right)\\ &+ 2A\sum_{n=1}^{\infty}C_n\int_0^1\cos(r_c\eta)\cos(k_n\eta)d\eta\\ &+ 2B\sum_{n=1}^{\infty}C_n\int_0^1\sin(r_c\eta)\cos(k_n\eta)d\eta\\ &+ 2AB\int_0^1\cos(r_c\eta)\sin(r_c\eta)d\eta.\end{aligned} \tag{D.84}$$

Recall the expression of $C_n = (c^2-1)\sqrt{1-r_n^2}\tilde{u}_n/c^2(1-r_n^{\nu 2})$, therefore

$$\sum_{n=1}^{\infty}C_n^2 = \kappa^2\frac{2\tan(r) + c(c^2-3)\tan(r_c) - r(c^2-1)\sec^2(r_c)}{r^5}. \tag{D.85}$$

Note also

$$\int_0^1 \sin(r_c\eta)\cos(k_n\eta)d\eta = \frac{k_n(-1)^{n+1}\sin(r_c) - r}{k_n^2 - r_c^2}, \tag{D.86a}$$

$$\int_0^1 \cos(r_c\eta)\cos(k_n\eta)d\eta = \frac{k_n(-1)^{n+1}\cos(r_c)}{k_n^2 - r_c^2}, \tag{D.86b}$$

$$\int_0^1 \cos(r_c\eta)\sin(r_c\eta)d\eta = \frac{\sin^2(r_c)}{2r_c}, \tag{D.86c}$$

The integrals that appear beside the factor AC_1 are

$$\int_0^1 \cos(r_c\eta)\cos(k_1\eta)d\eta = \frac{k_1\cos(r_c)}{k_1^2 - r_c^2}, \tag{D.87a}$$

$$\int_0^1 \sin(r_c\eta)\sin(k_1\eta)d\eta = \frac{r_c\cos(r_c)}{k_1^2 - r_c^2}, \tag{D.87b}$$

the integrals that appear beside the factor BC_1 are

$$\int_0^1 \sin(r_c\eta)\cos(k_1\eta)d\eta = \frac{k_1\sin(r_c) - r_c}{k_1^2 - r_c^2}, \tag{D.88a}$$

$$\int_0^1 \cos(r_c\eta)\sin(k_1\eta)d\eta = \frac{k_1 - r_c\sin(r_c)}{k_1^2 - r_c^2}, \tag{D.88b}$$

finally, the integral that combines A and B:

$$\int_0^1 \cos(r_c\eta)\sin(r_c\eta)d\eta = \frac{\sin^2(r_c)}{2r_c}. \tag{D.89}$$

Combining the two contributions, only the cross-terms corresponding to $2BC_n$ remain:

$$\begin{aligned}\frac{r^2}{2}\left\|\tilde{v}_w\right\|^2_{L^2([0,1])} - \frac{c^2}{2}\left\|\left.\frac{\partial\tilde{v}}{\partial\eta}\right|_w\right\|^2_{L^2([0,1])} &= -\sum_{n=1}^{\infty}\frac{(c^2k_n^2 - r^2)}{4}C_n^2 + \\ &+ \frac{c\,r}{2}\left[(A^2 - B^2)\frac{\sin(2r_c)}{2} + 2B\sum_{n=1}^{\infty}C_n + 2AB\sin^2(r_c)\right],\end{aligned} \tag{D.90}$$

recall that κ^2 is implicit (it is not being shown for it will be taken as a common factor in the end).

Therefore, the left-hand side of eq. (D.80), excluding κ^2,

$$\frac{c^2}{2}\left(\left\|\frac{\partial\tilde{u}}{\partial\xi}\Big|_w\right\|^2_{L^2([0,1])} - \left\|\frac{\partial\tilde{v}}{\partial\eta}\Big|_w\right\|^2_{L^2([0,1])}\right) + \frac{r^2}{2}\left\|\tilde{v}_w\right\|^2_{L^2([0,1])} =$$
$$= \sum_{n=1}^{\infty}\frac{c^2}{k_n^2(k_n^2-r^2)} - \sum_{n=1}^{\infty}\frac{(c^2k_n^2-r^2)}{4}C_n^2 +$$
$$+ \frac{c\,r}{2}\left[(A^2-B^2)\frac{\sin(2r_c)}{2} + 2B\sum_{n=1}^{\infty}C_n + 2AB\sin^2(r_c)\right]. \quad \text{(D.91)}$$

To come to the closure, calculate also the left-hand side by evaluating the contribution of the far-field:

$$\int_0^1 \tilde{u}_n d\eta = \frac{2}{k_n^3}\frac{1}{1-r_n^2}\int_0^1 -\sin(k_n\eta)d\eta = -\frac{2}{k_n^4}\frac{1}{1-r_n^2}, \quad \text{(D.92a)}$$

$$\int_0^1 (\tilde{u}_n)^2 d\eta = \frac{4}{k_n^6}\frac{1}{(1-r_n^2)^2}\int_0^1 \sin^2(k_n\eta)d\eta = \frac{4}{k_n^6}\frac{1}{(1-r_n^2)^2}\frac{1}{2} = \frac{2}{k_n^6}\frac{1}{(1-r_n^2)^2}, \quad \text{(D.92b)}$$

$$\int_0^1 \left(\frac{\partial\tilde{u}_n}{\partial\eta}\right)^2 d\eta = \frac{4}{k_n^4}\frac{1}{(1-r_n^2)^2}\int_0^1 \cos^2(k_n\eta)d\eta = \frac{2}{k_n^4}\frac{1}{(1-r_n^2)^2}, \quad \text{(D.92c)}$$

therefore,

$$\frac{1}{2}\left\{\frac{2}{k_n^4}\frac{1}{(1-r_n^2)^2} - r_n^2\frac{2}{k_n^4}\frac{1}{(1-r_n^2)^2}\right\} - \frac{2}{k_n^4}\frac{1}{1-r_n^2} =$$
$$\frac{1}{2}\frac{2}{k_n^4}\frac{1}{(1-r_n^2)^2}\left\{1-r_n^2\right\} - \frac{2}{k_n^4}\frac{1}{1-r_n^2} =$$
$$\frac{1}{k_n^4}\frac{1}{1-r_n^2} - \frac{2}{k_n^4}\frac{1}{1-r_n^2} = -\frac{1}{k_n^4}\frac{1}{1-r_n^2} = -\frac{1}{k_n^2(k_n^2-r^2)}. \quad \text{(D.93)}$$

Observe that

$$-\sum_{n=1}^{\infty}\frac{1}{k_n^2(k_n^2-r^2)} = \frac{r-\tan(r)}{2r^3}. \quad \text{(D.94)}$$

To conclude, retain only the contribution of the first mode and divide the right-hand side over left-hand side to obtain

$$\kappa(\nu,r) =$$
$$\sqrt{c^2 - \frac{2r^3}{r-\tan(r)}\sum_{n=1}^{\infty}\left[\frac{(c^2k_n-r^2)\bar{C}_n^2}{4} + \frac{c\,r\left(\frac{(\bar{A}^2-\bar{B}^2)\sin(2r_c)}{2} + 2\bar{B}\bar{C}_n + 2\bar{A}\bar{B}\sin^2(r_c)\right)}{2}\right]}, \quad \text{(D.95)}$$

where $\bar{C}_n = C_n/\kappa$ $\bar{A} = A/\kappa$, $\bar{B} = B/\kappa$. This concludes the evaluation of the dynamic J-integral.

Appendix E

DERIVATIONS FOR CHAPTER VI

E.1 Evaluating the PPIs

E.1.1 Configurational force in horizontal direction: $\hat{\mathrm{J}}_x = 0$

Recall, eq. (2.49) boils down to a contour integral in the plane strain case, in particular $\hat{\mathrm{J}}_x = 0$ becomes

$$\hat{\mathrm{J}}_x = \int_\Gamma \left[(\hat{W} - \hat{T})n_x - \hat{t}_i \hat{u}_{i,x}\right] dl \,. \tag{E.1}$$

E.1.1.1 Horizontal contour pieces

These contours are characterized by normal whose components are $n_x = 0$, $n_y = \pm 1$, therefore they have integrand $\hat{t}_i \hat{u}_{i,x}$, that is, the term corresponding to the tractions on the contour.

Bottom contour

See that this contour is such that there is no change in horizontal direction, $\hat{u}_{i,x} = 0$, whereas the free surface implies, Γ_3 and Γ_5, are traction free, $\hat{t}_i = 0$. Note that had we used a rigid bedrock as the one in section 2.6 or section 4.2, the result would have not changed.

Free surface

This piece does not contribute anything since there are no external tractions applied.

Excavation base

The contribution of the base of the excavation, Γ_5, $\hat{t}_i \hat{u}_{i,x}$ is

$$\int_{\Gamma_5} \left[-\hat{t}_i \hat{u}_{i,x}\right]_{y=0} dx = \int_{\Gamma_5} - \left[\hat{\tau}_{xy}\hat{u}_{,x} + \hat{\sigma}_{yy}\hat{v}_{,x}\right]_{y=0} dx = \int_{\Gamma_5} - \left[\hat{\sigma}_{yy}\hat{v}_{,x}\right]_{y=0} dx \,. \tag{E.2}$$

E.1.1.2 Vertical contour pieces

Far field

The contour corresponding to the far-field does not present gradients in the horizontal direction, hence

$$\int_{\Gamma_2} \left[(\hat{W} - \hat{T})\right]_{x\to\infty} dy \,, \tag{E.3}$$

we could expand this integral for the sake of more detail:

$$\int_{\Gamma_2} \frac{1}{2}\left[\frac{\hat{\tau}_{xy}^2}{\mu} - \rho\varpi^2\hat{u}^2\right]_{x\to\infty} dy = \int_{\Gamma_2} \frac{1}{2}\left[\mu\hat{u}_{,y}^2 - \rho\varpi^2\hat{u}^2\right]_{x\to\infty} dy\,. \tag{E.4}$$

Excavation wall

The one corresponding to the flank of the excavation is more convoluted, since the displacement field becomes more embroiled in the near field,

$$\int_{\Gamma_4} \left[(\hat{W}-\hat{T})(-1) - \hat{t}_i\hat{u}_{i,x}\right]_{x=W/2} dy = \int_{\Gamma_4} \left[-(\hat{W}-\hat{T}-\hat{\sigma}_{xx}\hat{u}_{,x}-\hat{\tau}_{xy}\hat{v}_{,x})\right]_{x=W/2} dy\,, \tag{E.5}$$

the integral can be conveniently expanded as

$$\int_{\Gamma_4} \frac{1}{2}\left[\frac{\hat{\sigma}_{xx}^2}{\lambda+2\mu} + \frac{\hat{\tau}_{xy}^2}{\mu} + \rho\varpi^2(\hat{u}^2+\hat{v}^2)\right]_{x=W/2} dy = \tag{E.6a}$$

$$\int_{\Gamma_4} \frac{1}{2}\left[(\lambda+2\mu)\hat{u}_{,x}^2 + \mu\hat{v}_{,x}^2 + \rho\varpi^2(\hat{u}^2+\hat{v}^2)\right]_{x=W/2} dy\,, \tag{E.6b}$$

Over-the-axis

Finally, the portion running over the antisymmetry axis:

$$\int_{\Gamma_6} \left[(\hat{W}-\hat{T})(-1) - \hat{t}_i\hat{u}_{i,x}\right]_{x=0} dy = \int_{\Gamma_6} \left[-(\hat{W}-\hat{T}-\hat{\tau}_{xy}\hat{v}_{,x})\right]_{x=0} dy\,, \tag{E.7}$$

which can be expanded as

$$\int_{\Gamma_6} \frac{1}{2}\left[\frac{\hat{\tau}_{xy}^2}{\mu} + \rho\varpi^2\hat{u}^2\right]_{x=0} dy = \int_{\Gamma_6} \frac{1}{2}\left[\mu\hat{u}_{,y}^2 + \rho\varpi^2\hat{u}^2\right]_{x=0} dy\,, \tag{E.8}$$

E.1.1.3 Balance equation

$$\begin{aligned}&\int_{\Gamma_2} \left[(\hat{W}-\hat{T})\right]_{x\to\infty} dy + \int_{\Gamma_4} \left[-(\hat{W}-\hat{T}-\hat{\sigma}_{xx}\hat{u}_{,x}-\hat{\tau}_{xy}\hat{v}_{,x})\right]_{x=W/2} dy + \\ &\int_{\Gamma_5} -\left[\hat{\sigma}_{yy}\hat{v}_{,x}\right]_{y=0} dx + \int_{\Gamma_6} \left[-(\hat{W}-\hat{T}-\hat{\tau}_{xy}\hat{v}_{,x})\right]_{x=0} dy = 0\,.\end{aligned} \tag{E.9}$$

Note that the contribution of Γ_2 cancels with the one of Γ_4 in case the excavation was absent altogether. Hence, this equation quantifies the perturbation introduced by the presence of the irregularity.

E.1.2 Configurational force in vertical direction: $\hat{\mathrm{J}}_y = 0$

Likewise,

$$\hat{\mathrm{J}}_y = \int_\Gamma \left[(\hat{W} - \hat{T})n_x - \hat{t}_i \hat{u}_{i,y}\right] dl\,. \tag{E.10}$$

E.1.2.1 Horizontal contour pieces

In this case the whole integrand, not only the direct contribution of the tractions, has to be considered.

Bottom contour

Beginning by the bottom contour, which does contribute in this direction,

$$\int_{\Gamma_1} \left[(\hat{W} - \hat{T})(-1) - \hat{t}_i \hat{u}_{i,y}\right]_{y\to-\infty} dy = \int_{\Gamma_1} -\left[(\hat{W} - \hat{T} - \hat{\tau}_{xy}\hat{u}_{,y})\right]_{y\to-\infty} dx\,, \tag{E.11}$$

equivalently,

$$\int_{\Gamma_1} \frac{1}{2}\left[\frac{\hat{\tau}_{xy}^2}{\mu} + \rho\varpi^2\hat{u}^2\right]_{y\to-\infty} dx = \int_{\Gamma_1} \frac{1}{2}\left[\mu\hat{u}_{,y}^2 + \rho\varpi^2\hat{u}^2\right]_{y\to-\infty} dx \tag{E.12}$$

Free surface

The traction free condition simplifies this one:

$$\begin{aligned}\int_{\Gamma_3} \left[(\hat{W} - \hat{T})\right]_{y=h} dy &= \int_{\Gamma_3} \frac{1}{2}\left[\frac{\hat{\sigma}_{xx}^2}{\lambda+2\mu} - \rho\varpi^2(\hat{u}^2+\hat{v}^2)\right]_{y=h} dx \\ &= \int_{\Gamma_3} \frac{1}{2}\left[(\lambda+2\mu)\hat{u}_{,x}^2 - \rho\varpi^2(\hat{u}^2+\hat{v}^2)\right]_{y=h} dx\end{aligned} \tag{E.13}$$

Excavation base

$$\begin{aligned}\int_{\Gamma_5} \left[(\hat{W} - \hat{T}) - \hat{\sigma}_{yy}\hat{v}_{,y} - \hat{\tau}_{xy}\hat{u}_{,y}\right]_{y=0} dx &= \int_{\Gamma_5} \frac{-1}{2}\left[\frac{\hat{\sigma}_{yy}^2}{(\lambda+2\mu)} + \frac{\hat{\tau}_{xy}^2}{\mu} + \rho\varpi^2\hat{v}^2\right]_{y=0} dx \\ &= \int_{\Gamma_5} \frac{-1}{2}\left[(\lambda+2\mu)\hat{v}_{,y}^2 + \mu\hat{u}_{,y}^2 + \rho\varpi^2\hat{v}^2\right]_{y=0} dx\,,\end{aligned} \tag{E.14}$$

Let us point out, for the sake of utmost clarity, that the absence of horizontal normal stresses from the prior expressions is not due to they actually vanishing over the contour, but rather to the fact that $\hat{u}_{,x} = 0$ on this contour as the excavation moves rigidly, then their corresponding addend $\hat{\sigma}_{xx}\hat{u}_{,x} = \lambda\hat{v}_{,y}\hat{u}_{,x} = 0$.

E.1.2.2 Vertical contour pieces

Far field

In this contour $-\hat{t}_i\hat{u}_{i,y} = -(\hat{\sigma}_{xx}\hat{u}_{,y}+\hat{\tau}_{xy}\hat{v}_{,y}) = 0$, hence the far-field does not contribute to the balance of configurational forces in vertical direction.

Excavation wall

In this case,

$$\begin{aligned}\int_{\Gamma_4}\left[-\hat{t}_i\hat{u}_{i,y}\right]_{x=W/2}dy &= \int_{\Gamma_4}\left[-(-\hat{\sigma}_{xx}\hat{u}_{,y}-\hat{\tau}_{xy}\hat{v}_{,y})\right]_{x=W/2}dy\\ &= \int_{\Gamma_4}\left[\hat{\sigma}_{xx}\hat{u}_{,y}\right]_{x=W/2}dy\,.\end{aligned} \tag{E.15}$$

Over-the-axis

Finally,

$$\int_{\Gamma_3}\left[(\hat{W}-\hat{T})\right]_{y=h}dy+\int_{\Gamma_6}\left[-\hat{t}_i\hat{u}_{i,y}\right]_{x=0}dy=\int_{\Gamma_6}\left[-(-\hat{\sigma}_{xx}\hat{u}_{,y}-\hat{\tau}_{xy}\hat{v}_{,y})\right]_{x=0}dy=0\,, \tag{E.16}$$

therefore this segment, just like the far field, does not contribute any configurational force along the vertical direction.

E.1.2.3 Balance equation

$$\begin{aligned}&\int_{\Gamma_1}-\left[(\hat{W}-\hat{T}-\hat{\tau}_{xy}\hat{u}_{,y})\right]_{y\to-\infty}dx+\int_{\Gamma_3}\left[(\hat{W}-\hat{T})\right]_{y=h}dy\\ &+\int_{\Gamma_4}\left[\hat{\sigma}_{xx}\hat{u}_{,y}\right]_{x=W/2}dy+\int_{\Gamma_5}\left[(\hat{W}-\hat{T})-\hat{\sigma}_{yy}\hat{v}_{,y}-\hat{\tau}_{xy}\hat{u}_{,y}\right]_{y=0}dx=0\end{aligned} \tag{E.17}$$

E.1.3 Configurational torques: $\hat{\mathrm{L}}_z = 0$

Finally, we consider the balance of configurational torques using the same contour. The identity we will obtain has a different character, as geometric parameters enter in differnet manner. The conservation law in this case dictates

$$\begin{aligned}\hat{\mathrm{L}}_z(\Gamma) &= \int_\Gamma \epsilon_{zij}\left[(\hat{W}-\hat{T})x_jn_i+\hat{t}_i\hat{u}_j-\hat{t}_k\hat{u}_{k,i}x_j\right]\,dl\\ &= -\int_\Gamma\Big[(\hat{W}-\hat{T})(xn_y-yn_x)+\hat{t}_y\hat{u}-\hat{t}_x\hat{v}\\ &\qquad -\hat{t}_x(x\hat{u}_{,y}-y\hat{u}_{,x})-\hat{t}_y(x\hat{v}_{,y}-y\hat{v}_{,x})\Big]\,dl=0\end{aligned} \tag{E.18}$$

The evaluation of this balance law involves more toil, as one must interpret it carefully.

E.1.3.1 Horizontal contour pieces

Bottom contour

Start by the bottom piece, $n_y = -1$ and $n_x = 0$, this contour runs from $x = 0$ to $x \to \infty$

$$\int_{\Gamma_1} \left[(\hat{W} - \hat{T})(-x) + \hat{\tau}_{xy}(x\hat{u}_{,y})\right]_{y\to-\infty} dx = \int_{\Gamma} \left[(\hat{W} - \hat{T} - \hat{\tau}_{xy}\hat{u}_{,y})(-x)\right]_{y\to-\infty} dx\,, \tag{E.19}$$

the integrand, as we are assuming the impinging wavefronts is unperturbed by scattering or reflections, is constant over the segment, and thus the integral is the value of the integrand times the length of the path. As we are taking limits to infinity, let us begin consider a value $x = ell$ in lieu of $x \to \infty$, and when the moment arrives we shall take $\ell \to \infty$. Likewise, let us say that the integrand is evaluated at a certain depth $y = -\ell$ Thus, eq. (E.19) becomes

$$\begin{aligned}\int_0^{\ell} \left[(\hat{W} - \hat{T} - \hat{\tau}_{xy}\hat{u}_{,y})(-x)\right]_{y=-\ell} dx &= \left[\hat{W} - \hat{T} - \hat{\tau}_{xy}\hat{u}_{,y}\right]_{y=-\ell} \int_0^{\ell} (-x)dx \\ &= -\left[\hat{W} - \hat{T} - \hat{\tau}_{xy}\hat{u}_{,y}\right]_{y=-\ell} \frac{\ell^2}{2}\,,\end{aligned} \tag{E.20}$$

see how the first factor can be expressed in different ways:

$$\left[\hat{W} - \hat{T} - \hat{\tau}_{xy}\hat{u}_{,y}\right]_{y=-\ell} = -\frac{1}{2}\left[\frac{\hat{\tau}_{xy}^2}{\mu} + \rho\varpi^2\hat{u}^2\right]_{y=-\ell} = -\left[\hat{W} + \hat{T}\right]_{y=-\ell}\,. \tag{E.21}$$

Free surface

Next, at the free surface, the contour runs from $x = \ell$ to $x = W/2$,

$$\int_{\Gamma_3} \left[(\hat{W} - \hat{T})(x)\right]_{y=h} dx\,. \tag{E.22}$$

the outcome of this contour is equivalent to the integrand of $\hat{\mathrm{J}}_y = 0$ times x.

Excavation base

The contribution of the base, unlike the two previous case is restricted to a finite contour, and note that $y = 0$ plays a role here,

$$\begin{aligned}&\int_{\Gamma_5} \left[(\hat{W} - \hat{T})(x) + \hat{\sigma}_{yy}\hat{u} - \hat{\tau}_{xy}(\theta x) - \hat{\tau}_{xy}(xu_{,y}) - \hat{\sigma}_{yy}(xv_{,y})\right]_{y=0} dx \\ &= \int_{\Gamma_5} \left[(\hat{W} - \hat{T} - \hat{\tau}_{xy}u_{,y} - \hat{\sigma}_{yy}v_{,y})(x) + \hat{\sigma}_{yy}\hat{u} - \hat{\tau}_{xy}\hat{u}\right]_{y=0} dx\end{aligned} \tag{E.23}$$

E.1.3.2 Vertical contour pieces

Let us proceed in similar fashion, keeping in mind we are using the finite distance ℓ so that we can deal with the infinite later.

Far field

In this case, y stretches from $y = -\ell$ to $y = h$.

$$\int_{\Gamma_2} \left[(\hat{W} - \hat{T})(-y) + \hat{\tau}_{xy}\hat{u}\right]_{x=\ell} dy\,, \tag{E.24}$$

See that, even though the integrand is not constant but easily integrable.

Excavation wall

The contribution of the wall in this case boils down to

$$\begin{aligned}
&\int_{\Gamma_4} \left[(\hat{W} - \hat{T})(y) - \hat{\tau}_{xy}\hat{u} + \hat{\sigma}_{xx}\frac{W}{2} + \hat{\sigma}_{xx}(x\hat{u}_{,y} - y\hat{u}_{,x}) + \hat{\tau}_{xy}(-y\hat{v}_{,x})\right]_{x=W/2} dy \\
&= \int_{\Gamma_4} \left[(\hat{W} - \hat{T} - \hat{\tau}_{xy}\hat{v}_{,x} - \hat{\sigma}_{xx}\hat{u}_{,x})(y) - \hat{\tau}_{xy}\hat{u} + \hat{\sigma}_{xx}\left(\frac{W}{2} - \theta x\right)\right]_{x=W/2} dy \\
&= \int_{\Gamma_4} \left[(\hat{W} - \hat{T} - \hat{\tau}_{xy}\hat{v}_{,x} - \hat{\sigma}_{xx}\hat{u}_{,x})(y) - \hat{\tau}_{xy}\hat{u}\right]_{x=W/2} dy\,.
\end{aligned} \tag{E.25}$$

Over-the-axis

The last one,

$$\begin{aligned}
&\int_{\Gamma_6} \left[(\hat{W} - \hat{T})(-yn_x) - \hat{\tau}_{xy}\hat{u} + \hat{\tau}_{xy}(-y\hat{v}_{,x})\right]_{x=0} dy \\
&= \int_{\Gamma_6} \left[(\hat{W} - \hat{T} - \hat{\tau}_{xy}\hat{v}_{,x})(y) - \hat{\tau}_{xy}\hat{u}\right]_{x=0} dy\,.
\end{aligned} \tag{E.26}$$

E.1.3.3 Balance equation

$$
\begin{aligned}
&- \left[\hat{W} - \hat{T} - \hat{\tau}_{xy}\hat{u}_{,y}\right]_{y=-\ell} \frac{\ell^2}{2} \\
&+ \int_{-\ell}^{h} \left[(\hat{W} - \hat{T})(-y) + \hat{\tau}_{xy}\hat{u}\right]_{x=\ell} dy \\
&+ \int_{\ell}^{W/2} \left[(\hat{W} - \hat{T})(x)\right]_{y=h} dx \\
&+ \int_{h}^{0} \left[(\hat{W} - \hat{T} - \hat{\tau}_{xy}\hat{v}_{,x} - \hat{\sigma}_{xx}\hat{u}_{,x})(y) - \hat{\tau}_{xy}\hat{u}\right]_{x=W/2} dy \\
&+ \int_{W/2}^{0} \left[(\hat{W} - \hat{T} - \hat{\tau}_{xy}u_{,y} - \hat{\sigma}_{yy}v_{,y})(x) + \hat{\sigma}_{yy}\hat{u} - \hat{\tau}_{xy}\hat{u}\right]_{y=0} dx \\
&+ \int_{0}^{-\ell} \left[(\hat{W} - \hat{T} - \hat{\tau}_{xy}\hat{v}_{,x})(y) - \hat{\tau}_{xy}\hat{u}\right]_{x=0} dy = 0\,.
\end{aligned}
\tag{E.27}
$$

E.2 Obtention of simplified formulae

We begin from table

	$\hat{\mathrm{J}}_x = 0$	$\hat{\mathrm{J}}_y = 0$
Γ_1		$-\frac{1}{2}\left(\frac{\hat{\tau}_{xy}^2}{\mu} + \rho\varpi^2\hat{u}^2\right)$
Γ_2	$\frac{1}{2}\left(\frac{\hat{\tau}_{xy}^2}{\mu} - \rho\varpi^2\hat{u}^2\right)$	
Γ_3		$\frac{1}{2}\left(-\rho\varpi^2\hat{u}^2\right)$
Γ_4	$-\frac{1}{2}\left(\frac{K^2(\hat{u}_0-\hat{u})^2}{\lambda+2\mu} + \rho\varpi^2((\hat{u}_0 - \theta_0 y)^2 + (\theta_0 W/2)^2)\right)$	$\theta_0 K(\hat{u}_0 - \hat{u})$
Γ_5	$-K{\theta_0}^2 x$	$-\frac{1}{2}\left(\frac{K^2(\theta_0 x)^2}{\lambda+2\mu} + \rho\varpi^2((\theta_0 x)^2 + \hat{u}_0^2)\right)$
Γ_6	$-\frac{1}{2}\left(\frac{\hat{\tau}_{xy}^2}{\mu} - \rho\varpi^2\hat{u}^2\right)$	

Table E.1: Summary of contributions to the PII, in terms of stresses

Recall that we use B as a shortcut for $W/2$ in this appendix. The dimensionless variables $\tilde{\theta_0} = \theta_0 h/\hat{u}_{f0}$, $\tilde{K} = Kh/(\lambda + 2\mu)$ and $\tilde{B} = B/h$ appear henceforth.

E.2.1 Horizontal balance

Bear in mind the main working assumption: the wavelength is greater than the geometrical features of the excavation.

E.2.1.1 Contribution of the wall, Γ_4

$$\int_{\Gamma_4} -\frac{1}{2}\left[\frac{\hat{\sigma}_{xx}^2}{(\lambda+2\mu)} + \rho\varpi^2(\hat{u}^2+\hat{v}^2)\right] dy \tag{E.28a}$$

$$= \int_{\Gamma_4} -\frac{1}{2}\left[\frac{K^2(\hat{u}_w - \hat{u}_{ff0})^2}{(\lambda+2\mu)} + \rho\varpi^2(\hat{u}_w^2 + (\theta B)^2)\right] dy \tag{E.28b}$$

flip the sign at this point

$$= \int_0^h \frac{1}{2}\left[\frac{K^2(\hat{u}_w - \hat{u}_{ff0})^2}{(\lambda+2\mu)} + \rho\varpi^2((\hat{u}_0 + \theta_0(z-h))^2 + (\theta_0 B)^2)\right] dy \tag{E.28c}$$

$$= \frac{1}{2}\frac{K^2}{(\lambda+2\mu)}\int_0^h (\hat{u}_w - \hat{u}_{ff0})^2 dy + \frac{1}{2}\rho\varpi^2\left[(\theta_0 B)^2 h + \int_0^h (\hat{u}_0 + \theta_0(z-h))^2 dz\right] = \tag{E.28d}$$

$$= \frac{1}{2}\frac{K^2}{(\lambda+2\mu)}\hat{u}_{ff0}^2 h\left[1 + \frac{\tilde{\theta}_0^2}{3} + \tilde{\theta}_0\left(\frac{2}{r^3} - \frac{(2+r^2)\cos(r)}{r^2}\right) + \frac{\cos(2r)}{2} - \frac{3\sin(2r)}{4r}\right] + \frac{1}{2}\rho\varpi^2\left[(\theta_0 B)^2 h + \hat{u}_{ff0}^2 h\left(\frac{\tilde{\theta}_0^2}{3} - \tilde{\theta}_0\cos(r) + \cos^2(r)\right)\right] \tag{E.28e}$$

E.2.1.2 Contribution of the base, Γ_5

This contour yields simply

$$\begin{aligned}\int_{\Gamma_5}[-\hat{\sigma}_{yy}\hat{v}_{,x}]dx &= \int_{\Gamma_5}[-K\hat{v}\hat{v}_{,x}]dx = \int_{\Gamma_5}[-K\theta_0^2 x]dx \\ &= \int_0^B [K\theta_0^2 x]dx = K\theta_0^2\frac{B^2}{2}\,.\end{aligned} \tag{E.29}$$

E.2.1.3 Contribution of the far field, Γ_2, and over-the-axis, Γ_4

The contribution of these two pieces boils down to :

$$\int_{\Gamma_2} \frac{1}{2}\Big(\mu\hat{u}_{,y}^2 - \rho\varpi^2\hat{u}^2\Big)dy + \int_{\Gamma_4} \frac{1}{2}\Big(\mu\hat{u}_{,y}^2 - \rho\varpi^2\hat{u}^2\Big)dy = \tag{E.30a}$$

$$\int_{-\ell}^{h} \frac{1}{2}\Big(\mu\hat{u}_{,y}^2 - \rho\varpi^2\hat{u}^2\Big)dy + \int_{0}^{-\ell} \frac{1}{2}\Big(\mu\hat{u}_{,y}^2 - \rho\varpi^2\hat{u}^2\Big)dy = \tag{E.30b}$$

$$= \int_{0}^{h} \frac{1}{2}\Big(\mu\hat{u}_{,y}^2 - \rho\varpi^2\hat{u}^2\Big)dy = \int_{0}^{h} \frac{1}{2}\Big(\mu\hat{u}_{,z}^2 - \rho\varpi^2\hat{u}^2\Big)dz \tag{E.30c}$$

$$= \frac{1}{2}\rho\varpi^2\hat{u}_{ff0}h\int_0^1 \Big(\sin^2(r\bar{z}) - \cos^2(r\bar{z})\Big)\,d\bar{z} \tag{E.30d}$$

$$= \frac{1}{2}\rho\varpi^2\hat{u}_{ff0}h\left(-\frac{\cos(r)\sin(r)}{r}\right). \tag{E.30e}$$

E.2.1.4 All together now

Hence, $\hat{\mathrm{J}}_x = 0$, in dimensionless form, yields

$$\begin{aligned}
&-\tilde{B}^2c^2\tilde{\theta}_0^2\tilde{K} + r^2\left(\left(\tilde{B}^2 + \frac{1}{3}\right)\tilde{\theta}_0^2 - \tilde{\theta}_0\cos(r) + \cos^2(r)\right)\\
&+ c^2\tilde{K}^2\left(\frac{\tilde{\theta}_0^2}{3} + \frac{2\tilde{\theta}_0}{r^2} - \frac{\tilde{\theta}_0\left(r^2+2\right)\cos(r)}{r^2} - \frac{3\sin(2r)}{4r} + \frac{1}{2}\cos(2r) + 1\right)\\
&- r\sin(r)\cos(r) = 0
\end{aligned} \tag{E.31}$$

E.2.2 Vertical balance

E.2.2.1 Contribution of the bottom contour, Γ_1, and free surface, Γ_3

The contribution of these two pieces was simplified into :

$$\int_{\Gamma_1} -\frac{1}{2}\Big(\mu\hat{u}_{,y}^2 + \rho\varpi^2\hat{u}^2\Big)dx + \int_{\Gamma_3} \frac{1}{2}\Big(-\rho\varpi^2\hat{u}^2\Big)dx = \tag{E.32a}$$

$$-\int_{\Gamma_3\cup[B,0]} \frac{1}{2}\Big(-\rho\varpi^2\hat{u}^2\Big)dx + \int_{\Gamma_3} \frac{1}{2}\Big(-\rho\varpi^2\hat{u}^2\Big)dx = \tag{E.32b}$$

$$-\int_{B}^{0} \frac{1}{2}\Big(-\rho\varpi^2\hat{u}^2\Big)dx = -\frac{1}{2}(-\rho\varpi^2\hat{u}_{ff0}^2)(-B) = -\frac{1}{2}\rho\varpi^2\hat{u}_{ff0}^2B\,. \tag{E.32c}$$

E.2.2.2 Contribution of the wall, Γ_4

$$\begin{aligned}\int_{\Gamma_4}[-\hat{\sigma}_{xx}\hat{u}_{,y}]dx &= \int_{\Gamma_5}[-K(\hat{u}_w-\hat{u}_{ff0})(-\theta)]dx \\ &= K\theta_0\int_{\Gamma_4}[(\hat{u}_w-\hat{u}_{ff0})]dx = -K\theta_0\int_0^h[(\hat{u}_w-\hat{u}_{ff0})]dx \\ &= -K\theta_0\hat{u}_{ff0}h\Big[-\frac{\tilde{\theta}_0}{2}+\cos(r)-\frac{\sin(r)}{r}\Big].\end{aligned} \tag{E.33}$$

E.2.2.3 Contribution of the base, Γ_5

$$\int_{\Gamma_5}-\frac{1}{2}\left[\frac{\hat{\sigma}_{yy}^2}{(\lambda+2\mu)}+\rho\varpi^2(\hat{u}^2+\hat{v}^2)\right]dx \tag{E.34a}$$

$$=-\frac{1}{2}\int_{\Gamma_5}\left[\left(\frac{K^2}{(\lambda+2\mu)}+\rho\varpi^2\right)\hat{v}^2+\rho\varpi^2\hat{u}_0^2\right]dx \tag{E.34b}$$

at this point we flip the sign

$$=\frac{1}{2}\int_0^B\left[\left(\frac{K^2}{(\lambda+2\mu)}+\rho\varpi^2\right)(\theta_0 x)^2+\rho\varpi^2\hat{u}_0^2\right]dx \tag{E.34c}$$

$$=\frac{1}{2}\left[\left(\frac{K^2}{(\lambda+2\mu)}+\rho\varpi^2\right)\theta_0^2\frac{B^3}{3}+\rho\varpi^2\hat{u}_0^2B\right]. \tag{E.34d}$$

E.2.2.4 All together now

The balance equation in this case is

$$\frac{1}{3}\tilde{B}^3\tilde{\theta}_0^2\left(c^2\tilde{K}^2+r^2\right)-\tilde{B}r^2+\tilde{B}r^2\cos^2(r)-2c^2\tilde{\theta}_0\tilde{K}\left(\frac{\tilde{\theta}_0}{2}+\frac{\sin(r)}{r}-\cos(r)\right)=0 \tag{E.35}$$

E.2.3 Perturbation series

We expand this equations assuming a perturbation series in terms of the parameter $r=\varpi c_s/H$ of both the rotation (presupposing that the first term scales as r^2) and the impedance:

$$\tilde{\theta}_0=\sum_{n=2}^{\infty}\tilde{\theta}_n r^n, \tag{E.36a}$$

$$\tilde{K}=\sum_{n=0}^{\infty}\tilde{K}_n r^n, \tag{E.36b}$$

If we gather leading-order terms of both horizontal and vertical balance, we reach a system of equations for both $\tilde{K}_0$ and $\tilde{\theta}_2$. The horizontal equilibrium yields

$$-60\tilde{B}^2\tilde{\theta}_2^2\tilde{K}_0 - \frac{20}{c^2} - 60\tilde{\theta}_2 + 20\tilde{\theta}_2^2\tilde{K}_0^2 + 25\tilde{\theta}_2\tilde{K}_0^2 + 8\tilde{K}_0^2 = 0\,, \tag{E.37}$$

whereas the vertical one

$$-3\tilde{B}c^{-2} - 2\tilde{K}_0\tilde{\theta}_2 - 3\tilde{K}_0\tilde{\theta}_2^2 + \tilde{B}^3\tilde{K}_0^2\tilde{\theta}_2^2 = 0\,. \tag{E.38}$$

This system can be solved in *Mathematica* (see notebook titled "Chapter6 Kinematic Interaction"). The choice of the solution attends to these criteria: 1) $K_0 > 0$ and 2) $\theta_2 < 0$ (the rotation is out-of-phase with the displacement, meaning that when the horizontal displacement in the far-field is positive, the rotation, following this convention, must be negative).